Geologic Map of the Carlsbad 30 x 60-Minute Quadrangle, Eddy and Otero Counties, New Mexico; and Culberson, Hudspeth, and Reeves Counties, Texas

By

Jon M. Krupnick[1], Tyler Askin[1], Bruce D. Allen[1], Michelle M. Gavel[2], and Victor J. Polyak[3]

[1]*New Mexico Bureau of Geology and Mineral Resources, 801 Leroy Place, Socorro, NM 87801*
[2]*TerranearPMC LLC, 4200 West Jemez Road, Los Alamos, NM 87544*
[3]*University of New Mexico, 1155 University Blvd SE, Albuquerque, NM 87106*

April 2026

New Mexico Bureau of Geology and Mineral Resources
Geologic Map 82

Scale 1:100,000

https://doi.org/10.58799/GM-82

This work was supported by the U.S. Geological Survey, National Cooperative Geologic Mapping Program (STATEMAP) under USGS Cooperative Agreement G23AC00578 and the New Mexico Bureau of Geology and Mineral Resources.

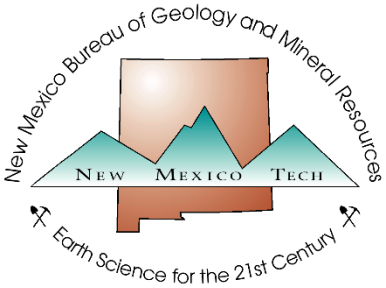

New Mexico Bureau of Geology and Mineral Resources
801 Leroy Place, Socorro, New Mexico, 87801-4796

GEOLOGIC SUMMARY

The Carlsbad 30x60-minute quadrangle (1:100,000 scale) spans several major geographic areas and geologic provinces, with a natural history that has provided important societal and scientific value for over a century. Prior to modern development, this area hosted indigenous societies for many millennia. Within this quadrangle, the Delaware Basin, part of the Permian Basin, features the city of Carlsbad and several towns that support major infrastructure for potash mining and oil and gas extraction within basinal Paleozoic sediments. This area is cut by the Pecos River valley and preserves a record of late Cenozoic fluvial systems. Prevailing winds source sands from the river valley to create major eolian deposits on the Mescalero Plain in the northeastern map area. Cave systems are abundant on the Gypsum Plain and in the Guadalupe Mountains, home to Carlsbad Caverns National Park. The Guadalupe Mountains encompass multiple wilderness areas and include exposures of shelf and reef sediments from the Permian sedimentary system and major geographical features such as the Seven Rivers Embayment and the Algerita Escarpment. Dropping westward, off the Algerita Escarpment, is a transition into the Rio Grande rift and the Salt Basin, represented by the remote and desolate Brokeoff Mountains as well as playa systems of the Crow Flats. Subsurface stratigraphy of Permian-through Cambrian-aged sedimentary rock and Mesoproterozoic basement is variably found in boreholes and well logs across the map area. The southern border of this quadrangle spans nearly 95 km across the border of New Mexico and Texas. This map is a compilation effort that brings together new data with decades of existing geologic mapping and research from various institutions and geologic field mappers.

The Permian sedimentary system dominates the exposed bedrock of this geologic quadrangle. Shelf deposits in the backreef, reefs on the shelf margin, and basin deposits are found preserved with much of their paleotopographic relief across the Northwest Shelf, Capitan Reef, and Delaware Basin. These features are part of the larger Permian Basin, which also encompasses the Central Basin Platform, Midland Basin, Marathon Shelf, Diablo Platform, and Val Verde Basin spanning southeastern New Mexico and west Texas. Deposition of the reef system exposed in this quadrangle occurred during the early to middle Permian. The typical stratigraphic configuration of these sediments is interbedded shelf deposits of clastics, evaporites, and carbonates grading and transitioning basinward into carbonate-dominated reef facies forming on the margin of the ancient shelf. Sand-dominated channels are found occupying broad topographic lows across the shelf before they cut across the reefs and drop as submarine mass-wasting deposits through foreslope sediments and splay out into deep basin lows. These sands aggraded on the basin floor along with shales and deep-water carbonates.

Prior to the deposition of the dominant shelf-reef-basin depositional system during the Cisuralian and Guadalupian periods, tectonics of the Ancestral Rocky Mountain (ARM) orogeny during the Pennsylvanian and early Permian deformed the landscape previously occupied by the Tabosa Basin into the topography that defines the stratigraphic architecture of the Delaware Basin. The change in this landscape is recorded by an unconformity at the base of

the early Permian Cisuralian (Wolfcampian) sediments. Sediments deposited during or before the early Permian are only found in the subsurface and include deposition during the Pennsylvanian, Mississippian, Devonian, Silurian, Ordovician, and Cambrian. These Paleozoic rocks are the targets of oil and gas plays within the Delaware Basin; preservation of these deposits is variable on the Northwest Shelf, where topographic highs during orogenic events may have resulted in erosion or nondeposition.

Lopingian strata followed the Guadalupian reef system as evaporites were deposited in a closed deep-water basin that shallowed upward as subsidence slowed and precipitation of salts buried the Guadalupian strata. The area experienced mixed clastic, evaporite, and carbonate deposition in nearshore and coastal environments through the late Permian and into the Triassic. The Western Interior Seaway (WIS) occupied this area during the Upper Cretaceous. Tectonic activity of the early Cenozoic uplifted the area kilometers above sea level, causing exhumation of Paleozoic and Mesozoic strata. No early Cenozoic strata deposited by traditional means are preserved in this quadrangle or the surrounding region.

Cretaceous sediments that collapsed into sinkholes or fractures within Lopingian strata are found, now exhumed, across the Gypsum Plain. These deposits are inferred to have collapsed after retreat of the WIS during the Upper Cretaceous or early Cenozoic, as regional uplift in the interior of the continent during the Laramide orogeny led to exhumation and erosion of contemporaneous strata. A brief period of late Eocene intrusive volcanism is preserved within Lopingian strata in the same area as the Cretaceous deposits and is also thought to be reworked into karst-collapse features. Karst processes may affect sediments of any age in a variety of manners across the entire map area.

Tectonic extension related to the Rio Grande rift uplifted the Guadalupe Mountains during the Miocene, and dissolution of Lopingian evaporites caused subsidence in the adjacent Delaware Basin. This may have resulted in uplift of paleohighlands to the west of the present-day Guadalupe Mountains, producing across-range sedimentation that deposited Ogallala sediments to the east and provided the framework for the development of the ancestral Pecos River sedimentary system. The system persisted in various forms from the Miocene into the middle Pleistocene, with an extensive history of stream capture, drainage reorganization, and climatic variability. The older sequence of sediments features a mature petrocalcic soil, with development starting at the end of a dominant aggradation regime that is now buried or inset by additional incision-dominated ancestral Pecos River sediments, which feature a less-developed petrocalcic horizon that was subsequently precipitated during the middle Pleistocene. Southward integration of the Pecos River is marked by either a change to an incisional regime or the development of fluvial terraces associated with the modern Pecos River. Rift extension continued until around this time, dropping fault blocks and grabens in the Brokeoff Mountains and moving the drainage divide along the Algerita Escarpment eastward.

Deposition of fans, piedmont aprons, colluvium, mass-wasting deposits, sheetwash, and eolian sediments are found draped as surficial deposits across the quadrangle and represent the most recent geologic history of the landscape. Cave entrances and sinkhole depressions are abundant in the landscape. The footprint of modern society is apparent within the Delaware Basin, where pumpjacks, agriculture, quarries, residences, and industrial development dot the landscape.

Figure 1: Sunset looking south-southwest from the Algerita Escarpment into Big Dog Canyon.

ACKNOWLEDGEMENTS

The authors would like to thank the STATEMAP program (grant number G23AC00578), Geologic Mapping Program Manager Dr. Matt Zimmerer, and State Geologist of the New Mexico Bureau of Geology and Mineral Resources, Dr. Mike Timmons, for their support of this project. Thank you to the New Mexico Geological Society (NMGS) for highlighting the unique geology of this field area during the 73rd annual Fall Field Conference in 2023, addressing the *Evaporite Karst of the Lower Pecos Region*. The NMGS also provided a platform for discussing topics related to this map through its annual spring meeting. Support and knowledge from the National Cave and Karst Research Institute located in Carlsbad was greatly appreciated. We would like to acknowledge the millennia of stewardship of this land from native people, and recent management of wilderness and public lands in this quadrangle by the Bureau of Land Management, National Park Service, and United States Forest Service. Processing and analysis of geochronology samples from both the Radiogenic Isotope Lab, at the University of New Mexico, and the New Mexico Geochronology Research Laboratory, at the New Mexico Institute of Mining and Technology, provided important data for this project. Thank you to the New Mexico Bureau of Geology and Mineral Resources Map Production Group for assistance with initial compilation of databases and transforming the map data into a beautiful final product.

Insight from colleagues was invaluable for this project. Thanks go to Dr. John Hawley, Dr. Steve Cather, Dr. Snir Attia, Dr. Veronica Prush, Dr. Brad Sion, and Dan Koning for constructive conversations about the late Cenozoic history of the area. Conversations with Dr. Veronica Prush, Kyle Gallant, Dr. Ron Broadhead, and Dr. Martin Reyes-Correa were essential for cross section construction, understanding of subsurface stratigraphy, and lateral relationships of Permian strata. Field trips led by Dr. Brian Hampton were critical for understanding these strata during the geoscience education of some authors. Communication with Steve Skotnicki built an understanding of piedmont alluvium facies and mapping of the Brokeoff Mountains. Special thanks to Frank Sholedice for report edits. Most importantly, thank you to friends and family for support, advice, and entertaining discussions about these mapping efforts.

TABLE OF CONTENTS

GEOLOGIC SUMMARY 2
TABLE OF CONTENTS 6
Geologic and Geographic Setting 9
Cave and Karst Systems 12
MOTIVATION 13
METHODS 14
Digital Compilation Methods 14
Simplification of Geodatabases 17
Attribute Table Fields 18
Field Methods 20
Cross Section Construction Methods 21
Uncertainties 23
Estimates of shortening 24
Estimate of net shortening 24
Estimate of shortening isolated to area east of rift extension 24
Estimate of lengthening isolated to area west of Huapache monocline 24
PREVIOUS WORKS 25
STRUCTURE AND TECTONICS 29
Precambrian Tectonism 30
Paleozoic Tectonism 30
Mesozoic and Early Cenozoic Tectonism 32
Cenozoic Tectonism 32
STRATIGRAPHY 33
Mesoproterozoic Erathem: Ectasian Period 34
Paleozoic Erathem: Cambrian–Pennsylvanian Periods 34
Cambrian–Ordovician subsurface stratigraphy 34
Ordovician subsurface stratigraphy 34
Silurian subsurface stratigraphy 35
Devonian subsurface stratigraphy 35
Mississippian subsurface stratigraphy 36
Pennsylvanian subsurface stratigraphy 36
Paleozoic Erathem: Permian Period 36
Cisuralian Epoch 36
Guadalupian Epoch 39
Reef environment 40
Backreef shelf environment: the Artesia Group 42
Post-depositional mineralization in shelf deposits 44
Basin deposition: the Delaware Mountain Group 45
Lopingian (Ochoan) Epoch 47
Mesozoic Erathem 48
Triassic deposits 48
Cretaceous outlier deposits 49

Cenozoic Erathem 50
Intrusive rocks 50
Relic deposits of the Neogene 50
Basin-fill and surficial deposits 50
Basin fill of the ancestral Pecos River system: the Gatuña Formation 52
Piedmont facies with tentative correlation to the Lower Gatuña Formation 63
Channel alluvium: Orchard Park terrace suite 65
Channel alluvium: Lakewood terrace suite 66
Channel alluvium: active channel, floodplain, and reactivated terraces 67
Piedmont and fan alluvium 68
Eolian deposits 70
Internally drained deposits 72
Mass-wasting and colluvial deposits 74
Anthropogenic deposits 75
INDUSTRY AND LAND USE 76
Oil and Gas 77
Potash 77
WIPP Site 77
Precious, Critical, and Industrial Minerals 78
REFERENCES 78
BIBLIOGRAPHY 89
APPENDIX 93
Description of Map Units 93
Description of Methods for Surficial Map Unit Compilation 129

TABLE OF FIGURES

Figure 1 4
Figure 2 9
Figure 3 11
Figure 4 12
Figure 5 13
Figure 6 17
Figure 7 18
Figure 8 26
Figure 9 28
Figure 10 29
Figure 11 35
Figure 12 39
Figure 13 40
Figure 14 41
Figure 15 39
Figure 16 40
Figure 17 41

Figure 18 42
Figure 19 43
Figure 20 44
Figure 21 45
Figure 22 46
Figure 23 48
Figure 24 49
Figure 25 51
Figure 26 52
Figure 27 54
Figure 28 55
Figure 29 55
Figure 30 58
Figure 31 60
Figure 32 62
Figure 33 63
Figure 34 68
Figure 35 69
Figure 36 70
Figure 37 71
Figure 38 72
Figure 39 69
Figure 40 70
Figure 41 71
Figure 42 72

TABLE OF TABLES

Table 1 21
Table 2 50
Table 3 60

INTRODUCTION

The map and report for the Carlsbad 30x60-minute quadrangle (1:100,000 scale) are a compilation effort that synthesize a wide range of geologic information into a single project. A bird's-eye view of the history is available in the geologic summary. The methods section details compilation techniques along with an appendix section that offers a description of methods for surficial map-unit compilation. An overview of existing mapping is provided in the previous works section. The structure and tectonics and stratigraphy sections steps through the tectonic history of the area and information regarding the deposition or formation of each grouping of map units. The stratigraphy section includes field and literature investigations of the Gatuña Formation, which exceeds the scope of other units in the stratigraphy section; however, research efforts are still ongoing. A short section on the industry of the area gives context for this project's motivation. The description of map units is

in the appendix and should be referred to for the most detailed lithologic descriptions made available through this project.

Geologic and Geographic Setting

This quadrangle occupies three major geographic areas that may each be split into detailed locations and geographic features (**Fig. 2**). The Guadalupe Mountains, Delaware Basin, and Brokeoff Mountains define the geography of this area. The Brokeoff Mountains are part of the Rio Grande rift physiographic province and exhibit extensional tectonic features, creating a low-elevation area with elongate, north-northwest-oriented mountains and valleys. The Guadalupe Mountains create highlands formed by compressional tectonics that contain broad dip slopes, forested hills, deep canyons, and wide valleys. The Delaware Basin is mainly a result of deep marine deposition and the dissolution of salts; it is dominated by broad gypsum flats, the Pecos River valley, human development, and sand-covered plains.

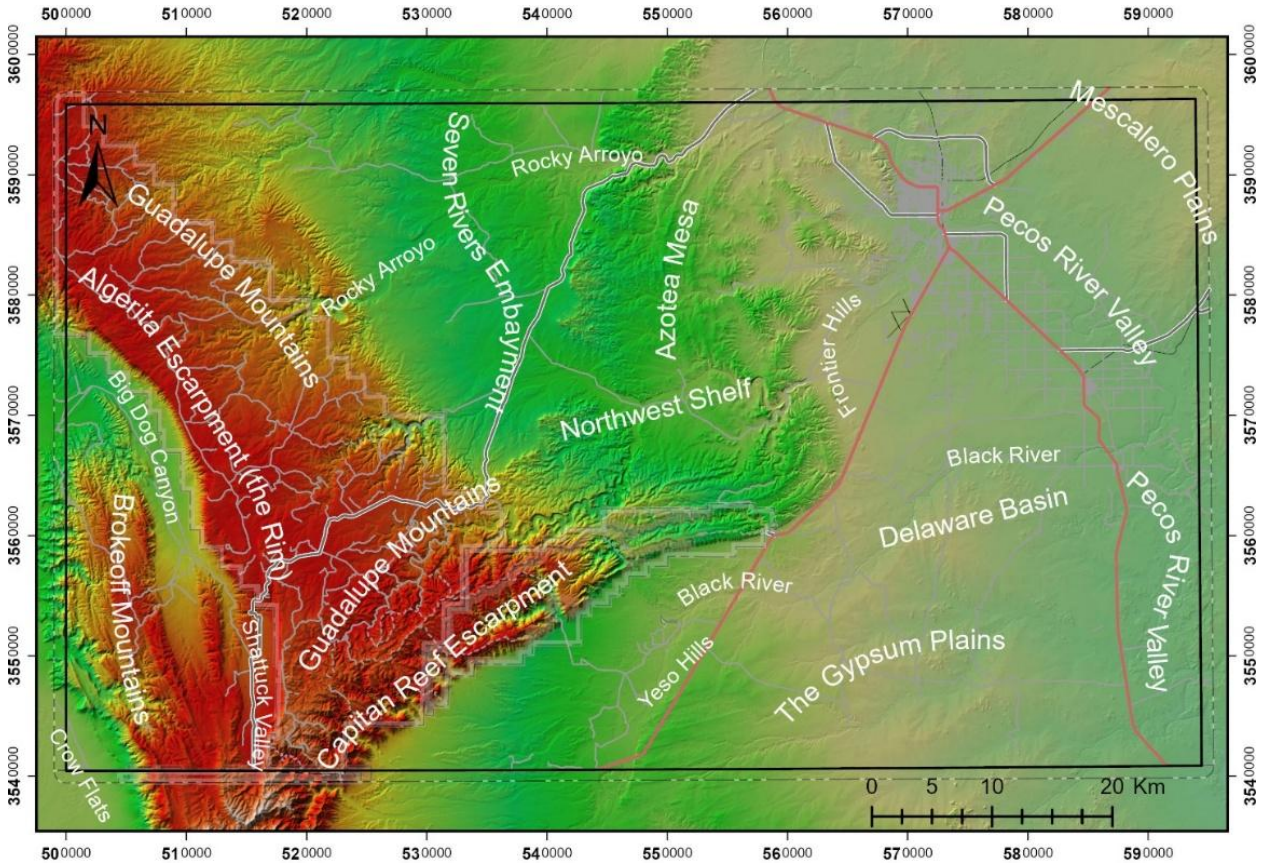

Figure 2: Geographic setting and shaded relief within the Carlsbad 30x60-minute quadrangle.

The Brokeoff Mountains are primarily federal lands managed by the Bureau of Land Management (BLM); there are also a few parcels managed by the State of New Mexico and private land in the vicinity of Shattuck Valley. Within the Brokeoff Mountains, the major geographic features are the Brokeoff Mountains, Big Dog Canyon, Shattuck Valley, Algerita Escarpment (the Rim), and Crow Flats. The Brokeoff Mountains are partly contained within the Brokeoff Mountains Wilderness Study Area managed by the BLM. Big Dog Canyon runs

alongside the Algerita Escarpment (**Fig. 1**) and is occupied by coalesced fan systems that dominantly exhibit aggradation, creating a smooth landscape with low amounts of incision. Crow Flats is part of the Salt Basin and has internally drained playa lakes and lacustrine sediments that are part of the Alkali Lakes Area of Critical Environmental Concern. The bedrock geology of the Brokeoff Mountains is dominated by the Guadalupian and Cisuralian shelf and shelf-margin deposits, including the Victorio Peak Limestone, Cutoff Formation, Glorieta Sandstone, Yeso Formation, and the tongue of the Cherry Canyon Formation, which have little to no exposure elsewhere on the map. These mountains are part of the Rio Grande Rift and are hydrologically connected to the Salt Basin (Kelley et al., 2020; Timmons and Sturgis, 2022).

Lands within the Guadalupe Mountains are managed by the United States Forest Service (USFS), BLM, National Park Service (NPS), State of New Mexico, and private landowners. This includes the Lincoln National Forest along the northwestern-trending branch of the mountains, as well as the BLM-managed Lonesome Ridge and Guadalupe Escarpment Wilderness Study Areas along the Capitan Reef Escarpment in the northeastern-trending branch of the mountains. Farther to the northeast is Carlsbad Caverns National Park, including the Carlsbad Caverns Wilderness Area and Mudgett's Wilderness Study Area along the park's northern boundary. BLM and state lands are concentrated in the Seven Rivers Embayment and in the lower-elevation portions of the mountains, around Azotea Mesa, in the north-central portion of this quadrangle. The broad dip slopes of San Andres Formation and Artesia Group shelf deposits, east of the Algerita Escarpment, are occupied by rocky forests and open grassy meadows; deep canyons (e.g., Rocky Arroyo) are cut as arroyos approach the Seven Rivers Embayment. Along the Capitan Reef Escarpment, the mountains are high relief, with open forests, shrub-covered hillslopes, high mesas, and deep valleys cutting down to the Delaware Basin. The Seven Rivers Embayment is open, vegetated with grasses and shrubbery, cut by numerous arroyos, and dotted with sinkhole depressions. Azotea Mesa is less forested, and relief and elevation decrease in this area. The mountains represent the ancient shallow marine northwest shelf of the Delaware Basin.

Figure 3: View across the Black River valley of the Guadalupe Mountains from the Gypsum Plains.

The Delaware Basin includes the Pecos River valley, Gypsum Plain, Mescalero Plains, and other geographic features that create a unique geologic story on this landscape. These lowlands are home to the City of Carlsbad and other smaller towns that support the potash, oil and gas, and agricultural industries in this region. The land is primarily managed by the BLM and State of New Mexico or owned by private citizens; however, there are parcels managed by the United States Fish and Wildlife Service (USFWS) and United States Bureau of Reclamation (USBR). Within the quadrangle, there are the Living Desert Zoo and Gardens State Park, managed by the New Mexico State Parks Division, and the Carlsbad Wildlife Refuge, managed by the USFWS and USBR. A small portion of Carlsbad Caverns National Park is present in the basin at Rattlesnake Springs west of the Black River valley. The BLM also manages the Chosa Draw Area of Critical Environmental Concern within this area. The Delaware Basin is occupied by outcroppings of Quaternary surficial cover, Cenozoic fluvial deposits, and Lopingian-Guadalupian marine basin sediments. The Gypsum Plain (**Figs. 2–4**) is a broad, low-relief highland of Lopingian marine evaporites that are intruded by the only igneous rocks in the map area at the Yeso Hills. To the west of the Gypsum Plain is the Black River valley and the piedmont alluvium system below the Capitan Reef Escarpment. Small areas of higher relief are present in the foothills of the mountains such as the Frontier Hills. The Pecos River valley runs from north to south across the eastern portion of this quadrangle and has broad floodplains utilized for agriculture. The Mescalero Plains are formed by the erosion-resistant Mescalero paleosol and covered in sand fields sourced from sediments eroded in the adjacent river valley.

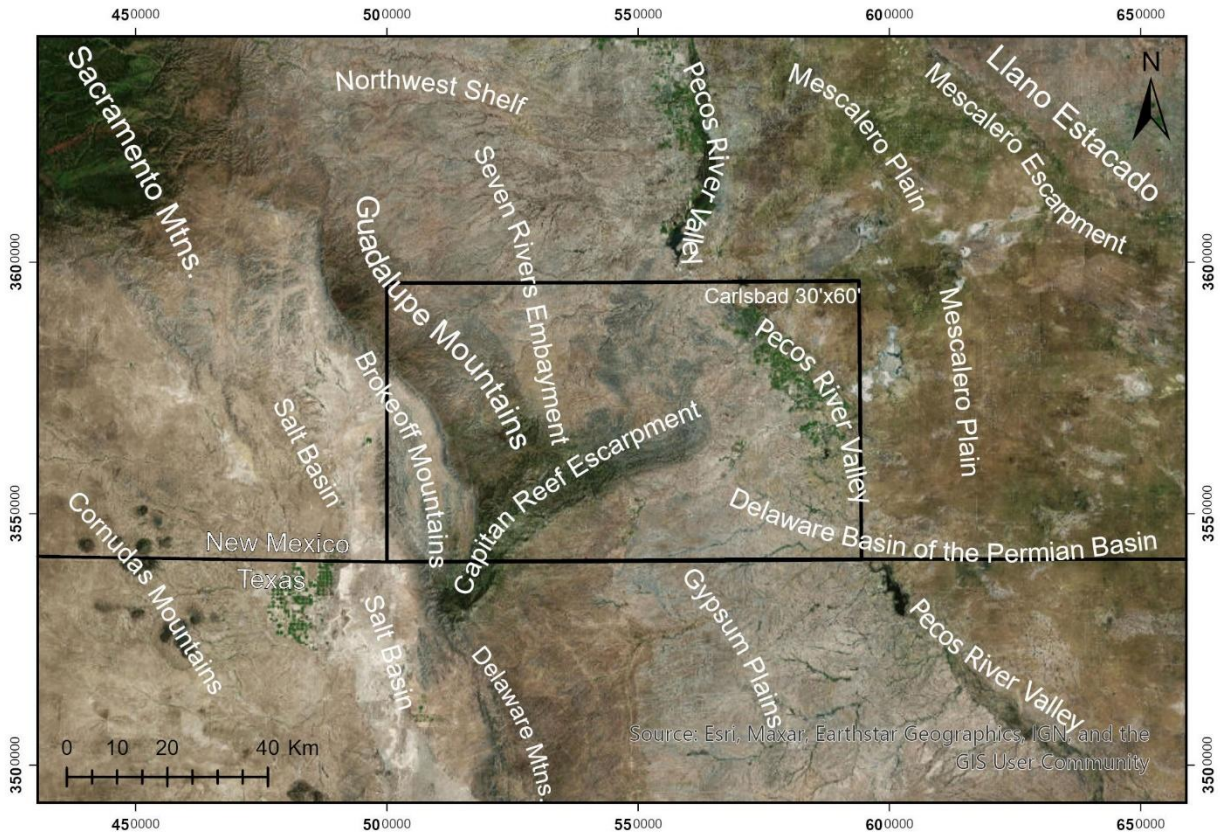

Figure 4: Regional geographic setting of the Carlsbad 30x60-minute quadrangle.

Within the larger region (**Fig. 4**), this quadrangle lies east of the Salt Basin and Cornudas Mountains, southeast of the Sacramento Mountains, north of the Delaware Mountains, and southwest of the Llano Estacado. This quadrangle includes portions of the Permian Basin, which encompasses the Delaware Basin. The geography of this quadrangle offers a good representation of regional geology because it incorporates aspects of all the adjacent features.

Cave and Karst Systems

Cave and karst systems dominate the geography of this quadrangle, evidenced by the presence of the National Cave and Karst Research Institute (NCKRI) and Carlsbad Caverns National Park. Additionally, caves and sinkholes in the Gypsum Plain, sinkhole depressions in the Seven Rivers Embayment, and salt dissolution modulating the history of the Pecos River valley are prevalent aspects of this landscape. This project does not focus on this aspect of the geology and only includes depression-fill and karst-collapse deposits as map units related to these systems. A dataset of cave entrances was mapped from lidar data but is not available to the public for safety and liability reasons. In and beneath the Guadalupe Mountains, cave systems have developed in the Capitan Formation and Artesia Group through sulfuric acid speleogenesis as water tables dropped synchronously with regional uplift in the late Cenozoic (Polyak et al., 1998, 2006, 2023). In the Gypsum Plain, caves are formed within the Castile Formation (**Fig. 5**). In the Seven Rivers Embayment, sinkhole depressions are found within the Queen Formation. Dissolution of Lopingian marine evaporites in the Delaware Basin is

responsible for collapses and subsidence of surface topography within the Gatuña Formation. This aspect of the landscape is discussed further in the geologic history section with field and literature investigations of the Gatuña Formation.

Figure 5: Sinkhole within the Castile Formation on the edge of the Gypsum Plain near the Yeso Hills dikes.

MOTIVATION

This project is guided by the objectives of the National Cooperative Geologic Mapping Program (NCGMP), which provided funding through the STATEMAP program to the Geologic Mapping Program within the New Mexico Bureau of Geology and Mineral Resources at the New Mexico Institute of Mining and Technology. The program aims to create surface (2D) and subsurface (3D) geologic mapping across the country to promote knowledge on critical minerals, energy resources, geologic hazards, water resources, land use, engineering and infrastructure, and environmental protection. Production of this map was recommended by the STATEMAP Advisory Committee.

This map synthesizes geologic mapping to the 1:100,000 scale across a 30x60-minute quadrangle that covers over 5,200 km², or around 1.29 million acres. This includes the charismatic Guadalupe Mountains, the desolate Brokeoff Mountains, and the economically important Delaware Basin. Industry practices and the large population of Carlsbad and other towns within the quadrangle necessitate geologic contexts for all motivating factors as they influence the safety of inhabitants, conservation of ecosystems, and development of local economies. The scale of this map is user-friendly and incorporates a large area, making it a useful map for professional or recreational consumers of this product.

METHODS

This section details the methods used to construct the Geologic Map of the Carlsbad 30x60-Minute Quadrangle (1:100,000 scale) by stepping through the digital compilation methods, geodatabase simplification, feature classes and fields, field methods, and previous works. The digital compilation methods include a brief overview of the work compiled, simplification of geodatabases, and digital mapping techniques. The geodatabase simplification methods explain the process that preceded the handoff of data from the cartography team to the field geologists. The feature classes and fields section details choices made regarding different map features in this quadrangle. Field methods include an explanation of resources used, objectives, and work completed in the field. The previous works section details the intricacies of the geologic maps previously mapped in this quadrangle and how they were incorporated in this product. A detailed breakdown of relations between surficial map units of various publications and the map units utilized in this compilation is provided in the appendix. Funding for this mapping effort began in September 2023, fieldwork was conducted from fall 2023 to spring 2025, and map products were completed during fall 2025.

Digital Compilation Methods

The Geologic Map of the Carlsbad 30x60-Minute Quadrangle (1:100,000 scale) represents over a century of geologic groundwork in the region that was compiled and added to by the authors of this study. An extensive history of oil and gas exploration, water resource investigations, cave and karst research, hazards work, and geologic mapping went into developing the bedrock and surficial framework of the units found in the map area. Regional small-scale maps (**Figs. 8 and 9**) at 1:125,000 to 1:187,500 scale (e.g., King, 1948; Hayes, 1964; Kelley, 1971; Bachman, 1980) were vital to the compilation because they established stratigraphic relations and major structures across broad areas, while localized intermediate- to large-scale maps at 1:24,000 to 1:62,500 scale (**Figs. 8 and 9**) provided details that allowed for modification of contacts, folds, and faults previously mapped at coarser scales. The previous works section of this report provides a deeper dive into existing maps and their use in this compilation.

The map production group at the New Mexico Bureau of Geology and Mineral Resources digitized all legacy geologic maps requested by the authors. These maps were processed with a Python code to smooth linework inappropriate for the 1:100,000 scale of this quadrangle. This code did not collapse small polygons or sharp shapes; rather, these sub-map-

scale features were highlighted for review by the authors. This process is detailed in the next section, simplification of geodatabases. Multiple geodatabases were provided to the authors: original digitized map data, smoothed (or simplified) map data, a database for drafts and compilation of simplified data, and a geodatabase for the map product itself. This mapping kit also included a geodatabase of geographical information for the map footprint and imagery, including orthoimages for stereophotogrammetric mapping, 4.5-m SPADTM digital elevation maps, and lidar imagery processed at 2-m resolution.

Between September 2023 and September 2024, efforts were focused on resolving known discrepancies in mapping and conducting new mapping of surficial Quaternary map units. Digitized legacy maps and smoothed line features were provided to authors in August 2024, at which point major digital mapping compilation efforts began. For a given area, the most detailed map data were chosen to be appended to the geodatabase. Mapping at 1:24,000 to 1:36,000 scale of 7.5- and 7.5x15-minute quadrangles covered a majority of the Delaware Basin and mountain front of the Guadalupe Mountains, while 1:62,000-scale maps captured the geology of the Brokeoff Mountains and a large portion of the interior of the Guadalupe Mountains. Large areas of the Seven Rivers Embayment, the northern Brokeoff Mountains, and the Guadalupe Mountains in the northwestern portion of the map area had not been mapped at intermediate to large scales and were compiled from small-scale regional maps. Additional linework and detail to existing contacts helped fit that mapping to the map scale of this publication throughout the mapping effort.

Areas with no detailed mapping are largely shallowly dipping, with limited contacts and structures. The northern Brokeoff Mountains offered more complexity; however, new mapping and field checking were limited by time constraints and the remote location of that area. Quaternary map units were not a priority of the existing regional, small-scale maps covering these areas, so work was completed to improve the detail of the dominantly alluvial (i.e., active channel, terraces, piedmont surfaces, fans) history in this area. The Indian Flats 7.5-minute quadrangle in the northeastern corner of the map area had also only been mapped as detailed as 1:187,500 scale by Kelley (1971), so new mapping at 1:100,000 scale was completed by the authors of this map.

Where coverage of intermediate- to large-scale mapping exists, maps were appended to the database starting from the southwest, in the Brokeoff Mountains, and working eastward and northward along the reef escarpment of the Guadalupe Mountains. As the appropriate scale was reached in these areas, quadrangles covering the Delaware Basin and Pecos River valley were appended and simplified. Quaternary map unit labels were adjusted using the field calculator in the attribute table of each feature class in ArcGIS Pro to fit the correlation of map units established for the Cenozoic in this study (see previous works and appendix). This correlation fits surficial deposits of shared origin but differing map-unit names from publication to publication into a single unified map unit schema. Any polygon at sub-map scale was either deleted or fit into a neighboring polygon if it was vital to the geologic understanding of the area. Polygons with “pinch points” below the map scale were either split or trimmed down to the portion that could be presented at 1:100,000 scale. For example, a polygon representing an alluvial channel that thins to less than around 150 m wide but widens in either direction would

be split into two polygons, while a thin alluvial channel that narrows at the head of its drainage would be reshaped so it was wide enough to be displayed on the map.

When compiling this quadrangle from existing data and new linework from fieldwork and digital mapping, the authors of this publication utilized field observations, lidar hillshade maps, satellite imagery, shaded-relief maps, topographic maps, photogrammetric imagery, and slope-aspect maps as primary tools. Lidar hillshade maps allowed for detailed analysis of landforms and textures within surficial deposits, identification of faults, and tracing of beds at the contact of bedrock units. Profiles derived from elevation imagery allowed for analysis of terrace heights above the grade of modern arroyo channels, which was a useful tool in distinguishing many surficial units. Satellite imagery was similarly useful because it allowed for the incorporation of colors to better distinguish features observed in elevation imagery. Stereophotogrammetric imagery was not heavily relied on for this project but was a useful tool that allowed for 3D viewing of the land surface. Shaded-relief and slope-aspect maps are derivatives of elevation imagery that provided additional details on the landscape (e.g., landforms mapped as fan alluvium had higher slopes than those mapped as piedmont alluvium). Mapping methods from the field are discussed in the field methods section, and observations from the authors of this publication in concert with observations from past mappers are detailed intermittently in the structure and stratigraphy sections as well as in the description of map units in the appendix.

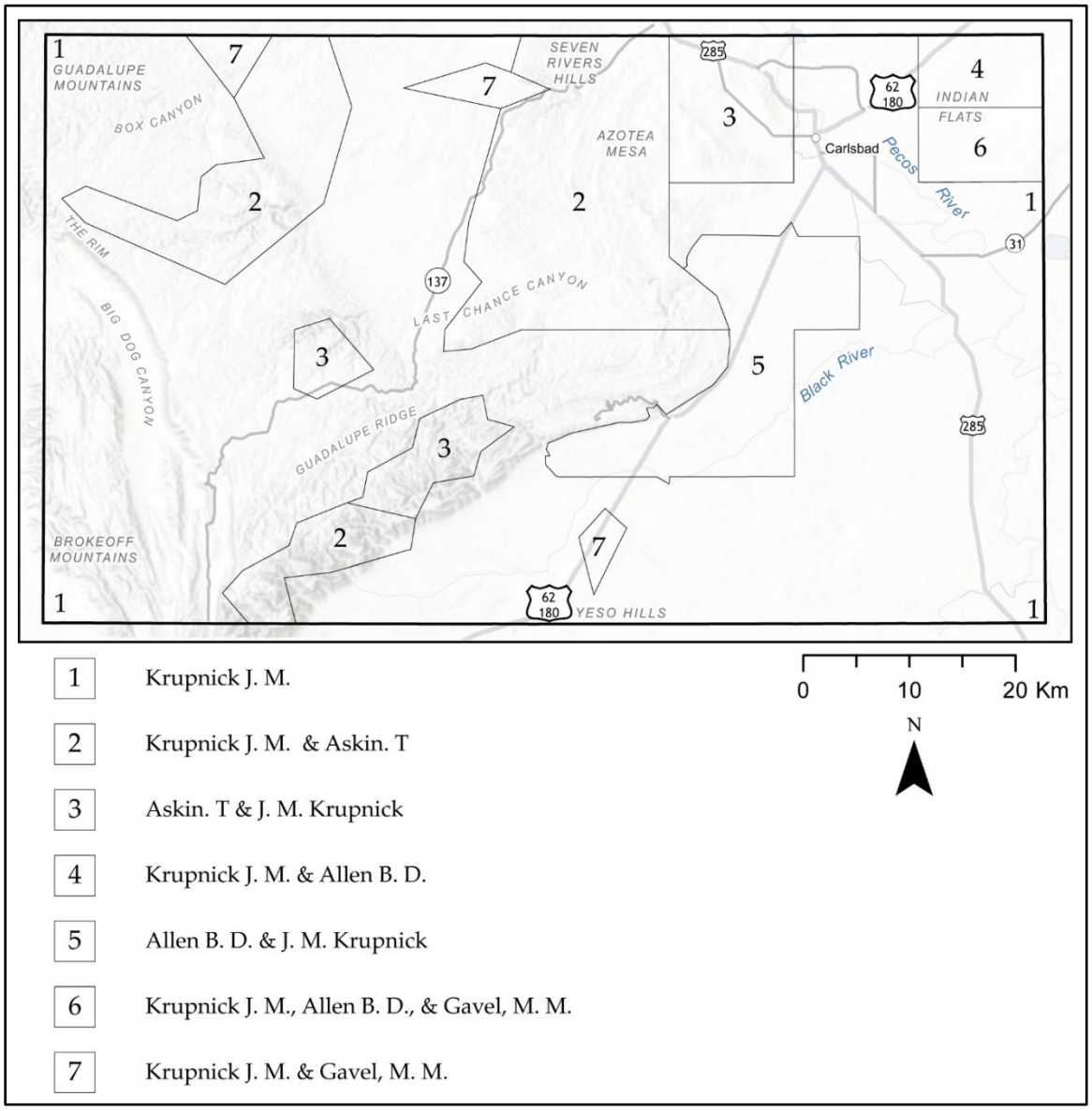

Figure 6: Contributions from authors of this map and report based on waypoint locations and data source identification of lines and points within the published map data.

Field mapper contributions to this product are displayed in Figure 6. This figure does not distinguish where field or computer methods were used; map users are encouraged to check the LocationSourceID fields in the attribute table of the map package data, especially the ContactsAndFaults feature class, for detail on where field methods were utilized. Note that Allen mapped several of the detailed quadrangles within the Delaware Basin area, but compilation efforts of that mapping were largely limited to Krupnick where symbolized.

Simplification of Geodatabases

Data from the original publications were simplified for the purpose of generalizing and compiling data from map scales as fine as 1:24,000 to build a 1:100,000-scale compilation map.

ContactsAndFaults feature classes from the original open-file geologic maps (OFGMs) GeMS (Geologic Map Schema) databases were modified using the Simplify Line tool using the Wang-Mülller simplification algorithm with a tolerance value of 110–180 m. The Retain Critical Bends (Wang-Müller) (algorithm='BEND_SIMPLIFY' in Python) algorithm applies shape recognition techniques that detect bends, analyze their characteristics, and eliminate insignificant ones. Points within the MapUnitPolysLabels feature class were repositioned to fix topological errors, and new polygons for the MapUnitPolys feature class were generated to reflect the changes of the simplified linework. Polygons with areas less than 13,000 m^2 and "pinch points" smaller than 80 m (threshold considered too small at 1:24,000 map scale) were flagged for deletion. Polygons with areas less than 39,000 m^2 and "pinch points" smaller than 330 m (threshold considered too small at 1:100,000 map scale) were flagged for review. These are cartographic thresholds that align with map-scale special accuracies, and some of these can be determined with general formulas.

Currently, GIS Services considers two general thresholds for determining if (1) polygons and (2) "pinch-points" are too small to display at this map scale. The polygon threshold is:

$$A = \pi ((2.228 \text{ mm} \times 100{,}000 / 1{,}000) / 2)^2$$

Where A is the minimum area of a polygon in square meters that can be displayed at a given map scale, 100,000 is the map scale, 1,000 is the conversion from millimeters to meters, and 2.228 is the minimum diameter of a polygon, in millimeters, that can be displayed *reasonably* on a printed layout.

Polygons with "pinch points" that are too narrow to display at the new map scale were selected using the Identify Narrow Polygon geoprocessing tool. The threshold size that was determined to be a "pinch point" too narrow to display at this map's scale is calculated by the following formulas:

$$3.3 \text{ mm} \times 100{,}000 / 1{,}000$$

$$3.3 \text{ mm} \times 24{,}000 / 1{,}000$$

Where 3.3 mm is the threshold of what can *reasonably* be displayed on a printed layout (large enough for a polygon color to be displayed to the eye with contact lines and a labelling leader), 100,000 is the map scale, and 1,000 is the conversion from millimeters to meters.

Attribute Table Fields

While most readers of this publication will review either the map or this report to understand how the authors made decisions in building such a major compilation project, the nuance of how information was compiled and represented is stored in the feature classes of the map's accompanying geodatabase. This section is not intended to elaborate on the usage of each field within feature classes or the NMBGMR GeMS database. This section explains how the database's schema was applied to this project. Anyone curious about those details should

consult the accompanying geodatabase's metadata or refer to the GeMS manual published by the USGS.

MapUnit, Label, and Symbol

The '+' modifier for combining units is only used to combine bedrock and surficial units into one polygon rather than two bedrock units. The exception to this is the combined Neogene and Permian units (e.g., **Pr+QNg**); however, the nature of Neogene units is largely surficial, and the span of time elapsed by the unconformity between the Permian units and Neogene units causes the use of the modifier to be essentially the same as between a Quaternary surficial unit and Permian bedrock unit. In the bedrock units, authors elected to create distinct, undivided map units for areas where polygons of one map unit drawn at an appropriate scale contain considerable outcrops of the underlying, or overlying stratigraphy (e.g., **Pag** and overlying **Paq** as **Pagq** rather than **Pag+Paq**).

IdentityConfidence and ExistenceConfidence

Map users are urged to consult the compiled large-scale maps (1:24,000, 1:36,000, or 1:62,500) for a detailed understanding of uncertainty within contacts. The use of queried contacts varied widely among publications involved in this compilation and would have resulted in a lack of unity and consistency across the map if the original queried symbols were used. Areas with queried contacts were targeted for fieldwork, and many are believed to have been resolved.

DataSourceID and LocationSourceID

DataSourceID and LocationSourceID are fields located in each feature class of map data within the Carlsbad 30x60-minute quadrangle geodatabase. As data were appended to the geodatabase of this project from the simplified geology geodatabase previously mentioned in Digital Compilation Methods, these fields were filled with data sources of the corresponding publication. For example, when first loaded into this project's geodatabase, data from the El Paso Gap 15-minute quadrangle (OFGM-315) would have DSOFGM315 in the DataSourceID field and LSOFGM315 in the LocationSourceID field. Line features and points that were not altered in any way by the authors of this publication retain their original DataSourceID and LocationSourceID values. Lines edited by the authors typically retain their original LocationSourceID and adopt the DataSourceID of the editing author because the general location of the feature was identified by the original publication, but the data no longer reflects that of the original publication. If the line was changed beyond recognition of the original data, then both fields are changed to correspond to the editing author. Long line segments that were only edited in part may have DataSourceID or LocationSourceID corresponding to this publication despite being largely representative of the original data. Efforts were made to split such lines and attribute these fields correctly; however, users are encouraged to compare the linework of this publication to that of the original, compiled data to verify the data source and location source of line and point features of interest.

Field Methods

Fieldwork was conducted during 4- to 5-day field excursions from fall 2023 through spring 2025 (**Fig. 7**). An estimated 10 weeks of fieldwork were completed between all contributing authors for work directly related to this publication (i.e., excluding fieldwork on prior quadrangles from authors on this quadrangle). Fieldwork targeted areas with limited detailed mapping and areas within detailed mapping where there were discrepancies between maps.

Figure 7: Walking a section of the Artesia Group above Slaughter Canyon previously measured by Hayes (1964).

The authors utilized mostly traditional field mapping techniques, including the use of paper maps on map boards, hand lenses, grain-size cards, hydrochloric acid, Munsell Color Charts, rock hammers, Brunton compasses, notes in field notebooks, and boots on the ground. Rather than traditional topographic maps, the authors mostly utilized printed layouts from

ArcGIS Pro that included existing linework, waypoints, roads, and topographic lines overlaid onto a lidar hillshade. In areas with existing mapping, authors regularly used those maps to identify bedrock units and gather observations to establish the schema for surficial map units in this publication.

Cross Section Construction Methods

The geologic cross section (A-A') for the Geologic Map of the Carlsbad 30x60-minute Quadrangle (1:100,000 scale) uses kink-band folding and shares attributes with fault-propagation fold geometries but does not include the rigor of the Suppe and Medwedeff (1990) geometric analysis. Geologic constraints from surface data and well logs caused the cross section to deviate from ideal model geometry. A line in the CartographicLines feature class was drawn parallel to tectonic transport, perpendicular to the strike of geologic structures, and to include as much of the bedrock geologic history as possible. This line is 94.45 km long, equivalent to the width of the map. It trends east-northeast across the Brokeoff Mountains, over the Algerita Escarpment (the Rim), down dip slopes in the central Guadalupe Mountains, across the Seven Rivers Embayment, and through Artesia Group strata before turning east-southeast over the buried Capitan Reef and into the Delaware Basin on the eastern side of the map.

API	Distance from CSX (Km)	Total Depth (m)	Latitude	Longitude
30-035-20007	6.54	1390	32.131783	-104.9366
30-035-00018	12.99	972	32.3012	-104.99369
30-015-00003	1.39	1888	32.23079	-104.7528
30-015-20752	0.66	1872	32.2487	-104.71216
30-015-00015	0.34	1067	32.2558	-104.69719
30-015-22022	1.93	2331	32.279411	-104.689781
30-015-00014	0.04	3850	32.26281	-104.68157
30-015-00013	2.67	3835	32.28943	-104.67842
30-015-22740	0.77	3100	32.28724	-104.62031
30-015-23103	1.00	3284	32.27287	-104.61124
30-015-00041	4.70	3661	32.338268	-104.568932
30-015-00044	0.01	3737	32.298613	-104.551612
30-015-21620	1.62	3300	32.33092	-104.48829
30-015-05913	0.24	3510	32.316734	-104.475578
30-015-20095	0.41	3416	32.324556	-104.440594
30-015-10560	2.06	3357	32.358414	-104.401939
30-015-00135	1.26	3746	32.365162	-104.348129
30-015-31529	3.97	3582	32.308853	-104.322182
30-015-20808	4.74	3645	32.287994	-104.283272
30-015-01112	2.05	656	32.321464	-104.188751
30-015-21599	0.49	3766	32.303337	-104.180244
30-015-23340	0.15	3886	32.277874	-104.116081
30-015-21786	2.91	3912	32.230282	-104.064819
30-015-23779	0.99	2627	32.241489	-104.043144

Table 1: Well logs used for geologic cross-section reconstruction in order from west (A) to east (A'). CSX – cross section. API number – American Petroleum Institute number.

An elevation profile was extracted from 4.5-m SPADTM data with 3x vertical exaggeration to a depth of 3048 m (10,0000 ft) below sea level along the cartographic line (A-A') and features the projected location of apparent dip indicators, contacts, faults, and folds. Bedding orientations within 3 km of the cross-section line were incorporated. Bedding and fault orientations were adjusted to match vertical exaggeration and apparent dip based on the obliquity between their strike direction's intersection with the cross-section line. This reconstruction utilizes well logs from 24 boreholes (**Table 1**) chosen based on proximity to the cross-section line and relevance of the data to the needs of the cross section. Surface geologic constraints were also used to constrain geometries at depth. Wells were projected to their total depth (T.D.) along the cross section at their actual elevation, rather than the elevation of the cross-section profile. Formation tops identified during the original logging of wells were used as constraints for cross-section geometries; the bibliography includes references of all well-log interpretations utilized. Faults were projected from their outcrop location to depth based on generalized fault dips because field constraints on fault orientations were not available. In the Delaware Basin and mountain front, depths of formation tops were checked against the 3D subsurface model of Lavery et al. (2024). Irregularities in contacts drawn between wells were smoothed out by interpolating the contacts based on distance from wells and perceived inconsistencies in picks within well logs. Contacts at the surface were projected at depth based on known structures and available dip ticks. Finally, lateral gradations between units were approximated based on picks at depth.

An absence of formation-top picks was noticeable through much of the Guadalupian strata (Artesia Group, Delaware Mountain Group, and Capitan Formation), Lopingian (Ochoan) strata, Cisuralian strata (San Andres Formation, Cutoff Formation, and Victorio Peak Formation), and early Paleozoic sediments (Ordovician and older). Within the Guadalupian strata, the top of the Delaware Mountain Group was typically the only unit logged. The Lopingian strata did not have formation tops, but records of halite presence in the well logs proved useful for distinguishing the Rustler Formation from the undivided Castile and Salado Formations map units. Logs commonly included picks for the Yeso, Abo, Hueco, Bone Spring, and Wolfcamp Formations in the Cisuralian strata, but San Andres, Victorio Peak, and Cutoff Formations picks were largely absent. The authors believe this is both a product of the loggers' objectives and nomenclature changes. Most wells stopped within the Pennsylvanian or Mississippian, but a few extended into the Ordovician, Cambrian-Ordovician, and Mesoproterozoic (Ectasian) basement rock. Time limitations prevented the authors from sourcing data from additional wells or refining picks from downhole geophysics logs.

Where surface and subsurface constraints were absent, contacts were interpreted based on available stratigraphic thickness estimates and the nature of lateral gradations from the literature (King, 1948; Boyd, 1958; Hayes, 1964). In these areas, the cross section should be considered schematic of stratigraphic relations. The same units that are largely absent from well logs experience drastic facies changes in a direction oblique to that of the cross-section transect. This likely results in discontinuities in some strata, and we therefore consider these aspects of the cross section to be schematic.

On the hanging wall of the blind thrust fault beneath the Huapache monocline, repeated stratigraphy was observed in well log 30-015-00014 throughout the early Paleozoic units, while thinning was observed in Pennsylvanian strata. This well did not indicate offset in units younger than Pennsylvanian, nor was there repeated stratigraphy in well 30-015-00013 that penetrated to the basement of the fault's foot wall. In agreement with past literature (e.g., Hayes, 1964), we hypothesize that thickening of Pennsylvanian units is indicative of growth strata. The repeated strata in well 30-015-00014 were in sequence and therefore not interpreted to have overturned, but instead, offset by a relatively high-angle thrust fault. Beds of Ordovician age on the hanging wall had greatly increased thickness in the well log, which we interpret to indicate an oblique intersection of those strata with the well due to steeply dipping beds. This well penetrated the Bliss Formation, while the adjacent well on the footwall intersected basement. The observed thickness of the Cambrian-Ordovician Bliss Formation is assumed to be the thickness observed in that well across the entirety of the cross section, despite possible fluctuations or truncation in some areas.

Between wells 30-015-00015 and 30-015-22022 on the hanging wall of the blind thrust, the projected formation tops had apparent offset of a back thrust, where formation tops in the more easterly well (30-015-22022) were a couple hundred meters higher than those of 30-015-00015. However, the authors chose to interpret that offset as a product of the wells' distance from the cross-section line. This decision was made because the picks from 30-015-00015 are proximal to the cross-section line, while 30-015-22022 is nearly 2 km away, which, when formation top locations are projected, could produce a false indication of a back-thrust structure. Possibilities for alternative interpretations of the subsurface stratigraphy and structures are endless, and this cross section represents one interpretation by the authors based on the surface and subsurface data available.

Uncertainties

A primary source of uncertainty is the difficulty in consistently aligning the cross-section line parallel to the direction of tectonic transport. Though generally parallel to the trends of structures and bedding, there are some locations where deviations from the dip direction of bedding plane measurements and mapped fault trends are considerable. This likely results in material transport in and out of the cross-section plane, violating assumptions of plane strain if efforts to reconstruct this cross section to a pre-deformation state were made. Bedding-parallel slickenlines were observed in the direction of tectonic transport within the San Andres Formation stratigraphy along the Algerita Escarpment. Stylolites, cleavage within ledge-forming carbonate beds, and the presence of evaporite beds and shales in the subsurface could all affect the deformation observed and the ability to reconstruct this cross section, primarily through volume loss out of the cross-section plane.

A further concern is the obliquity of the cross section to gradational back-shelf to reef and basin facies. In the transition from the Yeso and San Andres Formations (shelf) to the Victorio Peak Limestone (shelf-margin reef) and Bone Spring Formation (basin), the transect trends east-northeast, while facies gradation occurs in sediments trending south-southeast. This observation suggests variable thickness of these units in the subsurface that may be an artifact

of real or apparent paleotopography; however, this could also be the result of differing opinions and nomenclature changes recorded in well logs throughout the several decades of well data used in this study. Due to data and time constraints, the lateral gradations of these units were drafted to an idealized representation of the stratigraphy.

Estimates of shortening

Estimates of shortening are provided based on the entire width of the cross section, compressional deformation east of the Brokeoff Mountains, and extension west of the Huapache monocline.

Estimate of net shortening

Line length at the base of Wolfcamp/Hueco across the extent of the cross section:

L_0 = Initial length (sum of line lengths) = 95.65 km
L_f = Final length of section from A to A' = 94.45 km

$$e = (L_f - L_0)/L_0$$
$$e = (94.45\text{-}95.65)/95.65 = -0.0125$$
$$e \times 100\% = \underline{\%\ \text{shortening}}$$
$$-0.0125 \times 100\% = \underline{-1.25\%\ \text{shortening}}$$

Estimate of shortening isolated to area east of rift extension

Line length at the base of the Wolfcamp/Hueco across the extent of the cross section east of 30-015-00003:

L_0 = Initial length based on summed line lengths east of 30-015-00003 = 74.19 km
L_f = Final length of section from 30-015-00003 to A' = 72.94 km

$$e = (L_f - L_0)/L_0$$
$$e = (72.94\text{-}74.19)/74.19 = -0.0168$$
$$e \times 100\% = \underline{\%\ \text{shortening}}$$
$$-0.0168 \times 100\% = \underline{-1.68\%\ \text{shortening}}$$

Line length of the top of the Mississippian across the extent of the cross section east of 30-015-00003 to where Mississippian exits the cross-section plane:

L_0 = Initial length based on summed line lengths east of 30-015-00003 = 59.07 km
L_f = Final length of section from 30-015-00003 to A' = 56.95 km

$$e = (L_f - L_0)/L_0$$
$$e = (56.95\text{-}59.07)/59.07 = -0.0359$$
$$e \times 100\% = \underline{\%\ \text{shortening}}$$
$$-0.0359 \times 100\% = \underline{-3.59\%\ \text{shortening}}$$

Estimate of lengthening isolated to area west of Huapache monocline

Line length at the base of Wolfcamp/Hueco across the extent of the cross section west of 30-015-00003:

L_0 = Initial length based on summed line lengths west of 30-015-00003 = 21.46 km
L_f = Final length of section from A to 30-015-00003 = 21.51 km

$$e = (L_f - L_0)/L_0$$
$$e = (21.51\text{-}21.46)/21.46 = 0.00233$$
$$e \times 100\% = \underline{\%\ \text{elongation}}$$
$$0.00233 \times 100\% = \underline{0.233\%\ \text{elongation}}$$

Line length of the top of the Mississippian across the extent of the cross section west of 30-015-00003:

L_0 = Initial length based on summed line lengths west of 30-015-00003 = 21.58 km
L_f = Final length of section from A to 30-015-00003 = 21.51 km

$$e = (L_f - L_0)/L_0$$
$$e = (21.51\text{-}21.58)/21.58 = -0.00324$$
$$e \times 100\% = \underline{\%\ \text{shortening}}$$
$$0.00324 \times 100\% = \underline{-0.324\%\ \text{shortening}}$$

PREVIOUS WORKS

The Geologic Map of the Carlsbad 30x60-Minute Quadrangle (1:100,000 scale) utilized geologic mapping (**Figs. 8 and 9**) from nineteen 7.5-minute maps at 1:24,000 scale, one 15x7.5-minute map at 1:36,000 scale, and six 15-minute maps at 1:62,500 scale. Maps along the border that do not overlap with the map area of the present report include four 7.5-minute maps and one 15-minute map. Maps at other scales or dimensions (**Figs. 8 and 9**) include one 1:24,000-scale map, one 1:48,000-scale map, one 1:62,500-scale map, one 1:125,000-scale map, one 1:150,000-scale map, and one 1:187,500-scale map. Maps of unspecified scale (**Fig. 9**) from Bjorklund and Motts (1959) were consulted during this project. Additionally, the Hobbs Sheet (Barnes et al., 1976) at 1:250,000 scale borders the eastern edge of this quadrangle and was consulted for edge matching of contacts. Other geologic maps at various scales exist in and border this quadrangle that were not consulted or utilized for the compilation. Finally, geologic maps exist distal to the quadrangle that are not discussed here but were utilized to help develop the Quaternary map unit schema in this quadrangle; these quadrangles are referenced when relevant.

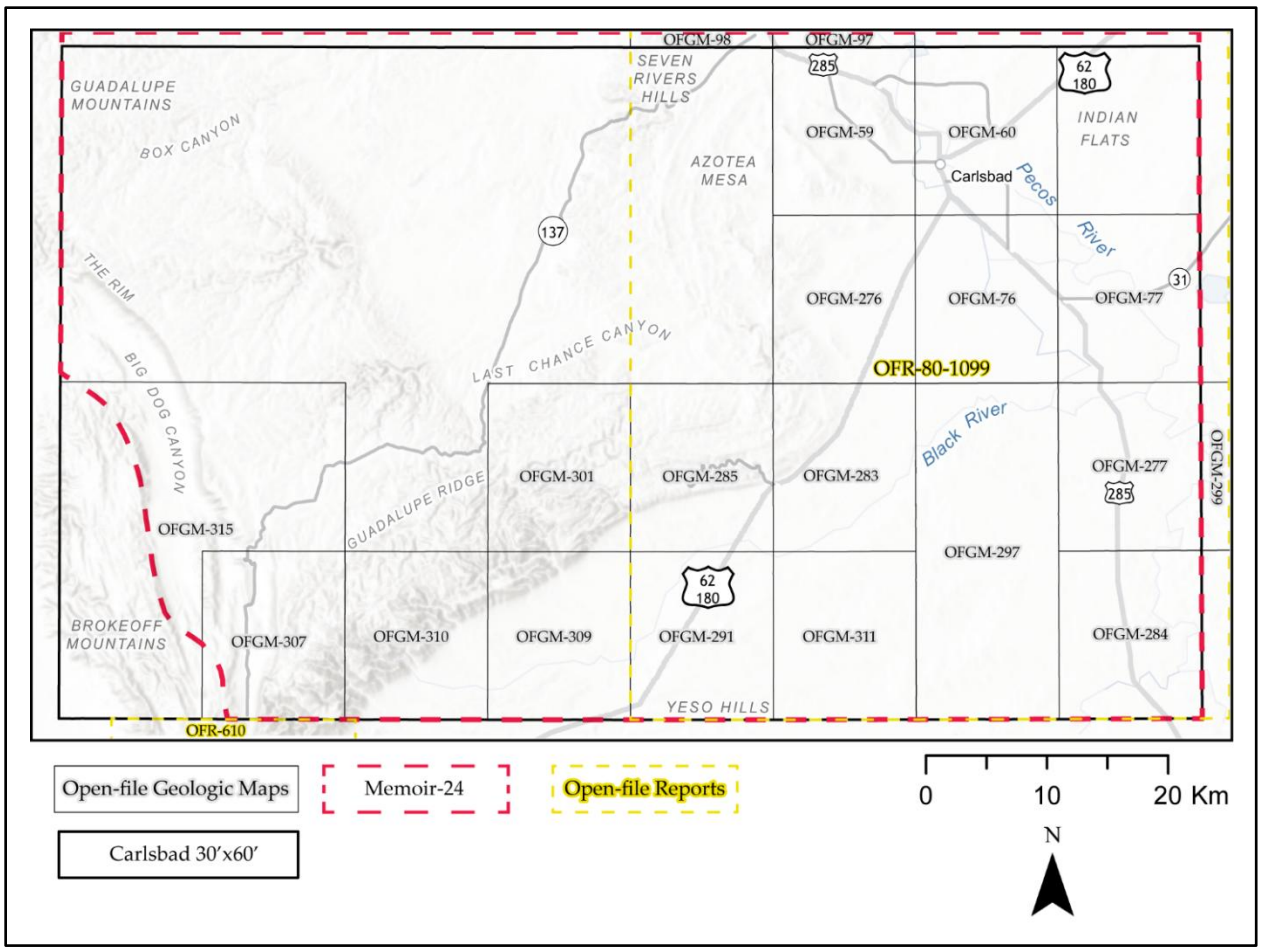

Figure 8: Index of geologic mapping for Open-File Geologic Maps, Memoirs, and Open-File Reports. These are all products of the New Mexico Bureau of Geology and Mineral Resources.

Recent Open-File Geologic Maps (OFGMs) from the New Mexico Bureau of Geology and Mineral Resources (NMBGMR) were the primary source of compiled data for this project; these include fifteen 7.5-minute geologic maps at 1:24,000 scale within the quadrangle. Locations of Open-file Geologic Maps, Memoirs, and Open-file Reports are shown in Figure 8. This includes, from southwest working east and north, the geologic maps of the El Paso Gap (OFGM-307), Gunsight Canyon (OFGM-310), Grapevine Draw (OFGM-309), Serpentine Bends (OFGM-301), Rattlesnake Springs (OFGM-291), Carlsbad Caverns (OFGM-285), Jumping Springs (OFGM-311), Black River Village (OFGM-283), Kitchen Cove (OFGM-276), Carlsbad West (OFGM-59), Otis (OFGM-76), Carlsbad East (OFGM-60), Red Bluff (OFGM-277), Malaga (OFGM-284), and Loving (OFGM-77). Five other geologic maps at 1:24,000 scale border the map, including three NMBGMR 7.5-minute quadrangles (geologic maps of Lake McMillian [OFGM-97], Seven Rivers [OFGM-98], and Pierce Canyon [OFGM-299]), one 7.5-minute United States Geological Survey (USGS) map (Geologic Map of the Cienega School Quadrangle [I-2630]), and the Geologic Map of the Guadalupe Mountains National Park (OFR-610) from NMBGMR. The Geologic Map of the Bond Draw and Cottonwood Hills 7.5-minute Quadrangles (OFGM-297) at 1:36,000 scale will also be discussed in this section.

OFGM-307 (Skotnicki, 2024a) was not heavily utilized in this publication because the same area was mapped in the El Paso Gap 15-minute quadrangle (OFGM-315; Skotnicki, 2024b) at a scale and extent more relevant to this compilation. OFGM-310 (Skotnicki and Allen, 2024), OFGM-309 (Allen and Skotnicki, 2024), OFGM-291 (Allen and Attia, 2021), OFGM-301 (Skotnicki and Attia, 2022), OFGM-285 (Skotnicki, 2021), OFGM-283 (Cikoski and Allen, 2020), and OFGM-276 (Cikoski, 2019a) were utilized to construct the schema for piedmont alluvium units and fan alluvium units along the reef escarpment. OFGM-310 contains the only outcrop of the Bell Canyon Formation in the quadrangle. The contact between the Yates and Tansill Formations was inconsistent between OFGM-310 and OFGM-309; the Carlsbad 30x60-minute quadrangle utilizes the contact of OFGM-309 because it agrees with other maps in the area. The contact between the Seven Rivers and Queen Formations in OFGM-301 was drawn too high in the section with a queried contact, causing the Queen to crop out farther east into Lechuguilla Canyon than what was revealed by field checking and computer methods in this study. OFGM-291 contains Paleogene intrusive deposits and karst-collapse deposits of Cretaceous strata, which are mapped in the MapUnitPoints feature class in this quadrangle. These karst-collapse deposits were also mapped in OFGM-311 (Allen, 2024) and found in OFGM-283 where they were not previously mapped. These deposits were also mapped in the northeastern portion of the quadrangle in OFR-80-1099 (Bachman, 1980); however, field checking of these deposits could not successfully identify them and they are thus not mapped. Additional karst-collapse deposits likely exist across this area that were not identified in this publication. Compilation efforts for the surficial map units of these quadrangles are detailed in the appendix, but it is important to mention that interpretations of age for the piedmont facies of the lower Gatuña Formation ranged from middle Quaternary to Miocene between these quadrangles.

OFGM-311, OFGM-291, OFGM-283, OFGM-297 (Allen and Attia, 2022), OFGM-284 (Cikoski, 2020), and OFGM-277 (Cikoski, 2019b) establish the stratigraphy and surficial units of the Gypsum Plain. There is good agreement among these maps between bedrock and surficial units. This area was extensively covered by loessal eolian deposits, sheetwash alluvium units, depression-fill deposits, and terrace deposits of Pecos River tributaries. OFGM-284 and OFGM-277, along with OFGM-77 (Pederson and Dehler, 2004b), OFGM-76 (Pederson and Dehler, 2004a), OFGM-59 (Dehler and Pederson, 2002), and OFGM-60 (Dehler and Pederson, 1998), establish the framework of the terrace units for this quadrangle and most of the Gatuña Formation polygons as well. These maps are supplemented with information from OFGM-97 (Dehler et al., 2005a) and OFGM-98 (Dehler et al., 2005b), which border this quadrangle to the north. Additionally, the map unit schema was informed by the Spring Lake 7.5-minute quadrangle (OFGM-214; McCraw et al., 2011), which is several quadrangles north of this map area's boundary. Mapping of the Gatuña Formation was also heavily informed by field checking within OFGM-299 (Attia and Allen, 2022) to the east of the quadrangle. I-2630 (O'Neill, 1998) is located west of the map in the southwestern corner, where it helped inform mapping of Crow Flats playa and lacustrine deposits. OFR-610 (Skotnicki and Knight, 2022) was utilized for its mapping of units that are only found within the subsurface or Brokeoff Mountains of the Carlsbad quadrangle. Some of these maps have intricate details (e.g., paleocurrent measurements) that were not included in this compilation because they were not consistently available on each map.

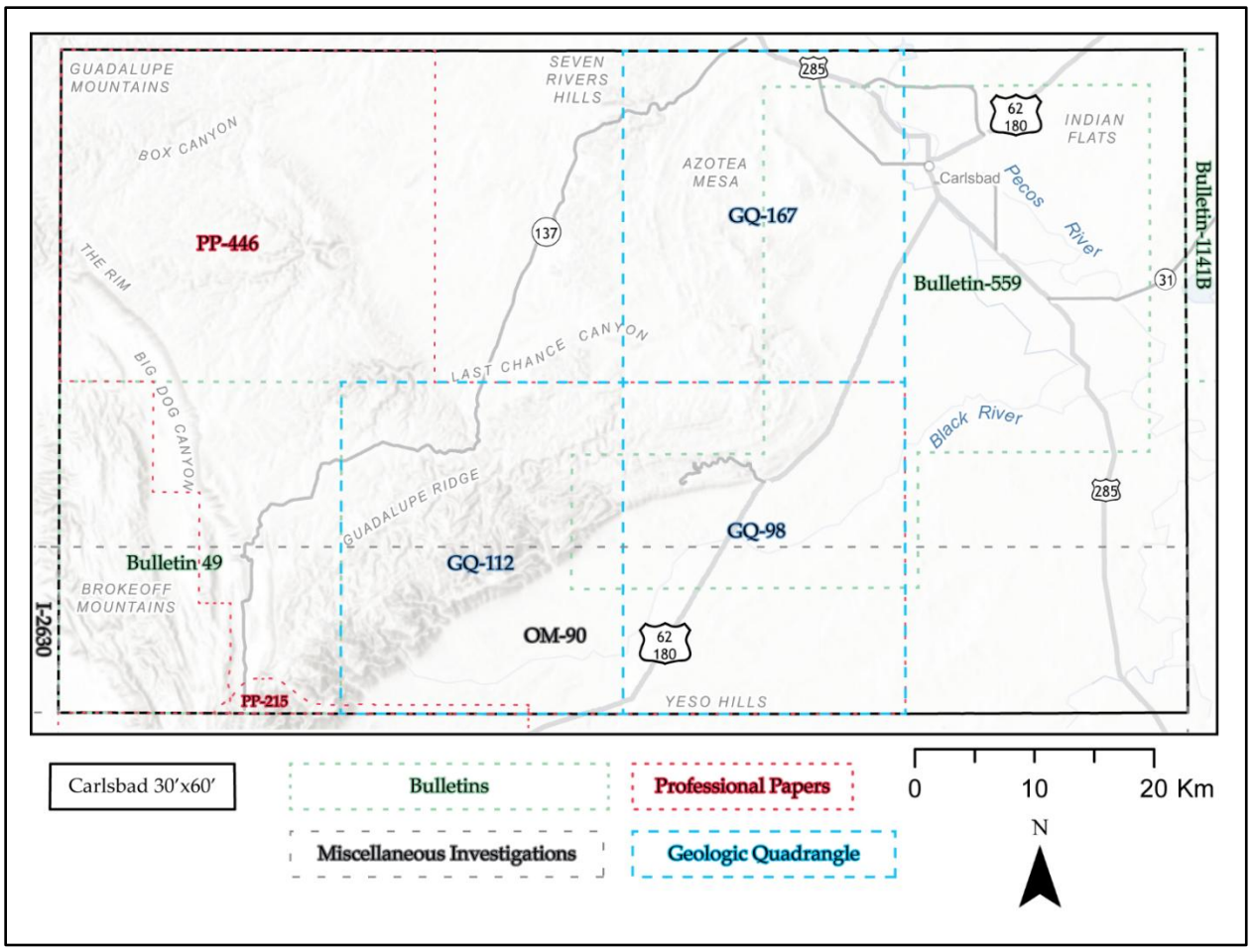

Figure 9: Index of geologic mapping for Bulletins, Professional Papers, Miscellaneous Investigations, and Geologic Quadrangles. These products are a mix of older NMBGMR and USGS publications.

In addition to the recently mapped 15-minute quadrangle (OFGM-315 at 1:62,500 scale), the Geology of the Carlsbad Caverns West Quadrangle (GQ-112; Hayes and Koogle, 1958), the Carlsbad Caverns East Quadrangle (GQ-98; Hayes, 1957), the West Carlsbad Quadrangle (GQ-167; Motts, 1962), the Geologic Map of the El Paso Gap Quadrangle (Bulletin-49; Boyd, 1958), and the Geologic Map and Section of the Nash Draw Quadrangle (Bulletin-1141B; Vine, 1963) were also utilized in this compilation. GQ-112, GQ-98, and GQ-167 are found overlapping the eastern mountain front of the Guadalupe Mountains and the piedmont alluvium deposited into the Delaware Basin. These maps were used primarily to check the logic of the 7.5-minute maps and to evaluate changes in geologic understanding and nomenclature through the decades. Bulletin-1141B is adjacent to the northeastern corner of this quadrangle and contained valuable information about outcrops of Triassic sedimentary deposits and the Gatuña Formation. The mapping from Bulletin-49 was not utilized, but the report contained valuable information, especially references to Skinner (1946), who described the Glorieta Sandstone north of Bulletin-49 along the Algerita Escarpment.

Small-scale maps and maps with irregular footprints (**Fig. 9**) overlap across the map area at a range of scales, including Geology of the Guadalupe Mountains-Carlsbad Region (Memoir-

24) at 1:187,500 scale (Kelley, 1971), Reconnaissance Map Showing Major Geologic Features, Pecos Region (OFR-80-1099) at 1:125,000 scale (Bachman, 1980), Geologic Map and Section of Guadalupe Mountains Area (PP-446) at 1:62,500 scale (Hayes, 1964), Geologic Map and Sections of Guadalupe Mountains (PP-215) at 1:48,000 scale (King, 1948), Regional Geologic Map of Parts of Culberson and Hudspeth Counties (OM-90) at 1:150,000 scale (King, 1949), and maps from OFR-59-9 (Bjorklund and Motts, 1959) at unspecified scales.

Memoir-24 covers a large area—the entire footprint of this quadrangle and the 30x60-minute map to the north—and was especially useful for contacts of members within the San Andres Formation and locations of facies gradations within Artesia Group formations. Memoir-24 also includes a plate showing geologic structures, which was useful for understanding regional tectonic trends. OFR-80-1099 helped with understanding of the Mescalero paleosol (caliche), which is discussed with the Gatuña Formation but was not mapped on this quadrangle. OFR-80-1099 also included outcrops of Triassic sediments that were not mapped in later 7.5-minute quadrangles or field checked during this project. Cretaceous deposits mapped in the northeastern corner of this map by OFR-80-1099 were field checked but not confirmed to be Cretaceous; rounded silicic pebbles resembling those from Cretaceous strata were observed, but no outcrop remnants were observed, and these pebbles are widely reworked into alluvial surficial units. PP-446 was mostly utilized for mapping of San Andres Formation member contacts between the Bonney Canyon Member (upper unit) and Rio Bonito Member (lower cherty unit). PP-446 also provided data on the Goat Seep Formation, fault geometries from the cross section, and information about unit contacts, unconformities, and lateral gradations in the report. PP-215 showed contacts of basin units south of the quadrangle and provided extensive information about these units in the report. PP-215 contains three separate plates: one showing Cenozoic landforms, one showing tectonic features, and one standard geologic map that includes cross sections. OM-90 overlaps across the southern portion of the map area and contains detailed mapping of structures in the Brokeoff Mountains; however, nomenclature of unit names has changed extensively since this publication. OFR-59-9 contains three plates: two are geologic maps of the Carlsbad area that were not consulted during this project, while the third plate shows lowland quaternary surfaces and was used often during this project to compare interpretations of the surficial geology with modern OFGMs.

STRUCTURE AND TECTONICS

The tectonic history of this quadrangle includes orogenic activity starting with continental accretion in the Proterozoic (Flawn, 1956), extension around the Precambrian to Phanerozoic boundary (Miall, 2008), convergent deformation in the Pennsylvanian–Permian (Hayes, 1964; Ye et al., 2006), tectonic subsidence and continued deformation throughout the Permian (Ewing, 1993; Hunt et al., 2003; Kosa and Hunt, 2005), regional uplift amongst overall quiescence in the Mesozoic, and rift extension during the Neogene. This section only attempts a broad overview of the literature of this area's tectonic history and map users are pointed to more comprehensive studies such as Horne et al. (2021) for a more in-depth overview.

Precambrian Tectonism

Boreholes penetrating basement rock in the quadrangle are limited, but granites of Ectasian age (Denison and Hetherington, 1969; Denison et al., 1971) are found below the Huapache monocline, and northward thrusting of basement rhyolites occurred during the Grenville orogeny in the region (Ewing, 1993; Ewing et al., 2019). Gravity data, field observations, and well data from Adams et al. (1993) show the presence of middle Proterozoic igneous basement rocks of variable compositions correlating to tectonic extension and the Grenville orogeny. Basement structures, including Phanerozoic deformation, are oriented with northwestward-striking faults with subordinate east-west structures (Horne et al., 2021). Rifting of the Rodinia supercontinent occurred during the end of the Proterozoic into the early Paleozoic, allowing for early basin sedimentation in what would become the Tabosa Basin (Walper, 1977; Miall, 2008).

Paleozoic Tectonism

The Guadalupe Mountains are a northeast-tilting block with a basement-cored thrust beneath the Huapache monocline on the east, the Bone Spring monocline, or Reef Anticline, along the reef escarpment to the southeast, and normal faults to the west on the Algerita Escarpment (Hayes, 1964). Northeast tilt is observable in the plunge of the Walnut Springs and Guadalupe Ridge anticlinal folds on the eastern periphery of the mountains (Hayes, 1964). Ancestral Rocky Mountain (ARM) and Marathon-Ouachita orogenic activity was likely responsible for early deformation in the quadrangle, with uplift in Pennsylvanian through Cisuralian time concurrent with basin subsidence, before waning tectonic subsidence until the late Cisuralian (King and Harder, 1985; Ye et al., 1996; Dickenson and Lawton, 2003; Kues and Giles, 2004; Rudolph, 2023).

The primary compressional feature observable in the quadrangle is the Huapache monocline, which grew over a blind thrust at depth along with other northwest-striking structures and subordinate northeast-striking structures (Horne, 2021). This fault causes repeated stratigraphic section in well 30-015-00014 within Ordovician to Mississippian strata, but Hayes (1964) suggests that crustal deformation from faulting below the Huapache monocline continued into the Cisuralian based on thickening of strata in nearby well logs while minor monoclinal folding continued through the Guadalupian based on structural measurements from the surface. This study's interpretations of steeply dipping beds on the hanging wall of a steep reverse fault structure are supported by Hayes (1964). Onset of thrust-sense motion on the fault beneath the Huapache monocline is thought to have occurred after the Mississippian and ceased before the latest Cisuralian due to an absence of offset in the San Andres Formation (Hayes, 1964). This study inferred roughly 20 m of offset in post-Pennsylvanian rocks and instead interpreted most of the stratigraphic thickening in early Cisuralian sediments to be related to deposition along paleotopography created by the thrust. Stratigraphic control from the well logs was limited to tops of the Hueco and Wolfcamp Formations in 30-015-00013 and 30-015-00014 such that offset in the Bone Spring and Victorio Peak Limestone was limited to wells distal from the fault. However, interpretations of thrust through the Wolfcamp Formation, Bone Spring Formation, and Victorio Peak Limestone that exceeds what is displayed in this study's cross section could likely be supported.

Figure 10: Near the Huapache monocline, a buckle at the contact of the Bonney Canyon Member and Fourmile Draw Member of the San Andres Formation.

The timing of movement along this thrust is unclear, but consistent fusulinid sequences within Pennsylvanian rocks on the hanging wall and footwall, despite drastic stratigraphic thickness differences, suggest slow movement that allowed for continuous but condensed sedimentation compared to rapid uplift and exhumation (Hayes, 1964). However, this is variable within the quadrangle because an absence of Pennsylvanian rocks on the hanging wall of the thrust within similar wells is observed near the northern boundary of this quadrangle (Hayes, 1964).

The contractional deformation (e.g., **Fig. 10**) during this time is proposed to be a product of varying vergence directions of the ARM and Marathon-Ouachita orogenies, which resulted in mixed deformation styles within the Permian Basin (Horne et al., 2021). The ARM orogeny is likely responsible for the development of east-verging faulting of the southernmost extension of the Pedernal uplift in this area, starting in the latest Mississippian, with high rates of erosion beginning in the Lower Pennsylvanian (Ye et al., 1996). The scale of exhumation in associated uplifts is reflected by regional deposition of clastics, with a shift from silicic to arkosic deposition occurring during the late Pennsylvanian as an increase in basement-derived clasts during deposition of the Strawn Formation (King and Harder, 1985; Ye et al., 1996).

Delaware Basin formation during the Paleozoic is largely attributed to ARM tectonism along with other major basins and uplift features in the Permian Basin; however, continued post-ARM activity (i.e., waning Permian tectonism) led to subsidence in the basin and uplift in the mountains (Fairhurst et al., 2021; Rudolph, 2023). Subsidence occurred to the greatest extent in the Delaware Basin, to the west of the Central Basin axis (Ewing, 1993). Small-magnitude deformation during the Guadalupian may be partly responsible for basin deepening as basinward dips in backreef sediments were found to be the result of differential subsidence in the Delaware Basin compared to the northwest shelf (Hunt et al., 2003)

The Bone Spring monocline developed after the Huapache monocline thrust around the boundary of the Cisuralian and Guadalupian, at the eastern flank of the Guadalupe Mountains, where the Victorio Peak Limestone reaches the shelf edge (Hayes, 1964). Uplift along the Bone Spring monocline is also responsible for the unconformity between the sandstone tongue of the Cherry Canyon Formation and the Cutoff Formation with the absence of the Brushy Canyon Formation or upper portions of the San Andres Formation on the shelf (King, 1948; Hayes, 1964). Deformation along the arch largely ceased by the deposition of the Cherry Canyon Sandstone and before the upper members of the San Andres Formation; however, localized angularity in the contact of the Grayburg and San Andres Formations is inferred to be a final bout of monoclinal deformation (Hayes, 1964). Hayes (1964) describes this unconformity within exposures of the San Andres and Grayburg Formations in Last Chance Canyon, the southernmost exposures of the San Andres Formation along the Algerita Escarpment, and within the Brokeoff Mountains 20 miles southwest of Last Chance Canyon. This publication utilized an observed angular unconformity along Algerita Escarpment as the northernmost extent of the unconformity while all contacts of Grayburg Formation onto San Andres were mapped as unconformable in Last Chance Canyon and the southern portion of the Brokeoff Mountains near the border with Texas.

Mesozoic and Early Cenozoic Tectonism

Mesozoic tectonism, including the Laramide orogeny, is likely absent in the map area. Hayes (1964) believed that regional epeirogenic uplift may have occurred during Laramide time and that the Walnut Canyon syncline and Guadalupe Ridge anticline are Laramide in age due to the deformation of Artesia Group sediments. However, basinward tilting of these same shelf strata was found to be the result of syndepositional (i.e., Paleozoic) tectonism along minor faults and folds near the shelf margin that acted to steepen dips and accentuate basin subsidence (Hunt et al., 2003; Kosa and Hunt, 2005). Some evidence from northeast-trending tectonic stylolites, small compressive faults, localized folding, and other small-scale tectonic features (e.g., deformed veins) may be indicative of Laramide tectonism in the Guadalupe Mountains (Erdlac, 1993).

Cenozoic Tectonism

In the present day, the Guadalupe Mountains stand out as a distinct uplift, with extension from Rio Grande rifting largely responsible for exposure of the Guadalupe Mountains (Rudolph, 2023). Onset of uplift occurred in the middle Oligocene to middle Miocene based on speleogenesis in cave systems of the Guadalupe Mountains (Decker, 2018). Uplift is recorded to

have continued from approximately 11 Ma to around 4 Ma based on speleogenesis occurring at decreasing elevations through time in the current mountain front of the Guadalupe Mountains from the water table dropping relative to the uplift of the mountains (Polyak et al., 1998, 2006, 2023). This deformation, which occurred during the Cenozoic, manifests itself in the Lopingian strata of the basin with folding in the Castile Formation evaporites (Anderson and Kirkland, 1978; Erdlac, 1993).

The Barrera Fault and Carlsbad Fault are portrayed offsetting Permian deposits along the eastern front of the Guadalupe Mountain where they meet the Delaware Basin. This fault was mapped by Kelley (1971) in Memoir-24 but was subsequently argued not to exist by Hayes and Bachman (1979) who did not observe any displacement. While observations in satellite and lidar imagery suggest the existence of a fault, Hayes and Bachman (1979) attributed that appearance to jointing and preferential growth of vegetation due to water availability along the mountain front.

Along the western mountain front, the Algerita Escarpment of the Rim Escarpment represents the edge of Rio Grande rift extension, with major faults, approaching 250 m of offset, bounding the extremities of the Big Dog Canyon graben (Hayes, 1964). Quaternary active stretches of the fault are tentatively observed in the northern portion of the Algerita Escarpment within this quadrangle and symbolized with queried scarps on normal fault. Prior studies suggest that the Guadalupe fault is late Pleistocene in age and limited to an extent that crosses the county line of Chaves and Otero Counties, New Mexico, to the north of the quadrangle (King, 1948; Kelley, 1971; Machette et al., 1998); however, offset was observed in Yeso Formation outcrops with remnant Quaternary deposits eroding off the footwall. On the footwall of the Guadalupe fault, or a smaller associated normal fault, subcrop of the Yeso Formation was present with a cover of gravels and boulders of mixed lithology. The surface is smooth and thin (<2 m), and no petrocalcic soil was observed. The gravels on the surface did contain discontinuous carbonate coatings; however, the absence of a mature soil could be due to a young age of the surface, erosion near the scarp where observations were made, lack of exposure, or absence of a soil in the case where this was not a stable Quaternary surface prior to faulting. When standing on the surface, the connection to the source drainage is still visible and the surface does not lie at a grade more than a couple meters above the adjacent active arroyo gulleys. Overall, the scarp is roughly 6–8 m in height and is primarily a bedrock fault inferred to have been active during the Quaternary due to the offset of lag gravels. Quaternary fault activity along the western escarpment of the Guadalupe Mountains is found to have reached a steady state where downcutting of arroyos and gulleys from erosion matches uplift along Quaternary active faults (Happel, 2017). Based on cosmogenic nuclide-derived erosion rates from in-situ bedrock along the Algerita Escarpment, the magnitude of uplift was greater and occurred more recently along the western bounding fault to the south of this quadrangle, across the border into Texas (Tranel and Happel, 2020).

STRATIGRAPHY

This section of the report begins with the oldest rock in the subsurface of the quadrangle, the Mesoproterozoic basement rock. It then addresses each age group of

sedimentary and surficial deposits in chronological order. This begins with early Paleozoic subsurface stratigraphy then works through the Permian, the Mesozoic, Oligocene intrusives, late Cenozoic basin-fill deposits, and Quaternary surficial cover.

Mesoproterozoic Erathem: Ectasian Period

Precambrian rocks in the region are not exposed at the surface but have been encountered in several deep wells. Most of the subsurface Precambrian rocks appear to be granitic, including quartz- and biotite-rich granite and possible granite pegmatite (Flawn, 1956; Hayes, 1964). To the northwest, metamorphosed sedimentary and volcanic rocks, such as chlorite phyllite and possible amphibolite, have also been documented, suggesting localized variation in basement composition. These findings support the delineation from Flawn (1956) of a cratonic margin underlying Texas and extending as far west as the Guadalupe Mountains. The granitic basement likely represents part of the stable craton, whereas the metamorphosed sequences may reflect more tectonically active margins, possibly associated with the northern, late Precambrian Red River mobile belt or the Van Horn orogeny to the south. Exposures of similar Precambrian rocks occur to the south in the El Paso and Van Horn areas.

Paleozoic Erathem: Cambrian–Pennsylvanian Periods

Cambrian–Ordovician subsurface stratigraphy

The oldest sedimentary unit overlying the Precambrian crystalline basement in the mapped area, as observed in well data, is correlated with the Bliss Sandstone. Regionally, the Bliss Sandstone is exposed in the Franklin Mountains and Baylor Mountains in Texas, as well as the Sacramento Mountains in New Mexico. Within the map area, the unit ranges in thickness from approximately 7 m near Last Chance Canyon to about 30 m to the northeast near Box Canyon. It is composed predominantly of light-gray to white, poorly sorted, coarse-quartz sandstone at the base and top, with a medial interval of medium-gray, fine- to medium-crystalline sandy dolomite. Based on lithologic and stratigraphic correlations, the Bliss Sandstone in this area is interpreted as being of late Cambrian to Early Ordovician age (Hayes, 1964).

Ordovician subsurface stratigraphy

The Montoya Group was deposited during a global transition from greenhouse to short-lived icehouse conditions in the Late Ordovician; it records a shift in marine environments on a broad, shallow-water carbonate platform (Jones, 2004). From oldest to youngest, it comprises the Upham, Aleman, and Cutter Formations. The Upham Formation locally includes the basal Cable Canyon Sandstone; a poorly sorted quartz sandstone and conglomerate derived from eroding Precambrian uplifts to the northwest. The Aleman Formation is dominated by interbedded carbonate and chert, with its lower facies reflecting deeper ramp deposition under cool-water conditions and limited storm influence. The overlying Cutter Formation reflects a return to shallower, normal marine conditions. The boundary between the Montoya and the overlying Silurian Fusselman Formation is commonly marked by the thin Sylvan Shale, where present. The Montoya Group ranges from 30 to 200 m thick and unconformably overlies the Simpson Group or, in places, the Ellenburger or Bliss Formation. It crops out in the Franklin,

Hueco, Sacramento, San Andres, and Caballo mountain ranges and reflects a passive margin setting influenced by fluctuating sea levels and the onset of the Hirnantian glaciation (Bruno and Chafetz, 1988; Brimberry, 1991; Jones, 2004; Pope, 2004).

The Middle Ordovician Simpson Group is described from drill cuttings in the area as dark-gray to dark greenish-gray shale and light-gray, coarse- to fine-grained sandstone and is capped by an unconformity. The upper unconformity marks a significant period of erosion related to post-depositional uplift (Jones, 2004). The Pedernal landmass of central and north-central New Mexico acted as a regional high during this time and served as a sediment source for Simpson sandstones and siltstones in southeastern New Mexico (Kottlowski, 1970). Near Last Chance Canyon, these Simpson-equivalent strata are approximately 12 m thick. East of Queen, thickness increases to about 21 m, but equivalent rocks appear to be absent a few kilometers southeast and around Texas Hill. Farther south, near the Black River, the Simpson equivalent is reported to be up to 57 m thick (Hayes, 1964).

Silurian subsurface stratigraphy

In the map area, the Fusselman Formation consists almost entirely of white to light-gray, coarse- to medium-crystalline dolomite (Hayes, 1964). Eight wells documented in Hayes (1964) penetrated the full thickness of the formation, which ranges from approximately 177 m near Texas Hill to about 226 m near Red Bluff Draw. During the Silurian, the axes of the Tobosa Basin represented relatively deeper marine settings where dense limestones and shales accumulated (Hill, 1996). In the Delaware Basin, the lower Silurian Fusselman Formation unconformably overlies the Upper Ordovician Montoya Group, with a marked lithologic transition. The upper surface of the Fusselman exhibits evidence of subaerial exposure and karstification, consistent with a regionally significant drop in sea level (Hill, 1996).

Devonian subsurface stratigraphy

The Woodford Shale is a black, organic-rich shale with minor black cherts, siltstones, sandstones, and greenish-colored shales. The unit is 0–100 m thick and estimated to be approximately 36 m thick in the map area (Broadhead, 2010). In the Permian Basin, the Woodford unconformably overlies Silurian and Lower Devonian carbonate strata of the Wristen Group and the Thirtyone Formation, and a pre-Woodford shale. The contact between the pre-Woodford shale and the Woodford Shale appears sharp on well logs, with pre-Woodford shales exhibiting a higher radioactivity signature than underlying carbonates but lower than the Woodford Shale (Broadhead, 2010).

The Fusselman Dolomite is sharply overlain by the Thirtyone Formation and the Percha Shale. The Thirtyone Formation is characterized by light-colored, siliceous, chert-rich limestone capped by an interval of crinoid-rich limestone and minor sandy limestone (Hill, 1996). Its thickness ranges from approximately 80 to 300 m. The overlying Percha Shale varies in thickness from about 6 to 21 m (Hayes, 1964). The Thirtyone Formation represents carbonate shelf deposition along the shallower margins of the Tobosa Basin, whereas the Percha Shale records deeper-water sedimentation during the Early to Middle Devonian.

Mississippian subsurface stratigraphy

The Barnett Shale ranges from approximately 60 to 140 m thick and thickens eastward across the region. It is composed primarily of dark-gray to black, hard, siliceous, fissile shale that is organic-rich and contains abundant pyrite, with minor interbeds of sandstone and limestone. In the Carlsbad area, an informal member known as the Chester interval is recognized; it consists of fine-grained sandstone, siltstone, argillaceous limestone, and shale. The Chester interval is interpreted as the initial progradation and influx of clastics from the Pedernal highlands, foreshadowing more extensive Pennsylvanian sedimentation in the Delaware Basin. The Barnett Shale represents deposition during a tectonically transitional period leading up to the Marathon orogeny, which ultimately subdivided the Tobosa Basin into the Midland and Delaware Basins (Hill, 1996).

Pennsylvanian subsurface stratigraphy

The Pennsylvanian Period includes, from base to top, the Morrow, Atokan, Strawn, Canyon, and Cisco Formations. These units are only found in the subsurface of this quadrangle, and the Cisco and Canyon Formations are mapped together in the cross section because they are relatively thin in most boreholes. The Morrow unconformably overlies the Mississippian Period strata and has coarse-grained clastics at its base related to the onset of Ancestral Rocky Mountain (ARM) tectonism; it also contains shales, limestones, and siltstones representing deposition from deep marine to deltaic environments (Hill, 1996). The Atokan conformably overlies the Morrow and contains sediments deposited in shallow marine and coastal environments during increased uplift of the Pedernal landmass; it includes limestones, shales, chert, and conglomeratic sandstones, with increasing shale abundance up section (Hill, 1996). The Strawn is unconformable over the Atokan and represents carbonate reef development, including limestones, shales, sandstones, and pebble conglomerates (Hill, 1996). The Canyon and Cisco Formations were deposited in deep marine basin settings with dominantly dolomite, chert, and siliciclastic sediments (Hill, 1996). The Pennsylvanian sediments are found to thicken greatly on the eastern footwall of the blind thrust beneath the Huapache monocline and thin dramatically on the hanging wall to the west.

Paleozoic Erathem: Permian Period

Cisuralian Epoch

The Cisuralian Epoch (formerly the Wolfcampian and Leonardian Epochs) in the Carlsbad 30x60-minute quadrangle contains backreef shelf, shelf-margin reef, and basin deposits like the Guadalupian Epoch. Most of the units of Cisuralian age are either only found in the subsurface or found cropping out in the Brokeoff Mountains (**Fig. 11**). In this section, we include the San Andres Formation and Cutoff Formation that straddle the Cisuralian–Guadalupian boundary (Hayes, 1959).

The Hueco Formation and Wolfcamp Formation are found above the basal Wolfcampian unconformity, which locally erodes the upper Pennsylvanian, and are overlain by and interfinger with the Abo Formation (Hayes, 1964). The Hueco Formation is distinguished from the underlying Pennsylvanian sediments based on fossil assemblages and the presence of an

unconformity; otherwise, it is visually similar (Hayes, 1964). The Hueco Formation contains siliceous limestone, dolomites, colorful shales, and fine-grained sandstones which are described as similar in appearance to the Bursum Formation found farther northwest away from the shelf margin (Hayes, 1964). The top of the formation grades shelfward into the Abo Formation and basinward into the basal Bone Spring Formation and Wolfcamp Formation (Pray, 1954; Bachman and Hayes, 1958; Hayes, 1964). In its basinward transition, where it consists of thick beds of crystalline dolomite, it is called the Abo Reef, a target for the petroleum industry elsewhere in the basin (Podpechan, 1959; LeMay, 1961; Hayes, 1964). The basinward transition into the Wolfcamp Formation occurs over a wide area due to immature development of the basin margins during early Permian times (Hayes, 1964). The sediments shift to dark-colored shales, crystalline limestones with chert, and micaceous sandstones, with the gradation starting farther shelfward and the base becoming increasingly close to the present shelf margin, moving upward in section (Hayes, 1964).

Located below the Cutoff Formation and San Andres Formation, the Yeso Formation, Victorio Peak Limestone, and Bone Spring Limestone represent a shelf-reef-basin transition and progradation during the Cisuralian. In the backreef shelf area, the Yeso Formation extends southward from its usual facies found in central New Mexico and presents as a dolomite-dominated marine unit grading into the Victorio Peak Limestone (Boyd, 1958; Hayes, 1964; Skotnicki, 2024b). The defining characteristic of the unit used to differentiate it from the Victorio Peak Limestone is the presence of gypsum or anhydrite, which are absent in the Victorio Peak Limestone. Because the sediments of the Yeso Formation are not typical of the formation within this quadrangle, it is a region of transitional facies (Hayes, 1964). The Yeso Formation is the oldest unit in the quadrangle because lateral progradation into the Victorio Peak Limestone makes the sediments decrease in age basinward and upward (Hayes, 1964). The Victorio Peak is the shelf-margin reef equivalent of the Yeso Formation and occupied the outer shelf and shelf margin; it progrades outward over shales of the basin-equivalent Bone Spring Formation (King, 1948; Hayes, 1964). The Bone Spring Formation is not exposed in the quadrangle but consists of cherty limestones, shales, shaly limestones, and fine sandstones (Hayes, 1964). The unit underlies and grades laterally into the base of the Victorio Peak Limestone; additionally, the lower portion of the Bone Spring Formation grades into the upper Hueco Formation approaching the shelf margin (King, 1948; Hayes, 1964).

Figure 11: Yeso Formation, San Andres Formation, and Grayburg Formation exposed along the Algerita Escarpment.

The Cutoff Formation is found on the shelf, where it overlies the Yeso Formation and Victorio Peak Limestone, and into the basin, where it overlies and grades downward and laterally into the Bone Spring Formation and laterally and upward into the Brushy Canyon Formation (Boyd, 1958; Hayes, 1964). Along the shelf-margin reef area, the Cutoff Formation was eroded by uplift on the Bone Spring monocline (Hayes, 1964). This unit includes thin limestones, siliceous shales that may be sandy, and sandstones (Hayes, 1964). At the base of the San Andres Formation and top of the underlying Yeso Formation, the Glorieta Sandstone is present for a few kilometers before pinching out toward the shelf margin. This outcrop was described by Skinner (1946), who found a few meters of the main sand body along the Algerita Escarpment. Additionally, he described underlying interbedded sands and carbonates, which are not mapped as Glorieta Sandstone in this publication. Well logs near the El Paso Gap 15-minute quadrangle mapped by Boyd (1958) and Skotnicki (2024b) were found to contain Glorieta Sandstone; however, its absence in satellite imagery and mapping of the area leads us to believe that it is the lower interbedded sand and carbonate portion rather than the primary sand body. Because of this, the Glorieta Sandstone is not mapped south of the extent described by Skinner (1946) and is excluded from the cross section.

Figure 12: Outcrops of the Fourmile Draw Member of the San Andres Formation.

The San Andres Formation represents shelf carbonates of Cisuralian to Guadalupian age that are found cropping out to the west of the Seven Rivers Embayment in the Guadalupe Mountains (Hayes, 1964; Kelley, 1971). Hayes (1964) split out a lower cherty unit, while Kelley (1971) expanded nomenclature he was using to the north to create three named members (from base to top: the Rio Bonito, Bonney Canyon, and Fourmile Draw Members). The basal Rio Bonito Member correlates to the lower cherty member of Hayes (1964). In this quadrangle, the Fourmile Draw Member (**Fig. 12**), which is characterized elsewhere by abundant gypsum, is minimally gypsiferous, and only isolated pods and thin beds of gypsum were observed near the northern map boundary.

Guadalupian Epoch

The Guadalupian Epoch in southwestern New Mexico was considered tectonically quiescent compared to the relatively recent epochs. The normal-marine conditions of the Marathon fold belt foreland basin evolved into a restricted marine setting, and a reef complex developed along the northwestern rim of the Delaware Basin, separating forereef and backreef environments (Kues and Giles, 2004). Wilson (1975, fig. 1) illustrates the general morphology of carbonate platforms and explains that facies analysis along a stratigraphic section enables the interpretation of depositional environments. A diagram of the Guadalupian shelf margin reveals a similar morphology (**Fig. 13**), and facies changes discussed in detail in the Description of Map Units will demonstrate the utility of the comparison.

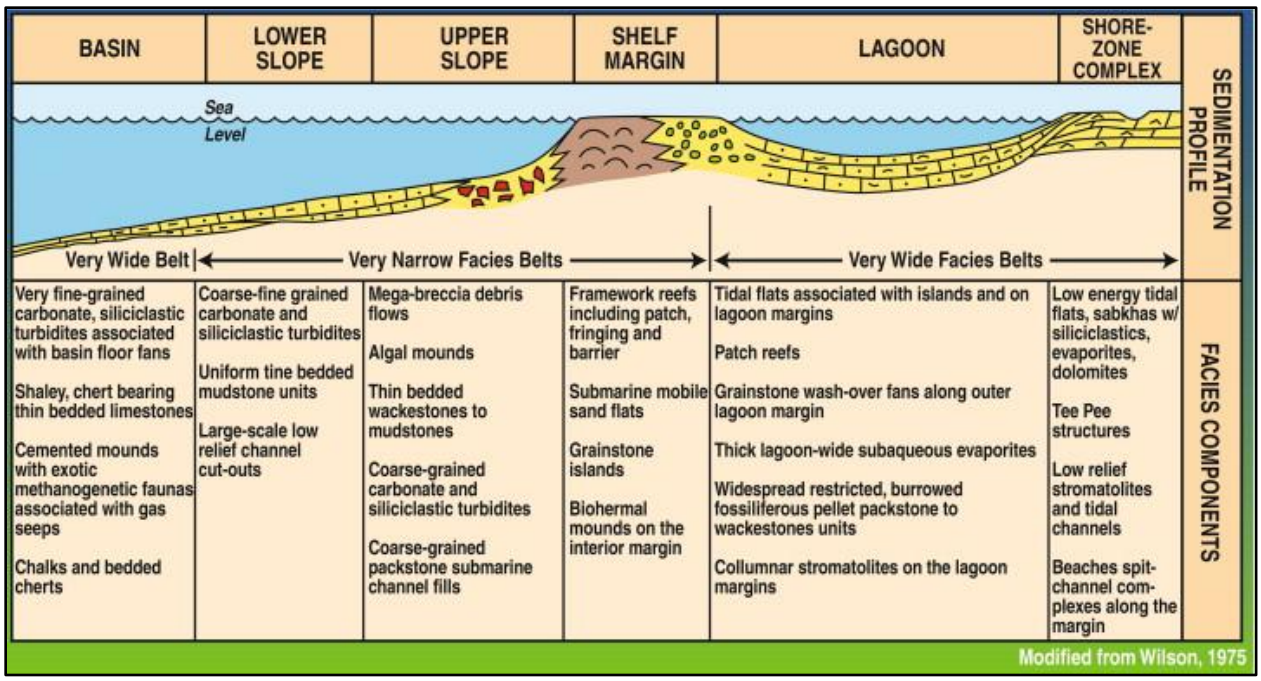

Figure 13: Carbonate shelf morphology diagram (Wilson, J.L., 1975, Carbonate facies in geologic history: New York, Springer-Verlag, 471 p. https://doi.org/10.1007/978-1-4612-6383-8).

Reef environment

The Goat Seep Dolomite is mostly a subsurface unit, with one exposed outcrop (150 m thick) in North McKittrick Canyon at the southern boundary of this map. The Goat Seep Dolomite is composed of massive to thick-bedded, fossiliferous carbonates and minor siliciclastic beds. It gradationally overlies the Cherry Canyon Tongue and laterally grades into the Cherry Canyon Formation to the southeast (basinward). The northwestern lateral contacts of the Goat Seep Formation grade into the Grayburg and Queen Formations. This unit represents initial reef development during the early Guadalupian Epoch and can be easily confused with the Capitan Formation; it can be differentiated by the significant dolomite presence (approximately 90% based on King [1948] and Hayes [1964]), whereas the Capitan Formation consists almost entirely of limestone. Note that King (1948) included time equivalent shelf units (i.e., the Grayburg and Queen Formations) to be included in the Goat Seep Dolomite; this causes an abundance of Goat Seep Dolomite to be mapped within his maps in the Brokeoff Mountains and Guadalupe Mountains in the southern map area.

The most prominent geologic feature of the Carlsbad 30x60-minute quadrangle is the Capitan Reef escarpment, which generally trends southwest to northeast across the center of the map. Kues and Giles (2004) summarized the fame of the Capitan Formation best: "The Capitan reef is the largest, best-preserved, most accessible, and most intensively studied Paleozoic reef complex in the world. Its structure stratigraphy, composition, diagenesis, paleontology, paleoenvironments, and growth have been the subject of hundreds of papers and numerous books. (p. 125)" The Capitan Formation is a 600-m-thick fossilized reef complex similar in morphology to the modern-day Great Barrier Reef in northern Australia. This formation is

disconformable over the Goat Seep Formation (Hayes, 1964) and laterally grades into the Artesia Group to the northwest and the Bell Canyon Formation to the southeast.

Figure 14: Foreslope talus breccia of the Capitan Formation.

There are two distinct facies within the Capitan Formation: the massive reef facies (**Fig. 16**) and forereef-slope facies (**Fig. 14**). The reef facies are devoid of bedding but contain a diverse assemblage of macrofossils, including sponges, corals, brachiopods, bryozoans, gastropods, crinoids, mollusks, fusulinids, and fossil algae. Newell (1953) noted that upwelling, nutrient-rich basin waters supported reef organisms, and there are faunal differences among basin, reef, and shelf biofacies. Forereef-slope facies consist of crudely bedded carbonate debris, talus blocks, and slides dipping basinward at 10–30°. Contacts between the reef-slope facies and the Brushy Canyon Formation serve as textbook examples of deep-marine turbidite systems and have been studied to understand the distribution and origin of hydrocarbon reserves (Kues and Giles, 2004). Contacts between the Capitan Formation and deep-marine basin environment are best seen to the south of McKittrick Canyon, but the reef facies are most exposed to the north. Even after termination as a marine environment, the Capitan Formation acts as a conduit for fluids between basin- and shelf-rock environments (Hill, 1993; Rice-Snow et al., 2006). The Capitan Formation is the host rock of world-renowned cave systems such as Carlsbad Caverns and Lechuguilla Cave, which formed from post-depositional acidic fluids from proximal, basin-derived hydrocarbon reservoirs interacting with the host carbonate rock (Polyak et al., 2006). Sandstone dikes, common throughout this unit, range from millimeter- to centimeter-scale and

are composed of siliciclastic material similar in lithology to the Yates and Bell Canyon Formations. Southward migration along the Capitan Formation (progressing up stratigraphy), reflects an overall retreat in sea levels as the climate changed to a more arid environment, possibly related to the final suturing of Gondwana to Laurentia (Kues and Giles, 2004).

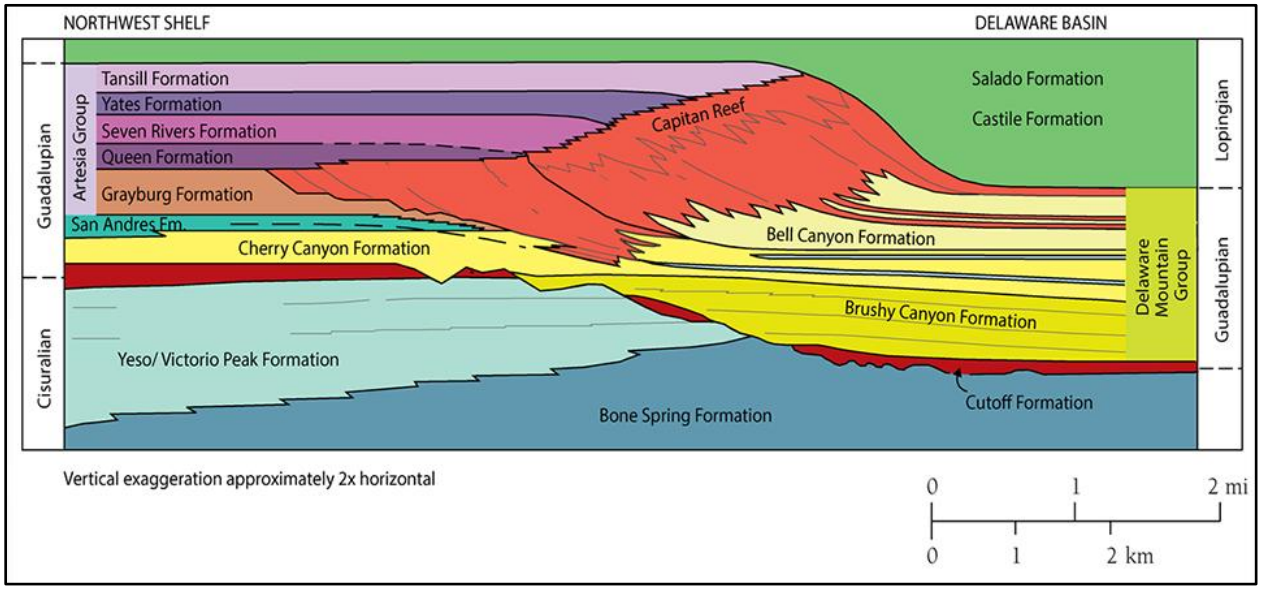

Figure 15: Permian stratigraphy diagram modified with facies boundaries (Modified from King, 1948 and Scholle, 2007).

Backreef shelf environment: the Artesia Group

The entire stratigraphic section of the Artesia Group (**Fig. 15**) is visible on this map. The Artesia Group, which occupies approximately a third of the map area, represents the backreef and shelf-lagoon facies of the Permian-aged carbonate platform. Units of the Artesia Group laterally grade from the north/northwest into the Capitan Formation and underlying Goat Seep Formation. Formations within the Artesia Group capture the cyclicity of sea levels during this time, but an overall retreat of the shoreline is observed as younger formations of the Artesia Group extend farther south toward the Delaware Basin (Kues and Giles, 2004). The northern extent of the Artesia Group reaches to northern New Mexico, on the eastern boundary of the Rio Grande rift, and is best documented by Kelley (1971). Distinct lithological differences exist between the formations of the Artesia Group, but they are subtle and often difficult to recognize without prolonged observation across the entire map area. Accordingly, this section describes the Artesia Group collectively, noting individual formations when necessary.

Figure 16: Contact of the Seven Rivers Formation of the Artesia Group with the Capitan Formation.

Within the Artesia Group, there are facies that change both laterally and vertically. Previous works have attempted to divide formations by facies indicators to better understand depositional environments at the time, but for the sake of scale, this project has kept the map units mostly undifferentiated. The exception to this is the distinction between carbonate and evaporite facies of the Artesia Group. Previous works have highlighted the boundaries of these facies where they are exposed at the surface; however, this work was unable to create a continuous, coherent boundary for each formation across the entire map area, and such boundaries were therefore not included. These facies boundaries represent a change in the local, carbonate-shelf depositional system from lagoonal or sabkha environments (evaporite-rich) to a more moderate-marine environment (carbonate-rich); the Seven Rivers Formation is the best example of this facies change, and for this reason is separated into two map units by a facies boundary (**Pas** and **Pase**). The evaporites in all these units are dominantly gypsum, and the concentration within a formation affects the likelihood that a formation is either present at the surface or eroded, which is the case for the Yates and Tansill Formations in the northern extent of this map; the gypsum is easily weathered and preferentially colonized by microorganisms in soils.

There is a subtle evolution of intraformational facies transitions in the Artesia Group; all formations exhibit facies changes, but the distinctions become more pronounced as formations get younger. Rocks near the reef are typically grain-dominated carbonates and exhibit oolitic/pisolitic textures. Fusulinid-rich, cross-laminated to planar beds are common and indicate deposition in shoal complexes. These grain-supported textures make rocks more porous and permeable, which supports marine circulation and allows for magnesium-rich fluids to increase dolomitization of near-reef deposits. As one travels away from the reef, rocks transition to mud-supported packstones and wackestones, ooids and pisoids become less frequent, fenestral fabrics and algal laminates become more common, and teepee structures and evaporite nodules begin to appear. Farther from the reef, dolomitic mudstones and silty carbonates become more common as fine-grained siliciclastic input increases and evaporite facies appear, indicating lower energy, possibly stagnant or restricted marine conditions of tidal-flat, lagoon, or sabkha environments. There are important chemical reactions related to evaporite precipitation and dolomitization of host rocks in arid, restricted marine environments during diagenesis that are relevant to understanding the Artesia Group but go beyond the scope of this report; this is covered in depth in Donatelli (2016).

Post-depositional mineralization in shelf deposits

In the Yates Formation, proximal to the underlying and overlying formation contacts, are trace, disseminated clusters of medium- to fine-grained iron-sulfide minerals (**Fig. 17**). These minerals were originally identified in the field as pyrite and marcasite. Crystals were black to reddish brown, commonly twinned, cubic, or radiating tabular prisms. There were also coarse- to medium-grained ooids of a metallic gray to black mineral, suspected to be goethite. Minerals were mostly found weathered from outcrops in areas where bedding was locally folded. These minerals are not commonly mentioned in previous mapping, but they do work as a remarkable marker for identifying the contact between the Yates and the Seven Rivers Formations across the entire map area.

Figure 17: A photo of typical mineral occurrences at the base of the Yates Formation.

X-ray diffraction analyses of two samples identified the minerals as goethite. Goethite appears in two forms: oolitic and as pseudomorphs of marcasite and pyrite. Hill (1993) conducted analyses of sulfur isotope ratios in Yates-hosted sulfides; the original pyrite and marcasite likely formed from sulfide gases that migrated from the basin and interacted with metal-chloride complexes that originated from the evaporite facies. These fluids were captured in structural and stratigraphic traps. Pliocene–Pleistocene uplift of the region lowered the water table and introduced oxygenated water to create the gossan deposits of goethite; the low concentration of these deposits makes them more of a geologic curiosity than an economic deposit, but these minerals highlight the subsurface migration of fluids between shelf and basin rocks.

Basin deposition: the Delaware Mountain Group

The Delaware Mountain Group contains three formations (from base to top): the Brushy Canyon, Cherry Canyon, and Bell Canyon Formations. Each of these has members (i.e., limestones or sands) that are named but not discussed in this report.

Figure 18: Brushy Canyon Formation of the Delaware Mountain Group.

The Brushy Canyon Formation (**Fig. 18**) is the lowest (oldest) formation of the Delaware Mountain Group and does not have a shelf or shelf-margin equivalent. Instead, the disconformity between the tongue of the Cherry Canyon Formation and Cutoff Formation, Bone Spring Formation, or Victorio Peak Limestone represents that time on the shelf (King, 1948; Hayes, 1964). This formation was deposited in deep waters as sediments dropped from the carbonate shelf into the Delaware Basin; it consists of shales, lenticular sandstones, and subordinate limestones (King, 1948; Hayes, 1964).

The Cherry Canyon Formation (**Fig. 19**) is the middle formation of the Delaware Mountain Group in the Delaware Basin. The formation conformably overlies the Brushy

Canyon Formation and underlies the Bell Canyon Formation (Hayes, 1964). It contains three named members (from oldest to youngest: Getaway, South Wells, and Manzanita Limestone Members) that are not discussed in this report (King, 1942; Hayes, 1964). The tongue of the Cherry Canyon Formation is exposed in the Brokeoff Mountains and along the Huapache monocline and is discussed in conjunction with other shelf sediments of the Guadalupian Epoch in the previous section. The tongue represents sands beneath the Getaway Limestone Member of the Cherry Canyon Formation and grades into the upper San Andres Formation on the shelf (Boyd, 1955, 1958; Hayes, 1959, 1964). A middle portion of the formation, including the Getaway Limestone Member to the South Wells Limestone Member, grades into the Goat Seep Formation at the shelf margin (King, 1942; Hayes, 1964). Above the South Wells Limestone Member, the Cherry Canyon Formation terminates between the Goat Seep Dolomite and the Capitan Formation (Hayes, 1964). Limestones of this formation, as well as the Bell Canyon Formation, thin and pinch out away from the mountain front in the basin (Hayes, 1964).

Figure 19: Tongue of the Cherry Canyon Formation of the Delaware Mountain Group.

The tongue of the Cherry Canyon Formation has a disconformable contact with the Cutoff Formation on the shelf (Hayes, 1964). The upper portions of the tongue of the Cherry Canyon Formation may grade into the lower Grayburg Formation; however, others suggest that the tongue grades into the upper San Andres Formation (Boyd, 1955; Hayes, 1964). This may be a source of error in the contact between the San Andres and Grayburg Formations within this quadrangle because we mapped the contact low in section around the presence of a thin sandstone horizon found along the Algerita Escarpment, according to mapping of Skotnicki (2024a, 2024b). Our pick for the contact is based on Skotnicki (2024a, 2024b) and Boyd (1955), while Hayes (1964) and Kelley (1971) considered the last remnants of sands grading from the tongue of the Cherry Canyon Formation to be correlative to the upper San Andres Formation, thus mapping the contact higher in section.

The uppermost (youngest) unit, the Bell Canyon Formation, includes interbedded sandstones and limestones, with five named members (from base to top: the Hegler, Pinery, Rader, McCombs, and Lamar Members) that conformably overlie the Cherry Canyon Formation (King, 1942; Hayes, 1964). The members of the Bell Canyon Formation grade shelfward into the Capitan Formation, where limestones of the Bell Canyon Formation thicken and sands thin, terminate, or grade into limestone facies of the Capitan Formation (King, 1942; Hayes, 1964).

Lopingian (Ochoan) Epoch

The Castile Formation and Salado Formation represent accumulations of evaporitic sediments from the late Permian (Lopingian, formerly Ochoan) period. The Castile is limited to the Delaware Basin where it overlies the Delaware Mountain Group. The Salado Formation was deposited in the basin, where it has a variably conformable contact with the Castile, and across the shelf where it is unconformable over the Artesia Group (Hayes, 1964; Kelley, 1971). The Castile Formation consists primarily of varved layers of gypsum and calcite, while the Salado is mostly halite that is absent due to dissolution at the surface. These formations are mapped together in this publication because the presence of the Salado Formation is limited to residual weathering products in most areas (Hayes, 1964).

Figure 20: Culebra Dolomite Member of the Rustler Formation in the Frontier Hills.

The Rustler Formation (**Fig. 21**) represents shelf and basin sedimentation in increasingly fresh waters during Lopingian time and includes sandstones, mudstones, evaporites, and carbonate lithologies (Kelley, 1971). The formation is split into four members, including, from base to top, the Virginia Draw, Culebra Dolomite, Tamarisk, Magenta, and Forty-niner Members. The formation is found unconformable over Artesia Group formations on the shelf outside of the map area and becomes conformable with the Salado Formation to the east where the Salado is present (Hayes, 1964; Kelley, 1971). The Rustler is observed to experience

significant slumping from the dissolution of underlying evaporites. The Culebra Dolomite Member (**Fig. 20**) is an important hydrogeologic unit.

Figure 21: Rustler Formation red beds at the eastern map boundary.

The Quartermaster Formation, variably and previously called the Dewey Lake Formation or Pierce Canyon Red Beds, is not mapped in this quadrangle despite being previously mapped in localized areas by Kelley (1971). Field observations suggest strong similarities in appearance (e.g., red beds with reduction spots) between the Quartermaster and Dewey Lake Formations. Channel sands in the Dewey Lake Formation appeared to be thicker, with a greater degree of scouring and increased presence of cross-bedding and ripple laminations. The formation has been argued to be of Permian and Triassic age (Schiel, 1988); however, fossil, magnetostratigraphic, and radiometric dates support deposition limited to the Permian (Roth et al., 1941; Fracasso and Kolker, 1985; Molina-Garza et al., 1989; Lucas and Anderson, 1993).

Mesozoic Erathem

Triassic deposits

No Triassic deposits were mapped in this quadrangle. Bachman (1980) mapped a collapse feature containing Triassic material; however, subsequent 1:24,000-scale mapping did not confirm its presence (Dehler and Pederson, 1998). Vine (1963) mapped Triassic deposits to the east of the northeastern map area in Bulletin 1141B, the Geologic Map and Section of the Nash Draw Quadrangle.

Cretaceous outlier deposits

Cretaceous karst-collapse deposits are found at nine separate outcrop locations on the Gypsum Plain in the Delaware Basin and in the Black River valley. More are likely to exist and could probably be identified using remote sensing with spectral imagery, combined with field verification. The deposits consist of sands, conglomerates, limestones, and siltstones of late Lower Cretaceous age assigned to the Washita Group (Lang, 1947; Scott et al., 1978; Kues and Lucas, 1993). The fauna (e.g., **Fig. 22**) observed in these outcrops is part of the Caribbean faunal province, which is separate from assemblages found to the north of Lovington (Kues and Lucas, 1993). Some hesitancy in the late Albian age designation was expressed by Kues and Lucas (1993), who believe that these deposits could be older due to the age ranges of constraining species. The mechanics of karst collapse that led to these sediments being preserved on the Gypsum Plain is unclear; possibilities include accumulation in depression-fill pits, cave collapses, and fissure fill (Lang, 1947; Hayes, 1964, Bachman, 1980; McKnight, 1986; Allen and Attia, 2021; Allen, 2024). Detrital sanidine $^{40}Ar/^{39}Ar$ samples are currently being processed to provide maximum depositional ages and provenance for these deposits that may help to constrain the age of and provide depositional context for conditions that separate this Caribbean faunal population from northern faunal groups.

Figure 22: An echinoderm fossil found among collapsed clastics and carbonates of Cretaceous sediments.

Cenozoic Erathem

The Cenozoic geologic history within the stratigraphic record of the Carlsbad 30x60-minute quadrangle starts with collapses of Cretaceous strata into karst systems on the Gypsum Plain and the intrusion of intermediate-mafic dikes and sills into Permian sediments in the Yeso Hills. Besides these two features, there is a distinct absence of strata in the Cenozoic before the start of Rio Grande rift extension. Exposures of the lower Gatuña Formation are inferred to be middle Miocene in age based on geochronology south of the quadrangle. It is difficult to distinguish the deposition of the Gatuña Formation apart from the east-flowing High Plains Ogallala piedmont alluvium system until stream capture reorganization and establishment of the ancestral Pecos River as a regional base level. Deposition of the Gatuña Formation and equivalent-aged sediments continued until the late middle-Pleistocene as basin-fill deposits and piedmont alluvium in the Pecos River valley and along the reef escarpment. Once the modern Pecos River entrenched below the level of the formation capping Mescalero paleosol, aggradation and cut-fill deposits of this basin-fill unit ceased and deposition of other surficial map units began, continuing to the present day.

Intrusive rocks

Intrusive rocks only occur in one area of this quadrangle, in the Yeso Hills, on the western side of the Gypsum Plain. These rocks were dated to 34.45 ± 0.28 Ma by Attia and Ricci (2023) and are suggested to be part of a greater trend of cordilleran magmatic peripheral belt. The textural and mineralogical characteristics of this map unit are described in the description of map units based on a host of sources (King, 1948; Pratt, 1954; Hayes, 1964; Calzia and Hiss, 1978; Allen and Attia, 2021; Attia and Ricci, 2023). Additional intrusives are found within well logs, and karst-collapse deposits containing igneous material have been observed on the Gypsum Plain (Calzia and Hiss, 1978). A sample from a suspected karst-collapse deposit of igneous material returned an $^{40}Ar/^{39}Ar$ geochronology emplacement age, using incremental heating of groundmass, of 28.167 ± 0.29 Ma. This age appears to be distinct from the in-situ intrusives mapped nearby; however, little context is available as the sample was found in subcrop and no outcrop was observed.

Relic deposits of the Neogene

Remnants of Neogene-aged rock in montane settings of this quadrangle were not mapped because their location was not identified and their correlation to the Neogene was not confirmed. Skotnicki and Knight (2021) mapped Tertiary sedimentary deposits in the Brokeoff Mountains along the southern quadrangle border in Texas in OFR-610. The mapped deposits are interpreted to be faulted synchronously to or after deposition (Skotnicki and Knight, 2021). The possibility of Neogene-aged sedimentary deposits in the Brokeoff Mountains and Guadalupe Mountains should be considered despite their absence on this map.

Basin-fill and surficial deposits

Deposits outlined in the following sections are ordered chronologically, beginning with the Gatuña Formation, interpreted as Cenozoic basin fill of the ancestral Pecos River system deposited prior to downcutting of the modern Pecos River. The late middle-Pleistocene to early

late-Pleistocene entrenchment of the modern Pecos River provided ample sands for the deposition of the Mescalero Sands (or Los Medaños Sands) on the Mescalero Plains, where buried paleosols preserve a climatic history of temperature and precipitation fluctuations through the late Pleistocene and Holocene (Hall and Gobble, 2023). Fluvial terraces and fill deposits of the late Pleistocene are preserved in the Pecos River, its tributaries, and minor washes. In the mountains, debris-flow deposits, colluvium, minor landslides, and alluvium were all deposited in narrow valleys cut into Permian carbonates. In the Salt Basin, an ephemeral lake persisted through the last glacial maximum when it dried up, was scoured by wind, and replaced by inset alkaline playa deposits.

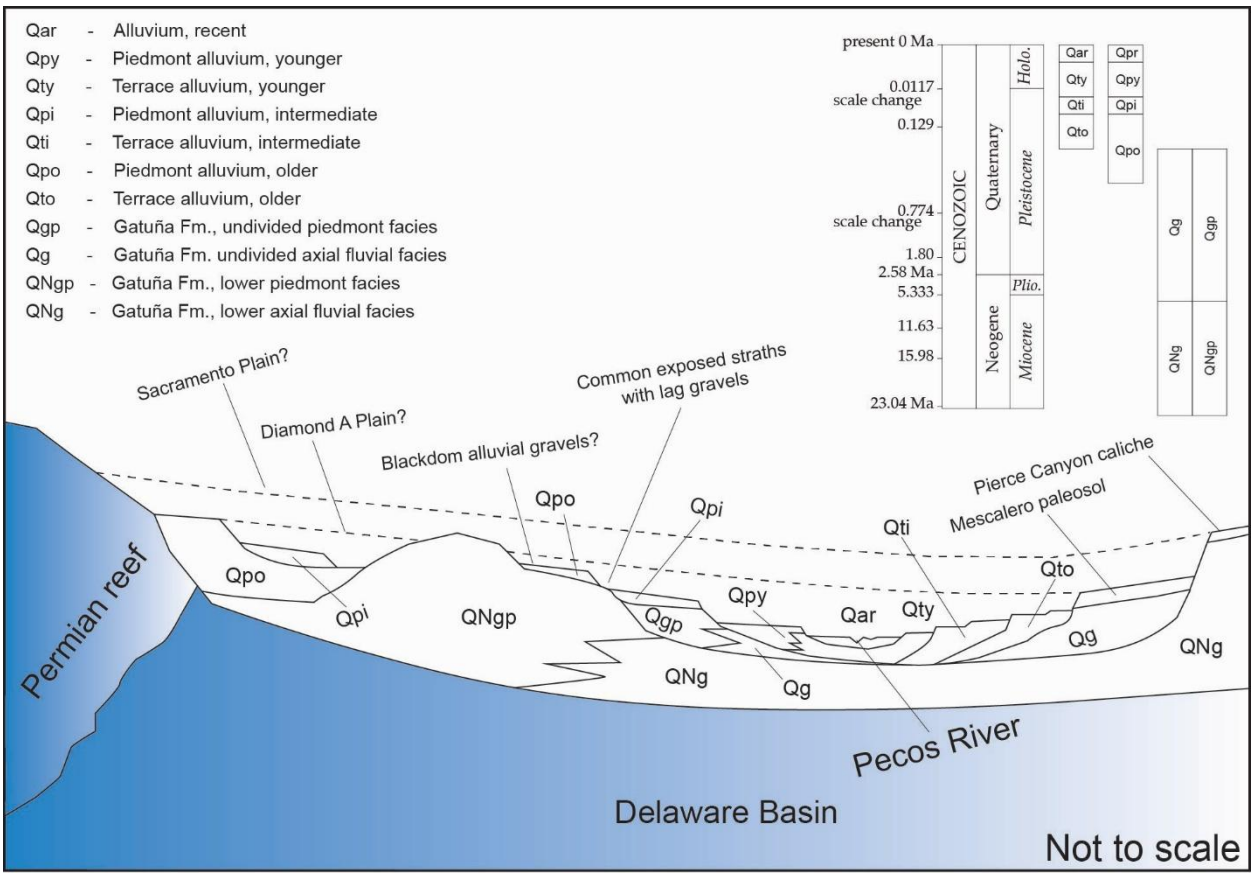

Figure 23: Idealized schematic of piedmont and channel alluvium units, including the ancestral Pecos River system basin-fill deposits.

Alluvial fan deposition is common, generally emanating from small, steep drainages along the reef escarpment and in the Brokeoff Mountains. Alluvial units (**Fig. 23**) in this quadrangle are split into five groupings: channel alluvium, piedmont alluvium, fan alluvium, sheetwash alluvium, and ancestral Pecos River system basin-fill deposits. Channel alluvium includes active channels, floodplains, reactivated terraces, and abandoned terraces in the Pecos River and its tributaries. Piedmont alluvium occurs below mountain escarpments in broad, coalesced, distributed fan and alluvial systems, with channel gradients and geomorphic surfaces steeper than channel alluvium and less steep than fan alluvium. Fan alluvium is mapped where high-energy transport of clastic material exits small catchments to meet valley

floors, creating steep, lobate, alluvial deposits that may aggrade or incise depending on location. Sheetwash alluvium is restricted to low-energy alluvial washes with dominantly aggradational characteristics. Figure 23 portrays an idealized schematic of landscape position and correlations between map units, petrocalcic soils, and geomorphic surfaces. Note that much uncertainty exists in correlations between older piedmont alluvium, the Gatuña Formation, and related soils and geomorphic surfaces (e.g., the Pierce Canyon caliche and Mescalero paleosol, described in detail below). Local sinkhole-related subsidence allowed for accumulation of closed depression-fill deposits, while regional subsidence affected trends in fluvial incision. Anthropogenic deposits dot the landscape as an unmistakable impression of humanity's mark in the Quaternary geologic record.

Basin fill of the ancestral Pecos River system: the Gatuña Formation

The Gatuña Formation has been a subject of controversy in the region and still requires a satisfying place in stratigraphic nomenclature, an understanding of its role in landscape history based on its internal stratigraphy, and improved temporal constraints, particularly on the end of deposition. Prior studies have built a wealth of data and mapping that this report will summarize and combine with new field observations and geochronological constraints to provide clarity on the formation's regional significance and evolution. The primary subjects of discussion in this section will be: the aggradation and incision history as interpreted by stratigraphic relationships between petrocalcic horizons and geomorphic surfaces; how these observations can be used to define mappable formation subunits; the possible existence of a piedmont facies along the Guadalupe Mountain front and its relationship to the standard basin-fill Gatuña Formation deposits; and the timing and differentiation of the Gatuña Formation from the Orchard Park terrace suite.

Figure 24: Valley-margin deposits of the lower Gatuña Formation in Pierce Canyon.

The Gatuña Formation (**Fig. 24**) represents basin-fill deposits in the Pecos River valley, extending from east-central New Mexico southward through this map area and into west Texas. The formation contains axial sands and gravels in cut-fill channels, muds in overbank facies with sand splays, and paludal evaporite deposits. The paleogeography of the Gatuña formation (**Fig. 25**) is discussed by Cather and Heizler (2023), who use detrital geochronology and provenance analysis in concert with paleocurrent measurements to investigate the northward drainage direction of the ancestral Pecos River system. Cather and Heizler (2023) support a north-flowing drainage for the ancestral Pecos River that may have continued until entrenchment of the south-flowing modern Pecos River. However, Hoagstrom et al. (2025) only support the notion of norward flow during the Miocene based on the genetic history of certain fish species across the Great Plains region. By the late Pliocene to early Pleistocene, stratigraphic and genetic evidence indicate that the Pecos River became endorheic in this area as fish speciated into endemic populations separate from their relatives in rivers to the north (Hill, 1996; Hoagstrom et al., 2025).

Age	Method/Phase	Formation/Target	Notes
90.7±6.7 ka	optically stimulated luminescence; quartz	Berino paleosol in Los Medaños Sands	***Hall and Gobble (2023)***. Postdates late Mescalero paleosol development in subsidence trough.
143±8.0 ka	optically stimulated luminescence; quartz	Mescalero paleosol of Gatuña Fm.	***Hall and Gobble (2023)***. Predates late Mescalero paleosol development in subsidence trough.
169±14 ka	uranium-series; calcite(?) in fossil	Orchard Park terrace	***Rosholt and McKinney (1980)***. Tentative evidence of a south-flowing system by MIS-6 if date and unit are accurate.
<210 to >50 ka	relative dating using fossil correlation	Orchard Park terrace	***Morgan and Lucas (2005)***. *Mammuthus* and *Bison Sp.* of Racholabrean age from inset terrace. Too old for C-14.
208±18 ka	uranium-series; calcite	Mescalero paleosol of Gatuña Fm.	***This study (2025)***. Minimum age for pedogenic calcite precipitation in Mescalero paleosol development.
328±21 ka	uranium-series; calcite	Mescalero paleosol of Gatuña Fm.	***This study (2025)***. Minimum age for pedogenic calcite precipitation in Mescalero paleosol development.
330±75 ka	uranium-series; calcite	Berino paleosol in Los Medaños Sands	***Rosholt and McKinney (1980)***. Date on Berino paleosol overlying Mescalero paleosol. Unclear accuracy.
420±60 ka	uranium-series; calcite	Mescalero paleosol of Gatuña Fm.	***Rosholt and McKinney (1980)***. Minimum age for pedogenic calcite precipitation in intermediate Mescalero paleosol.
530±330 ka	fission track dating; zircon	Lava Creek B ash in Gatuña Fm.	***Izett and Wilcox (1982)***. Original date for Lava Creek B ash in Nash Draw. Not accurate, reevaluated.
570±110 ka	uranium-series; calcite	Mescalero paleosol of Gatuña Fm.	***Rosholt and McKinney (1980)***. Minimum age for early calcite precipitation in Mescalero paleosol.
<600 to 420 ka	relative dating using soil indices	Mescalero paleosol of Gatuña Fm.	***Hawley (1993)***. Stage IV-V paleosol interpreted to be mid-Pleistocene, bracketed by existing dates.
630.9±1.2 ka	argon-argon; sanidine	Lava Creek B ash in Gatuña Fm.	***Jicha et al. (2016)***. Single Crystal Fusion (SCF) argon-argon date from *Jicha et al. (2016)*.
740±30 ka	argon-argon; detrital sanidine	Gatuña Formation	***Cather and Heizler (2023)***. Maximum depositional age (MDA) of sanidine grain in fluvial Gatuña Formation.
~1.6 to 0.21 Ma	relative dating using fossil correlation	Gatuña Formation	***Morgan and Lucas (2005); Miller (1982)***. Shad fossil with uncertain correlation: Blancan or Irvingtonian NALMA age.
1.32±0.02 Ma	argon-argon; detrital sanidine	Gatuña Formation	***Attia et al. (2023).*** Maximum depositional age (MDA) of sanidine grains in Gatuña Fm below Lava Creek B ash.
>2.58 Ma	relative dating using soil indices	Pierce Canyon caliche of Gatuña or Ogallala Fm.	***Hawley (1993)***. Stage VI paleosol interpreted to be Neogene based on soil profile development indices.
3.98±0.13 Ma	argon-argon; alunite and natroalunite	Speleothems in cave deposits	***Polyak et al. (1998)***. Dates speleogenesis at 1120 m in Guadalupe Mnts. as proxy for uplift above water table.
5.4±0.03 Ma	argon-argon; alunite and natroalunite	Speleothems in cave deposits	***Polyak et al. (2023)***. Dates speleogenesis at 1210 m in Guadalupe Mnts. as proxy for uplift above water table.
11.2±0.17 Ma	argon-argon; alunite and natroalunite	Speleothems in cave deposits	***Polyak et al. (2006)***. Dates speleogenesis at 2010 m in Guadalupe Mnts. as proxy for uplift above water table.
13.0±0.6 Ma	potassium-argon; volcanic glass	Ash of Yellowstone hot spot in Gatuña or Ogallala Fm.	***Powers and Holt (1993)***. Tentative to uncertain date due to ineffectiveness of K-Ar with volcanic glasses. Off map.

Table 2: Compiled and new geochronology and relative dates pertaining to the Gatuña Formation.

The Gatuña Formation is capped by petrocalcic horizons of varying stages of development, referred to by previous mappers as the Mescalero paleosol or Pierce Canyon caliche. Typically, soils of these units contain a <0.5-m-thick undulatory-tabular zone of nearly pure carbonate that is composed of tabular bands averaging around 10 cm thick. Beneath the undulatory-tabular zone is a 0.5- to 1-m zone of massive, cemented carbonate that may be fractured and recemented in a 3–5 m zone due to subsidence (Attia and Allen, 2022). This zone grades downward, with decreasing levels of carbonate and increasing proportions of parent material, occasionally terminating abruptly. These petrocalcic horizons commonly form in poorly sorted, well-rounded, gravels of variable lithologies, but is also observed in bedrock and fine-grained sediments.

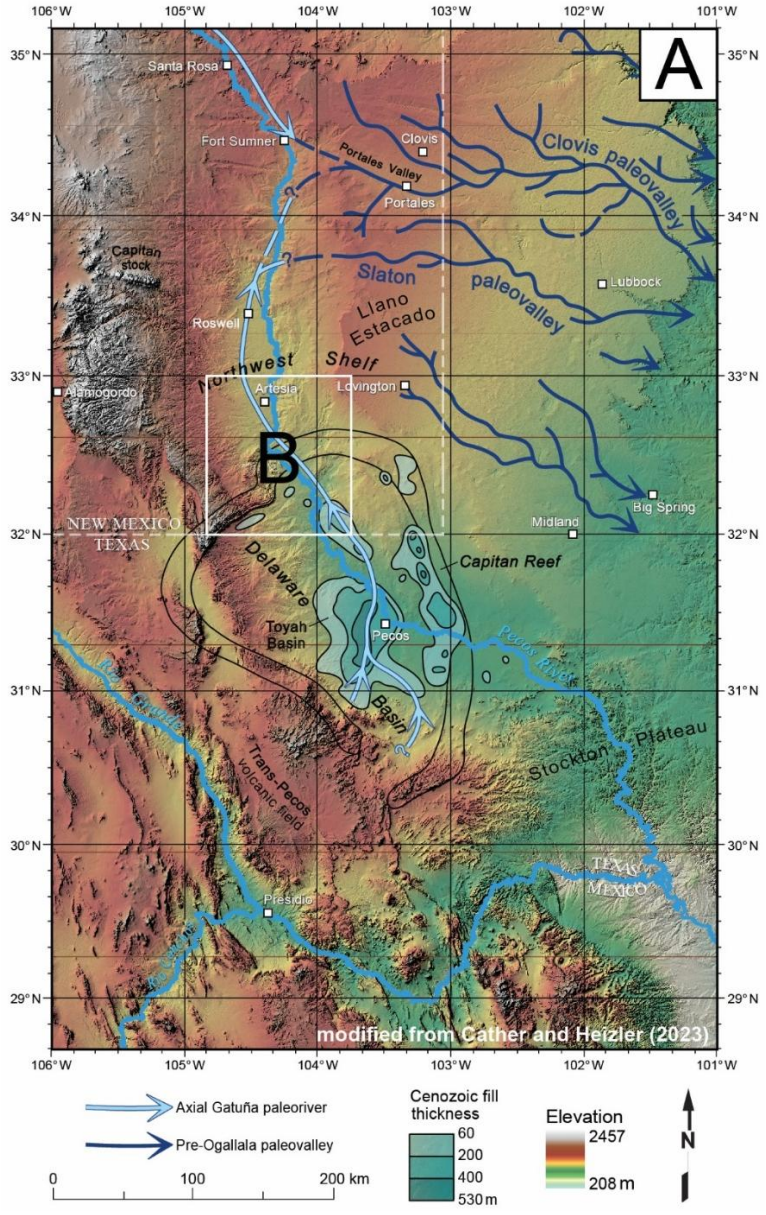

Figure 25: Map modified from Cather and Heizler (2023) showing paleoflow directions of Miocene (?) drainage systems (Krupnick et al., 2025).

The variability in the formation-capping petrocalcic horizon introduces the primary subject of controversy regarding the Gatuña Formation's evolution and field identification. Two petrocalcic horizons have been described capping the Gatuña Formation (**Table 2**, **Fig. 30**): a stratigraphically lower (topographically elevated; see **Fig. 23**) aggradation-dominated unit (lower Gatuña, map unit QNg) of Quaternary–Neogene age capped by a Stage V to VI petrocalcic horizon, termed the Pierce Canyon caliche by Hawley (1993). The second designation is an upper cut-fill unit of Quaternary age (upper Gatuña, map unit Qg) capped by a Stage IV to V petrocalcic horizon, termed the Mescalero paleosol. This report proposes that the Pierce Canyon caliche be grouped as temporally equivalent to the Mescalero paleosol, but simply developed on a topographically higher, and stratigraphically lower, spectrum of the Gatuña sequence associated with the end of net aggradation. To reflect this amendment, this report places all Gatuña capping petrocalcic horizons as the Mescalero paleosol but acknowledges a lower Quaternary–Neogene-aged petrocalcic horizon (Pierce Canyon caliche) and an upper Quaternary-aged portion (the Mescalero paleosol) because efforts to clarify the age relationship controversy neither supported nor ruled out a Neogene age for the earliest petrocalcic horizons (i.e., Hawley, 1993; Cikoski, 2019b, 2020). Age correlations presented in the map are queried pending further geochronologic data targeted at resolving the age of the geomorphic surface containing the Pierce Canyon caliche. Below, we discuss the known geochronological constraints on these various deposits and summarize new geochronology.

The proposed Neogene age for the start of lower Gatuña Formation deposition is loosely supported by existing geochronology (**Table 2**) from a potassium-argon (K-Ar) date by Powers and Holt (1993) on volcanic glass from an ash layer, dated to 13.0 ± 0.6 Ma, in fluvial facies south of the quadrangle near Orla, Texas. The middle Miocene age of these sediments suggests they are temporally equivalent to the Ogallala Formation, which is found nearby. Distinction between the two is primarily based on location, with the Gatuña Formation found within the Pecos River valley rather than on the high plains that form the Llano Estacado (**Fig. 26**). Additional evidence for the deposition of basin-fill sediments in the ancestral Pecos River valley throughout the Miocene is offered by records of uplift in the adjacent Guadalupe Mountains based on the timing of cave speleogenesis. Polyak et al. (1998, 2006, 2023) obtained argon-argon ($^{40}Ar/^{39}Ar$) dates, including those at 11.2 ± 0.17, 5.4 ± 0.03, and 3.98 ± 0.13 Ma at elevations of 2010, 1210, and 1120 m, respectively, in cave systems of the Guadalupe Mountains. These dates show how the mountains were progressively raised relative to the water table, allowing for dissolution and removal of material to form caves and the precipitation of the alunite and natroalunite samples used to constrain the timing of uplift (Polyak et al., 1998, 2006, 2023). As the mountains were exhumed by tilting from Rio Grande rift-related uplift, sediments were shed eastward down the dipslope of the range into either the Ogallala depositional system, or as Gatuña Formation sediments in the ancestral Pecos River valley.

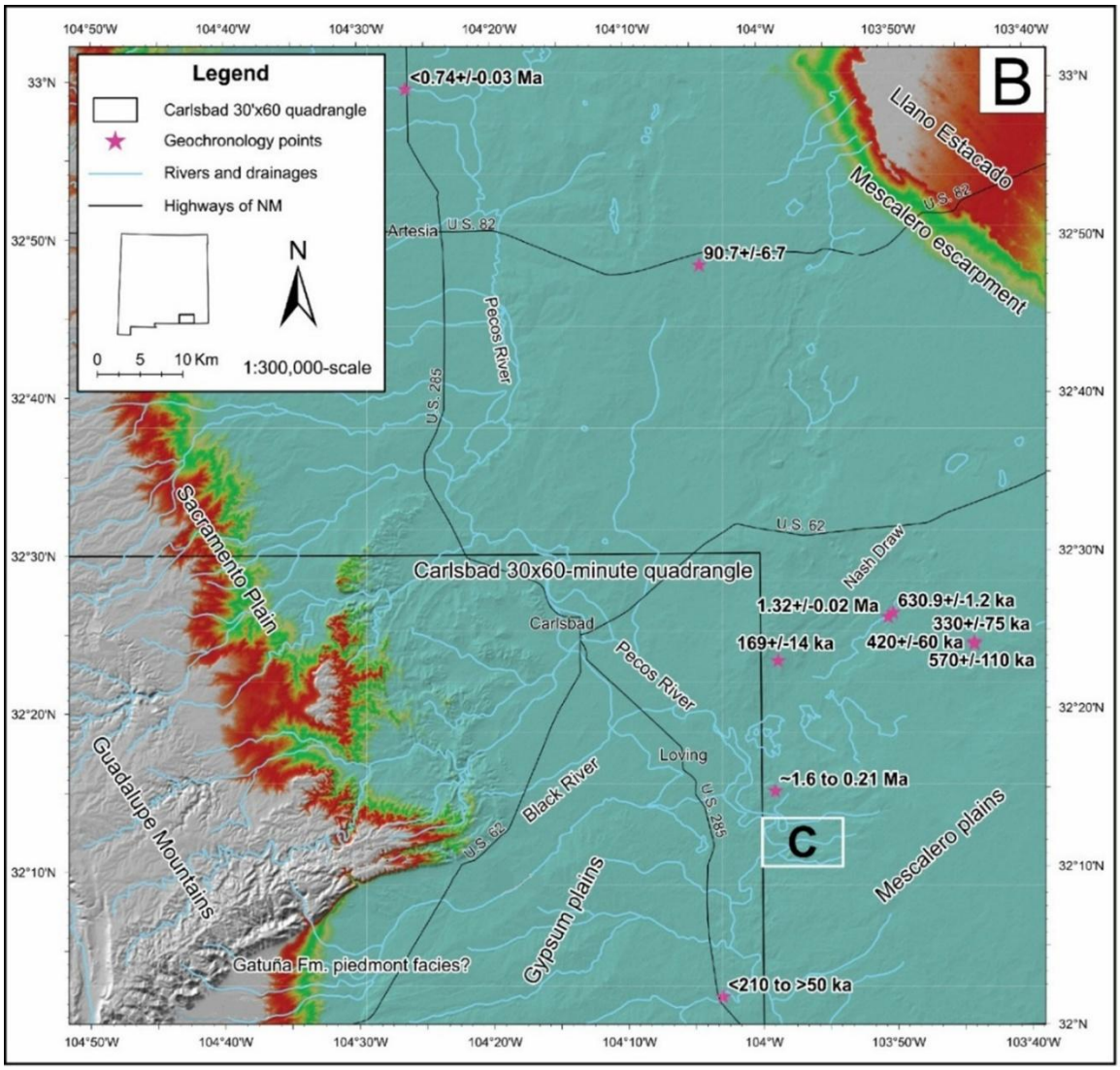

Figure 26: Regional map showing locations of geochronology and relative dating points. Includes inset of map 'C' containing compiled and new geochronology and relative dating points. Powers and Holt's (1993) date of 13.2 ± 0.02 Ma on an ash layer within fluvial facies of the Gatuña is located at approximately 31.68545° N, -103.68702° W NAD83, off the extent of this figure.

The ideal location to interpret this stratigraphic relationship of the petrocalcic horizons and investigate the proposed Quaternary–Neogene timing of early Mescalero paleosol development is at Pierce Canyon (**Fig. 27**), just east of the southeastern side of the Carlsbad 30x60-minute quadrangle where the term Pierce Canyon caliche was first used. In Pierce Canyon, Hawley (1993) observed an exceptionally well-developed Stage V to VI petrocalcic horizon that he considered to be Neogene in age and equivalent to the caprock of the Ogallala in the High Plains region. He also noted a distinct Stage IV to V petrocalcic horizon present on the northern rim of Pierce Canyon, which he differentiated and identified as the Mescalero paleosol. Cikoski (2019b, 2020) supported this sentiment and differentiated between a lower and upper Gatuña Formation based on the underlying or inset relations to petrocalcic soils of different degrees of development (**Fig. 30**). In contrast, Attia and Allen (2022) documented a

single petrocalcic horizon, which wrapped around the entire eastern rim of Pierce Canyon. Thus, they considered only the Quaternary-aged Mescalero paleosol to be present in the Pierce Canyon area. The sediments stratigraphically below the Mescalero paleosol were considered by Attia and Allen (2022) and Attia et al. (2023) to be entirely Quaternary-age based on a 1.32 ± 0.02 Ma $^{40}Ar/^{39}Ar$ maximum depositional age of detrital sanidine in Gatuña Formation sediments, and the stratigraphic position of those sediments below the Lava Creek B ash at Livingstone Ridge just northeast of Pierce Canyon (first described by Bachman, 1980). The first reported geochronologic date for this ash was 530 ± 330 ka by Izett and Wilcox (1982), which was reevaluated to 630.9 ± 1.2 ka by Jicha et al. (2016) based on a single-crystal fusion date. The presence of Quaternary grains below the cut-fill deposit, in which the Lava Creek B ash was preserved, suggests that the Gatuña Formation is of Quaternary rather than Neogene age above and below the depositional unconformity that may represent a contact between upper Gatuña Formation and the lower Gatuña Formation aggradation deposits.

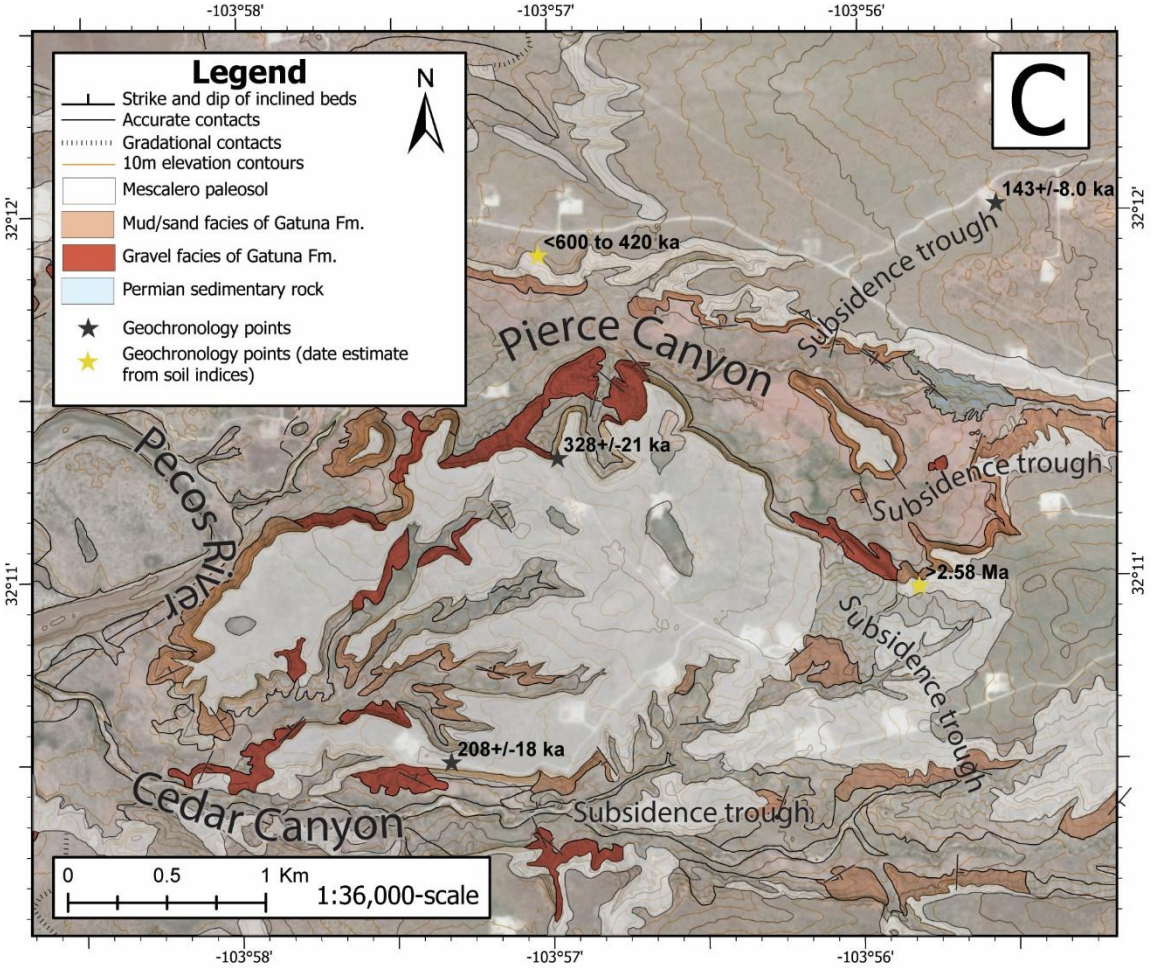

Figure 27: Map of Pierce Canyon area with new and compiled geochronology and relative dating points. Dates with '<' and '>' are relative dates based on soil development indices of Giles and Hawley (1981) and observations of Hawley (1993).

A fish genetics paper by Hoagstrom et al. (2025) investigated the history of the Pecos River, including the timing of its southward integration into the Rio Grande. In the late

early-Pleistocene to early middle-Pleistocene, before the deposition of the Lava Creek B ash, the downriver integration of the Rio Grande to the ultimate base level (sea-level) caused a base level drop in the lower Pecos River where it entered the Rio Grande as a tributary (Hoagstrom et al., 2025). Headward erosion initiated in the lower Pecos River causing northward incision towards the ancestral Pecos River in the region of the Carlsbad 30x60-minute quadrangle (Hoagstrom et al., 2025). The timing and occurrence of this event is based on the start of genetic interaction between two distinct endemic populations of fish: the Capitan area of endemism around the Carlsbad quadrangle and the Devils area of endemism of the lower Pecos River in Texas (Repasch et al., 2017; Hoagstrom et al., 2025). This integration could demark a switch from aggradation in the Quaternary–Neogene lower Gatuña Formation to incision and cut-fill deposition in the Quaternary upper Gatuña Formation.

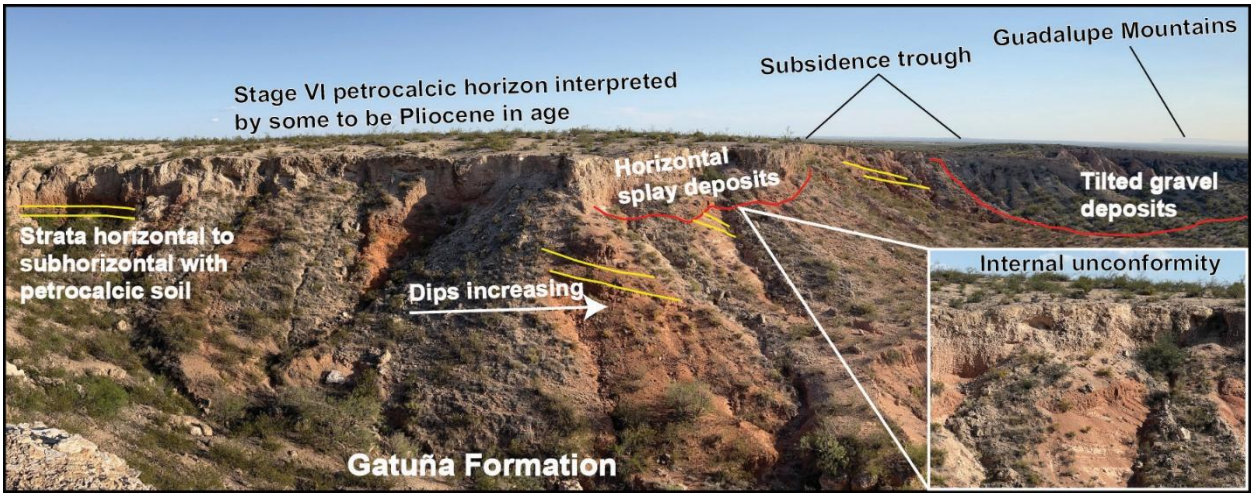

Figure 28: Annotated photo of Stage VI petrocalcic horizon on the south rim of Pierce Canyon taken from 32.18410° N, -103.92916° W NAD83.

Hall and Goble (2012, 2023) used two optically stimulated luminescence (OSL) dates to bracket the age of a petrocalcic soil, thought to be the Mescalero paleosol; however, field observations from one of the sampling locations indicated that the petrocalcic horizon may be developed in sheetwash alluvium fill postdating the Mescalero paleosol. At this location, in a subsidence trough on the northeastern side of Pierce Canyon, they assigned a tentative age of 143 ± 8 ka to Gatuña Formation sediments below the petrocalcic horizon (**Fig. 27**, **Table 2**). Eolian sands, above a similar petrocalcic horizon, in a subsidence trough north of the Carlsbad 30x60-minutes quadrangle (**Fig. 26**), were dated to 90.7 ± 6.7 ka (**Table 2**). If the soils bracketed by these dates were the Mescalero paleosol, it would provide a constraint on the minimum age for Gatuña Formation deposition. In this landscape, subsidence troughs seem to act as conduits for surface flow that may scour petrocalcic horizons and allow for the development of subsequent calcic soils adjacent to more-developed soils on older geomorphic surfaces. In this location we believe Hall and Goble (2023) observed a separate, younger, paleosol as it only exhibited Stage III carbonate development, which is less developed than the Stage IV to V horizons on the north rim of Pierce Canyon, and far less developed than the Stage V to VI horizon on the eastern side of the southern Pierce Canyon rim. Regardless, in that solution subsidence trough at Pierce Canyon, their data place the most probable period of calcic soil

precipitation during the dry and hot Marine Isotope Stage 5 (MIS-5) interglacial, indicating rapid development of this soil (Hall and Goble 2012; 2023). The presence of exceptionally arid conditions during this time in this region is supported by Railsback et al. (2015), who observed a lack of stalactite precipitation during the MIS-5 interglacial using $d^{18}O$ isotopes and uranium-series dating methods on precipitated calcite from a cave in the Guadalupe Mountains. The dry nature of this interglacial may contribute to the faster than usual development of a Stage III petrocalcic horizon in these young sediments that likely postdate the Gatuña Formation (Giles and Hawley, 1981).

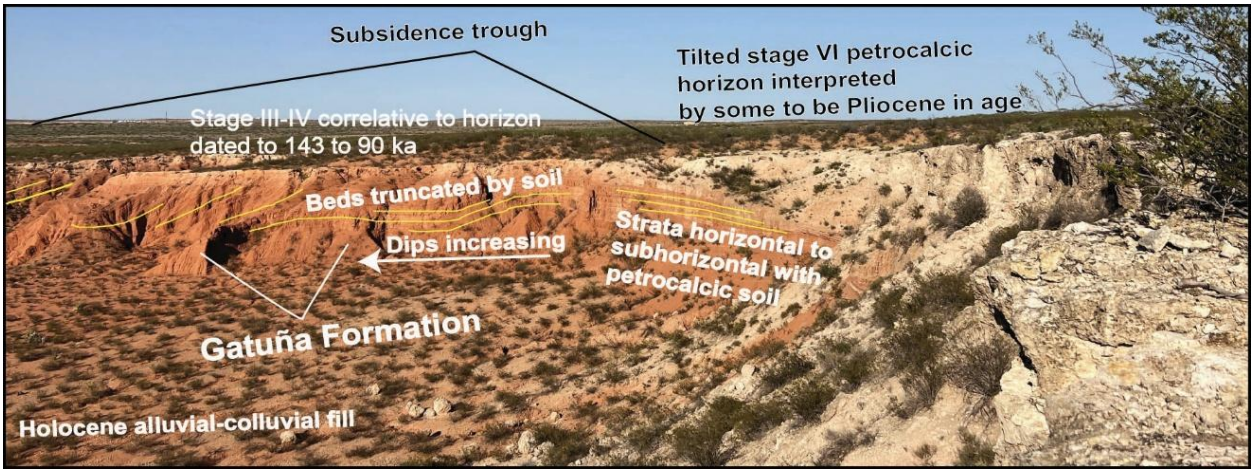

Figure 29: Annotated photo of Stage VI petrocalcic horizon on the south rim of Pierce Canyon being truncated by a Stage IV petrocalcic horizon developed in a subsidence trough (32.18440° N, -103.92843° W NAD83).

The maximum age for the inception of soil development, within the formation capping Mescalero paleosol, seems to be bracketed by the deposition of the Lava Creek B ash at 630 ± 1.2 ka (Jicha et al., 2016) and minimum precipitation dates of calcite in the soil. Uranium-series dates of 570 ± 110 and 420 ± 60 ka from Rosholt and McKinney (1980) support development of the Mescalero paleosol from the MIS-15 to the MIS-11 interglacial, with burial and development of the Berino paleosol (which lies above the Mescalero paleosol in Nash Draw) dated at 330 ± 75 ka during the MIS-9 interglacial. However, it is likely that the OSL date of Hall and Goble (2023) is more accurate for the age of the Berino paleosol, while the ages from Rosholt and McKinney (1980) are artificially old due to the incipient age of uranium-series methods when the samples were run.

The fossil record is an additional line of evidence helping to constrain the timing of the end of Gatuña Formation deposition and Mescalero paleosol development. **Table 2** shows fossils of tentative late middle Pleistocene (MIS-6) age from uranium-series dating by Rosholt and McKinney (1980) on bones that were found northwest of the map area in Nash Draw (**Fig. 26**). However, it is unclear whether the fossils were eroded from the Gatuña Formation or an inset terrace, and the date of these fossils is therefore unable to support Gatuña Formation deposition during the MIS-6 glacial. Because they could not be dated using radiocarbon methods, these fossils found in Gatuña Formation or subsequent terrace suites (i.e., the Orchard Park terrace suite) were inferred to date to the Rancholabrean North American fauna age

between 250 ka to ~50 ka (Morgan and Lucas, 2005). Neither of these fossil occurrences can precisely constrain an age for the end of Gatuña Formation deposition due to uncertainty in age of the fossil and identification of the deposit they were found in. Fossil or geochronological age constraints found within the Gatuña Formation that postdate MIS-7 would constrain its age to younger than what is currently understood by the literature and new data presented in this report.

Sample	^{238}U conc (ppb)		^{232}Th conc (ppt)		^{230}Th/^{232}Th (activity)		^{230}Th/^{238}U (activity)		δ^{234}U (measured)		δ^{234}U (initial)		age (uncorrected)		age (corrected)	
0716-2A-p1	366.3	± 2.3	168816	± 406	11.91	± 0.04	1.7964	± 0.0123	648	± 4	1725	± 67	351961	±13764	**346948**	**±13468**
0716-2A-p2	333.8	± 0.3	139963	± 209	12.98	± 0.04	1.7810	± 0.0046	658	± 2	1631	± 24	326274	±4633	**321555**	**±5055**
0716-2A-p3	333.8	± 0.3	166646	± 103	11.01	± 0.02	1.7461	± 0.0040	621	± 2	1582	± 25	336961	±4689	**331386**	**±5284**
0716-2A-p4	383.9	± 0.9	281604	± 526	7.66	± 0.04	1.8394	± 0.0089	627	± 2	2211	± 131	453397	±21072	**446586**	**±20319**
0716-3A-p1	545.0	± 0.4	150640	± 341	15.62	± 0.05	1.4130	± 0.0031	536	± 2	946	± 8	205830	±1462	**201630**	**±2519**
0716-3A-p2	515.7	± 0.5	97588	± 110	22.37	± 0.06	1.3853	± 0.0035	534	± 2	923	± 7	196560	±1452	**193663**	**±2023**
0716-3A-p3	589.5	± 0.6	47658	± 69	54.85	± 0.14	1.4509	± 0.0034	547	± 2	1002	± 7	215817	±1664	**214636**	**±1750**
0716-3A-p5	729.9	± 0.5	100066	± 96	32.34	± 0.07	1.4509	± 0.0032	536	± 2	993	± 7	220405	±1678	**218387**	**±1934**

Table 3: Raw data of Mescalero paleosol samples from the Radiometric Isotope Laboratory at the University of New Mexico. The weight of each subsample piece is less than 200 mg. Corrected ages in years before present (yr BP) use the ^{230}Th/^{232}Th atomic ratio value of 0.0000044 ± 50%. All errors are reported as absolute 2σ. All ratios are activity ratios. Decay constants used are 9.1705 × 10-6 for ^{230}Th and 2.82206 × 10-6 for ^{234}U (Cheng et al., 2013). δ^{234}U, reported as per milliliter (‰), = ([^{234}U/^{238}U]/[^{234}U/^{238}U]SE -1) × 1000, where [^{234}U/^{238}U] is the activity ratio and SE is secular equilibrium. yr BP is years before 2024 CE.

To continue deciphering the stratigraphic context of these deposits and soils, the authors returned to the Pierce Canyon 7.5-minute quadrangle to inform field observations within the Carlsbad 30x60-minute quadrangle. Guidance from Dr. John Hawley helped identify the specific outcrop that he considered to be Stage VI and of Neogene age, equivalent to the Ogallala caprock (**Figs. 28 and 29**). At this location, a solid 7- to 8-m-thick soil with a conformable relationship to underlying valley-margin strata was observed. The soil grades upward over the course of 4 m from pedogenic nodules into a solid plugged horizon capped by a 0.5- to 1-m laminar and undulatory carbonate that had an additional 1–2 m of petrocalcic soil subcrop on the erosional surface above it. Moving laterally in either direction, the dip of the angular unconformity between underlying beds and overlying soils increased from subhorizontal up to approximately 15°. In Figure 28, moving westward, away from the conformable soil and underlying sediments, dips increase, soils gradually thin and decrease in maturity, while the presence of internal angular unconformities with channel sands and gravels increased.

Scouring and subsequent soil development in solution subsidence troughs supports diachronous development of soils throughout the middle Pleistocene. To the north side of the Stage VI petrocalcic horizon, erosion truncates the soil within a subsidence trough grading toward the Pecos River in which subsequent soil development can be observed. It is at this transition from the well-developed Stage VI to the moderately developed Stage III to IV soil in the subsidence trough that a change from a conformable to an angular relationship between the soils and sediments is observed in tandem with the decrease in soil maturity; this type of relationship is hypothesized to explain the presence of the soil and sediments dated by Hall and Goble (2012; 2023). There is no increase in abundance of gravel-filled channels and internal

angular unconformities at this location because the subsidence trough is still active in the present day and only exhibits low-energy sheetwash flow. However, at the location shown in Figure 28, the subsidence channel may have developed concurrent with the ancestral Pecos River system, resulting in the observed channel deposits. Regardless, the processes remain constant: localized subsidence from dissolution of underlying evaporite rocks promotes the development of elongate washes that grade to a lower base level. Tilting of beds, scouring of existing petrocalcic development, and new development of calcic soils occurs within these washes to the present day (**Fig. 29**). During Gatuña time, this localized subsidence likely resulted in channelization and higher-energy sediment transport capable of scouring the soil and depositing horizontally bedded sediments over beds tilted by the subsidence trough before abandonment and subsequent development of the petrocalcic horizons. Cikoski (2019b) presented very similar observations and a hypothesis about the relationships of soil development and solution subsidence trough erosion in the adjacent Malaga 7.5-minute quadrangle. Observations from across the region therefore support the presence of an extremely developed soil with a conformable stratigraphic relationship to the underlying strata and did not indicate an inset relationship between two different soils with a time gap representing millions of years.

To support these field relationships and enhance the current geochronologic dataset, we collected two uranium-series dates from soils on the south side of Pierce Canyon and the north side of Cedar Canyon to the south (**Fig. 27**). Samples were submitted to the Radiometric Isotope Laboratory at the University of New Mexico. Samples collected at the most mature soil location, with conformable relationships to underlying strata, could not be processed for uranium-series geochronology because the collected material was too porous to properly trap daughter products in the uranium series decay chain. However, 2 km to the west and 3 km to the southwest (**Fig. 27**), of the mature soil described by Hawley (1993) samples were collected for analysis from soils that were traceable to this outcrop. These soils were approximately Stage IV to V in development and had angular relationships with the underlying stratigraphy. On the south rim of Pierce Canyon (**Fig. 27**), a sample was dated to 328 ± 21 ka (n=4) from carbonate nodules in the lower portion of the soil profile. To the south, on the north rim of Cedar Canyon (**Fig. 27**), a sample from a laminar horizon was dated at 208 ± 18 ka (n=4). Data for these samples are viewable in **Table 3**. Our geochronology data supports a minimum development age of middle Pleistocene for soil development at this location with punctuated precipitation of calcite during the MIS-9 and MIS-7 interglacial periods.

Geochronology and relative dating of the Mescalero paleosol in the literature reports a range of dates through the middle Pleistocene that would support diachronous soil development due to scouring and redevelopment in solution subsidence troughs; meanwhile, no additional support is given for a soil profile with development starting in the Neogene. To further constrain the timing for the end Gatuña Formation deposition, solid evidence of MIS-6 age for subsequent river terraces (the Orchard Park terrace suite) would offer some support that the Pecos River entrenched and integrated southward during the MIS-7 or MIS-6 glacial period. This would support the notion that the petrocalcic soil constrained to MIS-5 by Hall and Goble

(2023) is genetically related to the Orchard Park terraces during a period of stability after downcutting below the Mescalero paleosol (Krupnick et al., 2025).

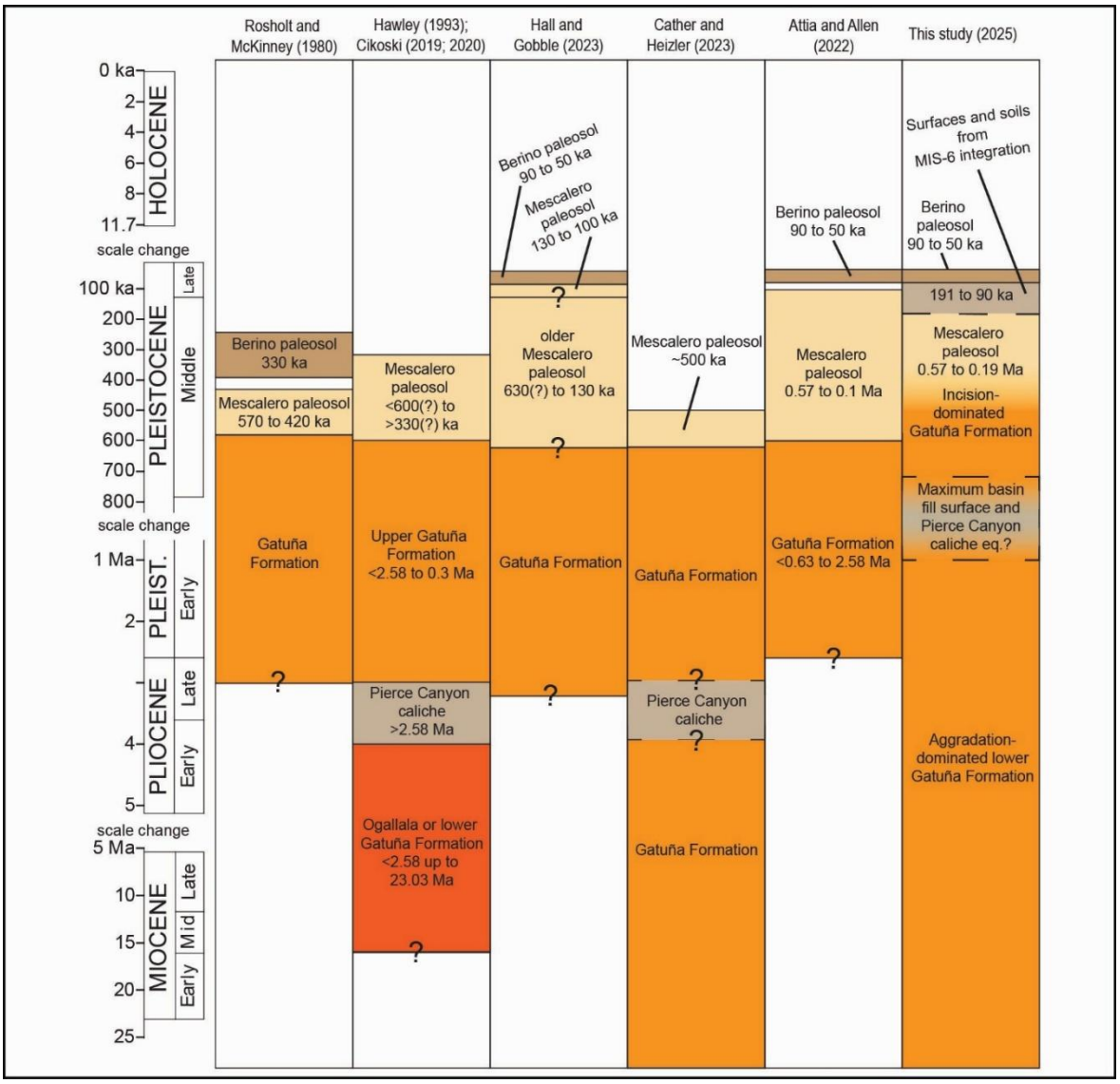

Figure 30: Stratigraphic correlation of the Gatuña Formation and its associated petrocalcic horizons.

To summarize, rather than the existence of a separate Neogene-aged soil horizon, discrepancies in geologic mapping seem to be a product of variability in soil development due to differences in geomorphic surface stability and deposition because of solution subsidence in the Delaware Basin throughout the late Cenozoic. We conclude that, based on the literature, the Gatuña Formation (**Fig. 30**) seems to have started depositing in a north-flowing system throughout the Miocene as uplift occurred on the periphery of the Rio Grande rift, exoreic deposition occurred into the Pliocene, and the Gatuña Formation aggraded until approximately 1–0.63, Ma at which point regional depositional trends shifted from aggradational to erosional, initiating downcutting of the Gatuña Formation. The existence of abnormally mature soil horizons, such as the Pierce Canyon caliche, likely represents the maximum aggradational surface of late early-Pleistocene to early middle-Pleistocene age. The ancestral Pecos River

system flowed southward through the middle- and late-Pleistocene, depositing upper Gatuña Formation sediments and developing petrocalcic soils on the Mescalero surface, which experienced localized and continued tilting, erosion, and development of calcic soils, with diachronous development observable through uranium-series geochronology ages. Landscape stability and hot, dry climates of the last major interglacial period (MIS-5) promoted rapid petrocalcic soil development; soils of that age are genetically related to inset deposits of the Orchard Park terrace suite rather than the Gatuña Formation and associated Mescalero paleosol.

Piedmont facies with tentative correlation to the Lower Gatuña Formation

Due to a lack of paleontological and direct geochronological age constraints, the timing of deposition for piedmont facies of the Gatuña Formation has been controversial, with some workers mapping them as the Blackdom terrace (Bjorklund and Motts, 1959), some placing them at or below the Quaternary–Neogene boundary (e.g., Cikoski, 2019a; Cikoski and Allen, 2020), while other workers map them as piedmont deposits of early to middle Pleistocene age coeval with Quaternary Gatuña Formation fluvial facies (Skotnicki and Attia, 2022; Allen and Skotnicki, 2024; Skotnicki and Allen, 2024). Piedmont facies are typically separated from the Gatuña Formation because direct field or geochronological evidence of their stratigraphic connection has not been established, and they do not represent the fluvial or valley-margin facies of the ancestral Pecos River that typically define the unit. This report reassigns these units as lower Gatuña Formation piedmont facies (map unit QNgp); however, this unit's correlation to the Gatuña Formation is tentative and is a topic for future work.

Fluvial and valley-margin facies of the Gatuña Formation are assumed to grade up slopes and interfinger with piedmont facies as fluvial facies shift to tributary piedmont alluvial deposits emanating from steep channels carrying locally derived sediments from the eastern side of the Gypsum Plains (**Fig. 26**). The Red Bluff 7.5-minute quadrangle (Cikoski, 2019b) maps mixed-composition Gatuña Formation deposits reaching up slopes and tributaries onto the Gypsum Plain before they are truncated by erosion, and we expect that these deposits once blanketed the Gypsum Plain not only in tributary channels but across its entire surface. The presence of gravels of Quaternary–Neogene age in collapse deposits on the western side of the Gypsum Plain indicates their presence across at least a portion of that area (Allen and Attia, 2021).

Figure 31: Lithified surface of a strath terrace cut into lower piedmont facies of the Gatuña Formation.

As described in more detail within the map unit description, these coarse conglomerate deposits are completely lithified by carbonate cement, form rounded knobs on the landscape west of the Black River, lack maximum-fill geomorphic surfaces, have few cut-fill features internal to the deposits, have rare to absent sand and muds facies, and are carved into strath terraces by piedmont alluvium erosion and sedimentation. Currently, no fossils or geochronology exists to constrain the age of these deposits, and no direct linkage to Gatuña Formation sediments (i.e., observed interfingering or grading between the two) was confirmed. The basal contact of the lower Gatuña piedmont facies (**QNg**) deposits overlies Lopingian basin strata, and they have been deposited with apparent high-energy aggradation and lack preserved geomorphic surfaces related to their maximum fill. Qualitatively, this suggests that these are associated with the basal Ogallala Formation (or Gatuña Formation in this area) erosional surface, which carved through existing sedimentary cover to underlying Permian evaporites and contributed to the initiation of dissolution-related subsidence in the Delaware Basin (Cather and Heizler, 2023). Uplift of the Guadalupe Mountains relative to the Delaware Basin during the Neogene (Polyak et al., 1998, 2006, 2023; Decker, 2018), combined with solution subsidence, would have created adequate drops in base level to support the continued high-energy aggradation that is suggested by their textural and stratigraphic characteristics. No maximum fill geomorphic surfaces are observable to date petrocalcic soils or analyze their height above the grade of the Pecos River.

Cikoski (2020) defines the differences of petrocalcic carbonate development and the cements in similar conglomerates for deposits on the eastern side of the Gypsum Plain in the Malaga 7.5-minute report. His observations suggest that unlike petrocalcic horizons, these gravels are not displaced, depositional features are preserved, and there is a lack of laminated or tabular soil horizons characteristic of well-developed soils (Cikoski, 2020). The ubiquitous groundwater derived carbonate cement that lithifies gravels throughout these deposits is inferred to have precipitated prior to the late middle-Pleistocene to early late-Pleistocene entrenchment of the Mescalero plain because aquifer conditions conducive to equal and pervasive cementation by groundwater would cease once these deposits were excavated to the level observed at the surfaces carved by older piedmont alluvium. Older piedmont alluvium commonly forms straths (**Fig. 31**) carved into these lithified deposits, leaving behind remnant deposits or gravel lags. We will submit samples of the carbonate cement in these deposits for uranium-series geochronology to obtain an age of cementation.

Channel alluvium: Orchard Park terrace suite

Much of the controversy regarding the Orchard Park terrace suite (**Fig. 32**) is about the timing of their entrenchment compared to the end of Gatuña Formation deposition, aspects of this topic were discussed in the previous section. This suite of terraces was named by Fielder and Nye (1933) for terraces found approximately 12–22 m above the modern river channel. In this quadrangle, the map unit older terrace alluvium (map unit Qto) includes correlative deposits within tributaries and small montane drainages that respond to different controls than those modulating the Pecos River. Throughout the quadrangle, the height above grade varies depending on tectonic history, lithology, catchment area, and proximity to knickpoints. Terraces typically have petrocalcic development between Stage III and IV but may reach up to Stage V soil development indices. Terraces mapped in this grouping may be of late Gatuña Formation age outside of the Delaware Basin, where direct comparison to Gatuña Formation deposits is not possible.

Figure 32: Older terrace alluvium in the Seven Rivers Embayment inferred to correlated to the Orchard Park terrace suite of the Pecos River with a well-developed Stage IV (?) soil profile (right).

Channel alluvium: Lakewood terrace suite

The first suite of inactive fluvial terraces (map unit **Qti**) above the Pecos River was originally described by Fielder and Nye (1933) as the Lakewood terrace, around 6–9 m above grade along the Pecos River north of the map area near Artesia and Roswell. This publication includes a lower terrace tread described by McCraw et al. (2007) and McCraw and Land (2008), and the upper treads may run as high as 12 m above grade, in agreement with McCraw et al. (2007). The lowest of McCraw et al.'s terraces are variably mapped as younger terrace alluvium (**Qty**) due to its low grade and common reactivation or deposition of sediments at its surface by flow sourced from axial drainages. Variation in elevation above Pecos River grade are variable due to scouring in active channels, lithological variations, geomorphological responses to tectonics or anthropogenic alteration on the landscape, and stream power differences across catchments in this large map area. These terraces were originally defined along the Pecos River, while this study includes major and minor tributaries, montane arroyos (**Fig. 33**), and alluvial systems draining into the endorheic Salt Basin as part of the Lakewood Terrace suite.

Terrace deposit lithologies are dependent on source catchments. Deposits along the Pecos River drainage or in streams eroding Gatuña Formation deposits show the most lithological variation. Bachman (1976) found that the presence of pink crystalline plutonic clasts derived from the Sangre de Cristo Mountains is a local defining characteristic of the map unit. The Pecos had not previously integrated northward into the southern Rocky Mountains (Bachman, 1976) during deposition of the older terraces representing the Orchard Park terrace suite, so the presence or absence of granitic clasts is excellent differentiator of Lakewood Terrace deposits. Field checking for this characteristic was not completed and should be considered tentative. In the Black River drainage, these terraces are commonly formed out of gypsite rather than other clastic materials (Allen and Attia, 2021, 2022; Allen, 2024; Allen and Skotnicki, 2024).

Figure 33: Intermediate terrace alluvium (not mapped due to scale) inferred to be correlative to the Lakewood terrace suite of the Pecos River.

Based on soil profiles from field observations and compiled maps, these terraces were assigned a late Pleistocene age, with deposition estimated to have occurred during the last glacial maximum (MIS-2). Soil development indices in petrocalcic horizons of the Lakewood Terraces range from Stage II+ to Stage III, which would typically identify these deposits as an older age. However, an abundance of windblown carbonate dust and host sediments of carbonate composition likely accelerate the development of calcic soils in this region, making relative ages difficult to compare with age indices developed elsewhere in the region (e.g., Gile et al., 1981). Additionally, abundant tufa cementation is prevalent in localized areas across the quadrangle and may lithify deposits of any age. Carbon dates compiled in Harris (1993), Van Devender (1980), and Elias and Van Devender (1992) may provide data for age constraints on the upper boundary of this unit or the lower boundary on the overlying active alluvial units; however, no effort was made in this publication to do so.

Channel alluvium: active channel, floodplain, and reactivated terraces

Active alluvium includes the active channel (**Fig. 34**) where sediments are mobilized, transported, and deposited with flow events, as well as the active floodplain (**Fig. 34**) where fine-grained muds are deposited as overbank water recedes and splays or accesory channels scour and deposit sediments adjacent to the main channel. Active channels are commonly scoured deeply at knickpoints. These units correlate in age to other alluvial units with recent (r) or younger (y) age modifiers from the piedmont, sheetwash, and fan alluvium groups.

Figure 34: Scouring in active alluvial channel (left) and active floodplain (right).

Occasionally, reactivated terraces are largely abandoned but are flooded during the largest storm events (e.g., centenial or millenial floods, tentatively). These low terraces are 3–6 m above the active channel and have previously been included in the Lakewood terrace suite (McCraw et al., 2007, 2011; McCraw and Land, 2008). Field observations and analysis of lidar imagery provide evidence for flow from the main channel (e.g., not sheetwash) on these surfaces. They are assumed to have been deposited as fill terraces during the latest Pleistocene to early Holocene, with reworking throughout the Holocene to the present. For a larger-scale map, these deposits would likely be split into a lower reactivated portion and a higher abandoned portion grouped into the Lakewood terrace suite; however, deposits at this map unit's height above grade are variably reactivated and mapped together.

Piedmont and fan alluvium

Older piedmont alluvium (**Fig. 35**) buries and forms straths on piedmont facies of the lower Gatuña Formation, is high above the grade of active channels (9–14 m), and has well-developed Stage III to V petrocalcic horizons. The age of these deposits is inferred to overlap with the end of fluvial and valley-margin facies of the Gatuña Formation deposition; however, age and stratigraphic relations are unclear. We expect that the highest aggradation portions of older piedmont deposits correlate to the Diamond-A Plain of Fielder and Nye (1933), which is the piedmont equivalent of the geomorphic surface associated with the Mescalero paleosol in the Pecos River valley and Mescalero Plains (Hornburg, 1949, Bachman, 1980; Rosholt and McKinney, 1980). Lag gravels of these piedmont deposits are commonly found on strath terraces cut into well-lithified lower Gatuña Formation piedmont deposits.

Figure 35: Older piedmont alluvium lag deposits on a strath of the lower piedmont facies of the Gatuña Formation.

Intermediate-aged fan and piedmont deposits are thought to correlate in age to the Lakewood terrace suite based on landscape position and soil development indices. Love and Land (2006) observed that piedmont deposits around Washington Ranch west of the Black River valley had multiple levels, or risers, which are interpreted to match incisional trends observed in Pecos River deposits. In areas that were previously internally drained but are now integrated (e.g., portions of the Brokeoff Mountains), fans that had aggraded in the past are observed to be incised by arroyos in their upper portions before younger fan alluvium progrades outward into low-relief deposits. A change from aggradation in a closed system, to incision in an integrated system, is supported by the presence of buried paleosols sequences that are now incised by headward erosion of streams integrated into the Salt Basin. The timing of this integration is unclear because multiple terraces were observed adjacent to the incised channel, which could indicate an older age for the buried paleosols.

Figure 36: Fans in the Brokeoff Mountains.

Piedmont and fan alluvium (**Fig. 36**) in this quadrangle are distinguished from each other based on fan alluvium's higher steepness in channels and on relic surfaces, smaller source drainages, higher-energy deposits, the smaller scale of deposits, and the location in the landscape close to the mountain front. Recent and younger piedmont alluvium share characteristics with recent alluvium and younger terrace alluvium. Recent and younger fan alluvium are distinguished based on their surface textures and inset or aggradational relationships with each other. Recent fan alluvium exhibits distinctive recent scouring and channelization that is either inset into or burying the underlying deposit. Meanwhile, younger alluvium has smoother topography among still-visible channelized scours and a slightly higher landscape position devoid of unvegetated recently scoured channels.

Eolian deposits

Eolian deposition in this quadrangle was mapped as two distinct units: eolian sediments, and sheetwash alluvium and loessal eolian sediments. The eolian sediment map unit (Qe) exhibits dune forms and forms thick, silicic deposits in raised topographic positions east of the Pecos River valley, while the sheetwash alluvium and loessal eolian sediments map unit (Qse) forms thin, reworked sand sheets of gypsic, calcic, or silicic composition, with common coppice dune forms primarily on the Gypsum Plain. At a finer scale than 1:100,000, many more divisions could be made in the eolian deposits of this area, as evidenced by the work of Hall and Goble (2006, 2011a, 2011b, 2023).

Figure 37: Dune forms on the Mescalero Plains.

Unconsolidated dunes and sand sheets (**Fig. 37**) on the Mescalero Plains occasionally overlie Permian bedrock or the Gatuña Formation but commonly overlie up to five older generations of sand sheets stabilized by pedogenic development. These deposits were studied using OSL, with results from decades of work summarized by Hall and Gobble (2023). The first episode (I) of eolian deposition and the oldest generation of the Mescalero Sands is the 90–50 ka 'Lower eolian sand' capped by the red to brown argillic Berino paleosol with secondary Stage I petrocalcic soil development (Hall and Goble, 2011, 2023). Hall and Goble (2023) describe the next episodes of eolian deposition to include the episode II 'Middle eolian sand' (33–20 ka) capped by a Bt paleosol horizon, the episode III 'Upper eolian sand' (18–5 ka) capped by a Bw and Bk paleosol horizon, the episode IV 'Holocene eolian sand' (12–2 ka) capped by the Eddy paleosol, the episode V 'Late Holocene eolian sand' (6–2 ka) capped by the Eddy paleosol, and finally the episode VI unconsolidated sands seen in Figure 37. The stabilized sand sheets are intermittently exposed between dunes in erosional areas, and, due to pedogenic development, they do not exhibit the same mobility as the overlying dunes. The sand sheets and associated argillic B horizon or sandy C horizon of the Berino paleosol are commonly found directly over the Mescalero paleosol. Rounded silicic pebbles are common on this landscape where they are reworked from the Gatuña Formation. Dune forms are largely limited to the Mescalero Plains or terraces within the Pecos River valley; elsewhere, eolian deposition is limited to loessal sand sheets.

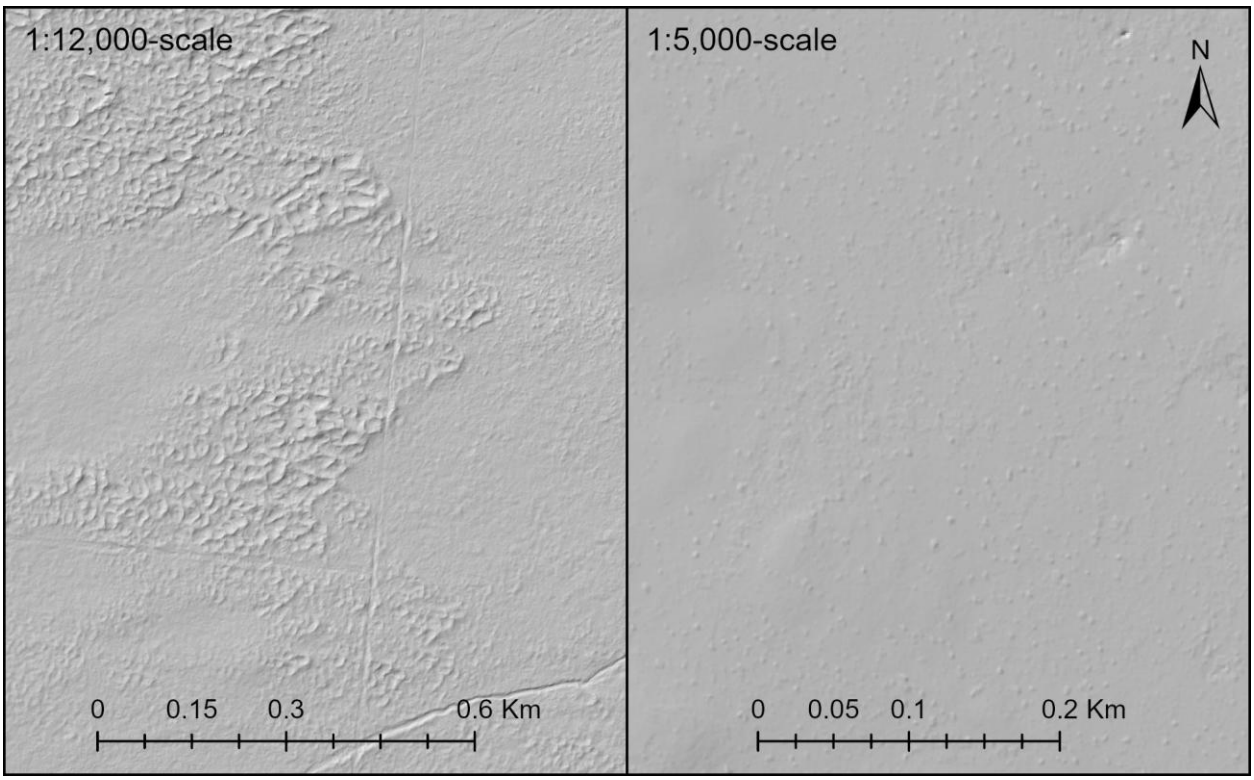

Figure 38: 1-m-resolution lidar image of dune forms (left) on the Mescalero Plains and loessal deposits with coppice dunes (right) on the Gypsum Plain.

Loessal deposits (**Fig. 38**) form a nearly ubiquitous cover in the Gypsum Plain, with prevalent deposits near the Pecos River valley and on piedmont deposits below the reef escarpment. These deposits vary in composition from dominantly gypsic or calcic to silicic depending on their location and the origin of the sediments. These deposits often exhibit coppice dune forms but are more commonly reworked by sheetwash processes into sand sheets that cover the underlying geology.

Internally drained deposits

Internally drained deposits in the quadrangle are split into three separate groups: lacustrine sediments, playa sediments, and depression-fill sediments. Lacustrine sediments are limited to the southwest corner where the quadrangle intersects pluvial Lake King (King, 1948). Playa sediments are found inset into lacustrine sediments, within the Brokeoff Mountains, and on either side of the Pecos River valley. Depression-fill deposits are found across the map area but primarily in the Delaware Basin and the Seven Rivers Embayment.

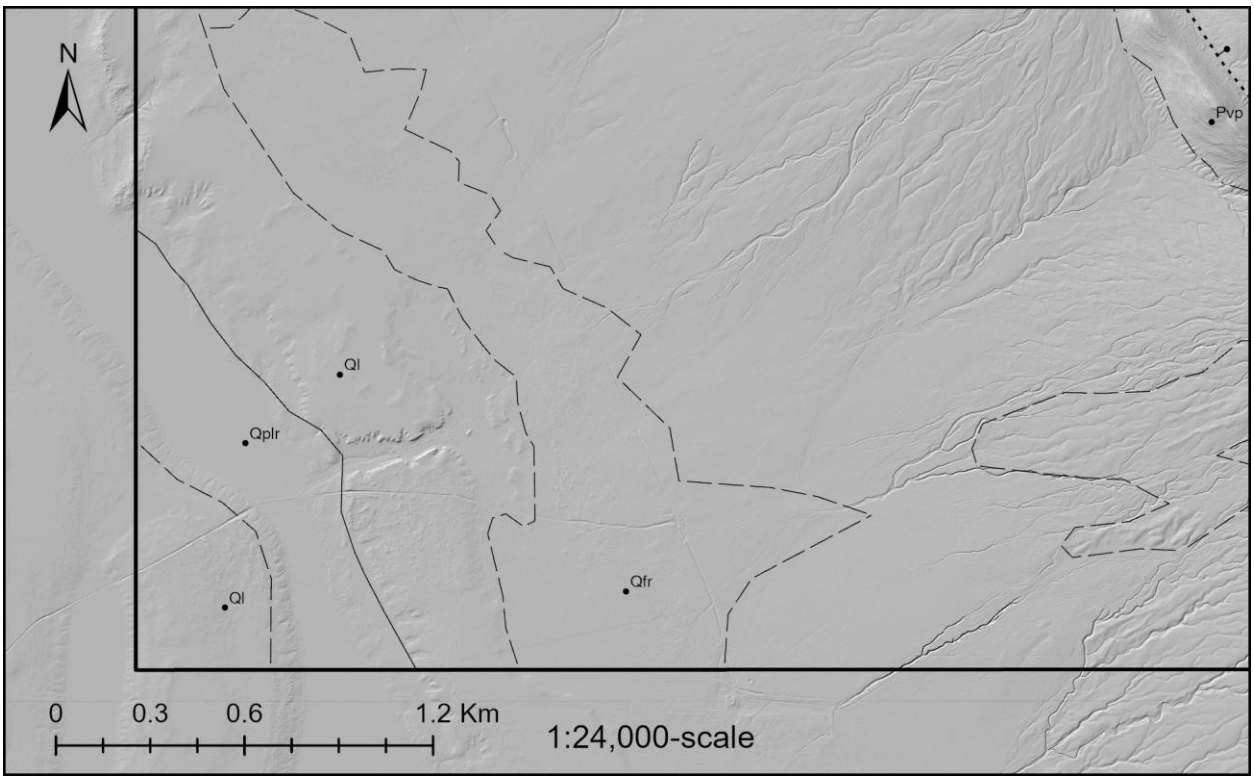

Figure 39: 1-m-resolution lidar image of Salt Basin at Crow Flats showing lacustrine sediments (Ql), recent playa sediments (Qplr), and adjacent recent fan alluvium sediments (Qfr).

Lake King (or pluvial Lake King) sediments (**Fig. 39**) are lacustrine deposits of late Pleistocene age that occupy the Salt Basin (**Fig. 40**) in Crow Flats within the southwest corner of the Carlsbad 30x60-minute quadrangle (Wilkens and Currey, 1996). These deposits were mapped by King (1948) on plate 23 of Professional Paper 215 and by O'Neill (1998) in the Geologic Map of the Cienega School Quadrangle (I-2630), with the most detailed study of these deposits by Wilkens and Currey (1996) and additional Salt Basin investigations by Veldhuis and Keller (1980), Goetz (1980), Kelley et al. (2020), and Timmons and Sturgis (2022).

Faulting, persisting into the Quaternary, dropped the Salt Basin graben, as part of the Rio Grande rift, causing internal drainage and accommodation for an endorheic basin; now, fault planes act as hydrologic barriers between brackish waters of the Salt Basin and comparatively fresh water in the Guadalupe Mountains (Goetz, 1980). Pluvial Lake King experienced four high stands during the latest Pleistocene between 22.57 and 15.94 ka, with cyclicity in lacustrine deposition loosely correlating to Dansgaard-Oeschger periodicity at 2550-yr recurrence intervals (Wilkens and Currey, 1996). Recent playa sediments (**Figs. 39 and 40**) occur in the lowest topographic positions of the basin within depressions created by eolian scouring and fed by ephemeral washes carrying alkaline waters to be evaporated (King, 1948). Basin fill in the Salt Basin, south of this map area, does not exceed 500 m according to geophysical gravity studies (Veldhuis and Keller, 1980). Unfortunately, deposits in the Salt Basin and Crow Flats were not able to be visited within the map area for field checking.

Figure 40: Recent playa deposits south of the map area in Texas. View looking north to Guadalupe Peak.

An isolated playa is present below the Algerita Escarpment in Big Dog Canyon of the Brokeoff Mountains, where an early Holocene playa lake level was observed as drab-gray, mixed clastic and evaporite sediments with prevalent carbonate nodules a few meters above the modern playa floor. Additional alkaline deposits are found in solution subsidence depressions in the vicinity of the Pecos River; these may include precipitation of minerals from waters extracted by potash mining. Other solution subsidence depressions without alkaline precipitates are mapped as depression-fill deposits.

Mass-wasting and colluvial deposits

No mass-wasting map units were mapped in this quadrangle due to the scale and nature of the landslides present. The map unit **Qac** comprises most of the landslides that do occur close to map scale by combining these, mostly debris-flow fans, with the adjacent alluvial and colluvial deposits. Steep gulleys with recent and older scars from debris flow initiation are observable throughout the map area, but especially along the Algerita Escarpment and in the steep drainages cutting the reef escarpment down to the Black River valley. Localized, infrequent, and very small rotational and translational slides were observed in lidar but not mapped due to their insignificance for the scope of the project. Note that some polygons mapped as fan alluvium may have experienced deposition more like that of a debris-flow fan

and exhibit high-energy deposition with debris-flow levies and inverse, kinetically graded deposits. This map unit (**Qac**) may also be mapped where no mass wasting is present, and instead mixed alluvial deposits are undivided with hillslope colluvium.

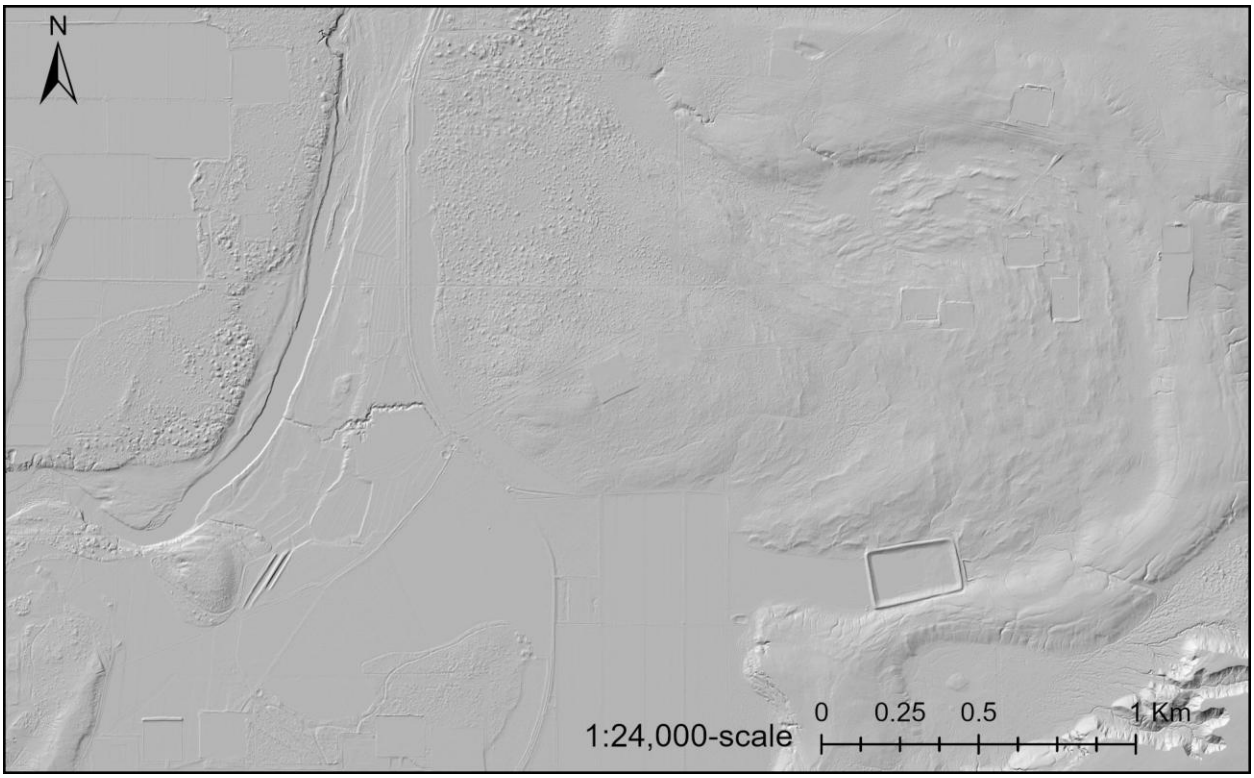

Figure 41: 1-m-resolution lidar image of solution subsidence collapse (32.26628° N, -104.00130° W NAD83) that is likely a form of mass wasting but mapped with the Gatuña Formation.

One feature (**Fig. 41**) on the eastern map boundary appears to be a large landslide inferred to be moving at very slow speeds accommodated by space created by incision and solution subsidence along the Pecos River. This could not be field checked and only a few areas with similar appearances are visible in lidar despite ubiquitous subsidence related to dissolution of underlying evaporite deposits.

Anthropogenic deposits

Evidence of anthropogenic activity is widespread across the quadrangle, especially within the Delaware Basin, where agricultural fields, grazing lands, cities and towns, well pads, mines and quarries, roads, irrigation ditches, and landfills are all present. Where an appreciable thickness and scale are achieved, the map unit artificial fill (**af**) was used to designate deposits originating from human activity (e.g., landfills, foundations, quarries, reservoir sediments). Shaded, overlaying polygons were used where disturbed land masked the underlying geology, but not of a significant thickness (e.g., tilled land, concrete, and/or roads).

Garbage may be found within any deposit designated as recent and on top of or in the upper portion of surficial and bedrock deposits of any age. The abundant cave and karst topography of this region complicates this because fissures, caves, and crevasses are common,

were used as dumping grounds, and can act as conduits to transport anthropogenic material deep into outcrops. It should be noted that unmapped deposits of stones, used as foundations for houses by indigenous people inhabiting this land, are found within the map area and should not be confused with naturally occurring geologic deposits. Many anthropogenic deposits exist on this landscape that are sub-map scale, and map users should refer to topographic maps or existing larger-scale geologic maps to check the origin of irregular deposits.

Figure 42: Sands consolidated by oil in the Mescalero Sands from anthropogenic activity. A leaking oil pipeline (now absent) consolidated these sands.

One peculiar observation (**Fig. 42**) was the presence of dark-brown, bimodally sorted, weakly consolidated sand with silicic pebbles on the Mescalero Plains. While visually similar to the preserved paleosols (e.g., the Berino paleosol) in the same sand fields, this location had a distinct fetid odor and was discontinuous laterally. After the second or third observation of these sands, it was concluded that an old, leaky, oil pipeline had run parallel to the road prior to its removal.

INDUSTRY AND LAND USE

The Carlsbad 30x60-minute quadrangle is on the periphery of the areas with the largest energy resource production in the state. Most industry occurs adjacent to this quadrangle, in areas to the north and east of this map, but the bedrock geology of this quadrangle is significant in understanding the geologic history that has led to the production of New Mexico's natural resources.

Oil and Gas

The Independent Petroleum Assessment of New Mexico (Winchester, 2024) ranked New Mexico as the second-largest oil producer in the United States, with 665.55 million barrels produced, accounting for 14.1% of U.S. production. The USGS (Gaswirth et al., 2018) estimated a reserve of 46.3 billion barrels of oil and 281 trillion cubic feet of gas in the Wolfcamp Formation and Bone Spring Formation, which extend beyond New Mexico into west Texas. As of today, most oil and gas is extracted through hydraulic fracturing of deep-basin deposits. In the past, hydrocarbon reservoirs could readily be found in the Artesia Group in classic structural and stratigraphic traps where hydrocarbons accumulated in porous and permeable rocks and were trapped by an impermeable seal. Nance (2004) estimated that cumulative oil production exceeded 254.5 million barrels from more than 236 reservoirs and that cumulative gas production exceeded 356.7 trillion cubic feet from 157 reservoirs. For more in-depth information regarding oil and gas production, refer to the NMBGMR's pages regarding petroleum resources.

Potash

The western edge of the Carlsbad potash district is in the Loving and Indian Flats 7.5-minute quadrangles, on the farthest eastern extent of the map area. This district is the largest potash-producing area in the United States, with an estimated 114 million tons of potash extracted since 1951. Potash is a mixture of potassium salts, the most important of which are sylvite (KCl) and langbeinite ($K_2SO_4 \cdot 2MgSO_4$); these salts are used in fertilizers, preservatives, detergents, and other industrial chemicals. The McNutt Member of the Salado Formation contains most of the important potash-bearing evaporite intervals and is extracted from underground. The McNutt Member is approximately 122 m thick and contains twelve 1- to 3-m-thick ore zones, which overlie relatively thick halite deposits (Griswold, 1982; Barker and Austin, 1993). The Salado Formation and McNutt Member exhibit stratigraphic sequences in two cycles: evaporites grading into muddy halite as seawater input (Type I) transitions to basin-brine with meteoric water and minor seawater interactions (Type II). The potash is the product of secondary, diagenetic precipitation of initial magnesium-rich evaporites (carnallite and polyhalite) from these halite-rich brines (Barker and Austin, 1993).

WIPP Site

The Salado Formation is the host rock for the Waste Isolation Pilot Plant (WIPP), located beyond the eastern edge of the map area. The WIPP site was authorized by Congress in 1979 to safely dispose of the United States military's "defense-generated" radioactive waste. The container for this waste is a series of excavated rooms approximately 655 m underground. The impermeability and plasticity of evaporites at depth were the primary reasons for storing hazardous waste in this location; once the facility reaches maximum capacity, the entrance will be sealed, and surface markers will be left to indicate the location of the buried radioactive waste. In 2022, The U.S. Department of Energy published a comprehensive list of criteria for material to be accepted at the WIPP site. The general criteria are any waste exceeding 100 nanocuries per gram that produces alpha radiation and has a half-life greater than 20 years, which are most radionuclides in the actinide series.

Precious, Critical, and Industrial Minerals

Three oxidized Mississippi-Valley Type (MVT) deposits are located around the Permian Basin; deposits are highly oxidized and small and contain minor amounts of lead, silver, and zinc (McLemore, 2006). Deposits are hosted in the Seven Rivers, Yates, or Tansill Formations. Outside of isolated prospects, there are no records of economic production, and the potential for base and precious metals in these deposits is low (McLemore, 2006). The main "mineral" produced in the region is aggregate. Quarries throughout the Pecos River valley extract caliche (precipitated calcium carbonate), which accumulates in the soils of arid regions. The quarries in this map area are typically extracting from the Gatuña Formation or younger Quaternary deposits. Caliche can be used to manufacture cement, but most of the caliche in the area contains 19–40% impurities, making it only suitable for road material (McLemore and Austin, 2017). Most quarries are near highways or populated cities due to the relatively low value of the material coupled with the high cost to transport it (McLemore and Austin, 2017). There are quarries that extract limestone from the Seven Rivers Formation for use in road construction and building material.

In the Guadalupe Mountains, groundwater resources are primarily drawn from the Goat Seep Formation, Capitan Formation, Queen Formation, and Seven Rivers Formation. The most significant aquifer system is the Capitan Formation; the carbonate acts as an aquifer that yields high-quality water and is commonly used for public and industrial supply (Hendrickson et al., 1952). Areas around Carlsbad rely on the Capitan Formation and alluvial aquifers, such as those along the Pecos River and in the Rustler Formation. Aquifers have become increasingly saline and are primarily used for agriculture or livestock. Groundwater depths vary regionally, ranging from less than 15 m in the Pecos River valley to over 152 m in upland areas near the Guadalupe Mountains. Groundwater in deeper formations such as the Capitan Formation is generally under confined conditions, whereas shallower units are unconfined and more susceptible to contamination from surface activities.

REFERENCES

Adams, D.C., Ouimette, M.A., and Moreno, F., 1993, Middle–Late Proterozoic extension in the Carlsbad region of southeastern New Mexico and west Texas, *in* Love, D.W., Hawley, J.W., Kues, B.S., Adams, J.W., Austin, G.S., and Barker, J.M., eds., *Carlsbad Region, New Mexico and West Texas*: New Mexico Geological Society 44th Annual Field Conference Guidebook, p. 137–144, https://doi.org/10.56577/FFC-44.137.

Allen, B.D., and Attia, S., 2021, Geologic Map of the Rattlesnake Springs 7.5-Minute Quadrangle, Eddy County, New Mexico: New Mexico Bureau of Geology and Mineral Resources Open-File Geologic Map 291, scale 1:24,000, 1 plate, p. 14, https://doi.org/10.58799/OF-GM-291.

Allen, B.D., and Attia, S., 2022, Geologic Map of the Bond Draw and Cottonwood Hills 7.5- Minute Quadrangles, Eddy County, New Mexico: New Mexico Bureau of Geology and Mineral Resources Open-File Geologic Map 297, scale 1:24,000, 1 plate, p. 16, https://doi.org/10.58799/OF-GM-297.

Allen, B.D., 2024, Geologic Map of the Jumping Spring 7.5-Minute Quadrangles, Eddy County, New Mexico: New Mexico Bureau of Geology and Mineral Resources Open-File Geologic Map 311, scale 1:24,000, 1 plate, p. 11, https://doi.org/10.58799/OF-GM-311.

Allen, B.D., and Skotnicki, S.J., 2024, Geologic Map of the Grapevine Draw 7.5- Minute Quadrangle, Eddy County, New Mexico: New Mexico Bureau of Geology and Mineral Resources Open-File Geologic Map 309, scale 1:24,000, 1 plate, p. 15, https://doi.org/10.58799/OF-GM-309.

Attia, S., and Allen, B.D., 2022, Geologic Map of the Pierce Canyon 7.5-Minute Quadrangle, Eddy County, New Mexico: New Mexico Bureau of Geology and Mineral Resources Open-File Geologic Map 299, scale 1:24,000, 1 plate, p. 37, https://doi.org/10.58799/OF-GM-299.

Attia, S., Heizler, M., and Ricci, J., 2023, Quaternary Age of the Gatuña Formation at Livingston Ridge, *in* Land, L., Jaoude, I.B., Hutchinson, P., Zeigler, K., Jakle, A., and Werff, V.B., eds., Evaporite Karst of the Lower Pecos Region: New Mexico Geological Society 73rd Annual Field Conference Guidebook, p. 103–111, https://doi.org/10.56577/FFC-73.103.

Anderson, R.Y., and Kirkland, D.W., 1970, Microfolding in the Castile and Todilto evaporites, Texas and New Mexico: Geological Society of America Bulletin, v. 81, p. 3259-3281, https://doi.org/10.1130/0016-7606(1970)81[3259:MITCAT]2.0.CO;2.

Attia, S., and Ricci, J., 2023, Latest Eocene $^{40}Ar/^{39}Ar$ Age from the Yeso Hills Dikes, Eddy County, New Mexico, *in* Land, L., Jaoude, I.B., Hutchinson, P., Zeigler, K., Jakle, A., and Werff, V.B., eds., Evaporite Karst of the Lower Pecos Region: New Mexico Geological Society 73rd Annual Field Conference Guidebook, p. 10, https://doi.org/10.56577/FFC-73.

Bachman, G.O., and Hayes, P.T., 1958, Stratigraphy of Upper Pennsylvanian and lower Permian rocks in the Sand Canyon area, Otero County, New Mexico: Geological Society of America Bulletin, v. 69, no. 6, p. 689-700, https://doi.org/10.1130/0016-7606(1958)69[689:SOUPAL]2.0.CO;2.

Bachman, G.O., 1976, Cenozoic Deposits of Southeastern New Mexico and an Outline of the History of Evaporite Dissolution: United States Geological Survey Journal of Research, v. 4(2), p. 135–149, https://pubs.usgs.gov/publication/70232221.

Bachman, G.O., 1980, Regional geology and Cenozoic history of Pecos region, southeastern New Mexico: United States Geological Survey Open-File Report Nos. 80–1099, 12 plates, p. 116, https://doi.org/10.3133/ofr801099.

Barker, J.M., and Austin, G.S., 1993, Economic geology of the Carlsbad potash district, New Mexico: *in* Love, D.W., Hawley, J.W., Kues, B.S., Adams, J.W., Austin, G.S., and Barker, J.M., eds., *Carlsbad Region, New Mexico and West Texas*: New Mexico Geological Society 44th Annual Field Conference Guidebook, p. 283–291, https://doi.org/10.56577/FFC-44.283.

Barnes, V.E., Eifler, G.K., Reeves, C.C., Kottlowski, F.E., Norman, D.M., Sherrod, C.H., and Hansen, J.J., 1976, Geologic atlas of Texas, Hobbs sheet: Bureau of Economic Geology, University of Texas at Austin, Geologic Atlas of Texas 17, scale 1:250,000.

Bjorklund, L.J., and Motts, W.S., 1959, Geology and water resources of the Carlsbad area, Eddy County, New Mexico: United States Geological Survey Open-File Report 59-9, 41 plates, p. 576, https://doi.org/10.3133/ofr599.

Boyd, D.W., 1955, Stratigraphy of the Brokeoff Mountains, New Mexico: in Society of Economic Paleontologists and Mineralogists, Permian Basin Sec., Permian Field Conference, October 1955: p. 47–51.

Boyd, D.W., 1958, Permian sedimentary facies, central Guadalupe Mountains, New Mexico: New Mexico Bureau of Mines and Mineral Resources Bulletin 49, p. 100, https://doi.org/10.58799/B-49.

Brimberry, D.L., 1991, Depositional and diagenetic history of the Late Ordovician Montoya Group, Sacramento Mountains, south-central New Mexico, *in* Johnson, K.S., ed., Late Cambrian-Ordovician geology of the southern Midcontinent: Oklahoma Geological Survey Circular, 1989 symposium, v. 92, p. 154–170.

Broadhead, R.F., 2010, The Woodford Shale in southeastern New Mexico: Distribution and source rock characteristics: *New Mexico Geology*, v. 32, no. 3, p. 79–88.

Brokaw, A.L., Jones, C.L., Cooley, M.E., and Hays, W.H., 1972, Geology and hydrology of the Carlsbad potash area, Eddy and Lea Counties, New Mexico: United States Geological Survey Open-File Report OFR-72-49, p. 105, https://doi.org/10.3133/ofr7249.

Bruno, L., and Chafetz, H.S., 1988, Depositional environment of the Cable Canyon Sandstone: A Mid-Ordovician sandwave complex from southern New Mexico: *in* Mack, G.H., Lawton, T.F., and Lucas, S.G., eds., Southwestern New Mexico: New Mexico Geological Society 39th Annual Field Conference Guidebook, p. 127–134, https://doi.org/10.56577/FFC-39.

Calzia, J.P., and Hiss, W.L., 1978, Igneous rocks in northern Delaware Basin, New Mexico and Texas, in Austin, G.S., ed., Geology and Mineral Deposits of Ochoan Rocks in Deleware Basin and Adjacent Areas: New Mexico Bureau of Mines and Mineral Resources Circular 159, p. 39–45, https://doi.org/10.58799/C-159.

Cather, S.M., and Heizler, M.T., 2023, A north-flowing precursor to the Pecos River in the Gatuña formation of southeastern New Mexico and Texas, *in* Land, L., Jaoude, I.B., Hutchinson, P., Zeigler, K., Jakle, A., and Werff, V.B., eds., Evaporite Karst of the Lower Pecos Region: New Mexico Geological Society 73rd Annual Field Conference Guidebook, p. 89–101, https://doi.org/10.56577/FFC-73.89.

Cheng, H.R., Edwards, L., Shen, C., Polyak, V.J., Asmerom, Y., Woodhead, J., Hellstrom, J., Wang, Y., Kong, X., Spötl, C., Wang, X., and Alexander, E.C., Improvements in ^{230}Th dating, ^{230}Th and ^{234}U half-life values, and U–Th isotopic measurements by multi-collector inductively coupled plasma mass spectrometry: Earth and Planetary Science Letters, v. 371–372(2013), p. 82–91, https://doi.org/10.1016/j.epsl.2013.04.006.

Cikoski, C.T., 2019a, Geologic Map of the Kitchen Cove 7.5-Minute Quadrangle, Eddy County, New Mexico: New Mexico Bureau of Geology and Mineral Resources Open-File Digital Geologic Map 76, scale 24,000, 1 sheet, p. 63, https://doi.org/10.58799/OF-GM-276.

Cikoski, C.T., 2019b, Geologic Map of the Malaga 7.5-Minute Quadrangle, Eddy County, New Mexico: New Mexico Bureau of Geology and Mineral Resources Open-File Geologic Map 277, scale 24,000, 1 plate, p. 62, https://doi.org/10.58799/OF-GM-277.

Cikoski, C.T., 2020, Geologic Map of the Red Bluff 7.5-Minute Quadrangle, Eddy County, New Mexico: New Mexico Bureau of Geology and Mineral Resources Open-File Geologic Map 284, scale 24,000, 1 plate, p. 31, https://doi.org/10.58799/OF-GM-284.

Cikoski, C.T., and Allen, B.D., 2020, Geologic Map of the Black River Village 7.5-Minute Quadrangle, Eddy County: New Mexico, New Mexico Bureau of Geology and Mineral Resources Open-File Geologic Map 283, scale 1:24,000, 1 sheet, p. 16, https://doi.org/10.58799/OF-GM-283.

Decker, D.D., Polyak, V.J., and Asmerom, Y., 2018, Spar caves as fossil hydrothermal systems—timing and origin of ore deposits in the Delaware basin and Guadalupe mountains, New Mexico and Texas, USA: International Journal of Speleology, v. 47, no. 3, p. 263–270, https://doi.org/10.5038/1827-806X.47.3.2173.

Dehler, C.M., and Pederson, J.L., 1998, Geologic map of the Carlsbad East 7.5-minute Quadrangle, Eddy County, New Mexico, New Mexico Bureau of Geology and Mineral Resources Open-File Geologic Map 060, scale 1:24,000, 1 sheet, p. 3, https://doi.org/10.58799/OF-GM-60.

Dehler, C.M., and Pederson, J.L., 2002, Geologic map of the Carlsbad West 7.5-minute Quadrangle, Eddy County, New Mexico: New Mexico Bureau of Geology and Mineral Resources Open-File Geologic Map 059, scale 1:24,000, 1 sheet, p. 4, https://doi.org/10.58799/OF-GM-59.

Dehler, C.M., Pederson, J.L., and Wagner, S.S., 2005a, Geologic map of the Lake McMillan South 7.5-minute Quadrangle, Eddy County, New Mexico: New Mexico Bureau of Geology and Mineral Resources Open-File Geologic Map 097, scale 1:24,000, 1 sheet, p. 4, https://doi.org/10.58799/OF-GM-97.

Dehler, C.M., Pederson, J.L., and Wagner, S.S., 2005b, Geologic map of the Seven Rivers 7.5-minute quadrangle, Eddy County, New Mexico: New Mexico Bureau of Geology and Mineral Resources Open-File Geologic Map 098, scale 1:24,000, 1 sheet, p. 3, https://doi.org/10.58799/OF-GM-98.

Denison, R.E., and Hetherington, E.A., 1969, Basement rocks in far west Texas and south-central New Mexico, in Kottlowski, F.E., and Lemone, D.V., eds., Border Stratigraphy Symposium: New Mexico Bureau of Mines and Mineral Resources Circular 104, p. 13, https://doi.org/10.58799/C-104.

Denison, R.E., Burke, W.H.J., Hetherington, E.A., and Otto, J.B., 1971, Basement rock framework of parts of Texas, southern New Mexico and northern Mexico, *in* Seewald, K., and Sundeen, D., eds., The geologic framework of the Chihuahua Tectonic Belt: West Texas Geological Society, p. 4–6.

Dickinson, W.R., and Lawton, T.F., 2003, Sequential intercontinental suturing as the ultimate control for Pennsylvanian Ancestral Rocky Mountains deformation: Geology, v. 31, no. 7, p. 609–612, https://doi.org/10.1130/0091-7613(2003)031<0609:SISATU>2.0.CO;2.

Donatelli, J.L., 2016, Dedolomitization and other diagenesis in the backreef setting of the Permian reef complex in Dark Canyon, New Mexico: [master's thesis]: Socorro, New Mexico, New Mexico Institute of Mining and Technology, p. 159, Table 1 XRD results,

Erdlac, R.J. Jr., 1993, Small-scale structures in the Guadalupe Mountains region: Implications for Laramide stress trends in the Permian Basin, *in* Love, D.W., Hawley, J.W., Kues, B.S., Austin, G.S., and Lucas, S.G., eds., Carlsbad Region, New Mexico and West Texas: New Mexico Geological Society 44th Annual Fall Field Conference Guidebook, p. 167–174, https://doi.org/10.56577/FFC-44.167.

Ewing, T.E., 1993, Erosional margins and patterns of subsidence in the late Paleozoic west Texas basin and adjoining basins of west Texas and New Mexico, *in* Love, D.W., Hawley, J.W., Kues, B.S., Austin, G.S., and Lucas, S.G., eds., Carlsbad Region, New Mexico and West Texas: New Mexico Geological Society 44th Annual Fall Field Conference Guidebook, p. 155–166, https://doi.org/10.56577/FFC-44.

Ewing, T.E., Barnes, M.A., and Denison, R.E., 2019, Proterozoic foundations of the Permian Basin, West Texas and southeastern New Mexico—a review, *in* Ruppel, S. C., ed., Anatomy of a Paleozoic basin: the Permian Basin, USA (vol. 1, ch. 3): The University of Texas at Austin, Bureau of

Economic Geology Report of Investigations 285; American Association of Petroleum Geologists Memoir 118, p. 43–61.

Fairhurst, B., Ewing, T., and Lindsay, B., 2021, West Texas (Permian) Super Basin, United States: Tectonics, structural development, sedimentation, petroleum systems, and hydrocarbon reserves: American Association of Petroleum Geologists Bulletin, v. 105, p. 1099-1147, https://doi.org/10.1306/03042120130.

Fiedler, A.G., and Nye, S.S., 1933, Geology and Ground-Water Resources of the Roswell Artesian Basin, New Mexico: United States Geological Survey Water Supply Paper No. 639, 40 plates, p. 372, https://doi.org/10.3133/wsp639.

Flawn, P.T., 1956, Basement rocks of Texas and southeast New Mexico: University of Texas, Bureau of Economic Geology, Publication 5605, p. 261.

Fracasso, M.A., and Kolker, A., 1985, Late Permian volcanic ash beds in the Quartermaster and Dewey Lake Formations, Texas panhandle: West Texas Geological Society Bulletin, v. 24, no. 6, p. 5-10.

Gaswirth, S.B., French, K.L., Pitman, J.K., Marra, K.R., Mercier, T.J., Leathers-Miller, H.M., Schenk, C.J., Tennyson, M.E., Woodall, C.A., Brownfield, M.E., Finn, T.M., and Le, P.A., 2018, Assessment of undiscovered continuous oil and gas resources in the Wolfcamp Shale and Bone Spring Formation of the Delaware Basin, Permian Basin Province, New Mexico and Texas: United States Geological Survey Fact Sheet 2018–3073, p. 6, https://doi.org/10.3133/fs20183073.

Gile, L.H., Hawley, J.W., and Grossman, R.B., 1981, Soils and Geomorphology in the Basin and Range Area of Southern New Mexico—Guidebook to the Desert Project: New Mexico Bureau of Mines & Mineral Resources Memoir 39, 2 sheets, p. 222, https://doi.org/10.58799/M-39.

Goetz, L.K., 1977, Quaternary faulting in Salt Basin graben, West Texas [master's Thesis]: Austin, TX, University of Texas, Austin, p. 136, https://doi.org/10.56577/FFC-31.83.

Griswold, G.B., 1982, Geology overview of the Carlsbad Potash Mining District: New Mexico Bureau of Mines and Mineral Resources Circular 182, p. 17-21.

Hall, S.A., and Goble, R.J., 2006, Geomorphology, stratigraphy, and luminescence age of the Mescalero Sands, southeastern New Mexico, *in* Land, L., Lueth, V.W., Raatz, W., Boston, P., and Love, D.L., eds., Caves and Karst of Southeastern New Mexico, New Mexico Geological Society 57th Annual Field Conference Guidebook, p. 297–310, https://doi.org/10.56577/FFC-57.297.

Hall, S.A., and Goble, R.J., 2011a, New optical age of the Mescalero sand sheet, southeastern New Mexico: New Mexico Geology, v. 33(1), p. 9–16, https://doi.org/10.58799/NMG-v33n1.9.

Hall, S.A., and Goble, R.J., 2011b, Geology and optical dating of sediments, *in* Railey, J.A., ed., Archaeology in Far Southeastern New Mexico: Albuquerque, SWCA Environmental Consultants, Report No. 2010-68, p. 309–335, (Locs. 11, 12, 13).

Hall, S.A., and Goble, R.J., 2012, Berino Paleosol, Late Pleistocene Argillic Soil Development on the Mescalero Sand Sheet in New Mexico. The Journal of Geology, 120(3), 333–345. https://doi.org/10.1086/664777.

Hall, S.A., and Goble, R.J., 2023, Quaternary and archaeological geology of the Mescalero Plain, southeastern New Mexico: New Mexico Bureau of Geology and Mineral Resources Bulletin 165, p. 216, https://doi.org/10.58799/B-165.

Happel, A.A., 2017, Evaluating Fault-Line Escarpment Exposure in the Guadalupe Mountains of West Texas and New Mexico [master's thesis]: Normal, Illinois, Illinois State University, p. 77.

Hayes, P.T., 1957, Geology of the Carlsbad Caverns East quadrangle, New Mexico, with a chapter on geologic development of the Carlsbad Caverns by B. T. Gale: United States Geological Survey Geological Quadrangle Map GQ-98, scale 1:62,500, https://doi.org/10.3133/gq98.

Hayes, P.T., 1959, San Andres limestone and related Permian rocks in Last Chance Canyon and vicinity, southeastern New Mexico: American Association of Petroleum Geologists Bulletin, v. 43, no. 9, p. 2197-2213, https://doi.org/10.1306/0BDA5EA9-16BD-11D7-8645000102C1865D.

Hayes, P.T., 1964, *Geology of the Guadalupe Mountains:* United States Geological Survey Professional Paper No. 446, scale 1:62,500, 3 plates, p. 69, https://doi.org/10.3133/pp446.

Hayes, P.T., and Koogle, R.L., 1958, Geology of the Carlsbad Caverns West quadrangle, New Mexico-Texas: United States Geological Survey Geological Quadrangle Map GQ-112, scale 1:62,500, https://doi.org/10.3133/gq112.

Hayes, P.T., and Bachman, G.O., 1979, Examination and Reevaluation of Evidence for the Barrera Fault, Guadalupe Mountains, New Mexico: United States Geological Survey Open-File Report 79-1520, p. 9.

Hawley, J.W., 1993, The Ogallala and Gatuña Formations in the southeastern New Mexico region: A progress report, *in* Love, D.W., Hawley, J.W., Kues, B.S., Austin, G.S., and Lucas, S.G., eds., Carlsbad Region, New Mexico and West Texas: New Mexico Geological Society 44th Annual Fall Field Conference Guidebook, p. 261–269, https://doi.org/10.56577/FFC-44.261.

Hendrickson, G.E., and Jones, R.S., 1952, *Geology and ground-water resources of Eddy County, New Mexico*: New Mexico Bureau of Mines and Mineral Resources, Ground-Water Report 3, Prepared in cooperation with the United States Geological Survey and the New Mexico State Engineer, 4 plates, p. 169, https://doi.org/10.58799/GW-3.

Hill, C.A., 1993, Sulfide/barite/fluorite mineral deposits, Guadalupe Mountains, New Mexico and west Texas: *New Mexico Geology*, v. 15, no. 3, p. 56–65, https://doi.org/10.58799/NMG-v15n3.56.

Hill, C.A., 1996, *Geology of the Delaware Basin, Guadalupe, Apache, and Glass Mountains, New Mexico and West Texas*: SEPM (Society for Sedimentary Geology) Special Publication 96, p. 480.

Hoagstrom, C.W., Davenport, S.R., and Osborne, M.J., 2025, Assembling the Pecos River Fish Fauna: Barrier Displacement on the Southern Great Plains, North America. Biology Reviews, v. 100, p. 1534–1556, https://doi.org/10.1111/brv.70012.

Horberg, C.L., 1949, Geomorphic history of the Carlsbad Caverns area, New Mexico: Journal of Geology, v. 57, no. 5, p. 464–476, https://doi.org/10.1086/625661.

Horne, E.A., Hennings, P.H., and Zahm, C.K., 2021, Basement-rooted faults of the Delaware Basin and Central Basin Platform, Permian Basin, West Texas and southeastern New Mexico, *in* Callahan, O.A., and Eichhubl, P., eds., The geologic basement of Texas: a volume in honor of Peter T. Flawn: The University of Texas, Bureau of Economic Geology Report of Investigations No. 286, https://doi.org/10.23867/RI0286C6.

Hunt, D.W., Fitchen, W.M., and Koša, E., 2003, Syndepositional deformation of the Permian Capitan reef carbonate platform, Guadalupe Mountains, New Mexico, USA: Sedimentary Geology, v. 154(3-4), p. 80–126, https://doi.org/10.1016/S0037-0738(02)00104-5.

Izett, G.A., and Wilcox, R.E., 1982, Map showing localities and inferred distributions of the Huckleberry Ridge, Mesa Falls, and Lava Creek ash beds (Pearlette family ash beds) of Pliocene and Pleistocene age in the western United States and southern Canada: United States Geological Survey Numbered Series No. 1325, https://doi.org/10.3133/i1325.

Jicha, B.R., Singer, B.S., and Sobol, P., 2016, Re-evaluation of the ages of $^{40}Ar/^{39}Ar$ sanidine standards and super eruptions in the western U.S. using a Noblesse multi-collector mass spectrometer: Chemical Geology, v. 431, p. 54–66, https://doi.org/10.1016/j.chemgeo.2016.03.024.

Jones, C.L., Cooley, M.E., and Bachman, G. O., 1973, Salt deposits of Los Medaños area, Eddy and Lea Counties, New Mexico: U.S. Geological Survey, Open-file Report 73-135, 67 p.

Jones, R.H., 2004, Patterns of Montoya Group deposition, diagenesis, and reservoir development in the Permian Basin, *in* Pope, M.C., and Read, J.F., eds., *Ordovician and Silurian Rocks of the Southern Midcontinent and Ozark Region*, SEPM Field Trip Guidebook, South-Central Section Meeting, Texas A&M University, College Station, Texas, March 2004, p. 75–90.

Kelley, V.C., 1971, *Geology of the Pecos country, southeastern New Mexico*: New Mexico Bureau of Geology and Mineral Resources Memoir 24, 7 plates, p. 75, https://doi.org/10.58799/M-24.

Kelley, S., Fichera, M., Evenocheck, E., Eberle, B.A., Person, M., Cadol, D., Newton, B.T., Timmons, S., and Pokorny, C., 2020, Assessment of Water Resources in the Salt Basin Region of New Mexico and Texas: Data Summary Report: New Mexico Bureau of Geology and Mineral Resources Open-file Report 608, p. 55, https://doi.org/10.58799/OFR-608.

King, P.B., 1948, *Geology of the southern Guadalupe Mountains, Texas*: United States Geological Survey Professional Paper 215, 13 plates, p. 183, https://doi.org/10.3133/pp215.

King, P.B., 1942, Permian of west Texas and southeastern New Mexico, pt. 2 of DeFord and Lloyd. eds., West Texas-New Mexico symposium: American Association of Petroleum Geologists Bulletin, v. 26, no. 4, p. 535–763, https://doi.org/10.1306/3D933468-16B1-11D7-8645000102C1865D.

King, P.B., 1948, Geology of the southern Guadalupe Mountains, Texas: United States Geological Survey Professional Paper 215, 23 plates, p. 183, https://doi.org/10.3133/pp215.

King, P.B., 1949, Regional geologic map of parts of Culberson and Hudspeth Counties, Texas: United States Geological Survey Oil and Gas Investigations Preliminary Map 90, https://doi.org/10.3133/om90.

King, W.E., and Harder, V.M., 1985, Oil and gas potential of the Tularosa basin–Otero platform–Salt basin graben area, New Mexico and Texas: New Mexico Bureau of Mines and Mineral Resources Circular 198, p. 1–36, https://doi.org/10.58799/C-198.

Koša, E., and Hunt, D.W., 2005, Growth of syndepositional faults in carbonate strata: Upper Permian Capitan platform, New Mexico, USA: Journal of Structural Geology, v.27(6), p. 1069–1094, https://doi.org/10.1016/j.jsg.2005.02.007.

Kottlowski, F.E., Flower, R.H., Thompson, M.L., and Foster, R.W., 1956, Stratigraphic studies of the San Andres Mountains, New Mexico: New Mexico Bureau of Mines and Mineral Resources Memoir 1, 5 plates, p. 132, https://doi.org/10.58799/M-1.

Krupnick, J.M., Polyak, V.J., and Asmerom, Y., 2025, Diachronous Development of the Mescalero Paleosol and Cessation of Gatuña Formation Deposition During the Middle-Pleistocene, Southeastern

New Mexico: Socorro, New Mexico, 15th April 2025, Conference Abstract, New Mexico Geological Society Spring Meeting.

Kues, B.S., and Lucas, S.G., 1993, Stratigraphy, paleontology and correlation of Lower Cretaceous exposures in southeastern New Mexico *in* Love, D.W., Hawley, J.W., Kues, B.S., Austin, G.S., and Lucas, S.G., eds., Carlsbad Region, New Mexico and West Texas: New Mexico Geological Society 44th Annual Fall Field Conference Guidebook, p. 16, https://doi.org/10.56577/FFC-44.

Kues, B.S., and Giles, K., 2004, The late Paleozoic ancestral Rocky Mountains system in New Mexico: The Geology of New Mexico, a Geologic History, v. 11, p. 95–136.

Lang, W.T.B., 1947, Occurrence of Comanche rocks in Black River Valley, New Mexico: American Association of Petroleum Geologists Bulletin, v. 31, no. 8, p. 1472–1478, https://doi.org/10.1306/3D933A19-16B1-11D7-8645000102C1865D.

Lavery, D., Reyes-Correa, M., Baca, A., Martin, L., and Attia, S., 2024, 3D Geologic Framework of the Delaware Basin, Eddy and Lea Counties, New Mexico: New Mexico Bureau of Geology and Mineral Resources Open-File Geologic Map 318, scale 1:250,000, https://doi.org/10.58799/OF-GM-318.

LeMay, W.J., 1961, Oil accumulations along Abo reefing, southeastern New Mexico [abs.]: American Association of Petroleum Geologists Bulletin, v. 45, no. 1, p. 125–126, https://doi.org/10.1306/BC743663-16BE-11D7-8645000102C1865D.

Love, D., and Land, L.A., 2006, Surficial Geology in the Vicinity of Washington Ranch, *in* Land, L., Lueth, V.W., Raatz, W., Boston, P., and Love, D.L., eds., Caves and Karst of Southeastern New Mexico, New Mexico Geological Society 57th Annual Field Conference Guidebook, p. 57–344, https://doi.org/10.56577/FFC-57.311.

Lucas, S.G., and Anderson, O., 1993, Stratigraphy of the Permian–Triassic boundary *in* Love, D.W., Hawley, J.W., Kues, B.S., Adams, J.W., Austin, G.S., and Barker, J.M., eds., *Carlsbad Region, New Mexico and West Texas*: New Mexico Geological Society 44th Annual Field Conference Guidebook, p. 219–230, https://doi.org/10.56577/FFC-44.

Lucas, S.G., and Morgan, G.S., 1996, Pleistocene vertebrates from the Pecos River valley near Roswell, Chaves County, New Mexico: New Mexico Geology, v. 18(4), p. 93–96, https://doi.org/10.58799/NMG-v18n4.93.

Machette, M.N., Personius, S.F., Kelson, K.I., Dart, R.L., and Haller, K.M., 1998, Map and Data for Quaternary Faults and Folds in New Mexico: United States Geological Survey Open-File Report 98–52, p. 358, https://doi.org/10.3133/ofr98521.

McCraw, D.J., Rawling, G., and Land, L.A., 2007, Preliminary geologic map of the Bitter Lake 7.5-minute Quadrangle, Chaves County, New Mexico: New Mexico Bureau of Geology and Mineral Resources, Open-File Geologic Map 151, scale 1:24,000, https://doi.org/10.13140/RG.2.1.3634.6087.

McCraw, D.J., and Land, L.A., 2008, Preliminary geologic map of the Lake McMillan North 7.5-minute Quadrangle, Eddy County, New Mexico: New Mexico Bureau of Geology and Mineral Resources Open-File Geologic Map 167, scale 1:24,000, https://doi.org/10.58799/OF-GM-167.

McCraw, D.J., Land, L.A., and Williams, S., 2011, Geologic Map of the Spring Lake 7.5-minute Quadrangle, Eddy County, New Mexico Bureau of Geology and Mineral Resources Open-File Geologic Map 214, scale 1:24,000, https://doi.org/10.58799/OF-GM-214.

McKnight, C.L., 1986, Descriptive geomorphology of the Guadalupe Mountains, southcentral New Mexico and west Texas: Baylor Geological Studies, Department of Geology, Baylor University, Waco, Texas, p. 40.

McLemore, V.T., 2006, Mineral deposits in Eddy County, New Mexico, and their relationship to karst processes, *in* Land, L., Lueth, V.W., Raatz, W., Boston, P., and Love, D.L., eds., Caves and Karst of Southeastern New Mexico, New Mexico Geological Society 57th Annual Field Conference Guidebook, p. 337–344, https://doi.org/10.56577/FFC-57.337.

McLemore, V.T., and Austin, G.S., 2017, Energy and Mineral Resources of New Mexico: Industrial Minerals and Rocks: New Mexico Bureau of Geology and Mineral Resources Memoir 50E, https://doi.org/10.58799/M-50E.

Miall, A.D., 2008, The southern midcontinent, Permian Basin, and Ouachitas, in Miall, A.D., ed., The sedimentary basins of the United States and Canada (ch. 8): Elsevier Sedimentary Basins of the World, v. 5, p. 297–327, https://doi.org/10.1016/S1874-5997(08)00008-7.

Molina-Garza, R.S., Geissman, J.W., and Vander Voo, R., 1989, Paleomagnetism of the Dewey Lake Formation (Late Permian), northwest Texas: end of the Kiaman superchron in North America: Journal of Geophysical Research, v. 94, p. 17881–17888, https://doi.org/10.1029/JB094iB12p17881.

Morgan, G.S., and Lucas, S.G., 2006, Pleistocene vertebrates from southeastern New Mexico, *in* Land, L., Lueth, V.W., Raatz, W., Boston, P., and Love, D., eds., *Caves and Karst of Southeastern New Mexico*: New Mexico Geological Society 57th Annual Field Conference Guidebook, p. 317–335. https://doi.org/10.56577/FFC-57.317.

Motts, W.S., 1962, Geology of the West Carlsbad quadrangle, New Mexico: United States Geological Survey Geologic Quadrangle 167, scale 1:62,500, https://doi.org/10.3133/gq167.

Nance, H.S., 2001, Guadalupian (Artesia Group) and Ochoan shelf succession of the Permian Basin: Effects of deposition, diagenesis, and structure on reservoir development: Bureau of Economic Geology Report of Investigations No. 261, The University of Texas at Austin, p. 53.

Newell, N.D., Rigby, J.K., Fischer, A.G., Whiteman, A.J., Hickox, J.E., and Bradley, J.S., 1953, *The Permian reef complex of the Guadalupe Mountains region, Texas and New Mexico, in a study in paleoecology*: San Francisco, California, W.H. Freeman & Co., p. 236, https://doi.org/10.1126/science.119.3099.727.a.

O'Neill, J.M., 1998, Geologic map of the Cienega School 7.5-minute Quadrangle, Otero County, New Mexico and Hudspeth County, Texas: United States Geological Survey Geologic Investigation Series I-2630, https://doi.org/10.3133/i2630.

Pederson, J.L., and Dehler, C.M., 2004a, Geologic Map of the Otis 7.5-minute Quadrangle, Eddy County, New Mexico: New Mexico Bureau of Geology and Mineral Resources Open-File Geologic Map 76, scale 1:24,000, p. 5, https://doi.org/10.58799/OF-GM-76.

Pederson, J.L., and Dehler, C.M., 2004b, Geologic Map of the Loving 7.5-minute Quadrangle, Eddy County, New Mexico: New Mexico Bureau of Geology and Mineral Resources Open-File Geologic Map 77, scale 1:24,000, p. 6, https://doi.org/10.58799/OF-GM-77.

Podpechan, F.W., 1959, New Empire Abo strikes rush to southeast New Mexico: Oil and Gas Journal, v. 57, no. 26, p. 148–151.

Polyak, V.J., McIntosh, W.C., Güven, N., and Provencio, P., 1998, Age and Origin of Carlsbad Cavern and Related Caves from $^{40}Ar/^{39}Ar$ of Alunite: Science, v. 279, issue 5358, p. 1919–1922, https://doi.org/10.1126/science.279.5358.1919.

Polyak, V.J., McIntosh, W.C., Provencio, P.P., and Guven, N., 2006, Alunite and natroalunite tell a story-the age and origin of Carlsbad Cavern, Lechuguilla Cave, and other sulfuric-acid type caves of the Guadalupe Mountains, *in* Land, L., Lueth, V.W., Raatz, W., Boston, P., and Love, D., eds., *Caves and Karst of Southeastern New Mexico*: New Mexico Geological Society 57th Annual Field Conference Guidebook, p. 203–209, https://doi.org/10.56577/FFC-57.203.

Polyak, V.J., Provencio, P., and McIntosh, B., 2023, Sulfuric acid speleogenesis at the new section level of Carlsbad Cavern roughly 6 Ma. *in* Land, L., Jaoude, I.B., Hutchinson, P., Zeigler, K., Jakle, A., and Werff, V.B., eds., Evaporite Karst of the Lower Pecos Region: New Mexico Geological Society 73rd Annual Field Conference Guidebook, p. 76–80, https://doi.org/10.56577/FFC-73.76.

Pope, M.C., 2004, Cherty carbonate facies of the Montoya Group, southern New Mexico and western Texas and its regional correlatives: A record of Late Ordovician paleoceanography on southern Laurentia: Palaeogeography, Palaeoclimatology, Palaeoecology v. 210, (issue) no. 2-4, p. 367–384, https://doi.org/10.1016/j.palaeo.2004.02.035.

Powers, D.W., and Holt, R.M., 1993, The upper Cenozoic Gatuña Formation of southeastern New Mexico, *in* Love, D.W., Hawley, J.W., Kues, B.S., Adams, J.W., Austin, G.S., and Barker, J.M., eds., *Carlsbad Region, New Mexico and West Texas*: New Mexico Geological Society 44th Annual Field Conference Guidebook, p. 271–282, https://doi.org/10.56577/FFC-44.271.

Pratt, W.E., 1954, Evidence of igneous activity in the northwestern part of the Delaware basin, in Stripp, T.F., ed., Guidebook of southeastern New Mexico: New Mexico Geological Society 5th Annual Fall Field Conference Guidebook, p. 143–147, https://doi.org/10.56577/FFC-5.

Pray, L.C., 1954, Outline of the stratigraphy and structure of the Sacramento Mountain escarpment, in New Mexico Geol. Soc. Guidebook, 5th Field Conf., October 1954: p. 92–107.

Railsback, L.B., Brook, G.A., Ellwood, B.B., Liang, F., Cheng, H., and Edwards, R.L., 2015, A record of wet glacial stages and dry interglacial stages over the last 560 kyr from a standing massive stalagmite in Carlsbad Cavern, New Mexico, USA: Paleogeography, Paleoclimatology, Paleoecology, v. 438, p. 256–266, https://doi.org/10.1016/j.palaeo.2015.08.010.

Repasch, M., Karlstrom, K., Heizler, M., and Pecha, M., 2017, Birth and evolution of the Rio Grande fluvial system in the past 8 Ma: progressive downward integration and the influence of tectonics, volcanism, and climate: Earth-Science Reviews, v. 168, p. 113–164, https://doi.org/10.1016/j.earscirev.2017.03.003.

Rice-Snow, S., and Goodbar, J., 2006, Terrain factors in Capitan aquifer recharge, northeastern Guadalupe escarpment, New Mexico, *in* Land, L., Lueth, V.W., Raatz, W., Boston, P., and Love, D., eds., *Caves and Karst of Southeastern New Mexico*: New Mexico Geological Society 57th Annual Field Conference Guidebook, p. 211–218, https://doi.org/10.56577/FFC-57.

Rosholt, J.N., and McKinney, C.R., 1980, Part 1: Uranium Series Disequilibrium Investigations Related to the WIPP Site, New Mexico, Part II: Uranium Trend Dating of Surficial Deposits and Gypsum Spring Deposit near WIPP Site, New Mexico: United States Geological Survey Open-File Report 80-879, p. 23.

Roth, R., Newell, N.D., and Burma, B.H., 1941, Permian pelecypods in the lower Quartermaster Formation, Texas: Journal of Paleontology, v. 15, p. 312–317.

Rudolph, K., 2023, The ancestral Rocky Mountain orogeny and evolution of the Permian Basin, *in* Land, L., Jaoude, I.B., Hutchinson, P., Zeigler, K., Jakle, A., and Werff, V.B., eds., Evaporite Karst of the

Lower Pecos Region: New Mexico Geological Society 73rd Annual Field Conference Guidebook, p. 98–102, https://doi.org/10.56577/FFC-73.

Schiel, K.A., 1988, The Dewey Lake Formation: end stage deposit of a peripheral foreland basin [master's thesis]: El Paso, University of Texas at El Paso, 181 p.

Scholle, P.A, Goldstein, R.H., and Ulmer-Scholle, D.S., 2007, Classic Upper Paleozoic reefs and bioherms of West Texas and New Mexico: a field guide to the Guadalupe and Sacramento Mountains of West Texas and New Mexico: New Mexico Bureau of Geology and Mineral Resources Open-File Report 504, p. 174, https://doi.org/10.58799/OFR-504.

Scott, R.W., Fee, D., Magee, R., and Laali, H., 1978, Epeiric Depositional Models for the Lower Cretaceous Washita Group, North-Central Texas: The University of Texas at Austin, Austin, Texas, Bureau of Economic Geology Report of Investigations No. 94, p. 24, https://doi.org/10.23867/RI0094D.

Skinner, J.W., 1946, Correlation of Permian of west Texas and southeast New Mexico: American Association of Petroleum Geologists Bulletin, v. 30, no. 11, p. 1857-1874, https://doi.org/10.1306/3D933887-16B1-11D7-8645000102C1865D.

Skotnicki, S.J., 2021, Geologic Map of the Carlsbad Caverns 7.5-Minute Quadrangle, Eddy County, New Mexico: New Mexico Bureau of Geology and Mineral Resources Open-File Geologic Map 285, scale 1:24,000, p. 21, https://doi.org/10.58799/OF-GM-285.

Skotnicki, S.J., and Attia, S., 2022, Geologic Map of the Serpentine Bends 7.5-minute Quadrangle Eddy County: New Mexico Bureau of Geology and Mineral Resources Open-File Geologic Map 301, scale 1:24,000, p. 20, https://doi.org/10.58799/OF-GM-301.

Skotnicki, S.J., and Knight, A.D., 2021, Geologic Map of the Guadalupe Mountains National Park, Culberson and Hudspeth Counties, Texas: New Mexico Bureau of Geology and Mineral Resources, Open-File Report 610, scale 1:24,000, p. 102, https://doi.org/10.58799/OFR-610.

Skotnicki, S.J., 2024a, Geologic Map of the El Paso Gap 7.5-Minute Quadrangle, Eddy and Otero Counties, New Mexico and Culberson County, Texas: New Mexico Bureau of Geology and Mineral Resources, Open-File Geologic Map 307, scale 1:24,000, 1 plate, p. 24, https://doi.org/10.58799/OF-GM-307.

Skotnicki, S.J., 2024b, Geologic Map of the El Paso Gap 15-Minute Quadrangle, Eddy and Otero Counties, New Mexico and Culberson and Hudspeth Counties, Texas: New Mexico Bureau of Geology and Mineral Resources Open-File Geologic Map 315, scale 1:62,500, p. 31, https://doi.org/10.58799/OF-GM-315.

Skotnicki, S.J., and Allen, B.D., 2024, Geologic Map of the Gunsight Canyon 7.5-Minute Quadrangle, Eddy County, New Mexico: New Mexico Bureau of Geology and Mineral Resources Open-File Geologic Map 310, scale 1:24,000, p. 9, https://doi.org/10.58799/OF-GM-310.

Suppe, J., and Medwedeff, D., 1990, Geometry and kinematics of fault-propagation folding: Eclogae Geologicae Helvetiae, v. 83, no. 3, p. 409–454.

Timmons, S., and Sturgis, L., eds., 2022, Hydrogeology and water resources of the Salt Basin, New Mexico and Texas: New Mexico Bureau of Geology and Mineral Resources Open-File Report 618, p. 154, https://doi.org/10.58799/OFR-618.

Tranel, L.M., and Happel, A.A., 2020, Evaluating escarpment evolution and bedrock erosion rates in the western Guadalupe Mountains, West Texas and New Mexico: Geomorphology, v. 368(6), p. 17, https://doi.org/10.1016/j.geomorph.2020.107335.

U.S. Department of Energy, 2022, Transuranic Waste Acceptance Criteria for the Waste Isolation Pilot Plant, Revision 8.0: U.S. Department of Energy, Carlsbad Field Office, DOE/WIPP-02-3122, p. 125, https://wipp.energy.gov.

Veldhuis, J.H., and Keller, G.R., 1980, An integrated geological and geophysical study of the Salt Basin graben, west Texas, *in* Dickerson, P.W., and Hoffer, J.M., eds., Trans-Pecos Region, Southeastern New Mexico: New Mexico Geological Society 31st Annual Field Conference Guidebook, p. 141–150, https://doi.org/10.56577/FFC-31.141.

Vine, J.D., 1963, Surface geology of the Nash Draw quadrangle, Eddy County, New Mexico: United States Geological Survey Bulletin 1141-B, p. 46, https://doi.org/10.3133/b1141B.

Walper, J.L., 1977, Paleozoic tectonics of the southern margin of North America: Transactions of the Gulf Coast Association of Geological Societies, v. 27, p. 230–241, https://doi.org/10.22201/igeof.00167169p.1989.28.5.1290.

Wilkins, D.E., and Currey, D.R., 1997, Timing and extent of late Quaternary paleolakes in the Trans-Pecos closed basin, West Texas and South-Central New Mexico: Quaternary Research, p. 306-315, https://doi.org/10.1006/qres.1997.1896.

Wilson, J.L., 1975, *Carbonate facies in geologic history*: New York, Springer-Verlag, p. 47, https://doi.org/10.1007/978-1-4612-6383-8.

Winchester, J., 2024, New Mexico remains No. 2 oil producing state: Independent Petroleum Association of New Mexico, December 5, https://ipanm.org/2024/12/05/new-mexico-remains-no-2-oil-producing-state/.

Ye, H., Royden, L., Burchfiel, C., and Schuepbach, M., 1996, Late Paleozoic deformation of interior North America—the greater Ancestral Rocky Mountains: AAPG Bulletin, v. 80, no. 9, p. 1397–1432, https://doi.org/10.1306/64ED9A4C-1724-11D7-8645000102C1865D.

BIBLIOGRAPHY

Bachman, G.O., 1974, Geologic Processes and Cenozoic History Related to Salt Dissolution in Southeastern New Mexico: United States Geological Survey Open-File Report 74-194, p. 81, https://doi.org/10.3133/ofr74194.

Bachman, G.O, and Machette, M.M., 1977, Calcic Soils and Calcretes in the Southwestern United States: United States Geological Survey Open-File Report 77-794, p. 163, https://doi.org/10.3133/ofr77794.

Bachman, G.O., 1981, Geology of Nash Draw, Eddy County, New Mexico: United States Geological Survey Open-File Report 81–31, 4 plates, p. 8, https://doi.org/10.3133/ofr8131.

Baird, D., 1964, Dockum (Late Triassic) reptile footprints from New Mexico: *Journal of Paleontology*; v. 38 (January 1964), no. 1, p. 118–125, https://www.jstor.org/stable/1301500.

Connell, S.D., Hawley, J.W., and Love, D., 2005, Late Cenozoic drainage development in the southeastern Basin and Range of New Mexico, southeasternmost Arizona, and western Texas, in Lucas, S.G., Morgan, G.S., and Zeigler, K.E., eds., New Mexico's Ice Ages: New Mexico Museum of Natural History & Science Bulletin No. 28, p. 125-150.

Cox, E.R., 1967, Geology and hydrology between Lake McMillan and Carlsbad Springs, Eddy County, New Mexico: United States Geological Survey Water Supply Paper WSP-1828, 6 plates, p. 48, https://doi.org/10.3133/wsp1828.

Decker, D.D., Polyak, V.J., Asmerom, Y., and Lachniet, M.S., 2018, U-Pb Dating of Cave Spar: A New Shallow Crust Landscape Evolution Tool: Tectonics, v. 27(1), p. 208–223, https://doi.org/10.1002/2017TC004675.

Decker, D.D., Land, L., and Luke, B., 2021, Geophysical Characterization of Playa Lakes in the Gypsum Karst of Southeastern New Mexico, USA: Oklahoma Geological Survey Circular 113, p. 79–92.

Department of the Interior, Geological Survey, 1955, Huapache Oil Unit, sec. 35, T. 23 S., R. 22 E., well no. 1 (30-015-00014). Humble Oil & Refining Company, operator. OCD Geospatial Hub.

Department of the Interior, Geological Survey, 1956, Huapache Oil Unit, sec. 23, T. 23 S., R. 22 E., well no. 2 (30-015-00013). Humble Oil & Refining Company, operator. OCD Geospatial Hub.

Department of the Interior, Geological Survey, 1959, Bandana Point Unit, sec. 13, T. 23 S., R. 23 E., well no. 1 (30-015-00044). Humble Oil & Refining Company, operator. OCD Geospatial Hub.

Department of the Interior, Geological Survey, 1960, North Caverns Unit, sec. 11, T. 23 S., R. 24 E., well no. 1 (30-015-05913). Gulf Oil Corporation, operator. OCD Geospatial Hub.

Department of the Interior, Geological Survey, 1961, Las Cruces D, sec. 12, T. 24 S., R. 21 E., well no. 1 (30-015-00003). Skelley Oil Company, operator. OCD Geospatial Hub.

Department of the Interior, Geological Survey, 1961, McMillan, sec. 15, T. 23 S., R. 19 E., well no. 1 (30-35-00018). E.P. Campbell, operator. OCD Geospatial Hub.

Department of the Interior, Geological Survey, 1965, Cueva Unit, sec. 28, T. 22 S., R. 25 E., well no 1 (30-015-10560). Monsanto Company, operator. OCD Geospatial Hub.

Department of the Interior, Geological Survey, 1967, Rock Tank Unit, sec. 7, T. 23 S, R. 25 E., well no. 1 (30-015-20095). Monsanto Company, operator. OCD Geospatial Hub.

Department of the Interior, Geological Survey, 1972, McKittrick Federal, sec. 25, T. 22 S, R. 25 E., well no. 1 (30-015-00135). Western Oil Producers, Inc., operator. OCD Geospatial Hub.

Department of the Interior, Geological Survey, 1975, Robinia Draw, sec. 3, T. 23 S., R. 24 E., well no. 1 (30-015-21620). Monsanto Company, operator. OCD Geospatial Hub.

Department of the Interior, Geological Survey, 1977, Huber Federal, sec. 27, T. 23 S., R. 22 E., well no. 1 (30-015-22022). Texas Oil & Gas Corporation, operator. OCD Geospatial Hub.

Department of the Interior, Geological Survey, 1979, Patterson Federal, sec. 20, T. 23 S., R. 23 E., well no. 1 (30-015-22740). Coquina Oil Corporation, operator. OCD Geospatial Hub.

Department of the Interior, Geological Survey, 1980, Last Chance, sec. 2, T. 23 S., R. 23 E., well no. 1 (30-015-23103). Harvey E. Yates Company, operator. Amoco Production Company. OCD Geospatial Hub.

Department of the Interior, Geological Survey, 1981, Phillips Federal, sec. 1, T. 24 S., R. 28 E., well no. 1 (30-015-23779). Harvey E. Yates Company, operator. OCD Geospatial Hub.

Department of the Interior, Geological Survey, 2001, Saragossa 17 Fed Com 1, sec. 17, T. 23 S., R. 26 E. (30-015-31529). Louis Dreyfus Natural Gas Corporation, operator. OCD Geospatial Hub.

Ewing, T.E., 2019, Tectonics of the West Texas (Permian) Basin origins, structural geology, subsidence, and later modification, in Ruppel, S. C., ed., Anatomy of a Paleozoic basin: the Permian Basin, USA (vol. 1, ch. 4): The University of Texas at Austin, Bureau of Economic Geology Report of Investigations 285; American Association of Petroleum Geologists Memoir 118, p. 63–96.

Flawn, P.T., 1954, Summary of southeast New Mexico basement rocks, in Stripp, T.F., ed., Guidebook of southeastern New Mexico: New Mexico Geological Society 5th Annual Fall Field Conference Guidebook, p. 114-116, https://doi.org/10.56577/FFC-5.114.

Frye, J.C., Leonard, A.B., and Glass, H.D., 1982, Western extent of Ogallala Formation in New Mexico: New Mexico Bureau of Geology and Mineral Resources Circular 175, p. 41, https://doi.org/10.58799/C-175.

Hall, S.A., and Goble, R.J., 2023, Late Middle Pleistocene OSL Age of the Upper Gatuña Formation, Southeastern New Mexico *in* Land, L., Jaoude, I.B., Hutchinson, P., Zeigler, K., Jakle, A., and Werff, V.B., eds., Evaporite Karst of the Lower Pecos Region: New Mexico Geological Society 73rd Annual Fall Field Conference Guidebook, p. 62–63, https://doi.org/10.56577/FFC-73.

Harris, A.H., 1993, Quaternary Vertebrates of New Mexico, New Mexico Museum of Natural History, in Lucas, S.G., and Zidek, J., eds., Vertebrate paleontology in New Mexico: New Mexico Museum of Natural History Bulletin No. 02, p. 179–197

Hawley, J.H., 2005, Five million years of landscape evolution in New Mexico: an overview based on two centuries of geomorphic conceptual-model development, in Lucas, S.G., Morgan, G.S., and Zeigler, K.E., eds., New Mexico's Ice Ages: New Mexico Museum of Natural History & Science Bulletin No. 28, p. 9–94.

Hayes, P.T., and Bachman, G.O., 1979, Examination and Reevaluation of Evidence for the Barrera Fault, Guadalupe Mountains, New Mexico: United States Geological Survey Open-File Report 79-1520, p. 13, https://doi.org/10.3133/ofr791520.

Hayes, P.T., and Bigsby, P.R., 1983, Mineral Resources potential of the Little Dog and Pup Canyons Roadless Area, Otero County, New Mexico: United States Geological Survey Miscellaneous Field Studies Map MF-1468, https://doi.org/10.3133/mf1468.

Hayes, P.T., Light, T.D., and Thompson, J.R., 1983, Mineral resource potential and geologic map of the Guadalupe Escarpment Wilderness Study Area, Eddy County, New Mexico: United States Geological Survey Miscellaneous Field Studies Map MF-1560-A, https://doi.org/10.3133/mf1560A.

Jones, C.L., and Madsen, B.M., 1968, Evaporite geology of fifth ore zone, Carlsbad district, southeastern New Mexico: United States Geological Survey Bulletin 1252-B, p. 30, https://doi.org/10.3133/b1252B.

Koop, A.N., Hirmas, D.R., Sullivan, P.L., and Mohammed, A.K., 2020, A generalizable index of soil development: Geoderma, v. 360(2020), p. 13, https://doi.org/10.1016/j.geoderma.2019.113898.

Lang, W.T.B., 1937, The Permian formations of the Pecos valley of New Mexico and Texas: American Association of Petroleum Geologists Bulletin, v. 21, no. 7, p. 833-898, https://doi.org/10.1306/3D932EDE-16B1-11D7-8645000102C1865D.

Lucas, S.G., 2023, The Guadalupian series and the Permian timescale, *in* Land, L., Jaoude, I.B., Hutchinson, P., Zeigler, K., Jakle, A., and Werff, V.B., eds., Evaporite Karst of the Lower Pecos Region: New Mexico Geological Society 73rd Annual Field Conference Guidebook, p. 82-88, https://doi.org/10.56577/FFC-73.82.

Lucas, S.G., 2004, The Permian Guadalupian stages: how politics and conodonts produced and unworkable chronostratigraphy: Permophiles – Newsletter of the Subcommission on Permian Stratigraphy No. 76, p. 9–11.

Lucas. S.G., Henderson, C.M., Krainer, K., Barrick, J.E., and Reynolds, S.J., 2024, Early Permian seaways in the American southwest: Journal of South American Earth Sciences, v. 148, p. 105–176, https://doi.org/10.1016/j.jsames.2024.105176.

Machette, M.N., 1985, Calcic soils of the southwestern United States, in Weide, D. L., ed., Soils and Quaternary Geology of the Southwestern United States: Geological Society of America Special Paper 203, p. 1–21.

Massari, F., Rio, D., Sgavetti, M., Prosser, G., D'Alessandro, A., Asioli, A., Capraro, L., Fornaciari, E., and Tateo, F., 2002, Interplay between tectonics and glacio-eustasy: Pleistocene succession of the Crotone basin, Calabria (southern Italy): Geological Society of America Bulletin, v. 114(1), p. 1183-1209, https://doi.org/10.1130/0016-7606(2002)114<1183:IBTAGE>2.0.CO;2.

Miall, A.D., and Blakey, R.C., 2008, Chapter 1: The Phanerozoic Tectonic and Sedimentary Evolution of North America, in Miall, A.D., ed., Sedimentary Basins of the World: The Sedimentary Basins of the United States and Canada: Elsevier, v. 5, p. 29, https://doi.org/10.1016/S1874-5997(08)00001-4.

Miller, R.R., 1982, First Fossil Record (Plio-Pleistocene) of Threadfin Shad, Dorosoma petenense, from the Gatuña Formation of Southeastern New Mexico: Journal of Paleontology, v. 56(2), p. 423–425.

Moore, S.L., Kleinkopf, M.D, Nowlan, G.A., and Corbetta, P.A., 1989, Mineral resources of the Brokeoff Mountains Wilderness Study Area, Otero County, New Mexico: United States Geological Survey Bulletin 1735-E, p. 22, https://doi.org/10.3133/b1735E.

Motts, W.S., 1968, The Control of Ground-Water Occurrence by Lithofacies in the Guadalupian Reef Complex near Carlsbad, New Mexico: Geological Society of America Bulletin, v.79(3), p. 283, https://doi.org/10.1130/0016-7606(1968)79[283:TCOGOB]2.0.CO;2.

Muehlberger, W.R., Belcher, R.C., and Goetz, L.K., 1978, Quaternary faulting in Trans-

Pecos Texas: Geology, v. 6(6), p. 337-340, https://doi.org/10.1130/0091-7613(1978)6<337:QFITT>2.0.CO;2.

New Mexico Bureau of Geology and Mineral Resources, 2003, Geologic Map of New Mexico: New Mexico Bureau of Geology and Mineral Resources Open-File Geologic Map 304, scale 1:500,000, 2 plates, https://doi.org/10.58799/116894.

New Mexico Oil Conservation Commission, 1957, Wester – Huapache Unit, sec. 33, T. 23 S., R. 22 E., well no. 1 (30-015-00015). Panoil Company, operator. Yates Drilling Company. OCD Geospatial Hub.

New Mexico Oil Conservation Commission, 1960, Bandana Point Unit, sec. 2, T. 23 S., R. 23 E., well no. 2 (30-015-00041). Humble Oil & Refining Company, operator. OCD Geospatial Hub.

New Mexico Oil Conservation Commission, 1962, Huapache – Wester, sec. 33, T. 23 S., R. 22 E., well no. 1 (30-015-20752). Panoil Company, operator. Yates Drilling Company. OCD Geospatial Hub.

New Mexico Oil Conservation Commission, 1971, West Dog Canyon Unit, SEC. 18, T. 25 S., R. 20 E., well no. 1 (30-35-20007). W.W. West, operator. OCD Geospatial Hub.

New Mexico Oil Conservation Commission, 1976, CNB Com. Sec. 11, T. 24 S., R. 28 E., well no. 1 (30-015-21786). Aminoil USA, Inc., operator. OCD Geospatial Hub.

New Mexico Oil Conservation Commission, 1976, Forehand #1-K, sec. 15, T. 23 S., R. 27 E. (30-015-21599). Husky Oil Company of Delaware, operator. OCD Geospatial Hub.

New Mexico Oil Conservation Commission, 1980, Cassidy Com, sec. 29, T. 23 S., R. 28 E., well no. 1 (30-015-23340). Belco Petroleum Corporation, operator. OCD Geospatial Hub.

New Mexico Oil Conservation Commission, 1980, Chadwick, sec. 9, T. 23 S., R. 27 E., well no. 1 (30-015-01112). Carper Drilling Company, Inc., operator. OCD Geospatial Hub.

New Mexico Oil Conservation Commission, 1980, Yates – King, sec. 22, T. 23 S., R. 26 E., well no. 1 (30-015-20808). J.M. Huber Corporation, operator. Carper Drilling Company, Incorporated. OCD Geospatial Hub.

Pazzaglia, F.J., 2005, River Response to Ice Age (Quaternary) Climates in New Mexico, in Lucas, S.G., Morgan, G.S., and Zeigler, K.E., eds., New Mexico's Ice Ages: New Mexico Museum of Natural History & Science Bulletin No. 28, p. 115–125.

Scholle, P.A., Ulmer, D.S., and Melim, L.A., 1992, Late-stage calcites in the Permian Capitan Formation and its equivalents, Delaware Basin Margin, west Texas and New Mexico: evidence for replacement of precursor evaporites: Sedimentology, v. 39, (issue 2), p. 207–234, https://doi.org/10.1111/j.1365-3091.1992.tb01035.x.

Sion, B.D., Philips, F.M., Axen, G.J., Harrison, B.J., Love, D.W., and Zimmerer, M.J., 2020, Chronology of terraces in the Rio Grande rift, Socorro basin, New Mexico: implications for terrace formation: Geosphere, v. 16(6), p. 1457-1478, https://doi.org/10.1130/GES02220.1.

Simpson, S., 2010, Holocene Thermal Feature Types in Archaeological Sites of the Mescalero Sands Environment, New Mexico [master's thesis]: Reno, Nevada, University of Nevada at Reno, p. 531.

Wilkins, D.E., and Currey, D.R., 1999, Radiocarbon chronology and C-13 analysis of

mid- to late-Holocene aeolian environments, Guadalupe Mountains National

Park, Texas: The Holocene, v. 9(3), p. 363–371, https://doi.org/10.1191/095968399677728249.

Willis, R., 1929, Preliminary Correlation of the Texas and New Mexico Permian: American Association of Petroleum Geologists Bulletin, v. 13, p. 1000-1031, https://doi.org/10.1306/3d93286f-16b1-11d7-8645000102c1865d.

APPENDIX

Description of Map Units

CENOZOIC ERATHEM

QUATERNARY SYSTEM

Anthropogenic (recent to late Holocene)

af – artificial fill

Short description: Areas artificially filled by anthropogenic activity that obscures or covers underlying geologic relations. Artificial fill may consist of any materials and includes quarries, tailings piles, drill

pads, dumps, dams, reservoir sediments, and major roads. Archeological sites are excluded from this map unit. Approximately 2–15 m thick.

Long description: Areas artificially filled by anthropogenic activity that obscures or covers underlying geologic relations. Artificial fill may consist of any materials and includes quarries, tailings piles, drill pads, dumps, dams, reservoir sediments, and major roads. Archeological sites are excluded from this map unit. Deposits are approximately 2–15 m thick. Areas where disturbed land masks the underlying geology without having a deposit of significant thickness (i.e., tilled land, concrete, and/or roads) are mapped with a separate, shaded, overlay polygon shown in the accompanying map's Explanation of Map Symbols. Compiled from new observations and synthesized descriptions of Dehler and Pederson (1998), Pederson and Dehler (2004a, 2004b), Cikoski (2019a, 2019b, 2020), Allen and Attia (2022), Skotnicki and Attia (2022), Allen (2024), and Allen and Skotnicki (2024).

Eolian deposits (recent to late Pleistocene)

Qe – Eolian sediments

Short description: Partially stabilized eolian sediments that are red-orange and tan-brown. Fine-grained, well-sorted, arenitic sand. Five generations of sand sheets stabilized by argillic or petrocalcic soil development with overlying unconsolidated parabolic or coppice dunes and sheet sands (Hall and Goble, 2023). In raised topographic positions in proximity to the Pecos River. Approximately 0–8 m thick.

Long description: Windblown, fine-grained, light-red to orange, brown, or tan sands forming hummocky terrain in thick dune fields moderately stabilized by vegetation and soil development. Includes parabolic dunes, coppice dunes, and sand sheets stabilized by soils and vegetation on the Mescalero Plain. Dune-form deposits and young sand sheets are unconsolidated, well-sorted, and arenitic and do not exhibit soil development. A dominant northeastern wind direction is observable from imagery. Unconsolidated dunes and sand sheets overlie Permian or Quaternary–Neogene bedrock or up to five older generations of sand sheets stabilized by pedogenic development. Studies establishing late-Pleistocene to Holocene eolian stratigraphy using optically stimulated luminescence are summarized by Hall and Goble (2023). The oldest episode dates to 90–50 ka and the youngest to 6–2 ka. Each event is capped by distinct paleosols reflecting periods of stabilization and pedogenic development. Dunes may locally exhibit light-tan to yellow color and a higher abundance of gypsum when in proximity to outcropping gypsum-rich facies of the Rustler Formation or gypsiferous facies of the Gatuña Formation. Well-rounded, siliceous pebbles and caliche clasts originating from underlying units are common in troughs between dunes. Found in alluvial channels, on river terraces, and in raised topographic positions northeast of the Pecos River on the southwestern margin of the Mescalero Plain. Deposit thicknesses range from 0 to 8 m. Compiled from new observations and synthesized descriptions of Dehler and Pederson (1998), Pederson and Dehler (2004b), Cikoski (2019b, 2020), and Hall and Goble (2023).

Qse – Sheetwash alluvium and loessal eolian sediments, interbedded

Short description: Thin mantle of lithologically heterogeneous deposits of loessal silts and eolian sands with reworking by sheetwash processes. Primarily coppice dunes or sheets of silt and sand. Poorly exposed and unconsolidated. Forms a thin veneer on raised surfaces. Deposits have weak argillic, gypsic, or calcic soil development. Approximately 0–3 m thick, occasionally 10 m thick or greater.

Long description: Thin, reworked eolian mantles of slope-, plane-, and piedmont-blanketing, fine- to coarse-grained, lithologically heterogeneous deposits of loessal silts and eolian sands with subordinate regolith, colluvium, and alluvial sediments. Dominantly reworked by sheetwash alluvial processes with subordinate reworking from channel alluvial processes. Form sheets, coppice dunes, and low-gradient alluvial aprons of sheetwash origin. Deposits tend to be tan to light-brown or yellowish-red, are pink to pale-red in areas underlain by red-hued bedrock, and are occasionally white to pale-gray at the surface or grading downward when in proximity to sources of gypsum. Dominantly silts, clays, and fine sands with trace pebbles or colluvial gravels in massive to poorly stratified deposits. Poorly exposed in outcrop but thin, flaggy, or tabular bedding and common dune forms inferred from surface morphology. Dominantly quartz with subordinate chert and carbonate input from local bedrock. Texturally mature, occasionally poorly sorted, and composed of subangular to subrounded clasts. Locally composed of gypsite from eolian sources or underlying lithology. Variable amounts of locally derived, angular, colluvial gravels from bedrock and well-rounded pebbles from piedmont and alluvial gravels sourced from low, isolated outcrops of underlying units. Rounded gravels are dominantly carbonate, chert, and quartzite with subordinate volcanic clasts. Weak soil development of Stage I petrocalcic horizon development with 2 mm concretions decreasing below 40 cm depth, with rare granular argillic pedogenic development. Soils feature occasional bioturbation and prismatic structures; commonly effervesces with HCl, with a thin organic film near the surface. May be equivalent to the Mescalero Sands. This unit is differentiated from map unit **Qe** due to a higher degree of input and reworking by alluvial processes and lacks the characteristic surface morphology of that unit. Deposits are found as a thin veneer on most raised surfaces, may be interspersed with sub-map-scale bedrock outcrops, and are moderately vegetated with shrubs and grasses. Commonly thickens along drainages, in low areas, and when aprons are sloping from highlands. Deposit thicknesses range from 0 to 3 m, but are sometimes greater. Compiled from new observations and synthesized descriptions of Dehler and Pederson (1998), Pederson and Dehler (2004a, 2004b), Cikoski (2019a, 2019b, 2020), Cikoski and Allen (2020), Allen and Attia (2021, 2022), and Allen (2024).

Colluvial deposits (Holocene to late Pleistocene)

Qac – Alluvium and colluvium, undifferentiated

Short description: Undifferentiated deposits of unconsolidated, poorly sorted rockfalls, debris flows, slumps, fans, colluvium, terraces, and valley floor alluvium found in steep, narrow drainages, along slopes, and in valley floors. May include mixed input from dry ravel, sheetwash, alluvial, and gravity-driven processes. Color and lithology are variable depending on location. May include sediments of any diameter. Approximately 1–10 m thick.

Long description: Undifferentiated deposits of unconsolidated, poorly sorted rockfalls, debris flows, alluvial fans, minor slumps, colluvium, terraces, and valley floor alluvium found in steep, narrow drainages, along escarpment slopes, and in valley floors. Locally derived from higher-relief surrounding landscapes and may include mixed input from dry ravel, sheet wash, alluvial, and gravity-driven processes. Deposits may be mixed, interbedded, or separated but not at sufficient map scale to differentiate. Color and lithology are variable depending on location. May include clays, silts, sands, cobbles, and boulders of any diameter. Found among canyon walls, along erosional escarpments, and associated with solution-subsidence troughs. Deposits are typically unconsolidated but may be cemented when in proximity to active channels. Weak to nonexistent soil development. Typically merge or underlie with downslope, surficial deposits. Deposits are approximately 1–10 m thick. Compiled from new

observations and synthesized descriptions of Allen and Attia (2021), Allen and Skotnicki (2024), and Skotnicki and Allen (2024).

Internally drained deposits (Holocene to late Pleistocene)

Qdf – Depression fill

Short description: Accumulations of muds and sands with varying amounts of gravel, regolith, or gypsite in shallow, closed, or previously closed sinkhole depressions. Depressions are recent karst features from solution subsidence of underlying Permian evaporitic rock or Quaternary evaporite deposits. May exhibit back rotation of beds. Approximately 1–3 m thick.

Long description: Accumulations of muds, sands, subordinate evaporites, and varying amounts of gravels and regolith in shallow, closed, or previously closed sinkhole depressions. Depressions are karst features from solution subsidence of underlying Permian evaporitic rock or Quaternary evaporite deposits. Includes inputs from sheetwash and eolian transport along depression margins. Minor input of pebbles and cobbles from underlying lithology or alluvial transport from upslope outcrops. Capture of water from internal drainage promotes vegetation growth and may exhibit ephemeral standing water. Circular to subcircular in shape and range from meter to kilometer scale; may include crevices or caves. Erosion is observed to link adjacent sinkhole features to become larger internally, or externally drained, sheetwash alluvial channel features. Fine-grained materials are typically very pale-brown to brown in color while coarse material matches the color of its locally derived material. No evidence of soil development is present. May exhibit characteristics of playa or ephemeral lacustrine features. Deposits are most prevalent on the Gypsum Plain, southeast of the Black River, where they are commonly associated with the Castile and Salado Formations but may be found on any Permian or Quaternary map unit. Deposits are approximately 1–3 m thick. Compiled from new observations and synthesized descriptions of Cikoski (2019a, 2019b, 2020), Cikoski and Allen (2020), Skotnicki (2021), Allen and Attia (2021, 2022), Allen and Skotnicki (2024), Skotnicki and Allen (2024), and Allen (2024).

Qplr – Playa sediments, recent

Short description: White to tan or gray, alkaline accumulations in ephemeral lakes and ponds. Euhedral gypsum, minor calcite, and dolomite with very fine sands and silts. Found in southwestern corner of map area, with minor deposits occupying closed depressions in the eastern map area and Brokeoff Mountains. Approximately 0.5–1 m thick.

Long description: White to tan or gray, alkaline accumulations in ephemeral lakes and ponds. Windblown and evaporitic euhedral gypsum with fine eolian sands and silts; minor proportions of evaporitic calcite and dolomite. Found in the southwestern corner of the map area in Crow Flats at the northeastern edge of the Salt Basin, at one location within the Brokeoff Mountains, and in the vicinity of the Pecos River. Deposits are inset into lacustrine deposits of late Pleistocene age or playa deposits of late Pleistocene to early Holocene age. Pluvial Lake King was abandoned at the end of the last glacial maximum, and subsequent wind erosion created depressions for seasonal accumulation of hypersaline waters (King, 1948; McKnight, 1986; Wilkins and Currey, 1997). Minor alkali accumulations, mapped as playa deposits**,** occupying closed depressions in the eastern map area, are distinguished from depression fill by their alkaline composition. Deposits are approximately 0.5–1 m thick. Compiled from new observations and synthesized descriptions of O'Neill (1998) and Cikoski (2019b).

Qplyr – Playa sediments younger and recent, undifferentiated

Short description: The map unit **Qplyr** is mapped where the map scale does not permit differentiation of map unit **Qply** and map unit **Qplr** when both are present on the landscape.

Long description: The map unit **Qplyr** is mapped where the map scale does not permit differentiation of map unit **Qply** and map unit **Qplr** when both are present on the landscape. This map unit does not indicate if younger or recent playa sediments are more predominant in a given polygon and instead assumes a noteworthy portion of each is present.

Qply – Playa sediments, younger

Short description: Drab-gray, alkaline accumulations and fine-grained eolian sediments forming terraces of relic, ephemeral lake and pond levels inset by active playas. Contain minor carbonate nodules and sediments composed of evaporite minerals with very fine sands and silts. Found in Brokeoff Mountains and in proximity to the Pecos River. Approximately 0.5–1 m thick in outcrop.

Long description: Drab-gray, fine-grained, eolian-transported silts and sands within evaporitic deposits representing higher playa levels now inset by recent playa deposits. May contain minor carbonate nodules. The unit typically exhibits a poorly vegetated, low erosional escarpment that has been scoured by wind. Found at one location in the Brokeoff Mountains and in proximity to the Pecos River. Assumed to be the latest Pleistocene to early Holocene in age. Compiled from new observations and synthesized descriptions of O'Neill (1998) and Cikoski (2019b).

Ql – Lacustrine sediments

Short description: Fine-grained, laminated sediments deposited in lacustrine environments of the Salt Basin. Sediments of a late Pleistocene lacustrine system in the southwestern map area are found in 0.1- to 1-cm-thick intervals with alternating layers of unconsolidated clays, silts, and sands interlayered with resistant, platy evaporite beds. Approximately 3 m thick in outcrop.

Long description: Light-tan to brown, fine-grained, laminated sediments deposited in lacustrine environments of the Salt Basin. Includes sediments of a late-Pleistocene lacustrine system in the southwestern map area. Lake terraces composed of sediments from the late Pleistocene, pluvial Lake King are laminated at 0.1- to 1-cm intervals with alternating layers of unconsolidated clays, silts, and quartz or gypsum sands. These sediment layers are interlayered with resistant, platy beds of halite, dolomite, and calcite with minor argillite. These ancient lake deposits are located in the northeastern Salt Basin at Crow Flats, where eolian erosion carved depressions that are now occupied by recent playa deposits of Holocene age. Subsidence during the late Neogene and early Quaternary led to accommodation in the Salt Basin, and the lake level was abandoned at the end of the last glacial maximum, leaving behind the sediments that are presently exposed. Deposits are approximately 3 m thick in observable outcrop but may extend far into the subsurface. Compiled from synthesized descriptions of King (1948), McKnight (1986), Wilkins and Currey (1997), and O'Neill (1998).

Alluvium deposits (recent to middle Pleistocene)

Qa – Alluvium of Quaternary age, undivided

Short description: Cross section only.
Long description: Cross section only.

Sheetwash alluvium deposits (recent to late Pleistocene)

Qsr – Sheetwash alluvium, recent

Short description: Unconsolidated, fine-grained, alluvial- and sheetwash-derived sands and muds with intercalated gravels in vegetated, active drainages and floodplains occupying the valley floor. Channels are broad and flat with active deposition by low-energy flows. Lacks continuously incised channels. Little to no soil development. Occasionally internally drained. Approximately 1–4 m thick.

Long description: Unconsolidated, fine-grained, poorly sorted, alluvial- and sheetwash-derived sands and muds with intercalated gravels in vegetated, active drainages and floodplains occupying valley floors and channel-flanking hillslopes. Channels are low-gradient, broad, and flat with active deposition of fine-grained sediments by low-energy flows and sheetwash punctuated by high-energy deposition of coarse materials. Generally, lacks prominent, continuously incised, active channels, although discontinuous channels may be present. Occasional input and incorporation of pebbles, cobbles, and boulders from tributary channels are found underlying or deposited onto the surface of these sediments. Minor colluvium input from intermittent exposures of bedrock along channel borders or in channels at cutbanks, gullies, and scoured sections. Minor eolian input and occasional reworking of channel sediments by eolian processes. Color reflects lithology of upstream catchment and adjacent hillslopes but is most often tan to pale-brown or gray. Occasional ephemeral springs and seeps; changes in vegetation indicate variable depth to the water table. May include hillslopes and areas of thin sheetwash cover. Little to no soil development is present. Occasionally, internally drained and associated with areas of solution subsidence. Deposits are approximately 1–4 m thick, but the thickness may be greater. Compiled from new observations and synthesized descriptions of Dehler and Pederson (1998, 2002), Cikoski (2019b), Cikoski and Allen (2020), Allen and Attia (2021, 2022), Allen and Skotnicki (2024), and Allen (2024).

Qsyr – Sheetwash alluvium younger and recent, undifferentiated

Short description: The map unit **Qsyr** is mapped where the map scale does not permit differentiation of map unit **Qsy** and map unit **Qsr** when both are present on the landscape.

Long description: The map unit **Qsyr** is mapped where the map scale does not permit differentiation of map unit **Qsy** and map unit **Qsr** when both are present on the landscape. This map unit does not indicate if younger or recent sheetwash alluvium is more predominant in a given polygon and instead assumes a noteworthy portion of each is present.

Qsy – Sheetwash alluvium, younger

Short description: Unconsolidated, laminated- to tabular-bedded muds and sands with subordinate gravels of alluvial and sheetwash origin forming terrace treads a few meters above modern, low-energy channels. Reworking by eolian processes. Locally includes gypsite. Subordinate gravels in lenticular horizons. Weakly to moderately developed soils. Approximately 1–10 m thick.

Long description: Unconsolidated, well-sorted, laminated- to tabular-bedded, tan to brown muds and sands with subordinate gravels of alluvial and sheetwash origin on channel-flanking hillslopes and

forming terrace treads above modern, low-energy channels. Includes gypsite accumulations deposited under the same circumstances. Sediments underlie terrace treads that are approximately 2–9 m above modern grade and overlie or are inset into bedrock or older surficial units. Dominantly fine-grained sediments transported by the abandoned channel or derived from hillslopes with local reworking by eolian processes. Subordinate pebbles and cobbles from tributary channels, colluvium input from exposed bedrock, and rare high-energy events in the dominantly low-energy main channel. Sands and gravels are found in broad, discontinuous, clast-supported, occasionally indurated, cross-bedded, lenticular beds that are surrounded by thick, tabular beds of fine-grained sediments. Sediments are locally gypsiferous, calcareous, or carbonaceous. Tufa is found as thin, lenticular masses or cementing sand and gravel horizons. Soils range from weakly to moderately well developed; commonly have moderately developed argillic horizons; thin, well-developed A horizons; and Stage I–II calcic horizons with carbonate nodules and partial gravel coatings. Gypsum and carbonate nodules are common even when other soil profile indices are absent. Occasional iron-oxide mottling is present at depths below the soil profile. These deposits tend to have sloped, rather than planated, terrace treads. Gypsite is white to light-gray, porous, and composed of clay, silt, sand, and granule-sized gypsum originating from Permian bedrock sources. Exhibits a thin cover of eolian dust and a decimeter-scale crust. Grades downward into higher energy deposits of rounded gypsum pebbles that are interbedded with siliciclastic sediments. The map unit is approximately 1–10 m thick, with local thicknesses reaching 30–50 m. Compiled from new observations and synthesized descriptions of Dehler and Pederson (2002), Cikoski and Allen (2020), Skotnicki (2021), and Allen and Attia (2022).

Fan alluvium deposits (recent to middle Pleistocene)

Qfr – Fan alluvium, recent

Short description: Gravels, sands, and muds which form distributive, coalesced alluvial fans emanating from low-stream-order drainages. Active, unvegetated channels and stabilized overbank splay deposits of late Holocene depositional events. Bar-and-swale topography is visible in elevation and satellite imagery at 1–2 m above active channels. Fans coalesce laterally. Approximately 1–4 m thick.

Long description: Gravels, sands, and muds that form distributive, coalesced alluvial fans emanating from low-stream-order drainages. This unit represents active alluvial channels and splay deposits of late Holocene depositional events. Includes stabilized overbank deposits and unvegetated, channelized areas of active deposition. Bar-and-swale floodplain topography is visible in elevation and satellite imagery at 1–2 m above active channels. Sediments are typically poorly exposed, poorly sorted, contain lithologies of the upstream catchment, are typically unconsolidated, and exhibit variable degrees of scouring and incision. Overbank portions of this deposit are commonly blanketed with eolian, colluvial, and sheetwash-derived sediments. Deposits often include lithologies of adjacent drainages as fans coalesce laterally. Deposits are occasionally cemented by tufa. Typically derived from drainages along the eastern escarpment of the Guadalupe Mountains, drainages within mountainous areas, off the western rim of the Guadalupe Mountains, and from drainages within the Brokeoff Mountains. May display an incisional or aggradational relationship with older deposits. Deposits do not commonly exhibit soil formation; however, up to Stage I calcic horizons may exist outside of the active channel. Approximately 1–4 m thick. Compiled from new observations and synthesized descriptions of Cikoski (2019a, 2019b, 2020), Cikoski and Allen (2020), and Skotnicki and Attia (2022).

Qfyr – Fan alluvium younger and recent, undifferentiated

Short description: The map unit **Qfyr** is mapped where the map scale does not permit differentiation of map unit fan **Qfy** and map unit **Qfr** when both are present on the landscape.

Long description: The map unit **Qfyr** is mapped where the map scale does not permit differentiation of map unit fan **Qfy** and map unit **Qfr** when both are present on the landscape.
This map unit does not indicate if younger or recent fan alluvium is more predominant in a given polygon and instead assumes a noteworthy portion of each is present.

Qfy – Fan alluvium, younger

Short description: Gravels, sands, and muds of coalesced alluvial fans emanating from low-stream-order drainages. Deposits and surfaces abandoned by incision or buried by deposition; reactivated during rare high-energy events. Smooth, faintly channelized surfaces visible in elevation and satellite imagery at 3–5 m above active channels. Up to Stage II pedogenic carbonate. Approximately 1–6 m thick.

Long description: Gravels, sands, and muds that form occasionally reactivated surfaces within systems of coalesced alluvial fans emanating from low-stream-order drainages. Represents deposits and surfaces abandoned by incision or buried by subsequent stream and fan deposition that may be reactivated only during rare high-energy events. Smooth to faintly channelized surfaces are visible in elevation and satellite imagery at approximately 3–5 m above active channels. Poorly sorted, angular to subrounded grains are derived from nearby bedrock and upstream catchment. Sediments are unconsolidated except at the surface by occasional pedogenic carbonate. Soil development ranges from nonexistent to moderately developed carbonate horizons up to Stage II. Commonly blanketed with eolian, colluvial, and sheetwash-derived sediments. Often includes lithologies of adjacent drainages as fans coalesce laterally. Typically derived from drainages along the eastern escarpment of the Guadalupe Mountains, off the western rim of the Guadalupe Mountains into Big Dog Canyon, or from drainages within the Brokeoff Mountains. Deposits are approximately 1–6 m thick. Compiled from new observations and synthesized descriptions of Cikoski (2019a, 2019b, 2020), Cikoski and Allen (2020), Skotnicki (2021), and Skotnicki and Attia (2022).

Qfyi – Fan alluvium younger and intermediate, undifferentiated

Short description: The map unit **Qfyi** is mapped where the map scale does not permit differentiation of map unit **Qfy** with map unit **Qfi** when both are present on the landscape.

Long description: The map unit **Qfyi** is mapped where the map scale does not permit differentiation of map unit **Qfy** with map unit **Qfi** when both are present on the landscape. This map unit does not indicate if intermediate or younger fan alluvium is more predominant in a given polygon and instead assumes a noteworthy portion of each is present.

Qfi – Fan alluvium, intermediate

Short description: Gravels, sands, and muds that form inactive remnant surfaces of alluvial fans; not reactivated during rare high-energy events. Smooth surfaces visible in elevation and satellite imagery at 6–9 m above active channels. Coarse facies alternate with pale, fine-grained horizons. Up to Stage III pedogenic carbonate and buried paleosols. Boulders at surface due to winnowing. Approximately 1–12 m thick.

Long description: Gravels, sands, and muds that form inactive remnant surfaces within systems of coalesced alluvial fans emanating from low-stream-order drainages. This unit represents deposits and surfaces abandoned by incision or buried by subsequent stream and fan deposition that are not reactivated even during rare high-energy events. Smooth surfaces are visible in elevation and satellite imagery at approximately 6–9 m above active channels. Poorly sorted, angular to subrounded grains are derived from nearby bedrock and upstream catchment. Coarse facies alternate laterally with tan to pink, fine-grained horizons. Sediments are unconsolidated except at the surface by pedogenic carbonate. Soil development is moderately to well-developed with carbonate horizons up to Stage III and may include buried soils. Surfaces are dominated by boulders and cobbles due to winnowing by eolian and sheetwash erosion; commonly blanketed with eolian, colluvial, and sheetwash-derived sediments. Often includes lithologies of adjacent drainages as fans coalesce laterally. Typically derived from drainages along the eastern escarpment of the Guadalupe Mountains, off the western rim of the Guadalupe Mountains into Big Dog Canyon, or from drainages within the Brokeoff Mountains. Approximately 1–12 m thick. Compiled from new observations and synthesized descriptions of Cikoski (2019a, 2019b, 2020), Cikoski and Allen (2020), Skotnicki (2021), and Skotnicki and Attia (2022).

Qfio – Fan alluvium, intermediate and older

Short description: The map unit **Qfio** is mapped where the map scale does not permit differentiation of map unit **Qfri** and map unit **Qfo** when both are present on the landscape.

Long description: The map unit **Qfio** is mapped where the map scale does not permit differentiation of map unit **Qfri** and map unit **Qfo** when both are present on the landscape. This map unit does not indicate if intermediate or older fan alluvium is more predominant in a given polygon but assumes a noteworthy portion of each is present.

Qfo – Fan alluvium, older

Short description: Gravels, sands, and muds of buried alluvial-fan deposits or isolated remnant surfaces in high landscape positions. Smooth topography around 9–12 m above active channels; moderately to deeply dissected by headward erosion. Surfaces cemented by pedogenic carbonate. Up to 500 m of accommodation is locally present (Veldhuis and Keller, 1980) with outcrops approximately 5–10 m thick.

Long description: Gravels, sands, and muds that form inactive remnant surfaces and buried deposits within systems of coalesced alluvial fans emanating from low-stream-order drainages. Represents deposits and surfaces either buried by subsequent deposition or abandoned by incision. In elevation and satellite imagery, these deposits exhibit smooth topography that is moderately to deeply dissected by headward erosion. Found approximately 9–12 m above active fan channels. Sediments are poorly sorted, contain angular to subrounded grains, and are derived from nearby bedrock and upstream catchments. Range from unconsolidated to strongly cemented by carbonate. Commonly blanketed with eolian, colluvial, and sheetwash-derived sediments. Often includes lithologies of adjacent drainages as fans coalesce laterally. Commonly expressed as isolated erosional remnants holding a high position in the landscape. Derived from drainages along the western rim of the Guadalupe Mountains and from drainages within the Brokeoff Mountains westward into the Salt Basin. Subsidence of the Salt Basin graben at Crow Flats and Big Dog Canyon created accommodation space for up to 500m of fan alluvium deposition (Veldhuis and Keller, 1980). At the surface, this unit is observed to be approximately 5–10 m thick. Compiled from synthesized descriptions of O'Neill (1998), Cikoski (2019a, 2019b, 2020), Cikoski and Allen (2020), Skotnicki (2021), Skotnicki and Knight (2022), and Skotnicki and Attia (2022).

Channel alluvium deposits (recent to middle Pleistocene)

Qar – Alluvium, recent

Short description: Unconsolidated, poorly sorted, unvegetated, gravel-dominated active channels with vegetated active floodplains 1–3 m above grade. Primarily carbonate compositions with minor sandstone in a carbonaceous or calcareous matrix. Localized perennial water. No soil in active channel, weak development in floodplain. Deposits are approximately 1–5 m thick.

Long description: Unconsolidated, poorly sorted, and unvegetated active channels with abundant gravels and adjacent vegetated active floodplains. This unit insets or overlies older units and may have intermittent exposures of unmapped Permian bedrock or older Quaternary sediments in cutbanks, gullies, and scoured reaches. Active channels commonly incise into the landscape and are dominated by subrounded boulders, cobbles, and pebbles of primarily carbonate compositions with minor sandstone in a carbonaceous or calcareous matrix of silts and sands. In the Delaware basin, subordinate siliceous pebbles appear in the active channel along with common gypsum from Permian bedrock units and conglomerates from older Quaternary units. In the Guadalupe Mountains, deposits are limited to clasts of Permian origin. May include anthropogenic material such as asphalt or scrap metal dumped in arroyo channels. In some reaches, active-channel deposits are comparatively fine-grained. In the vicinity of the Black River, deposits are commonly white to gray, gypsiferous, organic-rich, and contain occasional mollusks and tufa cementation. Soil development is nonexistent in active channels. Channels are locally filled with perennial water supported by groundwater discharge in several reaches of the Black River and Pecos River. Active floodplains are well-vegetated, located approximately 1–3 m above the active channel, characterized by bar-and-swale topography, and primarily composed of organic-rich clays, silts, and sands with relic channels of pebbles, cobbles, and boulders. Paleochannel fills within the floodplain are found in thin, lenticular beds of unconsolidated, poorly sorted, sub- to well-rounded, clast-supported, uncemented gravel and sand interbedded with poorly stratified, laminated or massive-bedded, carbonaceous sands and muds. Vegetation is either thick, shrubby vegetation or low-growing grasses that may trap eolian-transported sediments. Soil development is weak, but filaments and nodules of gypsum and carbonate may be present. Floodplains commonly have ephemeral seeps and springs. Occasional discontinuous, narrow channels of sands or gravels are present in floodplains that are activated during storm events. Deposits are approximately 1–5 m thick. Compiled from new observations and synthesized descriptions of Dehler and Pederson (1998, 2002), Pederson and Dehler (2004a), Cikoski (2019a, 2019b, 2020), Cikoski and Allen (2020), Skotnicki (2021), Allen and Attia (2021, 2022), and Allen (2024).

Qtyr – Recent alluvium and younger terrace alluvium, undifferentiated

Short description: The map unit **Qtyr** is mapped where the map scale does not permit differentiation of map unit **Qar** and map unit **Qty** when both are present on the landscape.

Long description: The map unit **Qtyr** is mapped where the map scale does not permit differentiation of map unit **Qar** and map unit **Qty** when both are present on the landscape. This map unit does not indicate if recent alluvium or younger terrace alluvium is more predominant in each polygon and instead assumes a noteworthy portion of each is present.

Qty – Terrace alluvium, younger

Short description: Unconsolidated, poorly sorted gravels, sands, and muds forming low, reactivated terraces 3–6 m above active channels. Smooth surfaces with minor bar-and-swale topography. Correlates to the lowest Lakewood terrace; experiences reworking and fine-grained deposition. Thin argillic horizons with Stage I petrocalcic horizon and rare carbonate nodules. Approximately 1–8 m thick.

Long description: Unconsolidated, poorly sorted gravels, sands, and muds forming low, occasionally reactivated terrace surfaces 3–6 m above grade of active channels. Similar in consistency to the active floodplain but experiencing less coarse deposition in the present day and exhibiting Stage I petrocalcic-soil development. Smooth surface morphology with minor bar-and-swale topography is visible in elevation and satellite imagery. Represents the lowest Lakewood terrace of McCraw et al. (2007, 2011) and McCraw and Land (2008) where the terrace is inferred to experience common reworking and deposition. Weakly developed profiles exhibit thin (5 cm) to thick (25 cm), darkened, organic-rich A horizons with a thin (10 cm) Stage I Bk horizon and small carbonate or gypsum nodules and stringers, depending on host sediment. Where soils are minimally developed or eroded, carbonate-coated clasts and rare carbonate nodules are present. Occasional argillic horizons and partial carbonate coating on gravels when found in sediments with lower abundance of carbonate material. Approximately 1–8 m thick. Compiled from new observations and synthesized descriptions of Dehler and Pederson (1998, 2002), Pederson and Dehler (2004a), McCraw et al. (2007, 2011), McCraw and Land (2008), Cikoski (2019a, 2019b, 2020), Cikoski and Allen (2020), Skotnicki (2021), Allen and Attia (2021, 2022), and Allen (2024).

Qtyi – Terrace alluvium younger and intermediate, undifferentiated

Short description: The map unit **Qtyi** is mapped where the map scale does not permit differentiation of map unit **Qty** and map unit **Qti** when both are present on the landscape.

Long description: The map unit **Qtyi** is mapped where the map scale does not permit differentiation of map unit **Qty** and map unit **Qti** when both are present on the landscape. This map unit does not indicate if younger or intermediate terrace alluvium is more predominant in a given polygon and instead assumes a noteworthy portion of each is present.

Qti – Terrace alluvium, intermediate

Short description: Alluvium underlying terrace treads of the Lakewood terrace suite at 6–9 m and 9–12 m above active channels. Sands and gravels in lenticular paleochannels cutting fine-grained sediments. Close to the mountains, carbonate dominates compared to siliceous compositions along the Pecos River. Stage II+ to III petrocalcic horizons. Tread heights are variable across the map. Approximately 1–12 m thick.

Long description: Alluvium underlying terrace treads of the Lakewood terrace suite at approximately 6–9 m and 9–12 m above grade of modern channels. Found inset into bedrock or older alluvial deposits and exhibits moderate soil development. Primarily composed of poorly exposed sands with lesser gravel and lenticular paleochannel fills cut into beds of fine-grained sediments. Unconsolidated, laminated to massive, irregular- or tabular-bedded sands, silts, and clays of variable composition. Sediments are poorly to moderately sorted, fining upward, occasionally well-sorted, and contain subrounded to subangular grains. Lenticular paleochannel fills are moderately thick, poorly sorted, massive to cross-bedded, moderately to well-rounded, and commonly cemented by carbonate. Along the Black River, these deposits are commonly composed of gypsite that forms a decimeter-scale crust of gypsic soil that is white to light-gray, porous, and composed of clays, silt, and sand that grades downward into siliceous

and gypsum gravels. Within proximity to the Guadalupe Mountains, the deposits are composed of carbonate lithologies with subordinate sandstones and siliceous clasts. Along the Pecos River, the deposits are dominated by siliceous sands with quartzose or igneous clasts interspersed into fine-grained sediments; the presence of pink, crystalline, plutonic clasts derived from the Sangre de Cristo Mountains is a local defining characteristic of the map unit**.** Soil profiles tend to have A and moderately developed Bk horizons that range from Stage II+ to III between the lower and higher terrace tread. The surfaces of the terrace treads tend to exhibit deposition and reworking by coppice dunes, as well as input of sands or gravel from tributary channels and sheetwash alluvium from hillslopes. Tread heights vary across the map area depending on stream order, lithology, catchment area, and proximity to knickpoints. Intermittent exposures of bedrock or older Quaternary sediments at the sub-map scale are common. Deposits are approximately 1–12 m thick. Compiled from new observations and synthesized descriptions of Fielder and Nye (1933), Dehler and Pederson (1998, 2002), Pederson and Dehler (2004a, 2004b), McCraw et al. (2007, 2011), McCraw and Land (2008), Cikoski (2019a, 2019b, 2020), Cikoski and Allen (2020), Skotnicki (2021), Allen and Attia (2022), and Allen (2024).

Qtio – Terrace alluvium intermediate and older, undifferentiated

Short description: The map unit **Qtio** is mapped where the map scale does not permit differentiation of map unit **Qti** and map unit **Qto** when both are present on the landscape.

Long description: The map unit **Qtio** is mapped where the map scale does not permit differentiation of map unit **Qti** and map unit **Qto** when both are present on the landscape. This map unit does not indicate if intermediate or older terrace alluvium is more predominant in a given polygon but assumes a noteworthy portion of each is present.

Qto – Terrace alluvium, older

Short description: Alluvium of the Orchard Park terrace suite forming treads and mesas at 12–22 m above active channels. First interval of entrenchment below the Mescalero paleosol and ancestral Pecos River deposits. Includes carbonate, siliciclastic, metamorphic, and igneous clasts. Stage III–IV petrocalcic carbonate. Occasional potholes. Approximately 1–12 m thick, up to 64 m thick in subsurface.

Long description: Alluvium underlying terrace treads of the Orchard Park terrace suite that form terraces and mesas at approximately 12–22 m above grade of modern channels. Deposits are found inset into or overlying bedrock and ancestral Pecos River alluvial fill; they exhibit moderate to strong calcic soil development. Gravels, sands, and fines derived from Pecos River during first interval of downcutting and entrenchment into the Mescalero paleosol and ancestral Pecos River sedimentary deposits. Deposits match the modern flow direction, rework sediments of the Gatuña Formation, and represent the assumed start of southerly flow seen in the contemporary Pecos River. Sediments are brown to light-brown, occasionally pink to red, medium- to coarse-grained sand and pebbles to cobbles with floodplain sands, silts, and clays. The floodplain consists of laminar to tabular beds of poorly sorted quartz and chert sands, silts, and clays with lesser channel fills of pebbles and cobbles. Gravels are commonly cemented by carbonate near their basal contact with underlying bedrock; gravels include limestone, dolomite, sandstone, chert, quartzite, caliche, and subordinate schist, volcanic, and plutonic rock. In Dark Canyon, this terrace level exhibits lower grades (10–18(?) m) with east to northeast paleoflows perpendicular to the Pecos channel in lenticular to tabular beds of cross-bedded, rounded cobbles and boulders cutting siliceous, sandy and silty, laminated or tabular to massive beds. Exhibits an inset relationship or low-angle unconformity with underlying Mescalero paleosol and Gatuña Formation sediments that have been

tilted by solution subsidence; a similar angular unconformity is found internal to the Gatuña Formation. The terrace surface is cemented by Stage III–IV petrocalcic carbonate soil with an occasional laminar horizon that is locally autobrecciated and overlying a plugged horizon approximately 2–3 m thick which envelops conglomerate and sandstone beds. A thin mantle of reddish-brown eolian and sheetwash sands commonly overlies this unit. The surface of the terrace may have potholes due to dissolution of underlying bedrock. Intermittent outcrops of Permian or older Cenozoic sedimentary units are present at the sub-map scale. Deposits are commonly 1–5 m thick, approximately 1–12 m thick in the largest outcrops, and up to 64 m thick in subsurface due to the effects of solution subsidence. Compiled from new observations and synthesized descriptions of Fielder and Nye (1933), Dehler and Pederson (1998), Pederson and Dehler (2004a, 2004b), McCraw et al. (2011), Cikoski (2019a, 2019b, 2020), and Allen and Attia (2022).

Piedmont alluvium deposits (recent to middle Pleistocene)

Qpr – Piedmont alluvium, recent

Short description: Unconsolidated gravels and sands that form unvegetated active channels and vegetated floodplains 1–2 m above active high-stream-order channels. Deposits aggrade, avulse, and planate close to the mountain front before channelizing. Little petrocalcic development. Bar-and-swale topography underlain by laminated fines with lenticular channel-fill gravel deposits. Approximately 1–5 m thick.

Long description: Unconsolidated and poorly exposed boulders, cobbles, and sands that form active channels and floodplains from high-stream-order piedmont alluvial systems draining highlands. These stream networks are sub-perpendicular to axial channels and are inset into bedrock or older piedmont alluvial gravels. Active channels are devoid of vegetation and are dominated by massively bedded boulders, cobbles, and sands. Deposits close to the mountain front exhibit rough topography with aggrading and avulsing streams that planate older deposits before channelizing farther from the mountain front. Floodplains adjacent to active channels are 1–2 m above the channel grade, are well vegetated, and have weak to nonexistent petrocalcic soil development. Surface is characterized by bar-and-swale topography and underlain by laminated carbonaceous and calcareous sands, silts, and clays with lesser winnowed pebble-to-boulder channel deposits present at the surface and lenticular channel-fill deposits in the subsurface. Lithology reflects upstream drainage. Deposits may coalesce laterally, leading to mixed representation from different catchments in each deposit. Locally includes colluvium or sheetwash input from older deposits or bedrock that occupies a higher landscape position. Intermittent exposures of bedrock or older piedmont alluvium-fill are exposed in channels or floodplains. Approximately 1–5 m thick. Compiled from new observations and synthesized descriptions of Cikoski (2019a), Cikoski and Allen (2020), Skotnicki (2021), Skotnicki and Attia (2022), Skotnicki and Allen (2024), and Allen and Skotnicki (2024).

Qpyr – Piedmont alluvium younger and recent, undifferentiated

Short description: The map unit **Qpyr** is mapped where the map scale does not permit differentiation of map unit **Qpr** and map unit **Qpy** when both are present on the landscape.

Long description: The map unit **Qpyr** is mapped where the map scale does not permit differentiation of map unit **Qpr** and map unit **Qpy** when both are present on the landscape. This map unit does not

indicate if younger or recent piedmont alluvium is more predominant in each polygon but assumes a noteworthy portion of each is present.

Qpy – Piedmont alluvium, younger

Short description: Unconsolidated and poorly exposed gravels and sands forming reactivated terrace surfaces 3–4 m above active high-stream-order piedmont alluvial channels. Smooth topography with minor bars and swales underlain by laminated sands and muds with lenticular channel-fill gravel deposits in the subsurface. Stage I–II petrocalcic horizons with argillic and A horizons. Approximately 1–6 m thick.

Long description: Unconsolidated and poorly exposed boulders, cobbles, and sands that form occasionally reactivated terrace surfaces inset into older piedmont alluvium in high-stream-order piedmont alluvial systems draining highlands. In elevation and satellite imagery, these deposits are visible as smooth terrace surfaces with minor bar-and-swale topography 3–4 m above active channels that are only reactivated in rare high-energy storm events. Deposits include laminated carbonaceous and calcareous sands, silts, and clays with lesser winnowed pebble-to-boulder channel deposits present at the surface and lenticular channel-fill deposits in the subsurface. Lithology reflects upstream drainage. Weak soil development with Stage I–II petrocalcic horizons with brown A horizons exhibiting minor argillic development. Deposits may coalesce laterally, leading to mixed representation from different catchments within each deposit. Locally includes eolian sediments and colluvium or sheetwash input from older deposits or bedrock that occupies a higher landscape position. Intermittent exposures of bedrock or older piedmont alluvium may be present. Deposits are approximately 1–6 m thick. Compiled from new observations and synthesized descriptions of Pederson and Dehler (2004b), Cikoski (2019a), Cikoski and Allen (2020), Skotnicki (2021), Allen and Attia (2021), Skotnicki and Attia (2022), Skotnicki and Allen (2024), and Allen and Skotnicki (2024).

Qpyi – Piedmont alluvium younger and intermediate, undifferentiated

Short description: The map unit **Qpyi** is mapped where the map scale does not permit differentiation of map unit **Qpy** and map unit **Qpi** when both are present on the landscape.

Long description: The map unit **Qpyi** is mapped where the map scale does not permit differentiation of map unit **Qpy** and map unit **Qpi** when both are present on the landscape. This map unit does not indicate if younger or intermediate piedmont alluvium is more predominant in each polygon but assumes a noteworthy portion of each is present.

Qpi – Piedmont alluvium, intermediate

Short description: Remnants of coalesced alluvial fan surfaces and correlative terraces inset into older deposits 5–8 m above active channels. Records multiple cut-fill episodes. Gravels with carbonate cement; equal parts fine-grain floodplain facies. Primarily carbonate composition; siliceous sands indicate a transition into Pecos River deposits. Stage II+ to III petrocalcic soils. Approximately 1–8 m thick.

Long description: Remnants of coalesced piedmont alluvial fan surfaces and correlative terrace treads inset into older alluvial deposits 5–8 m above the grade of active piedmont alluvium. It consists of boulders, cobbles, and sand channels with equal parts finer-grained sand and silt floodplain facies. Surfaces have moderate soil development. This unit records multiple aggradation or cut-fill episodes

inset into or overlying bedrock or older piedmont alluvium. Fine-grained facies are light-brown to pink, moderately sorted, massive to tabular-bedded sands, silts, and clays with subordinate pebbles intercalated with planar or lenticular gravel beds. Gravels occupy paleochannel fills or winnowed deposits at the surface and are poorly sorted, well-rounded, and commonly indurated with calcium-carbonate cement. Surfaces of treads exhibit bar-and-swale topography with increasing relief toward the mountain front. The lithology of the deposits depends on the source catchment, but gravels are primarily composed of carbonate with secondary sandstone and siliceous pebbles. Sands are primarily carbonate and chert with subordinate siliceous composition; a transition into dominantly siliceous sands may indicate a transition into, or reworking of, mainstem Pecos River deposits. Clasts are derived either from Permian units or from reworked older piedmont alluvial deposits no longer present in the source catchment. Soil development is commonly characterized by Stage II+ to III carbonate morphology featuring moderately thin, darkened A horizons, thick argillic horizons, pedogenic carbonate nodules, and complete coatings of carbonate on gravels that occasionally create plugged horizons. Commonly capped with eolian and sheetwash-derived sediments. Deposits are approximately 1–8 m thick. Compiled from new observations and synthesized descriptions of Pederson and Dehler (2004b), Cikoski (2019a), Cikoski and Allen (2020), Allen and Attia (2021), Skotnicki (2021), Skotnicki and Attia (2022), Allen and Skotnicki (2024), and Skotnicki and Allen (2024).

Qpio – Piedmont alluvium intermediate and older, undifferentiated

Short description: The map unit **Qpio** is mapped where the map scale does not permit differentiation of map unit **Qpi** and map unit **Qpo** when both are present on the landscape.

Long description: The map unit **Qpio** is mapped where the map scale does not permit differentiation of map unit **Qpi** and map unit **Qpo** when both are present on the landscape. This map unit does not indicate if intermediate or older piedmont alluvium is more predominant in a given polygon but assumes a noteworthy portion of each is present.

Qpo – Piedmont alluvium, older

Short description: Isolated remnants of coalesced alluvial-fan surfaces and correlative treads 9–14 m above active channels. Variably lithified channels and floodplain facies; fines distal to mountain front. Smooth topography incised by headward erosion. May be found as lags on planar straths. Carbonate, sandstone, and allochthonous siliceous clasts. Stage III–IV petrocalcic soils. Approximately 1–12 m thick.

Long description: Isolated remnants of coalesced piedmont alluvial-fan surfaces and correlative terrace treads inset into older alluvial deposits 9–14 m above grade of active piedmont alluvium. Consisting of well-cemented, discontinuously stratified boulders, cobbles, and sand channels showing eastward paleoflow with poorly exposed finer-grained sand and silt facies. Surface exhibits strong Stage III–IV petrocalcic soil development. This unit may record multiple aggradation or cut-fill episodes inset into or overlying bedrock or older piedmont alluvium. Fine-grained sediments consist of massive to tabular-bedded sands, silts, and clays that are subangular to rounded, well-sorted, and moderately indurated by calcium carbonate. Gravels are poorly sorted, subrounded to rounded, matrix- to clast-supported, and well consolidated by calcium-carbonate cement. Sediments fine distal to the mountain front. Surfaces exhibit smooth to rounded topography that may be incised by headward erosion. Occasionally, these deposits may only be a lag on straths planating older piedmont alluvium. Primarily composed of carbonate lithology with subordinate sandstones and occasional allochthonous siliceous pebbles. Sediments throughout the deposit are variably lithified by calcium-carbonate cement, and terrace treads

or deposit surfaces also exhibit a high degree of petrocalcic development. Development ranges from Stage III to IV horizons that are exposed at the surface due to stripped argillic horizons. Calcic horizons are commonly 2–3 m thick but up to 4 m thick, decreasing down section, with carbonate nodules, autobrecciation, and cemented gravels overlain by a laminar surface with minor pisolitic texture. Common cover of eolian and sheetwash-derived sediments. Occasional pockmarked texture from small depressions. Deposits are approximately 1–12 m thick, with drill logs indicating up to 64 m of fill beneath these deposits that likely includes older alluvial fill. Compiled from new observations and synthesized descriptions of Pederson and Dehler (2004a, 2004b), Cikoski (2019a), Cikoski and Allen (2020), Allen and Attia (2021), Skotnicki (2021), Skotnicki and Attia (2022), Allen and Skotnicki (2024), and Skotnicki and Allen (2024).

Qg – Gatuña Formation, fluvial and valley-margin facies

Short description: Poorly exposed sediments of the ancestral Pecos River adjacent to the modern drainage. Exhibits cut-fill channels, splays, paludal deposits, and overbank facies. Cemented gravel beds intercalated with sands and muds. Carbonate and siliceous lithologies with common metamorphic and igneous clasts. Capped by the Stage IV–V Mescalero paleosol. Approximately 5–15 but up to 45 m thick.

Long description: Poorly exposed, light-reddish-brown to pink, yellow to pale-brown, and white sediments of the ancestral Pecos River system found adjacent to the modern Pecos River drainage. Uncemented to well-cemented exotic and locally derived gravels, sands, and muds with subordinate gypsiferous intervals, capped by the petrocalcic Mescalero paleosol. Outcrops are crudely bedded with channel forms, cut-fill structures, splay deposits, paludal facies, and overbank floodplain deposits. Mud intervals are thinly laminated to tabular- or massive-bedded, noncalcareous claystones to siltstones with minor sand content and variable gypsiferous content; intercalated with lenticular channels or horizons of sand and gravel. Sands are very fine- to medium-grained, subangular to rounded quartz and chert that are horizontal-planar to massive- or cross-bedded, typically found in thin lenticular beds, as a matrix within conglomerate horizons, or interbedded with gravels. Gravels are intercalated with sands or muds; consist of pebble-, cobble-, and boulder-sized clasts that are subangular to well-rounded, poorly to moderately sorted, and clast-supported with a sandy matrix; and are found in medium to thick lenticular beds that are cross-stratified or undulatory and tabular. Clasts are dominantly large cobbles and boulders of carbonate and siliceous lithologies; this unit also contains common quartzite, chert, felsic to intermediate volcanic clasts, and occasional tan to gray porphyry, petrified wood, white vein quartz, schist, and granite. Gravels and sands are commonly cemented by calcium carbonate or contain clay or carbonate coatings that act to partially cement deposits. The well-indurated Stage IV to V petrocalcic horizon of the Mescalero paleosol caps the Gatuña Formation in many locations. This soil contains an undulatory-tabular laminar zone of nearly pure carbonate with trace parent material underlain by massive carbonate that is commonly fractured and recemented; the soil grades downward with decreasing levels of carbonate and increasing parent material, occasionally terminating abruptly. This formation is overlying or inset into itself, the lower Gatuña, or Permian bedrock units. Inset and overlain by Orchard Park and Lakewood terraces. Locally deformed into domes. Conglomeratic facies form mesas, knobs, and valley walls along the Pecos River; mud facies form slopes with badlands weathering. The unit is approximately 5–15 m thick, with thicknesses up to 45 m in regions with extensive subsidence of underlying strata. Compiled from new observations and synthesized descriptions of Motts (1962), Dehler and Pederson (1998, 2002), Pederson and Dehler (2004b), Cikoski (2019b, 2020), and Allen and Attia (2022).

Qgp – Gatuña Formation, piedmont facies

Short description: Poorly exposed gravel conglomerates of ancestral piedmont systems reflecting decreased stream power distal to the mountain front. Consolidated by carbonate cement. Carbonate with rare sandstone, metamorphic, and igneous clasts. Interfingers with fluvial facies. Rare sand beds terminate laterally. Knobs and deposits persist in alluvial channels. Approximately 10 m thick; pinches out westward.

Long description: Poorly exposed gravels and subordinate sands that tentatively represent piedmont gravels that flowed eastward into the ancestral Pecos River system from sources in the Guadalupe Mountains. These deposits are strongly consolidated by white to tan to pink, sparry carbonate cement that lacks pedogenic features. Gravels are predominantly gray to pinkish-gray, poorly sorted, rounded, and occasionally clast-supported, carbonate-pebble conglomerates with subordinate cobbles and boulders; they may represent a decrease in stream power distal from the Guadalupe Mountains. Deposits are well indurated, medium-bedded, cross-stratified, and lenticular, with beds pinching out or truncating laterally. Lithologies are primarily carbonates derived from local strata with rare sandstones, cherts, and quartzite and rare to absent volcanic and plutonic clasts that may indicate interfingering with fluvial and valley-margin Gatuña Formation facies. Also includes occasional reworked pebble conglomerates of autochthonous origin. Interbedded with rare sand horizons that are cross-stratified and lenticular, terminating laterally. Sands are poorly sorted, rounded, grain-supported, medium- to coarse-grained, and dominantly carbonate with subordinate quartz and chert grains. Sands are found as a matrix within conglomerate beds and are interbedded with poorly sorted pebbly sandstones. Outcrops weather to smooth, rounded knobs and mounds and are commonly found on the lower elevation of the Gypsum Plain west of the Pecos River and persisting upstream inset into bedrock along major tributaries to the Pecos River. May be observed to have an inset relationship with the lower Gatuña Formation and underlie the Mescalero paleosol or may have unclear field relationships that prevented a suggested possible affinity with the piedmont facies of the lower Gatuña Formation. The deposit thickens to greater than 10 m close to the Pecos River and thins to erosional pinch-outs westward toward the mountain front. Compiled from new observations and synthesized descriptions of Motts (1962), Dehler and Pederson (1998), Pederson and Dehler (2004a), Cikoski (2019a), Cikoski and Allen (2020), Allen and Attia (2021), Skotnicki (2021), Skotnicki and Attia (2022), Allen and Skotnicki (2024), and Skotnicki and Allen (2024).

QUATERNARY-NEOGENE SYSTEM

QNa – Alluvium of Quaternary and Neogene age, undivided

Short description: Cross section only.
Long description: Cross section only.

QNg – Gatuña Formation, lower fluvial and valley-margin facies

Short description: Muds, sands, gravels, and evaporites of the aggrading ancestral Pecos River capped by the Stage V to VI caliche. Thin beds of muds, lenticular sands, and gravel channels; local paludal gypsum. Siliceous lithologies, subordinate carbonate, and rare igneous clasts. Unconformable on Permian strata and overlain by the upper Gatuña Formation. Approximately 14 m thick; thickens in the subsurface.

Long description: Strongly colored, dominantly reddish-brown packages of silts, sands, muds, gravels, and evaporites deposited by an aggrading ancestral Pecos River sedimentary system. Typically crops out as thinly bedded, laminated muds and sands, lenticular sand bodies, and gravel-occupied paleovalleys.

This unit is locally gypsiferous and has brown to red, tan to orange, pink, and yellow fines, light-red to pale-brown sands, and light-brown to gray gravels. Sands are found interspersed in poorly sorted mud horizons and as lenticular to planar beds of rounded, poorly sorted, and fine-grained siliceous sands. Gravel bodies are moderately to well-cemented, poorly to moderately sorted, rounded to well-rounded, occasionally clast-supported, and found in paleovalleys or thin- to medium-thickness beds that are lenticular and contain trough cross-bedding. Include dominantly siliceous quartzite and chert with occasional sandstones, subordinate carbonate lithologies, and rare granites and felsic to intermediate extrusive volcanic clasts. The base of this unit is poorly exposed in the map area but lies unconformably on Permian strata, is inset or overlain by the upper Gatuña Formation, and underlies the well-developed petrocalcic Mescalero paleosol at the hypothesized maximum aggradation geomorphic surface. The differentiation of this unit from the upper Gatuña is tentative, and the distinction of this unit and the Ogallala Formation is controversial. Qualitative distinctions include greater degrees of sediment color vibrancy, cementation and consolidation of sediments, and degree of tilting or deformation. The Mescalero paleosol, termed the Pierce Canyon caliche when overlying these same deposits in previous mapping, is a 3- to 6-m-thick petrocalcic horizon of Stage V to VI carbonate morphology. It features an undulatory-tabular horizon up to 1 m thick with layers of decimeter-thick, porous, laminar carbonate and an indurated horizon with brecciation, pisolite textures, and recementation. This is underlain by a thick, fractured, recemented, carbonate-plugged horizon featuring concentrically coated gravels, pisolites, and carbonate nodules. This unit is up to 14 m thick in outcrop but thickens substantially in the subsurface within subsidence troughs. Compiled from new observations and synthesized descriptions of Motts (1962), Cikoski (2019b, 2020), Skotnicki (2021), and Allen and Attia (2021, 2022).

QNgp – Gatuña Formation, lower piedmont facies

Short description: Cemented conglomerates with rare fine-grained facies in rounded-planated interfluves of relic piedmont alluvium 30–50 m above active channels. Carbonate, sandstone, rare allochthonous chert or quartzite. Near ubiquitous calcium carbonate cement. Common tilting by solution subsidence or tectonism. Lacks fossil or radiometric age constraints. Approximately 5–25 m thick in outcrop.

Long description: Well-cemented, clast-supported conglomerates forming west-east-oriented, rounded-planated interfluves of relic piedmont alluvium gravels 30–50 m above modern grade. Transport is eastward from the Guadalupe Mountains and likely grades into sediments of the ancestral Pecos River. Overlies Permian strata and is inset by younger piedmont and terrace alluvium deposits. Conglomerate gravels are well-cemented and consist of subangular to rounded, poorly sorted boulders, cobbles, and pebbles that are clast-supported and dominantly consist of carbonate with subordinate sandstones locally derived from the Guadalupe Mountains with rare allochthonous pebbles of chert or quartzite. Gravels are imbricated and found in medium to thick beds that are lenticular and cross-stratified or occasionally tabular- to massively bedded. Conglomerates have a matrix of poorly sorted silt to coarse-grained carbonate and siliceous sands and are occasionally interbedded with pebbly sands. Fine-grained facies are characterized by subangular to rounded, moderately sorted quartz and lithics of fine- to medium-grained sands within a clay to silt matrix with occasional coarse sand and pebbles. Poorly exposed to absent beds of pink to reddish-brown sandy mudstone. Nearly ubiquitously moderate to strong cementation by calcium carbonate likely precipitated from groundwater. Ranges from discontinuous carbonate found between clasts to complete lithification; may include concentric laminae around clasts and occasional pisolitic textures. This unit forms rounded ridges that exhibit occasional planation of both constructional surfaces prior to incision and abandonment or truncation by subsequent erosion from a younger cycle of aggradation and incision. These planated surfaces feature rare Stage V petrocalcic soil

development. Inset by younger alluvial deposits and commonly found as well-cemented gravels in the floor of modern channels or intermittently exposed on terraces where younger deposits are discontinuous. Commonly slumped and tilted due to solution subsidence or possibly tectonism. Occasionally found where isolated remnant gravels were deposited by karst collapse onto the Gypsum Plain; this indicates easterly transport prior to the integration of the Black River. Due to a lack of paleontological and direct geochronological age constraints, the age and correlation of these deposits has been a subject of controversy and is an active topic of research. Deposits are up to 60 m thick (Hale, 1955) but extremely variable and typically 5–25 m observable in outcrop. Compiled from new observations and synthesized descriptions of Motts (1962), Dehler and Pederson (1998), Pederson and Dehler (2004a), Cikoski (2019a), Cikoski and Allen (2020), Allen and Attia (2021), Skotnicki (2021), Skotnicki and Attia (2022), Allen and Skotnicki (2024), and Skotnicki and Allen (2024).

PALEOGENE SYSTEM

EOCENE EPOCH

Intrusive rocks (Eocene)

PEi – Intrusive mafic-intermediate dikes

Short description: Dark-colored, poorly exposed basaltic andesite dikes in Permian rock on the Gypsum Plain. Feldspar phenocrysts in plagioclase groundmass, rare orthoclase and biotite, minor apatite, and altered ferromagnetic minerals (Pratt, 1954; Calzia and Hiss, 1978). Vesicles with silicic, calcitic, chloritic, or evaporitic fill. $^{40}Ar/^{39}Ar$ dates of 34.45 ± 0.28 (Attia and Ricci, 2023) to 28.167 ± 0.29 Ma.

Long description: Gray-green to black, intrusive, basaltic andesite dikes and connected high-angle sills that are highly weathered, poorly exposed, and visible in elevation and satellite imagery. Dike outcrops appear deformed but remain intact; outcrops are approximately 1 m wide and stain the Permian-aged, gypsic, host rock yellow to brown. Petrographic analysis, summarized by Calzia and Hiss (1978), described a groundmass composition consisting of plagioclase with rare orthoclase and biotite, minor apatite, and ferromagnetic minerals altered to chlorite or magnetite through resorption. Phenocrysts of feldspar are 3–6 mm long. Vesicles approximately 1 mm in diameter are abundant and may reach up to 1 cm. Vesicle fill is white and composed of chalcedony, anhydrite, calcite, or chlorite. Surrounding country rock is frequently incorporated into the dike margins. This unit is found in the Yeso Hills on the southwestern edge of the Gypsum Plain, above the Black River. Float from other vesicular intrusive rocks, identified by Pratt (1954) as trachyandesite, is found as apparent karst-collapse deposits on the Gypsum Plain at NE1/4 sec. 31, T. 25 S., R. 25 E.; characteristically similar float was found at NE1/4 sec. 12, T. 26 S., R. 24 E., with an $^{40}Ar/^{39}Ar$ geochronology sample yielding a 28.167 ± 0.29 Ma groundmass date. Argon geochronology of the Yeso Hills dikes by Attia and Ricci (2023) yielded a date of 34.45 ± 0.28 Ma. Additional intrusive rocks are found south of the Texas border and intermittently in the subsurface. Compiled from new observations and synthesized descriptions of King (1948), Pratt (1954), Hayes (1964), Calzia and Hiss (1978), Allen and Attia (2021), and Attia and Ricci (2023).

CENOZOIC-MESOZOIC ERATHEMS

PALEOGENE-CRETACEOUS SYSTEM

KPEu – Fracture fill of Cretaceous strata

Short description: Exhumed karst/fracture fill/collapse deposits of remnant Cretaceous clastic and carbonate strata found as isolated, weathered jumbles on the Gypsum Plain. Buff, massive to bedded, quartzose siltstone and sandstone with subordinate lithics. Rounded pebble conglomerate in coarse matrix. Tan to gray, variably fossiliferous wackestone and packstone. Albian in age (Lang, 1947; Kues and Lucas, 1993).

Long description: Isolated exposures of highly weathered, broken, and tilted blocks of remnant Cretaceous sandstone, conglomerate, and carbonate strata found on the Gypsum Plain resulting from exhumation of karst collapse or solution-subsidence infill deposits. Sandstones are yellow to tan-brown, subangular, well-sorted, moderately indurated, and quartzose. Sandstones are seen in outcrop as massively bedded, coarse-grained, channel sands or as planar- to cross-bedded, fine- to medium-grained sands or silty sandstones. These siliciclastic rocks comprise mostly quartz with subordinate feldspar, lithic fragments of chert, and iron minerals. Bivalve casts are common. Pebble conglomerates are clast-supported with a coarse sand matrix and calcium-carbonate cement. Pebbles are moderately to well-rounded, siliceous, and found occupying decimeter-thick channel beds. Carbonates are gray to tan, well-indurated wackestones to packstones commonly containing fossils of bivalves, ammonites, echinoderms, and other Cretaceous fauna. Fossil assemblages are variable at each outcrop and are absent at some locations. The mapped deposits, fissure-fill sandstone dikes in the Guadalupe Mountains, and reworking of rounded siliceous pebbles in Neogene surficial deposits support coverage of the map area by a Cretaceous sedimentary system. Lang (1947) and Kues and Lucas (1993) support correlation to the Albian-aged Washita Group of Texas. Collapse deposits of Permian or Cenozoic strata may be found alongside these Cretaceous outliers. Compiled from new observations and synthesized descriptions of Lang (1947), Hayes (1964), Kelley (1971), Kues and Lucas (1993), Allen and Attia (2021), and Allen (2024).

PALEOZOIC ERATHEM

PERMIAN SYSTEM

LOPINGIAN EPOCH

Pr – Rustler Formation

Short description: Clastics, evaporites, and carbonate in chaotic outcrops. From base: Virginia Draw, Culebra Dolomite, Tamarisk, Magenta, and Forty-niner Members. Base is red-brown, laminated sandstone and mudstones with reduction spots and gypsum. Resistant, brecciated, vuggy, crystalline dolomite. Upper is poorly exposed to absent bedded gypsum, gypsic mudstones, and sandy dolomites. The unit is 50–100 m thick or more.

Long description: The Rustler Formation is a lithologically heterogeneous unit composed of sandstones, mudstones, evaporites, and carbonates. Typical outcrops on the surface are irregular masses of gypsum, dolomite, and salt in large blocks scattered with chaotic bedding orientations. Previous 1:24,000 mapping across the Delaware Basin has characterized the Rustler Formation by members (Virginia Draw, Culebra Dolomite, Tamarisk, Magenta, and Forty-niner). Erosion has removed any identifiable outcrops of the Forty-niner Member from this map, and the Magenta Dolomite Member is only exposed in a few outcrops too small to display, on the farthest edge of this map, east of U.S. Route 285. The base of the Rustler Formation is marked by the Virginia Draw Member, which is pale-red to reddish-brown or deep orange-red siltstone to very fine-grained sandstone and gypsiferous mudstone. Beds are thin to

laminated, with cross-laminations, wavy bedding, reduction spots, and local gypsum nodules. The member is highly fractured and folded, forms colluvium slopes, and is commonly associated with solution-collapse breccias. The thickness of the member ranges from 75 to 130 m. The carbonate beds of the overlying Culebra Dolomite Member are the easiest to identify on this map, often forming low hills and ridges due to their relative resistance to erosion; beds are cream to white, finely crystalline, sugary dolomite and sandy limestone, and often exhibit low-angle cross-bedding. The dolomite is distinctly vuggy (1–10 mm scale) and extensively fractured or brecciated. Thickness of the member is 2–9 m. The overlying Tamarisk Member is light-gray, nodular gypsum interbedded with reddish-brown gypsiferous claystone/mudstone. Beds are brecciated to massive and commonly poorly exposed. This member is identified primarily by gypsum presence and stratigraphic position above the Culebra Dolomite Member; brecciated blocks of the overlying member subside in red muds. Thickness of the Tamarisk Member ranges from 9 to 82 m (local exposures typically <50 m). The Magenta Member is pale-gray to reddish-brown, sandy dolomite with subordinate siltstone. The Forty-niner Member is nearly absent and is white to gray, bedded gypsum. Frequent karstification and solution-collapse features, determined from subvertical contacts with the underlying Salado Formation, indicate early diagenetic dissolution of evaporites. Evaporitic intervals (especially gypsum and salt) point to episodic arid conditions, while siliciclastic input suggests intermittent periods of terrestrial influence. The Rustler Formation represents restricted marine to sabkha depositional settings, with strong evaporitic influence. The thickness of the undifferentiated Rustler Formation is highly variable but commonly 50–100 m, locally thicker where thick gypsum masses are preserved. Compiled from new observations and synthesized descriptions of Dehler and Pederson (1998, 2002), Pederson and Dehler (2004a, 2004b), Cikoski (2019a, 2019b, 2020), Cikoski and Allen (2020), Allen and Attia (2021, 2022), Attia and Allen (2022), and Allen (2024).

Prcs – Castile, Salado, and Rustler Formations, undivided

Short description: The map unit **Prcs** is mapped where the map scale does not permit division of map unit **Pcs** and map unit **Pr** when both are present on the landscape.

Long description: The map unit **Prcs** is mapped where the map scale does not permit division of map unit **Pcs** and map unit **Pr** when both are present on the landscape. This map unit does not indicate which formation is more predominant in a given polygon but assumes a noteworthy portion of each is present.

Pcs – Castile and Salado Formations, undivided

Short description: Thick, undivided sequence of evaporites and interbedded clastics and carbonates with extensive dissolution deformation. Castile Formation overlain by mostly absent Salado Formation. Laminations of white gypsum with gray calcite. Contact with Salado Formation at change to remnant interbeds and gypsum stained by leached clay minerals from dissolved halite. Approximately 750–1200 m thick.

Long description: Thick sequence of evaporites, including gypsum, anhydrite, halite, and potassium-rich salts, interbedded with claystone, siltstone, fine-grained carbonate sandstone, and minor carbonate mudstone. This unit is left undivided due to widespread dissolution, collapse brecciation, and karst modification within the Salado Formation, which makes it difficult to distinguish between the two evaporite deposits. Outcrops typically consist of gypsum breccia in a matrix of reddish-brown to yellow, clay-rich, crystalline gypsum and interbeds of light-gray to white, laminated gypsum, gypsum clay, and reddish-brown mudstone. Breccia blocks are massive to internally laminated and composed of angular, fine- to coarse-grained, crystalline gypsum and minor carbonate mudstone fragments. Contorted, folded,

or chaotic bedding is common due to salt dissolution and subsurface collapse. The unaltered Salado Formation is predominantly composed of halite (up to 90%), with interbedded anhydrite, gypsum, potash, dolomite, and claystone. Outcrops of the Salado Formation feature white to clear halite with gray or reddish bands of muddy halite. The upper portion is commonly brecciated, with selenite masses and variably weathered gypsum. Only leached and clay-rich remnants are typically exposed at the surface. Exposures are typically massive and poorly exposed and appear light pinkish-white, gray, or red on weathered surfaces. In the field, the unit may be identified by waxy, reddish clays, laminated or nodular gypsum, and collapse breccias. Karst features include solution-collapse troughs, subvertical fractures, and subsided breccia blocks. The McNutt Member of the Salado Formation contains important potash-bearing intervals and is the source of the largest domestic potash production in the United States (Barker and Austin, 1993). The Castile Formation consists of finely crystalline calcium sulfate (gypsum at the surface, anhydrite at depth) interlaminated with calcite and local halite intervals. Laminae are typically white to pale-gray gypsum and dark-gray calcite, with massive to faintly laminated textures. Halite beds and basal-laminated limestones are used to divide the unit into members. The contact between the Castile and Salado Formations is marked by a siliciclastic interval near the base of the Salado and by the base of a laminated limestone in the Castile. West of the Pecos River, the unit is primarily Castile Formation gypsum; to the east, the section thickens and includes more halite from the Salado Formation. Several researchers (Brokaw et al., 1972; Jones, 1973; Powers et al., 1978; Bachman, 1980; Cikoski, 2019b) have noted a directional thinning of the Salado Formation that was caused by a dissolution front that started up-dip, to the west; water preferentially dissolved halite and altered anhydrite to gypsum. Allen and Attia (2022) mark the Pecos River as a possible boundary between halite- and anhydrite-dominant outcrops. Thicknesses of the Castile and Salado Formations are estimated from drill logs; the Salado Formation thickness ranges from 300 to 650 m and the Castile Formation thickness is estimated to range from 445 to 585 m. Compiled from synthesized descriptions of Pederson and Dehler (2004a, 2004b), Cikoski (2019b, 2020), Allen and Attia (2021, 2022), and Cikoski and Allen (2020).

GUADALUPIAN-CISURALIAN EPOCH

Shelf Deposits

Pat – Tansill Formation of the Artesia Group

Short description: Shelf sediments of dolomite, limey mudstones, and clastics. Grades into the upper Capitan Formation. Common fossils and pisoliths increase toward the reef. Ocotillo Member forms a ledge of siltstone in the upper portion. Beds thicken and dolomite increases reefward. Lower contact with the Yates Formation at the change to slope-forming clastics. Approximately 30–50 m thick, up to 80 m thick at reef.

Long description: Pale-weathering, light-olive-gray to tan dolomitic grainstones, packstones, wackestones, and mudstones. Dolomitic beds are thin- to thick-bedded with minor dark-tan siltstone or quartz sandstone beds. Most dolomite beds are massive, but may have faint, localized fenestrae and layering. Intraclastic breccia, peloids, teepee structures, mud cracks, fine laminations, localized coated grains, and ripples are present. Fossiliferous grainstones and packstones occasionally contain crinoid fragments, brachiopods, ostracods, gastropods, and fusulinids. Pisoliths are common near reef fronts, decreasing in abundance shelfward, where carbonate mudstones with fenestral fabrics dominate. Siltstone interbeds are sparse and dark tan, while silty to clay-rich mudstones appear pale-brown to pink, particularly in the upper portions. Siliciclastic intercalations comprise translucent silica lenses and red, silty laminae with trace amounts of medium-grained quartz and feldspar. A persistent 3- to 4-m-thick,

ledge-forming siltstone named the Ocotillo Member occupies the upper part of the formation but is eroded in the northeast portion of the map area. The Tansill Formation can generally be divided into three facies: back-shelf, reef-transitional, and reef-facing. *Back-shelf facies* are thinly bedded carbonate mudstone and siltstone, exhibiting fenestral fabrics. Light-gray to tan dolomitic grainstones and packstones in thin, tabular beds transition (upward and shoreward) into mixed dolomite-siltstone-gypsum facies, characterized by slope-forming intervals and thin sandstone interbeds. Back-reef facies exhibit local features such as mud cracks, moldic porosity, and solution breccia. Fossils are sparse. The Tansill Formation grades laterally into the upper part of the Capitan Formation, characterized by a gradual increase in bioclastic material, thicker beds, and the prominence of pisolitic/oolitic textures. *Reef-transitional facies* are characterized by cliff-forming dolomites that alternate with ledge-forming mudstones and siltstones. Rare teepee structures and paleokarst fillings are observed near the reef. *Reef-facing facies* are interbedded, laminated, massive, and dominated by pisolitic/oolitic dolomites, with a lower siliciclastic content compared to back-shelf facies. Pisolites and ooids are more abundant, weathering to yellowish-tan to reddish-tan hues and ranging in size from millimeters to several centimeters. Thick dolomite beds display blocky weathering and small- to large-scale teepee structures. Cryptoalgal laminations, moldic porosity, and low-angle cross-bedding are prevalent. Fossils are more abundant, and evidence of bioturbation is present. Beds often alternate between vesicular and nonvesicular dolomite, which defines the bedding planes. The basal contact of the Tansill Formation is sharp, defined by the transition from slope-forming sandstone/siltstone of the Yates Formation to cliff-forming dolomites. Sugary dolomite and dolomitic limestone at the base exhibit planar to crinkly laminations, intraclastic breccia, and evidence of synsedimentary deformation. Solution breccia and localized cave formations are present near the basal contact. Average thickness is 30–45 m but up to 80 m near its lateral transition to the Capitan Formation. This unit is the uppermost formation in the Artesia Group that records the final pulse of Guadalupian Capitan reef. The contact between the Tansill and the underlying Yates Formation is commonly recognized as a break in slope. Compiled from synthesized descriptions of Hayes and Koogle (1958), Dehler and Pederson (2002), Cikoski (2019a), Cikoski and Allen (2020), Skotnicki (2021), Skotnicki and Attia (2022), and Allen and Skotnicki (2024).

Payt – Yates and Tansill Formations of the Artesia Group, undivided

Short description: The map unit **Payt** is mapped where the map scale does not permit division of map unit **Pay** and map unit **Pat** when both are present on the landscape.

Long description: The map unit **Payt** is mapped where the map scale does not permit division of map unit **Pay** and map unit **Pat** when both are present on the landscape. This map unit does not indicate which formation is more predominant in a given polygon but assumes a noteworthy portion of each is present.

Pay – Yates Formation of the Artesia Group

Short description: Gray-tan dolomite, pale siltstone, and sandstone in slope-forming unit with abundant siliciclastic beds. Thin- to medium-bedded and massive dolomites. Pisolites and oolites increase reefward as beds thicken and grade into the Capitan Formation. Interbedded fine-grained, calcareous, slope-forming siltstones and sandstones. Gypsum increases shelfward. Approximately 80 m thick and up to 150 m thick.

Long description: Light-gray to tan dolomite interbedded with gray-orange to pale-yellow-orange, calcareous, thin-bedded, fine-grained sandstone and siltstone. The Yates Formation is differentiated from

the overlying Tansill and underlying Seven Rivers Formations by the abundance of slope-forming, poorly exposed, siliciclastic beds; weathered outcrop surfaces are rounded, tabular beds in contrast to the blocky, angular beds of the Tansill and Seven Rivers Formations. Dolomite beds are medium- to thin-bedded, appear massive, fenestrate, vesicular, and often weather to dark-tan or light-gray. Bioturbation, intraclasts, and symmetrical ripple marks are frequently observed. Cryptoalgal laminations, "jelly-roll" structures, and mud cracks are locally observed. Pisolites and oolites increase toward the Capitan Formation, with grains up to 15 cm in diameter, exhibiting radial or concentric fabrics, but are noticeably less abundant than in the Tansill Formation. Dolomite beds thicken and laterally grade into limestone of the Capitan Formation. Interbedded sandstone and siltstones are fine-grained, yellowish brown, greenish-gray, pale-gray, or pink to red in color. Siliciclastic beds are planar or cross-laminated with internal structures such as climbing ripples, water-escape structures, and soft sediment deformation. Siliciclastic intervals are well-sorted and carbonate-cemented, with beds 0.3–4 m thick, friable, and often form slopes. Intervals erode to colluvium-dominated, vegetated slopes. Teepee structures and solution breccias are common near the Capitan Formation. The lateral grading and facies variations highlight a transition from a backreef shelf toward the Capitan reef. Trace, medium- to coarse-grained, disseminated clusters of goethite in botryoidal form or as pseudomorphs after marcasite and pyrite can be located at the base of the Yates Formation in a 3-m-thick zone, particularly near the reef front. These minerals were identified in outcrop or float and used to reliably identify the contact between the Yates and Seven Rivers Formations in the Dark Canyon area. Locally present west of Carlsbad, gypsum-rich siltstone and secondary gypsum have been remobilized into spherical concretions (0.5–1 m diameter), representing facies changes in the Yates north of this map, extending to Santa Rosa, New Mexico. Approximately 80 m thick and up to 150 m thick. Compiled from synthesized descriptions of Hayes and Koogle (1958), Kelley (1971), Dehler and Pederson (2002), Skotnicki (2021), Skotnicki and Attia (2022), Cikoski and Allen (2020), Allen and Skotnicki (2024), and
Skotnicki and Allen (2024).

Pasy – Seven Rivers and Yates Formations of the Artesia Group, undivided

Short description: The map unit **Pasy** is mapped where the map scale does not permit division of map unit **Pas** and map unit **Pay** when both are present on the landscape.

Long description: The map unit **Pasy** is mapped where the map scale does not permit division of map unit **Pas** and map unit **Pay** when both are present on the landscape. This map unit does not indicate which formation is more predominant in a given polygon but assumes a noteworthy portion of each is present.

Pas(e) – Seven Rivers Formation of the Artesia Group

Short description: Thick-bedded dolomite with sandstone, siltstone, and gypsum. Dolomite is white-gray and laminated. Laminated crystalline gypsum with siltstone interbeds increases shelfward and unit is labelled Pase. Siliciclastics are fine-grained and quartzose with minor lithics and clay minerals. Dolomites become calcic, fossiliferous, and pisolite-rich as beds grade into the reef. Approximately 120–180 m thick.

Long description: Light-gray to white, thick-bedded dolomite with sparse interbedded fine-grained sandstone/siltstone and gypsum in specific sections. Dolomite weathers to yellowish-gray to olive-drab. Local brecciation and intraformational faulting are common near transitions. Dolomite ranges from laminated to massive with pisolites near reef facies. Predominantly dolomite, transitioning into calcareous dolomite with fusulinid and mollusk fossils near reef facies. Siliciclastic beds are thin- to

medium-bedded, planar-laminated to cross-laminated, and pale-reddish-brown near evaporite facies; beds transition to very pale-orange near carbonate facies. Ripple marks are common, with occasional soft sediment deformation. Clasts are fine- to very fine-grained, poorly sorted in some intervals, and composed of quartz with minor feldspar and clay minerals. Gypsum nodules and minor carbonate clasts are present in some intervals. The Seven Rivers Formation is divided into two units by a sedimentary-facies boundary on the map. Carbonate facies (unit **Pas)** grade into the Capitan Formation toward the reef and shelf-margin, while a lateral transition to evaporite facies occurs in increasingly nearshore, back-shelf deposits. Carbonate facies grade shelfward into dolomitic intervals and laterally into evaporite facies away from the shelf. The reef facies exhibit pisolite-rich dolomite, indicative of higher-energy environments near the reef margin. Dolomite beds are 1–3 m thick, and up to 170 m in total thickness. The evaporite facies (unit **Pase**) is characterized by thin to massive, tabular beds of nodular, cream to yellow-gray, friable, alabaster gypsum. From elevation and imagery, the boundary between the carbonate and evaporite facies is identified by a respective change from steep cliffs to narrow, deeply incised catchments in piedmont slopes. The Seven Rivers Formation is exposed continuously from North McKittrick Canyon to East Hess Hills, but thins to transitional facies toward Seven Rivers Hills and El Paso Gap (10–15 km from the reef escarpment). Carbonate facies near the reef contain fusulinid coquinas, dolomitized mollusks, and abundant pisolites (<2.5 cm wide). Dolomite beds thicken (1.5–3 m) and exhibit massive bedding near the reef, which makes the gradational contact between the Seven Rivers Formation and the Capitan Formation inconspicuous. At the contact, 1–2 m of relief is carved into massive facies of the Capitan Formation and filled with thinly bedded calcareous siltstone of the Seven Rivers Formation. Overall formation thickness is 120–180 m near reef facies and thins laterally into the evaporite section. Compiled from new observations and synthesized descriptions of Hayes (1964), Kelley (1971), Dehler et al. (2005b), Cikoski (2019a), Cikoski and Allen (2020), Skotnicki (2021; 2024b), Skotnicki and Attia (2022), Allen and Skotnicki (2024), and Skotnicki and Allen (2024).

Paqs – Queen and Seven Rivers Formation of the Artesia Group, undivided

Short description: The map unit **Paqs** is mapped where the map scale does not permit division of map unit **Paq** and map unit **Pas** when both are present on the landscape.

Long description: The map unit **Paqs** is mapped where the map scale does not permit division of map unit **Paq** and map unit **Pas** when both are present on the landscape. This map unit does not indicate which formation is more predominant in a given polygon but assumes a noteworthy portion of each is present.

Paq – Queen Formation of the Artesia Group

Short description: Pale quartz siltstone and sandstone with thin beds of dolomite, gypsum, and mudstone; typically forming slopes. Siliciclastics in planar, Calcium-carbonate cemented, beds that decrease up section and reefward. Gypsums and muds increase shelfward. Dolomite thickens and increases up section in proximity to the gradational contact with the Goat Seep Formation. Approximately 120 m thick, thinning to 60 m thick.

Long description: Very pale-orange to pale-yellowish-brown, quartz siltstone and fine-grained quartz sandstone with subangular to subrounded grains. The clastic rocks form planar, thin to thick beds and are cemented with carbonate. Local thin interbeds of light-gray dolomite (10–30 cm thick) are present, especially in the upper portions of the formation, forming small, resistant ledges. In the uppermost 20 m, dolomite beds become thicker and more frequent, occasionally reaching several meters thick. The unit is

typically slope-forming, producing rust-yellow to rust-orange soils. The Queen Formation represents a mixed clastic-carbonate system that transitions laterally and vertically. Clastic beds dominate the lower and upper parts of the formation. Dolomitic beds become more common near the top, and toward the reef margin where the formation grades into the Goat Seep Formation. Toward the Seven Rivers Embayment in the northwest part of the map, dolomitic intervals transition to red-colored siltstone and mudstone; dolomites become increasingly replaced by gypsum, and the color changes from very pale-orange to reddish-brown. The type section for the Queen Formation was established by Moran (1954) in the west wall of Dark Canyon, about 8 km southwest of the town of Queen, New Mexico**.** The contact with the underlying Grayburg Formation is described by Hayes (1964) as conformable but arbitrarily placed based on subtle lithologic shifts. The contact with the overlying Seven Rivers Formation is described by Hayes (1964) as conformable, but Skotnicki and Attia (2022) describe the dolomite beds below the contact as dismembered, brecciated, irregular, and foundering in underlying siltstone, suggesting karstification and a localized erosional unconformity. The Queen Formation is approximately 120 m thick near the reef margin and thins to about 60 m toward the north and northwest. Compiled from synthesized descriptions of Hayes (1964), Kelley (1971), Skotnicki and Attia (2022), Skotnicki and Allen (2024), and Skotnicki (2024b).

Pagq – Grayburg and Queen Formations of the Artesia Group, undivided

Short description: The map unit **Pagq** is mapped where the map scale does not permit division of map unit **Pag** and map unit **Paq** when both are present on the landscape.

Long description: The map unit **Pagq** is mapped where the map scale does not permit division of map unit **Pag** and map unit **Paq** when both are present on the landscape. This map unit does not indicate which formation is more predominant in a given polygon but assumes a noteworthy portion of each is present.

Pag – Grayburg Formation of the Artesia Group

Short description: Dolomite, dolomitic limestone, sandstones, siltstones, and limestone. Tabular, laminated- to thin-bedded, fine-grained dolomite with fossils, ooids, and thick beds increasing toward the Goat Seep Formation. Thick-bedded, resistant, fine-grained quartzose sandstone with subordinate lithics. Forms smooth topography. Gypsum and fine-grained facies increase shelfward. Approximately 60–180 m thick.

Long description: Yellowish-gray to very pale-orange, laminated, fine-grained, calcareous dolomite, with minor fine-grained, locally oolitic limestone. Interbedded within the dolomite are locally resistant, pale-orange siltstone and well-sorted, subangular, very fine-grained quartzose sandstone beds with subordinate lithics and feldspars. Sands and silts are especially common and thicker in the lower part of the formation. Dolomite beds are typically tabular and thin-bedded (2–30 cm) but locally thicken up to 4 m near the reef; fusulinid molds and oolitic textures are common. Sandstone beds are typically 2–15 cm thick, but can locally reach 2 m. Calcite:dolomite ratios vary widely, but average approximately 4:96 based on spectrographic analyses by Boyd (1958) and versenate analyses by Haynes (1964). Beds are typically laminated to massive, with some intervals showing fenestral fabrics. The unit tends to form smoother, gently sloping hills compared to the underlying San Andres Formation, but steeper slopes and minor cliffs than the overlying Queen Formation. In the north, near Rocky Arroyo, gypsum becomes abundant, sinkholes are common, and gypsum forms red-and-white, banded beds several meters thick. The lower contact with the San Andres Formation is locally unconformable in surface exposures from

Last Chance Canyon, southwestward to the Algerita Escarpment, and in the Brokeoff Mountains near the border with Texas; the extent of this unconformity is not well constrained. Outside those areas, this contact is largely conformable and marked by a distinct lithologic change from coarser, more massive dolomite to finer-laminated textures and the occasional presence of a discontinuous calcium-carbonate-cemented, white-weathering-tan, well-sorted, fine-grained, moderately to well-sorted, round-weathering, massive sandstone. The upper contact with the Queen Formation is conformable but arbitrarily placed, based on a subtle increase in clastic content and a darker gray appearance in the Queen. The transition to the Goat Seep Formation to the south and southeast is gradational, marked by thickening carbonate beds, coarser grain sizes, and increased dolomite cementation of sandstones. The Grayburg Formation is typically between 60 and 180 m thick. Compiled from new observations and synthesized descriptions of Kelley (1971), Hayes (1964), Skotnicki and Attia (2022), and Skotnicki (2024b).

Pcg – Cherry Canyon Sandstone Tongue of the Delaware Mountain Group and Grayburg Formation of the Artesia Group, undivided

Short description: The map unit **Pcg** is mapped where the map scale does not permit division of map unit **Pcc** and map unit **Pag** when both are present on the landscape.

Long description: The map unit **Pcg** is mapped where the map scale does not permit division of map unit **Pcc** and map unit **Pag** when both are present on the landscape. This map unit does not indicate which formation is more predominant in a given polygon but assumes a noteworthy portion of each is present.

Pcc – Cherry Canyon Sandstone Tongue of the Delaware Mountain Group

Short description: Shelf sandstone tongue correlative to the lowest sands of the deep-marine basin facies. Discontinuous beds of poorly exposed fine quartz and arkose sand. Grades into the upper San Andres Formation and is disconformable over the Cutoff Formation on the shelf; conformable over the basinal Brushy Canyon Formation. Approximately 60–90 m thick in the Guadalupe Mountains and up to 200 m thick in the Brokeoff Mountains.

Long description: The Cherry Canyon Formation and Cherry Canyon Sandstone Tongue consists of thin- to medium-bedded, light-orange to buff quartz siltstone and very fine-grained sandstone, interbedded with medium- to thick-bedded, gray to tan, fossiliferous dolomite and limestone. Sandstone and siltstone beds are typically fine-grained, arkosic to subarkosic, thinly laminated, and poorly sorted, containing predominantly quartz and minor altered feldspar grains. Carbonate intervals (the Getaway, South Wells, and Manzanita Members) are characterized by tan to dark-gray, fossiliferous, dolomitic limestone and thin carbonate beds that thin toward the deeper basin. Ripple marks, varvelike laminations, and irregularly bedded channel fills are common, particularly in the lower two-thirds of the unit. Bedding is generally thin to thick and somewhat discontinuous due to the presence of submarine channels. In outcrop, the unit is typically poorly exposed and tends to form low slopes. In the subsurface, the Cherry Canyon is described as buff to brown, fine-grained sandstone and siltstone, with persistent carbonate intervals that thin basinward. Neutron density-porosity log signatures display a distinct, laterally continuous marker compatible with lithologic changes at formation boundaries. The Cherry Canyon Formation represents sandstone channels on the shelf that continue basinward as deep marine siliciclastic and carbonate sedimentation within the Delaware Basin. Sandstone and siltstone beds were deposited largely by submarine channel and levee systems. In the basin, the Cherry Canyon Formation conformably overlies the Brushy Canyon Formation. On the shelf margin and shelf, the lowest portions of the Cherry Canyon Sandstone, below the lowest limestone, are disconformable over the Cutoff Formation and

Victorio Peak Limestone and grade into the upper San Andres Formation. The central portion of the unit, from the lowest limestone to the middle limestone, grades shelfward into the Goat Seep Formation. The upper portion of the unit pinches out between the Goat Seep Formation and Capitan Formation. Moving basinward, the limestones of the Cherry Canyon thin and disappear, making differentiation of Delaware Mountain Group formations difficult in the subsurface. The unit varies in thickness from 340 to 435 m in the subsurface of the map area, is approximately 60–90 m thick in outcrops of the Guadalupe Mountains and is up to 200 m thick in the Brokeoff Mountains. Compiled from synthesized descriptions of King (1942, 1948), Boyd (1955, 1958), Hayes and Koogle (1958), Hayes (1959, 1964), Kelley (1971), Cikoski (2019b), Cikoski and Allen (2020), Allen and Attia (2021), and Allen (2024).

Psag – San Andres Formation and Grayburg Formation of the Artesia Group, undivided

Short description: The map unit **Psag** is mapped where the map scale does not permit division of map unit **Psa** and map unit **Pag** when both are present on the landscape.

Long description: The map unit **Psag** is mapped where the map scale does not permit division of map unit **Psa** and map unit **Pag** when both are present on the landscape. This map unit does not indicate which formation is more predominant in a given polygon but assumes a noteworthy portion of each is present.

Psa – San Andres Formation, undivided

Short description: Dolomite and dolomitic limestone with fetid odor, fossils, chert nodules at the base, and clastics increasing up section. Includes, from lowest to highest, the Rio Bonito, Bonney Canyon, and Fourmile Draw Members. The base grades laterally into the Cutoff Formation and downwards into the Yeso Formation or Glorieta Sandstone, the middle pinches out basinward, and the upper grades laterally into the Cherry Canyon Sandstone and is locally unconformable under the Grayburg Formation. Approximately 350 m thick.

Long description: Thin- to thick-bedded, light- to dark-gray dolomite and dolomitic limestone unit that contains chert nodules near the base, a fetid odor and fossils in the middle member, and an upper member of interbedded dolomite, limestone, and silty sandstone that becomes increasingly gypsic around the northern map boundary. Includes three members described separately from lowest to highest: Rio Bonito, Bonney Canyon, and Fourmile Draw. The lower portion of the formation grades into the Cutoff Formation, the middle of the formation pinches out basinward, and the upper portion grades into the Cherry Canyon Sandstone. Forms shallowly dipping, undulatory dip slopes in the highlands of the Guadalupe Mountains and cliffs along the Algerita Escarpment. Locally unconformable below the Grayburg Formation from Last Chance Canyon, southwestward across parts of the Algerita Escarpment and Brokeoff Mountains (Hayes, 1964). Locally unconformable between the Rio Bonito and Bonney Canyon Members; extent of local unconformity not displayed on map (Hayes, 1964). The undifferentiated unit is approximately 350 m thick. Compiled from new observations and synthesized descriptions of Boyd (1955, 1958), Hayes (1959, 1964), Kelley (1971), and Skotnicki (2024).

Psaf – Fourmile Draw Member of the San Andres Formation

Short description: Upper ledge-forming member of the San Andres Formation with crystalline dolomite, tabular limestones, sandstones, and gypsum pods. Common pitted textures, rare laminations and fossils, and absent chert. Shelfward increase in gypsum abundance. Interbedded sandstones may correlate to the

Cherry Canyon Sandstone; upper contact with Artesia Group may be locally unconformable. Less than approximately 115 m thick.

Long description: The uppermost member of the San Andres Formation is ledge-forming dolomite beds of consistent thickness interbedded with tabular limestones, occasional sandstones, and rare, discontinuous pods of gypsum. Carbonate beds are drab-yellow-olive and light- to medium-gray, finely to medium-crystalline dolomite. Weathered and fresh surfaces are approximately the same color and weather to pitted or vuggy textures with botryoidal calcite fill, especially in tabular limestone beds. Occasionally micritic or oolitic and clastic in nature. Forms consistent, evenly spaced, ledge-forming beds (0.1–1.5 m thick) of massive, occasionally laminated dolomite interbedded with tabular, rounded limestones, weathering light-gray. Chert is absent, fossils are rare, contacts between beds are commonly styolitic, and localized brecciation occurs. Beds may split and rejoin around interbedded, silty gypsum pods in the northern map area. Gypsum increases shelfward, north of the map area, and begins to appear around Texas Hill. This unit is preferentially deformed into undulatory dip slopes indicated by brecciation at the outcrop scale, where carbonates are interbedded with gypsum. The upper portion of the unit is interbedded with yellow-brown, fine-grained sandstone that may be correlative to the Cherry Canyon Sandstone, which is known to have a gradational relationship moving toward the shelf. Contact with the overlying Grayburg Formation of the Artesia Group is conformable but may be locally unconformable from Last Chance Canyon southwestward to the Algerita Escarpment and Brokeoff Mountains near the border with Texas (Hayes, 1964). Kelley (1971) described the contact with underlying members as transitional and vague, attributing differences in this area primarily to minor changes in composition, texture, and color. Less than approximately 115 m thick. Compiled from new observations and synthesized descriptions of Boyd (1955, 1958), Hayes (1959, 1964), Kelley (1971), and Skotnicki (2024).

Psab – Bonney Canyon Member of the San Andres Formation

Short description: Thin-bedded middle member of the San Andres Formation with brown-gray, crystalline dolomite and dolomitic limestone. Consistent beds form alternating vegetated slopes and ledges. Common vugs, fossils, and fetid odor. Absent chert. Thins and becomes dolomitic and unrecognizable toward the shelf margin. Lower contact is variably conformable and marked by the presence of chert. Approximately 60–180 m thick.

Long description: The middle member of the San Andres Formation is thin-bedded, porous, brownish-gray to dark-brown or gray and light-gray to tan-brown, finely crystalline dolomite and dolomitic limestone. Forms consistent (0.25 to 2 m thick) beds that form alternating vegetated slopes and ledges with occasional thick, cliff-forming beds. Occasional medium-gray beds of micritic texture with small calcite-filled vugs. Commonly has deep centimeter-scale pits and vuggy weathering with calcite fill that decrease up section. Absent chert, common fetid odor, occasional laminae, and abundant recrystallized fossils. Fossils include brachiopods, fusulinids, and crinoids. Occasionally interbedded with light-gray dolomitic limestones with rounded weathering of decimeter-scale massive beds. The unit thins toward the shelf margin, where it becomes unrecognizable, and thickens shelfward beyond the map area. The lower contact is distinct and unconformable to the south and becomes conformable northward. Increasingly dolomitic shelfward to the northwest, and limestones increase in abundance toward the shelf margin. Largely similar in composition and texture to the underlying Rio Bonito Member but does not contain chert. Unit is approximately 60–180 m thick. Compiled from new observations and synthesized descriptions of Boyd (1955), Hayes (1964), Kelley (1971), and Skotnicki (2024).

Psar – Rio Bonito Member of the San Andres Formation

Short description: Lower member of the San Andres Formation has gray, thick- to variably bedded, homogenous, crystalline dolomites with chert abundant up section. Dolomitic limestone increases up section and toward the shelf margin. Conformable over the Yeso Formation down section of the first cherty bed or at the Glorieta Sandstone as it pinches out. Grades basinward into the Cutoff Formation. Approximately 110 m thick**.**

Long description: The lowermost member of the San Andres Formation consists of moderately thick beds of light- to medium-gray dolomite and dolomitic limestone with brown-orange-weathering chert increasing up section. Beds are 0.5–2 m thick but occasionally as thin as 0.1 m or as thick as 10 m, weathering to olive-gray ledges or slopes. Beds are massive, planar or tabular, and occasionally lenticular. Texturally homogenous fine to medium crystalline dolomites and dolomitic limestone. Cherts may be present or absent at the base of the member that is otherwise characterized by thin beds of occasionally laminated, microcrystalline, dolomitic limestone with occasional pisolites. Chert is light- to medium-gray and brown, weathering to light-orange or brown, is found in variable abundance from bed to bed, and increases up section. Chert is found as irregularly shaped nodules, pods, and lenticular beds. Vugs and pitted textures are common. Overall, this member does not vary laterally but is increasingly calcic up section and basinward, while dolomitic compositions increase shelfward. Conformable with the underlying Yeso Formation either at, or just up section of the contact between thin-bedded, non-cherty and thick-bedded, cherty dolomite, or at the highest sandy siltstone bed in the Yeso Formation that may be the Glorieta Sandstone. Separated from the Yeso Formation where the Glorieta Sandstone is present. This lower member grades gradually and indistinctly into the Cutoff Formation. This member is approximately 110 m thick**.** Compiled from new observations and synthesized descriptions of Boyd (1955, 1958), Hayes (1964), Kelley (1971), and Skotnicki (2024b).

Pgl – Glorieta Sandstone

Short description: Described and traced to the Algerita Escarpment by Skinner (1946). Poorly exposed gray, weathering to yellow, frosted, coarse, well-rounded, lightly quartzitic sandstone. Overlain by a discontinuous limestone conglomerate and underlain by sandy dolomitic limestone. Conformably separates the Yeso Formation from the lower San Andres Formation where present. Approximately 3 m thick.

Long description: Traced to its position in this quadrangle and described by Skinner (1946) as a poorly exposed, gray, weathering to yellow, coarse-grained sandstone that is frosted, well-rounded, and lightly quartzitic. Overlain by a discontinuous limestone conglomerate and underlain by a lower unit of dolomitic limestone with abundant sands that grades and interbeds into the underlying Yeso Formation. Thins to 3-m-thick before grading laterally into the upper Yeso Formation just below the contact with the San Andres Formation at sec. 20, T. 23S., R. 20E. along the western side of the Guadalupe Mountains on the Algerita Escarpment above Big Dog Canyon. Conformably separates the Yeso Formation from the lower San Andres Formation. Progressively south, the San Andres Formation lies conformably on the Yeso Formation. Description is compiled from synthesized descriptions of Skinner (1946) and Hayes (1964).

Pyv – Yeso Formation and Victorio Peak Limestone, undivided

Short description: The map unit **Pyv** is mapped where the map scale does not permit division of map unit **Pyo** and map unit **Pvp** when both are present on the landscape.

Long description: The map unit **Pyv** is mapped where the map scale does not permit division of map unit **Pyo** and map unit **Pvp** when both are present on the landscape. This map unit does not indicate which formation is more predominant in a given polygon but assumes a noteworthy portion of each is present.

Pyo – Yeso Formation

Short description: Dolomitic- to calcic-carbonates with subequal crystalline gypsum, flaky shale, and quartzose sandy siltstone. Conformable upper contact below cherty carbonate beds or at the Glorieta Sandstone. Disparate from the standard Yeso Formation as changes in strata are marked by a gradation and nomenclature change to the Victorio Peak Limestone when evaporites are absent. Approximately 0–180 m thick.

Long description: This unit comprises dolomite and dolomitic limestone interbedded with gypsum, limestone, shale, and sandy siltstone that forms slopes in the Brokeoff Mountains and grades into the Victorio Peak Limestone towards the shelf margin. Dolomites, dolomitic limestones, and limestones are light- to dark-gray in thin to medium planar beds around 0.25 m thick. These beds have sugary microcrystalline textures, a light fetid odor when broken, rare chert, and rare fossils. Chert is abundant in the rare beds where it is found. Fossils include crinoids and fusulinids. Gypsum is subequal in abundance to carbonates, crystalline, and white to dark-gray, weathering to light-brown to orange. Shales are infrequent, thinly bedded, and have a flaky texture. Occasional beds of slope-forming, yellow to gray, sandy, thin-bedded siltstone with quartzose compositions. The top of the unit has a sandy siltstone that is tentatively a southern pinch-out of the Glorieta Sandstone extending roughly 7–8 km into the quadrangle along the Algerita Escarpment. This clastic bed thickness is approximately 3 m and grades into the uppermost Yeso Formation and the base of the San Andres Formation. The Yeso Formation in this area represents a transition from the classic shelf-facies characteristic of central New Mexico into the reef facies of the Victorio Peak Limestone. The presence of gypsum and anhydrite, which decreases toward the shelf margin, is the defining characteristic of this unit when compared to the Victorio Peak Limestone. Beds are progressively younger toward the shelf margin due to progradation. The conformable contact with the overlying San Andres Formation occurs either above the sandy siltstone of the Glorieta Sandstone or where thin non-cherty dolomite transitions to thick-bedded dolomite that has progressively abundant chert up section. The unit is approximately 0–180 m thick. Compiled from new observations and synthesized descriptions of Boyd (1958), Hayes (1964), Kelley (1971), and Skotnicki (2024b).

Pa – Abo Formation

Short description: Cross section only.
Long description: Cross section only.

Shelf-margin reef deposits

Pcp – Capitan Formation

Short description: Fossiliferous limestone, dolomite, and carbonate breccia. Vertical cliffs of unstratified massive reef facies composed of accreted organic debris. Transitions into breccia foreslope facies with thick inclined beds of dolomitized talus. Grades shelfward into the Artesia Group and basinward into the Bell Canyon Formation and is disconformable on the Goat Seep Formation. Approximately 600 m thick.

Long description: Massive, fossiliferous, gray to very light-gray limestone, dolomite, and limestone/dolomite breccia. Outcrops generally appear massive and structureless, with a paucity of bedding in the main reef core. Surfaces are often pitted or vuggy, with centimeter- to decimeter-scale elongate voids variably filled with coarse-grained, light-yellow, palisade calcite spar. Local zones are faintly brecciated, with dark-gray angular carbonate clasts floating in a lighter-gray matrix. The unit forms steep slopes and imposing, nearly vertical cliffs, particularly in canyon walls such as Big Canyon and Slaughter Canyon. Brecciation is common toward the slope facies, where fragmented reef debris, calcarenite, and fossil reef talus are cemented and partly dolomitized. The brecciated member can be visually separated from the massive reef facies by its steeper dips, thick beds, and slope-forming nature. Sandstone dikes ranging from "wispy" fractures to meter-scale, shelf-parallel dikes are common, especially near the top of the formation, and may indicate karstic processes. Conspicuous fractures filled with microbial remains are frequent. The Capitan Formation represents the preserved Capitan Reef itself, formed primarily by organic skeletal accretion that was buried by marine carbonate cement as the Guadalupian carbonate shelf aggraded and prograded into the Delaware Basin. The reef core is massive and unstratified, whereas the forereef slope consists of crudely bedded carbonate debris, talus blocks, and slides dipping basinward at 10–30°. The reef contains a diverse assemblage of macrofossils, including sponges, corals, brachiopods, bryozoans, gastropods, crinoids, mollusks, fusulinids, and fossil algae. Non-dolomitized primary-reef textures consist of undisturbed fossil frameworks, bioclastic calcarenite, and microcrystalline limestone. The massive member (reef core) transitions downslope into a breccia member representing the forereef slope facies. The massive member supports the vertical cliffs and is devoid of bedding. The breccia member forms ragged slopes, with coarse, angular cobbles and boulders derived from the reef core and adjacent shelf carbonates. To the northwest, the massive reef grades into shelf carbonates of the Seven Rivers, Yates, and Tansill Formations of the Artesia Group; to the southeast, it transitions into the siliciclastic sediments of the Bell Canyon Formation. The unit has a disconformable contact with the underlying Goat Seep Formation (Hayes, 1964). The massive reef member varies from approximately 75 to 230 m thick (averaging 122 m). The breccia member can reach up to 536 m thick, with an overall maximum combined thickness of nearly 610 m. Compiled from synthesized descriptions of Hayes (1964), Kelley (1971), Cikoski and Allen (2020), Skotnicki (2021, 2024a, 2024b), Skotnicki and Attia (2022), Allen and Skotnicki (2024), and Skotnicki and Allen (2024).

Pgs – Goat Seep Formation

Short description: Massive to thick-bedded shelf-margin carbonate consisting of gray dolomite with minor siliciclastic beds. Dominantly massive with low-angle, basinward-dipping foreslope deposits. Porous karstic weathering of dolomitized carbonates with few primary structures. Grades shelfward into the Artesia Group and basinward into the Cherry Canyon Sandstone. Up to 150 m thick where exposed.

Long description: Massive to thickly bedded shelf-margin reef carbonates consisting of light-gray dolomite with minor siliciclastic beds. Exposed only in North McKittrick Canyon within the Guadalupe Mountains in the southern portion of the map area. This unit represents early reef development during the Guadalupian period, grading into shelf equivalents of the Grayburg and Queen Formations of the Artesia Group; it is thought to correlate to basinal equivalents of the Cherry Canyon Sandstone of the Delaware Mountain Group despite an absence of observable exposures of this transition. The lower portion gradationally overlies the Cherry Canyon Sandstone Tongue and is composed of thickly bedded to massive dolomite that is thought to grade into shelfward-thickening limestone beds of the Cherry Canyon Sandstone. The upper portion is dominantly massive with foreslope deposits near the top of the unit. Foreslope deposits dip basinward at lower angles than Capitan Formation foreslope breccia facies

and contain wackestones and siliciclastic beds that are recorded to persist into subsurface well logs. Siliciclastic beds found in the upper part of the unit may be remnants of sandy upper Cherry Canyon Sandstone beds that pinch out toward the shelf. This unit exhibits porous to vuggy and karstic weathering of thoroughly dolomitized carbonates with few remaining primary structures and finely crystalline to sugary textures that may exhibit microbrecciation, remnant fossils, and intermixed very fine quartz grains. Overall, this unit is very similar in appearance and characteristics to the Capitan Formation. Up to 150 m of section is exposed; the base of the units is not visible in this quadrangle. Compiled from synthesized descriptions of King (1942, 1948), Newell et al. (1953), Boyd (1958), Hayes (1964), and Skotnicki (2024).

Shelf-margin deposits

Pco – Cutoff Formation

Short description: Slope-forming, dolomitic limestone, siltstones, and shale. Lower shales and chert grade into the basal San Andres Formation. Gypsum and siltstone high in the unit increase shelfward; limestones increase and grade into the Bone Spring Formation at the shelf margin. Overlies the Victorio Peak Limestone and is equal in age to the absent Brushy Canyon Formation. Approximately 70–90 m thick.

Long description: Medium- to dark-gray, weathering to light-gray, thin- to medium-bedded, slope-forming, dolomitic limestone interbedded with occasional siltstones, dark-gray shale, and shaly limestone. Dark-gray limestones are thinly bedded, about 0.1 m thick, and separated by interbeds of centimeter-scale dark shale and black chert that are found in the lower portion of the unit. Limestones may be massively bedded with micritic textures and a fetid odor. Siltstones are gray to orange, quartzose, and have vugs filled with calcite. The upper portion is dominated by light-gray dolomite that becomes more calcic and limestone-dominated toward the shelf margin in Texas. Siltstones and occasional gypsum become more prevalent shelfward as the lower portion of the unit grades inconspicuously into the lower San Andres Formation. The Cutoff Formation overlies the Victorio Peak Limestone, grades into the upper Bone Spring Formation, and is time equivalent to the lower Brushy Canyon Formation of the Delaware Mountain Group, which is absent on the shelf. Approximately 70–90 m thick. Compiled from synthesized descriptions of Warren (1955), Boyd (1958), Hayes (1964), and Skotnicki (2024b).

Pvc – Victorio Peak Limestone and Cherry Canyon Sandstone Tongue of the Delaware Mountain Group, undivided

Short description: The map unit **Pvc** is mapped where the map scale does not permit division of map unit **Pvp** and map unit **Pcc** when both are present on the landscape.

Long description: The map unit **Pvc** is mapped where the map scale does not permit division of map unit **Pvp** and map unit **Pcc** when both are present on the landscape. This map unit does not indicate which formation is more predominant in a given polygon but assumes a noteworthy portion of each is present.

Pvp – Victorio Peak Limestone

Short description: Dolomitic limestone with rare chert and thin sandstone interbeds near the base; thin, slope-forming limestone with dolomite and rare chert in the middle; and gray, thick, fine-grained bioclastic limestones at the top. Grades basinward into the upper Bone Spring Formation and shelfward

into the Yeso Formation and lower San Andres Formation. Approximately 85 m thick where exposed, and up to 240 m thick in Texas.

Long description: Shelf-margin reef facies with dolomitic limestone near the base, thin-bedded limestone in the middle, and thick limestone at the top of the unit. Dolomitic limestones are orange to light- or medium-gray, fine-grained, and found in 0.25- to 2-m-thick beds, with rare chert and interbeds of fine-grained sandstone. Olive-gray to light- or medium-gray, thin-bedded limestones and subordinate dolomite beds form slopes in the middle of the unit. These beds are less than 0.5 m thick and have occasional irregularly shaped, light-gray weathering to orange, chert nodules. Interbedded sandstones are tan, fine-grained, and calcareous. The upper unit is gray, fine-grained, thick-bedded limestone found in beds up to 2 m thick. This portion of the unit is bioclastic with common fossils of silicified crinoids and brachiopods. Throughout the unit, beds are massive, largely devoid of chert, and ledge or cliff forming, except for in the middle of the unit. Grades basinward into the upper Bone Spring Formation. The lower and middle portions grade shelfward into the Yeso Formation, where gypsum becomes prevalent, while the upper portion grades shelfward into the lower portion of the San Andres Formation. The cliff-forming upper portion becomes increasingly thick-bedded and cliff-forming south of the map area in the southern Guadalupe Mountains. Differences between the upper portion of this unit and the lower San Andres are largely unperceivable in the Brokeoff Mountains, where they grade into one another laterally. Approximately 85 m of the unit is exposed in the map area, whereas it reaches a thickness up to 240 m in Texas. Compiled from synthesized descriptions of Boyd (1958), Kelley (1971), Hayes (1964), and Skotnicki (2024b).

Ph – Hueco Formation

Short description: Cross section only.
Long description: Cross section only.

Basin deposits

Delaware basin sediments

Pdbc – Bell Canyon Formation of the Delaware Mountain Group

Short description: Basin limestone and sandstone. The exposed upper member (Lamar Limestone) consists of irregular to massive beds of fine, micritic, and bituminous limestone overlain by siltstones and limestones. Conformable with Cherry Canyon and the overlying Castile Formation, grades into the Capitan Formation. Limestones thicken reefward and thin basinward. Approximately 200 m thick at the type section in Texas.

Long description: Interbedded basinal limestone and sandstone with only the upper portion of the unit exposed in the map area. The Lamar Limestone is found along the reef escarpment at the southern map boundary along with outcrops of what is tentatively either the McCombs or Pinery Limestone in Black Canyon (Hayes, 1964). From base to top, the limestones are named Hegler, Pinery, Rader, McCombs, and Lamar; they are observed to be more calcic than the dolomitic limestones of the Cherry Canyon Sandstone. The Bell Canyon Formation features turbidite deposits near the basin margin that may include poorly sorted deposits with meter-scale limestone clasts in a sandy matrix. Limestones are typically dark gray, massive, and occur in beds around 1 m thick, and interbedded with limey and tabular to laminated sandstones and siltstones. The Lamar Limestone is dark gray; has thin to thick, irregular, and massive

beds; and is fine-grained, micritic, and bituminous. Contains occasional silicified, submillimeter-scale fossiliferous material and occasional chert. Where exposed, the Lamar Limestone may be overlain by a couple of meters of interbedded, brown, thin siltstones and flaggy limestones. This unit is conformable with the underlying Cherry Canyon Formation, is overlain conformably by the Castile Formation, and grades shelfward into the Capitan Formation. Approaching the reef, limestone members thicken and sandstones grade into limestone or pinch out. In the subsurface distal from the mountain front, limestones thin and disappear, making differentiation of Delaware Mountain Group formations difficult in the subsurface. At the type section in Texas, the unit is greater than 200 m thick. Compiled from synthesized descriptions of King (1942, 1948), Hayes and Koogle (1958), Hayes (1964), and Skotnicki and Allen (2024).

Pdc – Cherry Canyon Formation of Delaware Mountain Group

Short description: Cross section only.
Long description: Cross section only.

Pdbs – Brushy Canyon Formation of Delaware Mountain Group

Short description: Cross section only.
Long description: Cross section only

Pbs – Bone Spring Formation

Short description: Cross section only.
Long description: Cross section only.

Pw – Wolfcamp Formation

Short description: Cross section only.
Long description: Cross section only.

Carboniferous to Cambrian Systems

Tabosa Basin sediments

IPu – Pennsylvanian, undivided

Short description: Cross section only.
Long description: Cross section only.

IPcc – Cisco Formation and Canyon Group, undivided

Short description: Cross section only.
Long description: Cross section only.

IPs – Strawn Formation

Short description: Cross section only.

Long description: Cross section only.

IPa – Atoka Formation

Short description: Cross section only.
Long description: Cross section only.

IPm – Morrow Formation

Short description: Cross section only.
Long description: Cross section only.

Mu – Mississippian, undivided

Short description: Cross section only.
Long description: Cross section only.

DMw – Woodford Shale

Short description: Cross section only.
Long description: Cross section only.

Du – Devonian, undivided

Short description: Cross section only.
Long description: Cross section only.

SDu – Silurian and Devonian, undivided

Short description: Cross section only.
Long description: Cross section only.

Ou – Ordovician, undivided

Short description: Cross section only.
Long description: Cross section only.

OSf – Fusselman Dolostone

Short description: Cross section only.
Long description: Cross section only.

Om – Montoya Group

Short description: Cross section only.
Long description: Cross section only.

Os – Simpson Group

Short description: Cross section only.
Long description: Cross section only.

Oul – Lower Ordivican, undivided

Short description: Cross section only.
Long description: Cross section only.

COb – Bliss Formation

Short description: Cross section only.
Long description: Cross section only.

Mesoproterozoic Erathem

Ectasian System

Y2 – Precambrian plutonic igneous rocks

Short description: Cross section only.
Long description: Cross section only.

Description of Methods for Surficial Map Unit Compilation

This section is separate from the description of map units and describes how polygons and descriptions of surficial map units from different publications were compiled into the surficial map unit schema used in this map.

CENOZOIC ERATHEM

QUATERNARY SYSTEM

Anthropogenic (recent to late Holocene)

af – artificial fill

Compilation description: The map unit **artificial fill (af)** includes map units: *'human disturbed areas (hd)'* of Pederson and Dehler (2004b); *'disturbed ground (dg)'* of Cikoski (2019b); *'disturbed areas (d)'* of Allen and Attia (2022), Allen and Skotnicki (2024), and Allen (2024); *'disturbed ground and artificial fill (daf)*' of Skotnicki and Attia (2022); *'disturbed areas (hd)'* of Dehler and Pederson (1998) and Pederson and Dehler (2004a); *'artificial fill (af)'* of Cikoski (2019a), Cikoski (2019b), and Cikoski (2020).

Eolian deposits (recent to late Pleistocene)

Qe – Eolian sediments

Compilation description: The map unit **eolian sediments (Qe)** includes map units: *'Quaternary sand covering caliche (Qsc)'* of Dehler and Pederson (1998); *'eolian sand (Qes)'* of Pederson and Dehler (2004b); *'dune deposits (Qed)'* of Cikoski (2019b) and Cikoski (2020).

Qse – Sheetwash alluvium and loessal eolian sediments, interbedded

Compilation description: The map unit **sheetwash alluvium and loessal eolian sediments, interbedded (Qse)** includes map units: *'aeolian deposits (Qaes)'* and *'Quaternary eolian sands (Qe)'* of Dehler and Pederson (1998); *'alluvial and eolian deposits (Qaes)'* of Pederson and Dehler (2004a) and Pederson and Dehler (2004b); *'eolian sand (Qes)'* of Pederson and Dehler (2004b); *'alluvial and eolian sediment (Qae)'* of Cikoski (2019a); *'slope wash alluvium (Qsw)'* of Cikoski (2019b) and Cikoski (2020); *'alluvial and eolian deposits in swales (Qsw)'* of Cikoski and Allen (2020); *'eolian and alluvial sediments (Qae)'* of Cikoski (2020); *'eolian/alluvial surface deposits (Qae)'* and *'alluvial aprons (Qacs-Qafn)'* of Allen and Attia (2022); *'windblown silt, fine sand and slope-wash mud blanketing relatively flat area to the east of Black River (Qae)'* of Allen and Attia (2021); *'windblown silt and fine sand (Qae)'* of Allen (2024); *'eolian deposits (Qe)'* of Cikoski (2019b); *'mixed eolian, alluvial, and colluvial surface deposits (Qae)'* of Cikoski and Allen (2020).

Colluvial deposits (Holocene to late Pleistocene)

Qac – Alluvium and colluvium, undifferentiated

Compilation description: The map unit **alluvium and colluvium, undifferentiated (Qac)** includes map units: *'undivided alluvium and colluvium (Qac)'* of Skotnicki and Allen (2024); *'undivided valley alluvium and colluvium in the Guadalupe Mountains (Qac)'* of Allen and Skotnicki (2024); and *'accumulations of alluvium and colluvium along steep slopes and associated down-slope alluvial aprons (Qac)'* of Allen and Attia (2021). It may also include any other active or inactive alluvial, colluvial, or sheetwash units that are not able to be differentiated at this scale. Sections, or entire polygons, of map units from existing publications that are mapped as **alluvium and colluvium, undifferentiated (Qac)** in this publication may also be assigned to other units. *'Qac'* of Allen and Skotnicki (2024) is variably mapped as **alluvium recent (Qar)**.

Internally drained deposits (Holocene to late Pleistocene)

Qdf – Depression fill

Compilation description: The map unit **depression fill (Qdf)** includes map units: *'closed basin deposits (Qaed)'* of Skotnicki and Allen (2024); *'sinkholes (Qs)'* of Skotnicki (2021); *'externally drained collapse features (Qsl)'* of Skotnicki (2021), *'eolian/alluvial deposits in depressions (Qaed)'* of Allen and Attia (2022); *'accumulations of eolian and alluvial silt, sand, clay, and minor gravel in closed or nearly closed depressions (Qaed)'* of Allen and Attia (2021) and Allen (2024); *'alluvium and eolian silt, sand, clay and gravel in closed or nearly closed depressions (Qvaed)'* of Allen and Skotnicki (2024); *'depression fill (Qdf)'* of Cikoski (2019a), Cikoski (2019b), Cikoski and Allen (2020), and Cikoski (2020). Previous mapping utilized point features (e.g. *collapse structure or sinkhole (23.09)* of Cikoski and Allen (2020)) or map unit points (e.g. *sinkholes (Qs)* of Skotnicki (2021)) for features below map scale. Individual polygons may include multiple combined features in an effort to maintain representation at this map-scale despite presence of other surficial or bedrock units separating sub-map-scale deposits.

Qplr – Playa sediments, recent

Compilation description: The map unit **playa sediments, recent (Qplr)** includes map units *'depression fill (Qdf)'* of Cikoski (2019b), 'playa deposits (Qp)' of Skotnicki (2024b), 'playa lake deposit (Qp)' of Pederson and Dehler (2004b), and *'alkali lake deposits (Qak)'* of O'Neill (1998) which is a 7.5-minute, 1:24,000-scale, map to the west of the southwestern most 7.5-minute quadrangle in this 30 x 60-minute sheet.

Qply – Playa sediments, younger

Compilation description: The map unit **playa sediments, younger (Qply)** includes map units *'depression fill (Qdf)'* of Cikoski (2019b).

Ql – Lacustrine sediments

Compilation description: The map unit **lacustrine sediments (Ql)** includes map unit *'lake sediments (Ql)'* of O'Neill (1998), a 7.5-minute, 1:24,000-scale, map to the west of the southwestern most 7.5-minute quadrangle in this 30'x60' sheet.

Alluvium deposits (recent to middle Pleistocene)

Sheetwash alluvium deposits (recent to late Pleistocene)

Qsr – Sheetwash alluvium, recent

Compilation description: The map unit **sheetwash alluvium, recent (Qsr)** includes map units: *'Quaternary valley fill (Qvf)'* of Dehler and Pederson (1998), *'Quaternary deposits, younger (Qy)'* of Dehler and Pederson (2002), *'younger alluvium (Qay)'* of Cikoski (2019b), *'alluvium in active drainages (Qay)'* of Allen and Attia (2022), *'recent alluvium (Qayh)'* of Cikoski and Allen (2020)), *'sand, mud, gravel and gypsite underlying the upper Black River valley floor (Qvae)'* of Allen and Skotnicki (2024), *'valley-floor sand, mud, gravel and gypsite underlying floodplains in larger drainages bordered by gypsum bedrock (Qvae)'* of Allen and Attia (2021), and *'valley-floor sand, mud, gravel and gypsite underlying floodplains in larger drainages (Qvae)*' of Allen (2024) and Allen and Attia (2022). Sections, or entire polygons, of map units from existing publications that are mapped as **sheetwash alluvium, recent (Qsr)** in this publication may also be assigned to other units. *'Qay'* of Cikoski (2019b), *'Qvae'* of Allen (2024), *'Qy'* of Dehler and Pederson (2002), and *'Qvf'* of Dehler and Pederson (1998) are variably mapped as **sheetwash alluvium, younger (Qsy)**. *'Qy'* of Dehler and Pederson (2002), *'Qayh'* of Cikoski and Allen (2020), and *'Qvae'* of Allen and Attia (2022) are variably mapped as **alluvium, recent (Qar)**. *'Qy'* of Dehler and Pederson (2002) is variably mapped as **terrace alluvium, younger (Qty).** *'Qayh'* of Cikoski and Allen (2020) is variably mapped as **piedmont alluvium, recent (Qpr)**.

Qsy – Sheetwash alluvium, younger

Compilation description: The map unit **sheetwash alluvium, younger (Qsy)** includes map units: *'Quaternary deposits, younger (Qy)'* of Dehler and Pederson (2002), *'older Holocene sedimentary deposits (Qy)'* of Skotnicki (2021), *'Black River valley-border alluvium (Qbr)'* and *'valley-floor gypsite along major drainages (Qvg)'* of Allen and Attia (2022), *'older Black River terrace alluvium (Qtb1)'* and *'older gypsiferous Black River terrace alluvium (Qtbg)'* of Cikoski and Allen (2020). Note that *'valley-floor gypsite along major drainages (Qvg)'* is very distinct in composition but extent of exposure is insufficient for map scale and the processes that created those deposits are largely the same as **sheetwash alluvium, younger (Qsy), terrace**

alluvium, younger (Qty), or **terrace alluvium, intermediate (Qti)**. Sections, or entire polygons, of map units from existing publications that are mapped as **sheetwash alluvium, younger (Qsy)** in this publication may also be assigned to other units. *'Qy'* of Dehler and Pederson (2002), *'Qy'* of Skotnicki (2021), *'Qvg'* & *'Qbr'* of Allen and Attia (2022), and *'Qtb1'* & *'Qtbg'* of Cikoski and Allen (2020) are variably mapped as **terrace alluvium, younger (Qty)** but seem to more often exhibit processes and deposition characteristic of unit **sheetwash alluvium, younger (Qsy)** at that time. *'Qy'* of Skotnicki (2021) is variably mapped as **piedmont alluvium, intermediate (Qpi)** when along piedmont tributary channels. *'Qy'* of Dehler and Pederson (2002) is variably mapped as **alluvium, recent (Qar)** and **sheetwash alluvium, recent (Qsr)**.

Fan alluvium deposits (recent to middle Pleistocene)

Qfr – Fan alluvium, recent

Compilation description: The map unit **fan alluvium, recent (Qfr)** includes map units: *'piedmont fan deposits (Qpf)'* of Skotnicki and Attia (2022), *'small-scale fan alluvium (Qaf)'* of Cikoski (2019a), and *'fan alluvium (Qay)'* of Cikoski (2019b), Cikoski and Allen (2020), and Cikoski (2020). Sections, or entire polygons of map units from existing publications that are mapped as **fan alluvium, recent (Qfr)** in this publication may also be assigned to other units. *'Qpf'* of Skotnicki and Attia (2022), and *'Qfy'* of Cikoski and Allen (2020) are variably mapped as **piedmont alluvium, recent (Qpr)**. *'Qpf'* of Skotnicki and Attia (2022) is variable mapped as **fan alluvium, younger (Qfy)** and **piedmont alluvium, younger (Qpy)**.

Qfy – Fan alluvium, younger

Compilation description: The map unit **fan alluvium, younger (Qfy)** includes map units *'piedmont fan deposits (Qpf)'* of Skotnicki and Attia (2022), '*Older Holocene sedimentary deposits' (Qy)'*, *'Late Pleistocene sedimentary deposits (Ql)'*, and *'Quaternary or Tertiary sedimentary deposits (QTc2)'* of Skotnicki (2021), *'younger subunit of the older alluvium (Qao2)'* of Cikoski (2019a), 'Quaternary deposits, younger (Qy)' of Dehler and Pederson (2002), *and 'younger piedmont alluvium (Qpy)'* of Allen and Skotnicki (2024) and Skotnicki and Allen (2024). Sections or entire polygons of map units from existing publications that are mapped as **fan alluvium, younger (Qfy)** in this publication may also be assigned to other units. *'Qpy'* of Allen and Skotnicki (2024) is variably mapped as **piedmont alluvium, recent (Qpr)** and **fan alluvium, recent (Qfr)**. *'Qpf'* of Skotnicki and Attia (2022) is variably mapped as **fan alluvium, intermediate (Qfi) and fan alluvium, older (Qfo)**.

Qfi – Fan alluvium, intermediate

Compilation description: The map unit **fan alluvium, intermediate (Qfi)** includes map units 'older alluvium, undivided (Qao)' of Cikoski (2019a) and 'late Pleistocene sedimentary deposits (Ql)' of Skotnicki (2021). Sections, or entire polygons, of map units from existing publications that are mapped as **fan alluvium, younger (Qfy)** in this publication may also be assigned to other units. *'Qao'* of Cikoski (2019a) is variably mapped as **piedmont alluvium, intermediate (Qpi)** and occasionally mapped as **terrace alluvium, intermediate (Qti)**.

Qfo – Fan alluvium, older

Compilation description: The map unit **fan alluvium, older (Qfo)** includes map unit *'old alluvial fan deposits (Qfo)'* of O'Neill (1998) which borders the Carlsbad 30'x60' sheet to the west of the southwestern

most 7.5-minute quadrangle. It also includes map unit *'older alluvium fan deposits (Qso)'* and *'oldest alluvium fan remnants (Qco)'* of Skotnicki and Knight (2022) which covers the Guadalupe Mountains south of the Texas-New Mexico border.

Channel alluvium deposits (recent to middle Pleistocene)

Qar – Alluvium, recent

Compilation description: The map unit **alluvium, recent (Qar)** includes map units: *'historic alluvium (Qah)'* of Cikoski (2019a), Cikoski (2019b), and Cikoski (2020), *'Quaternary alluvium (Qal)'* of Dehler and Pederson (1998) and Pederson and Dehler (2004a), *'Quaternary deposits, younger (Qy)'* of Dehler and Pederson (2002), *'younger subunit of the younger subunit (Qay2)'* and *'gravel-dominated deposits of the younger subunit of the younger alluvium (Qay2g)'* of Cikoski (2019a), *'youngest terrace/floodplain deposits (Qtp3)'* and *'young terrace and floodplain deposits along the Black River (Qtby)'* of Cikoski (2019b), *'recent alluvium (Qayh)'* and *'youngest Black River terrace alluvium (Qtb2)'* of Cikoski and Allen (2020), *'younger alluvium (Qay)'* of Cikoski (2020), *'active channel deposits (Qyc)'* of Skotnicki (2021), *'alluvium along active drainages (Qay)'* of Allen and Attia (2021), *'alluvium in active drainages (Qay)'* and *'valley-floor alluvium (Qvae)'* of Allen and Attia (2022), and *'valley-floor sand, mud, gravel, and gypsite underlying floodplains and low terraces of larger drainages (Qvae)'* and *'alluvium in active drainages (Qay)'* of Allen (2024). Sections, or entire polygons, of map units from existing publications that are mapped as **alluvium, recent (Qar)** in this publication may also be assigned to other units. *'Qayh'* of Cikoski and Allen (2020), *'Qay'* and *'Qvae'* of Allen and Attia (2022), *'Qy'* of Dehler and Pederson (2002), *'Qvae'* of Allen (2024), and *'Qay'* of Allen and Attia (2021) are variably mapped as **sheetwash alluvium, recent (Qsr)**. *'Qayh'* of Cikoski and Allen (2020) and *'Qay2'* & *'Qay2g'* of Cikoski (2019a) are variably mapped as **piedmont alluvium, recent (Qpr)**. *'Qtp3'* & *'Qtby'* of Cikoski (2019b), *'Qvae'* of Allen (2024), *'Qy'* of Dehler and Pederson (2002), and *'Qay'* of Allen and Attia (2021) are variably mapped as **terrace alluvium, younger (Qty)**. *'Qay2'* and *'Qay2g'* of Cikoski (2019a) are variably mapped as **fan alluvium, recent (Qfr)**. Map unit *'youngest Lakewood terrace alluvial deposits (Qlt3)'* of McCraw et al. (2011) tends to be mapped with **terrace alluvium, younger (Qty)** as it is only 2- to 3-m-above grade of the active channel and commonly experiences reactivation during storm events.

Recent alluvium and younger terrace alluvium, undifferentiated – Qtyr

Qty and Qti – Terrace alluvium, younger and Terrace alluvium, intermediate

Compilation description: Differentiation between the map units **terrace alluvium, younger (Qty)** and **terrace alluvium, intermediate (Qti)** was not recognized during the initial phase of map unit schema development. Qty was broken out to indicate the lowest levels of the Lakewood terrace suite that experience reactivation and ongoing deposition while Qti represents inactive surfaces and deposits. The map units **terrace alluvium, younger (Qty)** and **terrace alluvium, intermediate (Qti)** includes map units: *'alluvial sand mainstem (Qasm1)'* of Dehler and Pederson (1998), Pederson and Dehler (2004a), and Pederson and Dehler (2004b), *'alluvial gravel mainstem (Qagm2)'* of Dehler and Pederson (1998), Pederson and Dehler (2004a), and Pederson and Dehler (2004b), *'Black River valley-border alluvium (Qbr)'* and *'Black River valley-border alluvium (Qbr)'* of Allen (2024) and Allen and Attia (2022), *'Quaternary deposits, younger (Qy)'* of Dehler and Pederson (2002), *'Quaternary sand sheet, sometimes overlying Quaternary terrace (Qss & Qss/Qt2)'* of Dehler and Pederson (1998), *'older subunit of the younger alluvium (Qay1)'*, *'Gravel-dominated deposits of the older subunit of the younger alluvium (Qay1g)'*, *'older alluvium, undivided (Qao)'*, *'younger subunit of the older alluvium (Qao2)'*, and *'sand-dominated deposits of the younger subunit of the older alluvium (Qao2s)'* of Cikoski (2019a), *'younger terrace deposits (Qtp2)'*, *'older terrace deposits (Qtp1)'*, and *'young terrace and*

floodplain deposits along the Black River (Qtby)' of Cikoski (2019b), *'older gypsiferous Black River terrace alluvium (Qtbg)'* of Cikoski and Allen (2020), *'younger terrace deposits (Qt2)'* of Cikoski (2020), *'older Holocene sedimentary deposits (Qy)'* of Skotnicki (2021), *'valley-floor gypsite (Qvg)'* of Allen and Attia (2022), *'older Black River terrace alluvium (Qtb1)'*. Characterization of these deposits build on work of Fielder and Nye (1933), McCraw et al. (2007), and McCraw and Land (2008), but utilizes descriptions of map units *'young Lakewood terrace alluvial deposits (Qlt2)'* and *'older Lakewood terrace alluvial deposits (Qlt1)'* of McCraw et al. (2011) north of the Carlsbad 30x60-minute quadrangle. Map unit *'youngest Lakewood terrace alluvial deposits (Qlt3)'* of McCraw et al. (2011) tends to be mapped with **terrace alluvium, younger (Qty)** as it is only 2- to 3-m-above grade of the active channel and commonly experiences reactivation during storm events. Sections, or entire polygons, of map units from existing publications that are mapped as **terrace alluvium, younger (Qty)** in this publication may also be assigned to other units. *'Qy'* of Dehler and Pederson (2002) and *'Qtby'* of Cikoski (2019b) are variably mapped as **alluvium, recent (Qar)**. '*Qagm2'* of Dehler and Pederson (1998), Pederson and Dehler (2004a), and Pederson and Dehler (2004b), *'Qss & Qss/Qt2'* of Dehler and Pederson (1998) and *'Qbr'* of Allen (2024) are variably mapped as **terrace alluvium, older (Qto)**. *'Qy'* of Dehler and Pederson (2002) & Skotnicki (2021), *'Qtb1'* & *'Qtbg'* of Cikoski and Allen (2020), and *'Qbr'* & *'Qvg'* of Allen and Attia (2022) are variably mapped as **sheetwash alluvium, younger (Qsy)**. *'Qy'* of Skotnicki (2021), *'Qao'*, *'Qao2'*, and *'Qao2s'* of Cikoski (2019a) are variably mapped as **piedmont alluvium, younger (Qpy)**. *'Qao*' of Cikoski (2019a) is variably mapped as **fan alluvium, younger (Qfy)**.

Qto – Terrace alluvium, older

Compilation description: The map unit **terrace alluvium, older (Qto)** includes map units: *'Orchard Park alluvial-plain deposits (Qop)'* of Allen and Attia (2022), *'alluvial sand and gravel mainstem (Qasgm2)'* of Pederson and Dehler (2004b), *'alluvial sand and gravel piedmont (Qagp2)'* of Pederson and Dehler (2004a), *'alluvial gravel mainstem (Qagm2)'* of Dehler and Pederson (1998), Pederson and Dehler (2004a), and Pederson and Dehler (2004b), *'alluvial gravels of Dark Canyon (Qagdc2)'* of Dehler and Pederson (1998) and Pederson and Dehler (2004a), *'Quaternary terrace (Qt1)'* of Dehler and Pederson (1998) and *'older terrace deposits (Qt1)'* of Cikoski (2020), *'older subunit of the older alluvium (Qao1)'* of Cikoski (2019a), *'conglomerates along the Pecos River (Qgca)'*, *'conglomerates along the Black River (Qgcb)'*, and *'conglomerate-dominated facies (Qgc)'* of Cikoski (2019b), *'upper Gatuña Formation (Qg)'* of Cikoski (2019b) and Cikoski (2020), and *'coarser-grained faceis of the upper Gatuña Formation (Qgc)'* of Cikoski (2020). Characterization of these deposits builds on work of Fielder and Nye (1933) and utilizes descriptions of map unit *'Orchard Park terrace alluvial deposits (Qot)'* of McCraw et al. (2011) north of the Carlsbad 30'x60'. Sections, or entire polygons, of map units from existing publications that are mapped as **terrace alluvium, older (Qto)** in this publication may also be assigned to other units. *'Qagm2'* of Pederson and Dehler (2004b) and *'Qagdc2'* of Dehler and Pederson (1998) & Pederson and Dehler (2004a) are variably mapped as **terrace alluvium, intermediate (Qti)**. *'Qagm2'* of Dehler and Pederson (1998), *'Qao1'* of Cikoski (2019a), and *'Qagp2'* of Pederson and Dehler (2004a) are variably mapped as **piedmont alluvium, older (Qpo)**. *'Qagm2'* of Pederson and Dehler (2004b), *'Qagm2'* of Dehler and Pederson (1998), *'Qt1'* of Dehler and Pederson (1998), 'Qao1' of Cikoski (2019a), and *'Qgc'* of Cikoski (2020) are variably mapped as **Gatuña Formation, lower fluvial and valley-margin facies (QNg)**. Portions of *'Qgc'*, *'Qgcb'*, *'Qgca'*, *and 'Qg'* of Cikoski (2019b) and *'Qg'* of Cikoski (2020) are tentatively mapped as **Gatuña Formation, lower fluvial and valley-margin facies (QNg)**. These units are tentative because they are described by Ckowski (2019b; 2020), as sediments overlying the Pierce Canyon Caliche of Hawley (1993) and underlying the Mescalero paleosol or "Mescalero Caliche" of Bretz and Horberg (1949). Hawley (1993) described the Pierce Canyon Caliche as being age equivalent to the Pliocene aged Ogallala Caprock but genetically related to the Gatuña fluvial system. Attia and Allen (2022) in OFGM-299 found that the interpretation of two caliches

of distinct ages was misguided. Their field observations found that offsetting of the caliche was caused by solution subsidence and made the Gatuña Formation sediments to appear as overlying the Mescalero paleosol and thickening of the caliche due to solution subsidence related fracturing and subsequent recementation locally makes the caliche appear thicker. This produced an illusion of a thick middle Gatuña caliche that was down section of the Mescalero paleosol and acted as a division between underlying *'lower Gatuña Formation (Tg)'* and *'upper Gatuña Formation (Qg)'* of Cikoski (2019b). Locally, the units *'Qgc'*, *'Qgcb'*, *'Qgca'*, *'Qg'* of Cikoski (2019b) and *'Qg'* of Cikoski (2020) may not actually lie over the Mescalero paleosol, Cikoski's Pierce Canyon Caliche, and thus should be mapped as Gatuña Formation rather than with the map unit **terrace alluvium, older (Qto)**.

Piedmont alluvium deposits (recent to middle Pleistocene)

Qpr – Piedmont alluvium, recent

Compilation description: The map unit **piedmont alluvium, recent (Qpr)** includes map units: *'younger piedmont alluvium (Qpy)'* of Skotnicki and Allen (2024), *'piedmont fan deposits (Qpf)'* of Skotnicki and Attia (2022), *'active channel deposits (Qpf)'* of Skotnicki (2021), *'fan alluvium (Qfy)'* of Cikoski and Allen (2020), *'alluvium along active drainages (Qay)'* and *'younger piedmont alluvium (Qpy)'* of Allen and Skotnicki (2024), *'Gravel-dominated deposits of the younger subunit of the younger alluvium (Qay2g)* of Cikoski (2019a), *'recent alluvium (Qayh)'* of Cikoski and Allen (2020), *'youngest terrace deposits (Qty)'* of Skotnicki and Attia (2022), *'older Holocene sedimentary deposits (Qy)'* of Skotnicki (2021), *'younger alluvium, undivided (Qay)'* of Cikoski (2019a) and Cikoski and Allen (2020), and *'younger subunit of the younger subunit* (Qay2)' of Cikoski (2019a) and Cikoski and Allen (2020). Sections, or entire polygons, of map units from existing publications that are mapped as **piedmont alluvium, recent (Qpr)** in this publication may also be assigned to other units. *'Qayh'* of Cikoski and Allen (2020) is variably mapped as **interbedded sheetwash and alluvium, recent (Qsr)**. *'Qpf'* of Skotnicki and Attia (2022) is variably mapped as **fan alluvium, younger (Qfy)**. *'Qpf'* of Skotnicki and Attia (2022) and *'Qy'* of Skotnicki (2021) are variably mapped as **piedmont alluvium, younger (Qpy)**. *'Qay2g'* of Cikoski (2019a), *'Qayh'* of Cikoski and Allen (2020), and *'Qay2'* of Cikoski (2019a) & Cikoski and Allen (2020) are variably mapped as **alluvium, recent (Qar)**. *'Qay2'* of Cikoski (2019a), *'Qay2g'* of Cikoski (2019a), *'Qfy'* of Cikoski and Allen (2020), and *'Qpf'* of Skotnicki and Attia (2022) are variably mapped as **fan alluvium, recent (Qfar)**.

Qpy and Qpi – Piedmont alluvium, younger and piedmont alluvium, intermediate

Compilation description: Differentiation between the map units **piedmont alluvium, younger (Qpy)** and **piedmont alluvium, intermediate (Qpi)** was not recognized during the initial phase of map unit schema development. Qpy was broken out to indicate piedmont deposits and surfaces equivalent to the lowest levels of the Lakewood terrace suite that experience reactivation and ongoing deposition while Qti represents inactive surfaces and deposits. The map units **piedmont alluvium, younger (Qpy)** and **piedmont alluvium, intermediate (Qpi)** includes map units: *'younger piedmont-slope sand, gravel, and mud (Qpy)'* of Allen and Attia (2021), *'intermediate piedmont alluvium, younger subunit (Qpi2)'* of Skotnicki and Allen (2024), *'intermediate piedmont alluvium, younger map unit (Qpi2)'* of Allen and Skotnicki (2024), *'alluvial sand piedmont (Qasp1)'* of Pederson and Dehler (2004b), *'older subunit of the younger alluvium (Qay1)'* of Cikoski (2019a), *'gravel-dominated deposits of the older subunit of the younger alluvium (Qay1g)'* of Cikoski (2019a), *'older alluvium, undivided (Qao)'* of Cikoski (2019a), *'younger subunit of the older alluvium (Qao2)'* of Cikoski (2019a), *'sand-dominated deposits of the younger subunit of the older alluvium (Qao2s)'* of Cikoski (2019a), *'older subunit of the younger alluvium (Qay1)'* of Cikoski and Allen (2020), *'intermediate terrace deposits (Qti)'* of Skotnicki and Attia (2022), *'piedmont fan deposits (Qpf)'* of Skotnicki and Attia

(2022), *'late Pleistocene sedimentary deposits (Ql)'* of Skotnicki (2021), and *'older Holocene sedimentary deposits (Qy)'* of Skotnicki (2021). Sections, or entire polygons, of map units from existing publications that are mapped as **piedmont alluvium, younger (Qpy)** in this publication may also be assigned to other units. *'Qay1'* of Cikoski (2019a), *'Qay1g'* of Cikoski (2019a), and *'Qao'* of Cikoski (2019a) are variably mapped as **terrace alluvium, younger (Qti)**. *'Qao'* of Cikoski (2019a) and *'Qpf'* of Skotnicki and Attia (2022) are variably mapped as **fan alluvium, younger (Qfy)**. *'Qpf'* of Skotnicki and Attia (2022) is variably mapped as **fan alluvium, recent (Qfr)** and **piedmont alluvium, recent (Qpr)**.

Qpo – Piedmont alluvium, older

Compilation description: The map unit **piedmont terrace, older (Qpto)** includes map units: *'intermediate piedmont-slope sand, gravel, and mud (Qpi)'* of Allen and Attia (2021), *'intermediate piedmont alluvium, older map unit (Qpi1)'* of Allen and Skotnicki (2024), *'intermediate piedmont alluvium, older subunit (Qpi1)'* of Skotnicki and Allen (2024), *'alluvial sand and gravel piedmont (Qagp2)'* of Pederson and Dehler (2004a), *'alluvial sand piedmont (Qsp2)'* of Pederson and Dehler (2004a), *'alluvial sand and gravel piedmont (Qasgp2)'* of Pederson and Dehler (2004b), *'alluvial sand piedmont (Qasp2)'* of Pederson and Dehler (2004b), *'older subunit of the older alluvium (Qao1)'* of Cikoski (2019a), *'intermediate alluvium, undivided (Qai)'* of Cikoski and Allen (2020), *'upper Gatuña Formation (Qgcc)'* of Cikoski and Allen (2020), *'upper Gatuña Formation – conglomeratic facies (Qgc)'* of Cikoski and Allen (2020), *'upper Gatuña Formation – fine-grained facies (Qgf)'* of Cikoski and Allen (2020), *'oldest terrace deposits (Qto)'* of Skotnicki and Attia (2022), *'middle Pleistocene sedimentary deposits (Qm)'* and *'Quaternary or Tertiary sedimentary deposits, younger unit (QTc2)'* of Skotnicki (2021). Sections, or entire polygons, of map units from existing publications that are mapped as **piedmont alluvium, older (Qpo)** in this publication may also be assigned to other units. *'Qagp2'* of Pederson and Dehler (2004a) and *'Qao1'* of Cikoski (2019a) are variably mapped as **terrace alluvium, older (Qto)**.

QUATERNARY–NEOGENE SYSTEM

Qg and QNg – Gatuña Formation, fluvial and valley-margin facies and Gatuña Formation, lower fluvial and valley-margin facies

Compilation description: The map unit **Gatuña Formation, fluvial and valley-margin facies (Qg)** and the map unit **Gatuña Formation, lower fluvial and valley-margin facies (QNg)** includes map units: *'older alluvium (Qo)* of Motts (1962); *'undifferentiated Gatuña Formation (QTg)'* of Cikoski (2020) and Cikoski (2019b); *'undifferentiated siltstone/sandstone-dominated Gatuña Formation (QTgs)'*, *'undifferentiated coarser-grained deposits of Gatuña Formation age (QTgc)'*, *'undifferentiated finer-grained deposits of the Gatuña Formation (QTgf)'*, *'sand- and mud-dominated facies (Qgs)'*, *'gravel-dominated facies (Qgg)'*, *'lower Gatuña Formation (Tg)'*, *'conglomerate-dominated facies (Qgc)'*, and *'conglomerates along the Pecos River (Qgca)'* of Cikoski (2019b); *'Gatuña Formation (TQg)'*, *'alluvial gravel mainstem (Qagm2)'*, and *'Quaternary terrace (Qt1)'* of Dehler and Pederson (1998); *'Quaternary deposits, older (Qo)'* of Dehler and Pederson (2002); *'old Pecos River gravel deposits (Qrg)'* of Allen and Attia (2022); *'Gatuña Formation (QTg)'* of Pederson and Dehler (2004b); *'coarser-grained facies of the lower Gatuña Formation (Tgc)'* and *'finer-grained facies of the lower Gatuña Formation (Tgf)'* of Cikoski (2020). Sections, or entire polygons, of map units from existing publications that are mapped as **Gatuña Formation, fluvial and valley-margin facies (Qg)** and **Gatuña Formation, lower fluvial and valley-margin facies (QNg)** in this publication may also be assigned to other units. *'Qagm2'* of Dehler and Pederson (1998) is variably mapped as **terrace alluvium, older (Qto)**. *'Qagm2'* and *'Qt1'* of Dehler and Pederson (1998), *'Qo'* of Dehler and Pederson (2002), and *'QTgs'*, *'QTgc'*, *'QTg'*, *'QTgf'*, *'Qgs'*, *'Qgc'*, & *'Qgca'* of Cikoski (2019b) are variably mapped as **terrace alluvium, older (Qto)**. *'Qgg'* of Cikoski (2019b),

'Qrg' of Allen and Attia (2022), and *'QTgc'* of Cikoski (2020) are variably mapped as **Gatuña Formation, piedmont facies (Qgp)** and **Gatuña Formation, lower piedmont facies (QNgp)**.

Qgp and QNgp – Gatuña Formation, piedmont facies and Gatuña Formation, lower piedmont facies

Compilation description: The map unit **Gatuña Formation, piedmont facies (Qgp)** and **Gatuña Formation, lower piedmont facies (QNgp)** includes map units: *'Quaternary Dark Canyon fan (Qf1b)'* and *'alluvial gravels of Dark Canyon (Qagdc2)'* of Dehler and Pederson (1998); *'lower Gatuña Formation (Tgc)'* of Cikoski and Allen (2020); *'Gatuña Formation, piedmont facies (Tgp)'* of Cikoski (2019a)'; *'older piedmont (Qpo)'* of Allen and Attia (2021);*'older alluvium (Qo)'* of Motts (1962); *'older piedmont alluvium (Qpo)'* of Skotnicki and Allen (2024) and Allen and Skotnicki (2024); *'oldest terrace deposits (Qto)'* of Skotnicki and Attia (2022);*'piedmont conglomerate remnants at high levels on the Gypsum Plain (QTg)'* of Allen and Attia (2021); *'Quaternary or Tertiary sedimentary deposits, younger unit (QTc2)'* and *'Quaternary or Tertiary sedimentary deposits, older unit (QTc1)'* of Skotnicki (2021); and *'alluvial sand and gravel piedmont (Qagp2)'* of Pederson and Dehler (2004a). Sections, or entire polygons, of map units from existing publications that are mapped as **Gatuña Formation, piedmont facies (Qgp)** and **Gatuña Formation, lower piedmont facies (QNgp)** in this publication may also be assigned to other units. *'Tgp'* of Cikoski (2019a), *'QTc2'* of Skotnicki (2021), and *'Qpo'* of Skotnicki and Allen (2024) & Allen and Skotnicki (2024) are variably mapped as **piedmont terrace, older (Qpto)**. *'Qf1b'* of Dehler and Pederson (1998) and *'Qpo'* of Allen and Attia (2021) are variably mapped as **Gatuña Formation, fluvial and valley-margin facies (Qg)**. *'Qagdc2'* of Dehler and Pederson (1998) and *'Qagp2'* of Pederson and Dehler (2004a) are variably mapped as **terrace alluvium, older (Qto)**.